Title
NONLINEAR-SPECTROSCOPIC STUDIES OF HIGHLY EXCITED STATES OF MOLECULES IN SUPERSONIC BEAMS

Author
Page, R.H.

Publication Date
1987-04-01

Lawrence Berkeley Laboratory
UNIVERSITY OF CALIFORNIA

Materials & Chemical Sciences Division

NONLINEAR-SPECTROSCOPIC STUDIES OF HIGHLY EXCITED STATES OF MOLECULES IN SUPERSONIC BEAMS

R.H. Page
(Ph.D. Thesis)

April 1987

Prepared for the U.S. Department of Energy under Contract DE-AC03-76SF00098

DISCLAIMER

Nonlinear-Spectroscopic Studies of Highly Excited States of Molecules in Supersonic Beams

Ralph Henry Page
Ph.D. Thesis

Lawrence Berkeley Laboratory
University of California
Berkeley, California 94720

April 1987

This work was supported by the U.S. Department of Energy under Contract Number DE-AC03-76SF00098.

NONLINEAR-SPECTROSCOPIC STUDIES OF HIGHLY EXCITED STATES OF MOLECULES IN SUPERSONIC BEAMS

Ralph Henry Page

ABSTRACT

This thesis describes nonlinear optical spectroscopic experiments on molecules and molecular clusters in supersonic beams. First, the absorption spectrum of water dimers in the O-H stretching region (~3400-3800 cm^{-1}) was obtained with a resolution of ~ 2 cm^{-1}, by monitoring vibrational predissociation. The O-H stretching frequencies of the dimer were found to be shifted by hydrogen bonding, with respect to those of the monomer. In a similar, lower-resolution experiment, $(H_2O)_{19}$ clusters were studied. The effect of the cluster temperature on the absorption spectrum was discussed.

A tunable, narrowband (~ 1.5 cm^{-1} resolution) XUV source in the 904-1024 A region has been developed using frequency tripling in a pulsed jet of gas. Rotationally resolved photoionization spectra of H_2O and D_2O were then obtained with this source. The spectra were assigned, and the energies of some excited states were accurately determined. Autoionizing Rydberg series in the spectra were identified. Lifetimes of the autoionizing states were deduced to be between 0.1 and 1 psec.

XUV-UV and XUV-visible double-resonance experiments on H_2 are described. The former probed the ion-pair production in the ($H^+ + H^-$)

continuum, and detected previously-unobserved Rydberg series which converge to high vibrational levels ($v^+ \sim 10$) of H_2^+. The latter probed the region slightly below the ionization potential and detected electronic states with medium principal quantum number ($n \sim 5$). Predissociation properties of these levels were found to vary greatly with the symmetries of their electronic configurations.

Two infrared-ultraviolet double resonance experiments on benzene were performed. In both, vibrational state selection of the benzene molecules was accomplished using resonantly-enhanced two-photon ionization (R2PI). In the first, the overtones of C-H stretches in electronic-ground-state benzene and the benzene dimer were studied with a resolution of ~ 1 cm^{-1}. The spectra showed newly-resolved vibrational features with bandwidths less than a few cm^{-1}, undetected in room-temperature absorption experiments. A tendency toward "local mode" behavior was observed as the C-H stretching quantum number was raised from 1 to 3. The dimer's C-H stretching fundamental spectrum showed combination bands with van der Waals intermolecular vibrations, and widths of rotational bands provided evidence to support the argument that the dimer is T-shaped.

In the second experiment, hitherto unknown frequencies of C-H stretching and bending modes in benzene's first excited singlet state were determined. Also, the state mixing present in the region of the fundamental C-H stretches associated with the electronic ground state was probed. This provided evidence which confirms a recent analysis that showed that the C-H stretching admixture contains four states

instead of three, as was previously thought. A reassignment of the benzene UV spectrum is suggested, with the result that the C-H stretches of different symmetry in the excited electronic state all have their frequencies increased by ~ 20 cm^{-1} from the ground electronic state. A Fermi resonance in the excited state was also detected.

TABLE OF CONTENTS

ACKNOWLEDGMENTS

Many people deserve to be acknowledged at this time. However, some will probably be overlooked, just because I'm too tired to think of anything but finishing with this business. Those who believe they've been passed over will just have to get me to buy them a beer sometime.

First I must thank my advisor, Y. R. Shen, for helping me to learn to try hard at my research. Ron's constant quest for logic, clarity, and reasonableness have also been transmitted to me in some small measure; his approach to physics is certainly one I would make my own if I knew how. His commitment to trying to improve my writing was also above and beyond a normal effort on the part of an advisor. It certainly wasn't easy for either of us!

Thanks are also due to Gil Nathanson, who also generously sacrificed his time in order to see if this work is understandably described. We also turned out to have an important interest in common: food!

My co-advisor, Y. T. Lee, was a very positive influence on my life during my seven years in his group. His enthusiasm, and willingness to come running to the laboratory are certainly the marks of a man who loves science and is eager to share his excitement with students. Y. T. is truly "a master." Also, he was able to provide a superbly equipped laboratory for me to use for experiments which were extremely laser-intensive and expensive. For a guy like me who likes machines and gadgets, this was heaven. The sound of dueling Quanta-Ray lasers, screaming dye pumps, whirring Roots blower, tired mechanical pumps, and gale force air conditioner, is a fond memory. Both Ron and Yuan were supportive in helping me to attend conferences and to find employment.

Several people actually endured my presence in the laboratory. Matt Vernon and Jim Lisy helped me get acquainted with molecular beam research. Their spirited discussions concerning what to do next certainly did lead to rapid experimental results. Other coworkers included Jim O' Brien, John Hepburn ("Captain Collimation", my hero), Jeremy Frey, Tim Minton, Harry Tom, Bob Larkin, and Andy Kung. I have learned something different from each one of them.

Prof. Bob Byer kindly let me borrow crystals for the optical parametric oscillator (OPO) I built, and shared his voluminous knowledge on various aspects of laser practice with me. I certainly feel a kinship with, and sympathy for, students who build lasers for use on experiments. Without the help of someone like Bob, I might never have gotten anywhere with the thing.

Prof. Bob Field has been an inspiration to me, in the form of a spectroscopist who gets useful answers about questions concerning the behaviour of molecules. He has helped me to analyze some of the data in this tome.

People whose attitudes I admired, or marveled at, did much to make the laboratory life something worth getting used to. Chenson Chen, Harry Tom, Scott Anderson, Matt Vernon, Doug Krajnovich, Tom Turner, John Hepburn, and Rob Continetti were great morale boosters.

Many of the support staff at LBL also made it a fun place to work. It was always enjoyable to run across a maintenance machinist at 4 a.m. and chat for a while, or to get a cup of bad coffee and hear a good story at Fred and Ed's. Charlie Taylor and Tony Moscarelli were expert and generous teachers of machine shop practice. The library staff in Bldg. 50 was very helpful to me, and always kept a sense of humor about

them. Likewise, Camille Wanat of the Physics Library has gone out of her way to show me how to find things quickly.

I have often been thankful for the administrative help and good advice of Ann Weightman and Rita Jones, each in her own way a tenacious ally and, at times, a worthy opponent. Life in the Shen and Lee groups would be difficult without the presence of these talented women.

Favorite friends and brewing partners entered my life in the forms of Veit Elser and Jim Austin. Their sense of fun, desire to explore, and balanced perspective were often a delight to me in the first few years of graduate school. Others who shared my nonscientific life in an important way were Sean O' Gara, Disa Gambera, Persis Drell, Jim Welch, Larry Golding, Gene Commins, and Erwin Hahn. Still more people who have helped me get through life are Mark and Bonnie Tincknell, Georg Raffelt, Mitchio Okumura, Rick Brudzynski, Xiang-Dong Zhu, and Anne-Marie Schmoltner.

A few have cared very deeply about me during my stay in Berkeley. Rita Jones caused me to see myself in a new way, and helped me to learn to be more aware of the feelings of others. Clearly, there is plenty of room for my improvement in that regard! My mother and my brother have also been very supportive during difficult times. Whatever else I may have accomplished in this time, learning about people was by far the most important.

I. INTRODUCTION

The title of this thesis is "Nonlinear Spectroscopic Studies of Highly Excited States of Molecules in Supersonic Beams." Supersonic beams were used to prepare rotationally cold samples of molecules and clusters of molecules in a collision-free environment. Such an environment is appropriate for the study of isolated molecule spectroscopy and dynamics. The kinds of beams we used were not thick enough to absorb a noticeable amount of light of any color, so ordinary absorption spectroscopy was out of the question. We used various nonlinear spectroscopic techniques in order to get absorption spectra of the species under study. All of the experiments described here involved changing the populations of molecules in the ground and excited states, so they could be broadly classified as saturation spectroscopy experiments. Within that category, the double resonance technique was used to study some excited states selectively. Other, more mundane nonlinear optical methods were used in the course of doing the experiments. These included multiphoton ionization, tunable infrared generation with an optical parametric oscillator, and tunable extreme ultraviolet generation by frequency tripling.

The use of the sophisticated laser and molecular beam techniques was simply a means of achieving the goal of understanding more about the highly-excited states. These states are interesting because when molecules are excited to them, something happens. And the "thing" that happens is usually not well understood. There is usually some sort of decay, exclusive of fluorescence. Examples of decays relevant to this thesis include intramolecular vibrational relaxation, vibrational

predissociation, electronic predissociation, and autoionization. Each of these will be described in turn.

It is very exciting to use spectroscopy to study molecular dynamics of highly excited states. It is slightly less exciting, but exceedingly important, to detect and identify the highly excited states beforehand, or at least simultaneously. Who would dare to discuss the dynamics of a system without first describing its eigenstates, at least in a crude way? An embarrassingly large part of this thesis is devoted to hard-core spectroscopy, a fact which has caused the writer and his advisors considerable frustration. Consequently, people who hate spectroscopy will have difficulty understanding many of the details, but it is hoped that they do not completely smother the bit of useful information that can lead to increased insight concerning the physics of molecules.

A longstanding problem in experiments on van der Waals molecules is to explain the dynamics of vibrational predissociation. In this process, as it is customarily described, a cluster absorbs a photon whose energy is larger than its binding energy. The cluster eventually falls apart. Most experiments and theories are aimed at discovering how the intramolecular vibrational modes of a cluster's constituents are coupled to the intermolecular modes of the cluster itself. Large-amplitude motion in these latter modes is a harbinger of dissociation. The zeroth-order description treats the intramolecular vibrations as "local modes" which are only weakly affected by the van der Waals bonds. An excitation of a high-frequency mode (C-H or O-H stretch) eventually decays into the low-frequency intermolecular modes. Theories of vibrational predissociation have something in common with

those of intramolecular vibration relaxation (IVR)!

Spectroscopically, the effects of predissociation show up as homogeneous linewidths on the absorptions: the decay may occur on timescales of μsec or psec, which is much shorter than the radiative lifetimes of msec for fundamental vibrational modes. Also, the vibrational spectra of clusters are slightly different from those of their monomer building blocks. The monomer's fundamentals are shifted slightly by the van der Waals interaction, and combination bands of the fundamentals with van der Waals (intermolecular) modes are observed. The rotational structure of a vibrational band is different too, because the cluster has a different shape and different moments of inertia. In general, the rotational structure of cluster vibrational transitions is quite difficult to resolve. Failure to resolve rotational structure has led some people to conclude that they observe homogeneously-broadened bands due to states with psec lifetimes. The $(C_2H_4)_2$ system is a famous example in which groups have reported both psec[1] and nsec[2] lifetimes; this controversy lives on. Pump-probe experiments have reliably determined the vibrational predissociation lifetimes of $(NO)_2$ clusters to be several tens of psec.[3] An example of a highly-resolved spectrum of a van der Waals molecule is that of $(HF)_2$,[4] whose lines are much more widely spaced than those of most clusters. Assignments of the rotational lines led to a determination of the structure of the dimer, and to an understanding of the tunneling motion of its two protons.

Some of our own work has been on water clusters, namely, $(H_2O)_2$ and $(H_2O)_{19}$. The hydrogen bonds in water clusters are far stronger than van der Waals bonds; they distort the monomers and change their

vibrational frequencies drastically. Research on water clusters is largely aimed at determining their structures, and understanding the hydrogen bonds. We did not measure predissociation rates or determine structures of clusters. Our spectra tell mostly about the O-H stretching modes present in the clusters, and are useful for comparisons with spectra of monomers and condensed phases. Chapter II includes accounts of the H_2O cluster experiments I did.

The benzene dimer, $(C_6H_6)_2$, is an example of a "genuine" (not hydrogen bonded) van der Waals molecule, whose IR spectrum in the C-H stretching region is not very different from the monomer's. Since the structure and intermolecular potential of this dimer have been calculated, experimental work on it is especially interesting. During an experiment on benzene's local modes (Chapter III), I obtained the C-H stretching spectrum of $(C_6H_6)_2$. The spectrum yielded a van der Waals mode frequency of ~ 30 cm^{-1}, and gave evidence that the dimer is T-shaped.

A problem which is philosophically related to vibrational relaxation in clusters is that of local modes in large molecules. In particular, overtones of high-frequency vibrations appear to be localized in two ways: first, it often appears that only a single bond (e.g. C-H or O-H) is vibrating, so the vibration is localized in space. Second, the vibrational bandwidth appears to be limited to less than ~ 100 cm^{-1}, regardless of the energy of the vibration. The vibration is localized in frequency, as opposed to a phonon band in a cyrstal, in which the absorption spectrum is rather diffuse. The burning question when discussing the local mode features in an absorption spectrum is whether the bands are homogeneously or

inhomogeneously broadened. After all, observed linewidths of ~ 100 cm^{-1} are much greater than the known homogeneous linewidth (~ 10^{-8} cm^{-1}) of a single rovibrational transition in a fundamental vibrational band. The benzene molecule has been a favorite molecule for local mode studies of C-H "oscillators".[5] My experiment, described in Chapter III, describes results on its C-H stretching v= 1, 2, and 3 levels. The temptation to study these vibrations in the benzene dimer as well as the monomer was too great to resist. My results on the monomer and dimer support the contention that the "local" description of C-H stretching vibrations becomes increasingly good as the quantum number v is raised.

The experiment on benzene's local modes was of the double resonance variety, which meant that I had to understand the IR and UV spectra in some detail. While learning about the UV spectrum, it became clear that with the same setup, it was possible to study the C-H stretches in benzene's lowest excited singlet state. This prospect seemed very attractive because there is current interest in modeling the excited-state force fields of large molecules, especially benzene.[6] Benzene's high symmetry and rather well-understood spectroscopy make it a prime candidate for a complete calculation of its vibrational potential. But a thorough list of experimental vibrational frequencies is needed as input data. Heretofore unknown frequencies in the excited state have included some C-H stretching and bending frequencies. Our ability to create ground-state populations in these modes gave access, via "vertical" electronic transitions, to their excited- state homologs. Information derived from our study, described in Chapter IV, can be directly applied to the determination of the excited-state force field:

C-H stretching and bending frequencies were determined. We have provided a new picture of the excited-state vibrations. This venture into hard-core spectroscopy was not to be the last.

Although studies of vibrationally-excited states are interesting, work on the electronically-excited states is also very challenging. One is forced to think about the electrostatic interactions that hold molecules together in the first place, and about the couplings between different electronic states. Such couplings can be caused by vibrational and rotational motion, or can appear to be present just because a zeroth-order description of a wave function is insufficienlty sophisticated. The study of perturbations in molecules is at the same time very involved and very incomplete.[7]

Electronic perturbations are manifested in a couple of striking dynamical processes. The first, predissociation, can occur when a molecule is excited to a state whose energy exceeds the dissociation limit in the lowest electornic state. The molecule then fragments into neutral particles. The second, autoionization, can occur when the excited state is above the ionization potential. In this process, an electron is ejected. Of course, there are more exotic decay channels which occur at different thresholds. Dissociative ionization ($AB^* \rightarrow A + B^+ + e^-$) and ion-pair production ($AB^* \rightarrow A^+ + B^-$) are examples.

Observation of these various processes can tell a lot about the quantum mechanics of molecules by revealing the magnitudes of the couplings between different states. Spectroscopy is well suited to poking around in the excited-state manifold, and detecting the perturbations. Shapes and widths and intensities of spectral lines can be analyzed to give a wealth of information about lifetimes, branching

ratios, molecular geometries....

Since molecules are so complicated, only the smallest ones are really understood in detail. In particular, good theories[8] exist to describe the dynamics of the excited states of H_2. There are also many calculations[9] of its excited-state energy levels. This theoretical work can always be tested spectroscopically, but sometimes the spectroscopy is difficult: New technology many be required, or sophisticated techniques may be needed to simplify the generally complex spectra. Our simultaneous use of XUV and double-resonance methods is a good example of spectroscopic novelty.

We developed a continuously tunable XUV source, described in Chapter V. It used the technique of frequency tripling in a pulsed free jet of gas, and was conveniently employed for generating light in the 900-1000 A range. XUV light is good for creating highly-excited electronic states. "Things" that happen in these states include the aforementioned autoionization and predissociation. The dynamics of electronically- excited small molecules have always been interesting, especially because they can often be calculated.

We did not really have that in mind when the decision was made to test the XUV source by obtaining high-resolution spectra of H_2O^+ and D_2O^+. In order to make good use of an experimental spectrum, and not look stupid, it is necessary to assign the spectrum first so as to know exactly what states one is talking about. Then one can explain why the various states have their respective properties. The high-quality spectra we obtained have largely been assigned; the task of assignment included consideration of asymmetric rotor energy levels and selection rules, nuclear spin statistics, linear ↔ bent transitions,

Renner-Teller coupling, and ℓ uncoupling. The autoionizing states of water were displayed as never before, and overall lifetimes of the states, including predissociation, appear to be between 1 and ~ 0.1 psec. This "stress test" of the XUV source and its operator(s) is described in Chapter VI.

Experiments on the highly-excited electronic states of small molecules also included studies of H_2. By using two lasers, we did double-resonance experiments in two ranges of final energy. The first, at ~ 140000 cm^{-1}, was nominally a study of the ion-pair ($H^+ + H^-$) decay channel. What we actually ended up being concerned with was the newly-detected Rydberg states associated with high vibrational levels ($v^+ \sim 10$) of the H_2^+ core. The Rydberg states of H_2 have historically been important as a means of understanding general properties of molecular Rydberg states, including predissociation, autoionization, ℓ uncoupling, and perturbations. We made a bit of progress by confirming the positions of some H_2^+ vibrational levels, and detecting a peculiarity in the shapes of resonance lines due to Rydberg series. The majority of the spectral features we revealed remain uninterpreted.

The second (short) experiment on H_2 was in the ~ 122000 cm^{-1} region, just below the ionization potential. We detected a few states with medium principal quantum number; the important decay phenomena included radiation and predissociation. It was revealed that the predissociation rate varies by five orders of magnitude, depending on the symmetry of the electronic wavefunction. This result is of real value because the mechanism of predissociation can be rather reliably guessed. Also, predissociated states, known to exist, have not been well studied. This experiment serves mainly to demonstrate the

technique. These experiments on H_2 are discussed in Chapter VII.

References

1. G. Fischer, R. E. Miller, P. F. Vohralik, and R. O. Watts, J. Chem. Phys. 83, 1471 (1985).

2. K. G. H. Baldwin and R. O. Watts, Chem. Phys. Lett. 129, 237 (1986).

3. M. P. Casassa, A. M. Woodward, J. C. Stephenson, and D. S. King, J. Chem. Phys. 85, 6235 (1986).

4. A. S. Pine and W. J. Lafferty, J. Chem. Phys. 78, 2154 (1983).

5. K. V. Reddy, D. F. Heller, and M. J. Berry, J. Chem. Phys. 76, 2814 (1982).

6. K. Krogh-Jespersen, R. P. Rava, and L. Goodman, J. Phys. Chem. 88, 5503 (1984).

7. H. Lefebvre-Brion and R. W. Field, Perturbations in the Spectra of Diatomic Molecules (Academic Press, New York, 1986).

8. M. J. Seaton, Rep. Prog. Phys. 46, 167 (1983).

9. L. Wolniewicz and K. Dressler, J. Chem. Phys. 82, 3292 (1985).

II. A.

Volume 106, number 5 CHEMICAL PHYSICS LETTERS 4 May 1984

INFRARED PREDISSOCIATION SPECTRA OF WATER DIMER IN A SUPERSONIC MOLECULAR BEAM

Ralph H. PAGE *, Jeremy G. FREY **, Y.-R. SHEN * and Y.T. LEE ‡
Materials and Molecular Research Division, Lawrence Berkeley Laboratory, University of California, Berkeley, California 94720 USA

Received 14 March 1984

The infrared absorption spectrum of the hydrogen-bonded water dimer, $(H_2O)_2$, formed in a supersonic expansion, was recorded in the region of the OH stretch by monitoring the predissociation resulting from the absorption of the radiation. The conditions were such that there was minimal contribution to the observed spectrum from higher water polymers. The observed features show considerable structure, with widths that appear to be limited by the optical resolution of 2 cm^{-1}. A combination band of the OH stretch with the water bend and an overtone of the bending vibration were also observed.

1. Introduction

The previous investigations of the infrared vibrational spectra of water clusters in the gas phase [1] had shown that the dimer spectrum differs markedly from that of the higher polymers, and was also distinctively different from the absorptions in bulk liquid water. However, the beam conditions and laser resolution were such that few conclusions could be drawn about the possibilities of obtaining high-resolution vibrational spectra of the dimer.

Accurate information about the ground state of $(H_2O)_2$ is available from the molecular beam electric resonance (MBER) work of Dyke et al. [2]. The microwave and radiofrequency transitions observed show that the ground-state structure is trans-linear, with a linear hydrogen bond, in contrast to the higher polymers which have a cyclic structure. The B value of the almost symmetric top could be accurately determined [$(B + C)/2$ = 6160.7 MHz], but the A constant is less certain (approximately 7 cm^{-1}). From the centrifugal distortion constants Dyke et al. estimated that the hydrogen stretching vibration of one water molecule against the other occurs at about 140 cm^{-1}.

A better knowledge of the vibrational spectrum of the dimer would give much needed information on the properties of the hydrogen bond, and the influence of hydrogen bonding on the donor and acceptor units. While some information is available from matrix studies, the matrix certainly precludes the possibility of obtaining much structural information because the rotational spectrum is supressed. The aim of this work was to investigate the water dimer spectrum under conditions in which there was minimal contamination of the spectrum by higher polymers and at sufficient resolution to indicate if the rotational transitions could be observed, or if in fact predissociation linewidth would be larger than the rotational spacing. The observation of the $(HF)_2$ spectrum at high resolution in a gas cell [3] indicated that the former possibility was very likely.

2. Experimental

The water dimers were formed in a supersonic expansion through a nozzle of 50 μm diameter, of helium at pressures from 1 to 4 atm, which had bubbled

* Also associated with the Department of Physics, University of California, Berkeley, California 94720, USA.
** NATO/SERC Post-Doctoral Fellow.
‡ Also associated with the Department of Chemistry, University of California Berkeley, California 94720, USA.

0 009-2614/84/$ 03.00

through a water reservoir held at a temperature of 15, 25 or 35°C. The nozzle was held at a temperature of 90°C to prevent condensation of the water vapor. After two stages of differential pumping and a flight path of about 0.15 m, the molecular beam was ionized by an electron bombardment ionizer and the resulting ions mass analyzed with a quadrupole mass spectrometer. The $(H_2O)_2$ fragmented in the ionizer to give predominantly the relatively stable H_3O^+ ion and so the dimer is detected at mass 19. The beam conditions were such that the amount of trimer present in the beam was kept very low. A measure of the trimer content of the molecular beam is given by the ratio of the mass 19 signal to that at mass 37 (this is only approximate because of the uncertainty in the fragmentation patterns), and this indicates that the dimer to trimer ratio was better than 20 : 1.

1 mJ, 10 ns pulses of tunable infrared radiation at about 2 cm^{-1} resolution and 10 Hz repetition rate were obtained from an optical parametric oscillator (OPO) of the Byer design [4] pumped by a Quanta Ray Nd : YAG laser in the far field. Damage to the optical components prevented the oscillator from running at the higher resolution that would be obtained by the use of intracavity line-narrowing elements. The wavelength calibration was performed using a monochromator.

The infrared radiation overlapped the molecular beam in an anti-parallel direction, and was brought to a focus near the nozzle. This is not an ideal arrangement because it leads to non-uniform power density along the molecular beam, however, the optical properties of the OPO beam were such that a narrow parallel beam was almost impossible to produce. Over most of the interaction region the laser beam had a slightly larger diameter than the molecular beam, which ensured that all of the molecular beam that was sampled by the ionizer could have interacted with the radiation.

The energy contained in an OH stretch is considerably greater than that required to break the hydrogen bond, and so upon absorption of such an energetic infrared photon, the dimer molecules predissociate, consequently reducing the number of water dimers reaching the detector. The experiment is performed by scanning the infrared radiation while looking for a depletion or "hole burning" in the mass 19 signal. The recorded signal is accumulated for between 2000 and 4000 laser shots at each wavelength. The power of each laser shot was recorded and used to normalize the depletion signal to the laser power. Since the spectra of interest lie in regions of very high atmospheric water absorption, the whole optical path from the OPO to the window into the molecular beam vacuum system had to be continuously flushed with dry nitrogen.

Spectra were recorded from 3500 to 3900 cm^{-1} and around 3200 and 5300 cm^{-1}. No spectra could be recorded between 3450 and 3500 cm^{-1} because the OH impurity in the $LiNbO_3$ crystal of the OPO caused the output power to be anomalously low in this region.

The power dependence of the major peaks was checked and found to be linear within the accuracy of the measurements.

Any problems that the focusing of the radiation onto the nozzle might have produced could be investigated since the dimer signal arriving at the nozzle was "time resolved", using a multi-channel scaler with a 1 μs channel width. The laser pulse is only about 10 ns long, which means that the arrival time at the detector of the molecules that interact with the radiation translates directly into the position of the dimer molecules along the molecular beam, whose velocity is about 1 mm/s, when the molecule absorbed the radiation.

No such "nozzle" effect was observed in the idler range, but in the more intense signal range an apparent decrease in the dimer population at the nozzle could be seen. This did not affect the molecules downstream, which had already left the nozzle before the laser pulse arrived. It does indicate that in the high-density region just in front of the nozzle the signal beam is strongly absorbed over a wide frequency range.

3. Results

The water dimer absorptions in the OH stretching region that we observed are shown in fig. 1. An assignment that is in reasonable agreement with the matrix isolation spectra [5] is possible if the shoulder on the low-frequency side of the 3730 cm^{-1} absorption is taken to be the υ_3 of the donor. The main peaks in the spectrum are respectively assigned as υ_1(donor) at 3545 cm^{-1}, υ_1(acceptor) at 3600 cm^{-1}, υ_3(acceptor) at 3730 cm^{-1} and υ_3(donor) at 3715 cm^{-1}.

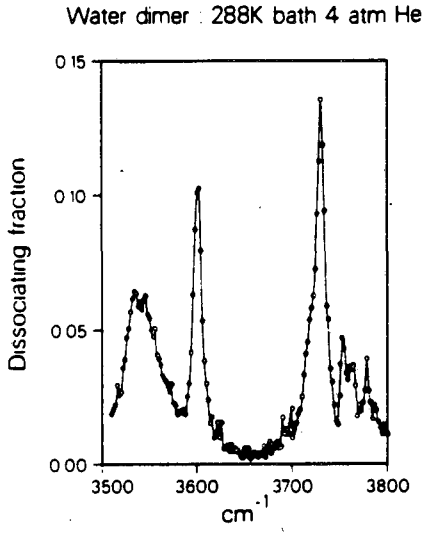

Fig. 1

and are compared to the matrix values in table 1. Some of the vibrations recorded in this work are shifted by more than 20 cm^{-1} from the matrix results.

Over the range of stagnation pressures used (from less than 1 atm to greater than 4 atm) the 3730 and 3600 cm^{-1} bands become significantly narrower with increasing pressure. This is consistent with the increased degree of cooling in the harder expansions. If large amounts of higher polymers were present in the beam, then we might have expected to see a large linewidth at higher pressure as these conditions are more favorable for the formation of the polymers. The structure on the 3550 cm^{-1} band is reproducible; however, because of the unknown, though low rotational temperature (estimated to be about 10 K), the apparent perpendicular band nature of this feature cannot be conclusively substantiated. That this molecule should show perpendicular and/or parallel bands could be expected since it is very nearly a symmetric top, with the top axis lying along the hydrogen bond and defined by two oxygen atoms.

Table 1
Stretching vibrations of $(H_2O)_2$ (cm^{-1})

		N_2 matrix [3]	This work
acceptor	υ_1	3627.2	3600
	υ_3	3715.0	3730
donor	υ_1	3550.0	3545
	υ_3	3698.8	3714

The existence of the rotational structure in the gas phase spectrum makes it difficult to compare the peak intensities with the matrix work.

The peaks to the high- and low-frequency sides of the 3730 cm^{-1} band are almost certainly combination of the υ_1 modes of the donor and acceptor molecules with the low-frequency vibrations of the hydrogen bonds. Theoretical calculations [6] and the MBER data indicate that the stronger bands at 3753, 3760 and 3778 cm^{-1} should be assigned to combinations involving the hydrogen bond stretch, the out-of-plane bending of the hydrogen bond and the in-plane bending of the hydrogen bond, respectively. If this is the case then these modes are lowered by about 10 cm^{-1} when the OH stretches in the water molecules are excited. This vibrational shift would cause the diagonal hot bands to be displaced from the fundamental and may account for the greater width of the 3550 cm^{-1} band. This band would be expected to be more profoundly influenced by the water–water stretching motion since it mainly involves the stretching of the hydrogen-bonded hydrogen.

While the assignment of the these side peaks to combination bands seems reasonable, it cannot be completely ruled out that they arrise from absorption of other complexes such as $(H_2O)_3$ or $(H_2O)_2He_n$.

Weak absorptions were observed at 3186 and 5333 cm^{-1}, which were assigned to combinations of two HOH bends (υ_2 modes) and an OH stretch with an HOH bend, respectively. Owing to signal-to-noise limitations only a single absorption could be observed in each region. Even so these data are consistent with the OH stretching frequencies being reduced upon forming the hydrogen bond while the bending vibrations are stiffened.

This work indicates that it is possible to obtain infrared spectra of the water dimer free of contamination from higher polymers. The spectrum shows a rotational envelope and it is likely that with increased resolution the rotational structure can be recorded; this would greatly enhance the feasibility of obtaining structural information on the vibrationally excited states of the water dimer.

Acknowledgement

This work was supported by the Director, Office of Energy Research, Office of Baisc Energy Sciences, Chemical Sciences Division of the US Department of Energy under Contract No. DE-AC03-76SF00098.

References

[1] M.F. Vernon, D.J. Krajnovich, H.S. Kowk, J.M. Lisy, Y.-R. Shen and Y.T. Lee, J. Chem. Phys. 77 (1982) 47.
[2] T.R. Dyke, K.M. Mack and J.S. Meunter, J. Chem. Phys. 66 (1977) 498.
[3] A.S. Pine and W.J. Laferty, J. Chem. Phys. 78 (1983) 2154.
[4] S.J. Brosnan and R.L. Byer, IEEE J. Quantum Electron. QE-15 (1979) 415.
[5] L. Fredin, B. Nelander and G. Ribbegard, J. Chem. Phys. 66 (1977) 4065;
R.M. Bentwood, A.J. Barnes and W.J. Orville-Thomas, J. Mol. Spectry. 84 (1980) 391.
[6] J.C. Owicki, L.L. Shipman and H.A. Scheraga, J. Phys. Chem. 79 (1975) 1794.

II. B. INFRARED VIBRATIONAL PREDISSOCIATION SPECTRA OF LARGE WATER CLUSTERS

I. Introduction

We are always trying to understand the behavior of water better; to do so, it is necessary to understand the forces within and between water molecules. The chemical bonds that cause the molecules to exist are largely understood, but the forces between molecules (i.e. hydrogen bonds) are still challenging us. Hydrogen bonds occur when an H atom of one molecule is strongly attracted to an O atom of another. They are too strong and too complex to be accurately modeled by simple perturbation theory or first-principles calculations. Consequently, a semi-empirical approach, guided by theory and intuition, is used in which the intermolecular potential is represented by a complicated formula with many terms and adjustable parameters.

The quality of such a potential function is judged by its ability to describe experimentally observable properties of all phases. These include, for example, the molecular electric dipole and quadrupole moments, and bulk properties such as the density, crystal structure, compressibility, specific heat, and second virial coefficient. But a potential should also describe the properties of dimers and other clusters; indeed, it makes perfect sense to try to construct an intermolecular potential by considering at first a pair of molecules. Logically, one could add the extra complexity of more molecules once the basic interaction in a dimer had been worked out.

Studies with molecular beams, currently the only medium which contains clusters completely free of perturbations from neighboring

atoms and molecules, have recently been reported.[1-4] To date the experimental results have included values for electric dipole moments of clusters,[4] the microwave spectrum and structure of the dimer,[4] and cluster infrared absorption spectra.[1-3] This work has provided important data for developing and testing models of the intermolecular potential energy function. The Watts group has found the "RWK2-M" potential, [Named after Reimers, Watts and Klein (Ref. 5), and modified to treat the O-H bonds as Morse oscillators] which reproduces the monomer's properties and simultaneously fits many of the thermodynamic data of the bulk phases. By using this potential and the "quantum simulation" calculation technique, they have reproduced the O-H stretching frequencies of the water dimer almost exactly,[6] and partially accounted for the trimer spectrum. But the infrared absorption spectra of larger clusters, and of the liquid and solid phases, are not accurately predicted thus far.[7-9] This is a symptom of hydrogen bonding, a rather strong intermolecular force: the molecules affected by it experience significant changes in shape, charge distribution, and vibrational frequencies. Hydrogen-bonded molecules do not retain the monomeric properties which were used in the creation of a pair potential function. Thus the pair potential cannot exactly describe clusters larger than the dimer.

It is clearly useful to obtain cluster IR spectra as a function of cluster size. This can lead to a step-by-step improvement in the intermolecular potential function. Dimer O-H stretching spectra have been reported.[2,3] Also, spectra have been obtained with samples whose polymer size distribution includes a range of n-mers.[1-3] In this communication, we report on the differences between our spectra of

medium-sized (6 - 19 subunits) water clusters and the "large-cluster" spectra of the Watts group. The two sets of experimental techniques have different biases, with respect to cluster size distribution, that lead to somewhat different spectral appearances and interpretations. The key experimental difference is the use of a mass spectrometer instead of a bolometer to detect the clusters.

II. Experimental

Lately, this group and the Watts group have reported IR absorption spectra of water clusters in the 3000-4000 cm^{-1} O-H stretching region.[1-3] To obtain the spectra, both groups observe IR-pumping-induced vibrational predissociation (VPD), in which an IR photon has enough energy to fragment a cluster: $(H_2O)_n + h\nu_{IR} \rightarrow (H_2O)_m + (H_2O)_{n-m}$. A detector which responds to the decrease in parent $(H_2O)_n$ concentration or to the increase in fragment concentration is used to monitor the intensity of VPD. Consideration of the cluster dissociation energies suggests that the most likely dissociation channel has $m = 1$: a monomer is "evaporated". Depending on a cluster's geometry, splitting it into two polymers could require the fracture of more than one ~2000 cm^{-1} hydrogen bond. At energies below ~ 4000 cm^{-1}, the infrared photons used to excite O-H stretches are not sufficiently energetic to do so. If one assumes that the VPD probability (thought to be unit in the O-H stretching range) is only weakly dependent on total photon energy, then the IR frequency (ν_{IR}) dependence of the VPD signal is the same as the $(H_2O)_n$ cluster IR absorption cross section.

VPD spectra are obtained as follows: A rare-gas/water mixture is expanded into vacuum through a nozzle and skimmed, forming a supersonic

molecular beam. The cluster size distribution in the beam depends on the nozzle stagnation pressure and fraction of water in the gas mixture. It also depends on the choice of seed gas and on the nozzle temperature and diameter. The degree of cooling achieved in the expansion increases with the number of collisions experienced by the atoms and molecules. From geometrical arguments, the "collision number" scales roughly as $p_o d$, where p_o is the pressure of gas behind the nozzle of diameter d. To form stable clusters, the cooling must be sufficient to dissipate the heat of condensation. Formation of large clusters is supposedly favored when the nozzle temperature is lowered toward the dew point of the gas mixture, when the fraction of water is increased, or when the nozzle stagnation pressure is increased with the water fraction constant.

Detection of polymers is accomplished in two ways: the Watts group has used a bolometer operating at 1.8 °K to sense the total power in the molecular beam, which condenses on its surface. For a given beam velocity, the signal depends on the mass flux and internal energies of all the beam constituents. Clusters of a particular size cannot be selectively studied without interference from larger and smaller clusters. On the other hand, this group has used an RF quadrupole mass spectrometer with electron-bombardment ionization. It gives a signal dependent on the number density of the selected cluster ion, which, due to ion fragmentation, is always smaller than, or the same size as, the parent cluster. [A technical detail of the ionization process is that an ionized water cluster tends to expel an OH radical, leaving behind a stable "solvated proton". Therefore, the $(H_2O)_n$ cluster is detected by tuning the mass spectrometer to the mass of $(H_2O)_{n-1}H^+$.] Fragmentation

can only be ignored when the largest polymer present in the sample is the one selected for detection.

Tunable infrared light illuminates the molecular beam. Absorption of a photon fragments a cluster; the fragments recoil with a non-negligible amount of kinetic energy which causes most of them to exit the beam.[1] The measurement of VPD is accomplished by noting the depletion of clusters in the molecular beam. Fragments scattered out of the beam do not contribute to the bolometer signal, nor do they give an ion signal at the original cluster mass. Monomers absorb light and remain vibrationally excited until they fluoresce, strike a surface, or are destroyed by ionization. Vibrating monomers contribute to the bolometer signal; since they deliver heat to it, they give a signal opposite in sign to the VPD signal. They do not cause a change in the cluster signal obtained with mass-spectrometric detection.

Whereas the Watts group used a Kr-ion-pumped color center laser to generate tunable IR light, we have used a pulsed, Nd:YAG laser-pumped optical parametric oscillator (OPO).[10] It covers the requisite 3000-3800 cm^{-1} range, but has a ~ 25 cm^{-1} gap at ~ 3500 cm^{-1} where its $LiNbO_3$ crystal has an absorption. With the pump laser running at 10 Hz, the average IR power available at the beam machine was 5-15 mW; the peak power, assuming ~ 5 nsec output pulses, was thus on the order of 100 KW. This would make the peak intensity about 1 MW/cm^2, since the IR beam was ~ 3 mm in diameter, being loosely focused into the molecular beam, which it overlapped collinearly. We used a Scientech calorimeter for IR power measurements and placed its detector near the point where the IR beam entered the vacuum chamber. This told us the power actually reaching the molecular beam, and prevented errors due to

atmospheric absorption, which can be important in the 2.7μ region. The new data we report here were obtained with the OPO in its low (~ 5 cm^{-1}) resolution mode. We used a monochromator for wavelength calibration.

III. Results

In this experiment we were specifically interested in looking at large clusters. Thus the mass spectrometer was tuned to detect the largest possible cluster, and managed to reach m/e = 325, corresponding to $(H_2O)_{18}H^+$. This ion comes from $(H_2O)_{19}$ and larger clusters.

The supersonic beam came from an argon/water mixture with total pressure 1 atm and H_2O at 80°C, for an H_2O fraction of 44%. We kept the 70μ-dia. nozzle at 100°C. An estimate of the cluster size distribution comes from comparing cluster ion count rates. With the sensitivity used, the monomer $(H_2O)^+$ signal overwhelmed the detector; dimer and trimer count rates exceeded 1 μHz, the tetramer $(H_2O)_3H^+$ rate was 600 kHz, hexamer $(H_2O)_5H^+$ gave 300 kHz, and the large cluster ions (17-19) had rates ~ 30 kHz. We emphasize the point that most of the water molecules in the mixture remained as monomers and small clusters.

The $(H_2O)_{19}$ absorption spectrum, obtained while detecting $(H_2O)_{18}H^+$, is shown in Fig. 1. It is actually the fractional depletion in the cluster signal normalized to the laser power at each wavelength. We observed that the cluster signal could be attenuated ~ 10% at the strongest absorptions in the spectrum. Inability to measure the fluctuating OPO power accurately was the major cause of error. Data points were excluded from the spectrum when the laser power dropped below a certain value; this accounts for the missing points at

3425 and 3500 cm^{-1}. A couple of representative error bars are shown; their heights are proportional to the cross section at each wavelength. A smooth curve has been drawn through the data points, whose spacing is 25 cm^{-1} except at the sharp ~ 3715-cm^{-1} feature, where the interval is ~ 12 1/2 cm^{-1}. The IR absorption spectra of liquid water at ~ 40°C [11] and polycrystalline ice Ih at 150°K [12] are plotted on the same axes. The liquid spectrum's amplitude has been adjusted to approximate that of the $(H_2O)_{19}$ spectrum around 3500 cm^{-1}.

For comparison, the spectrum of the $(H_2O)_6$ cluster, also obtained by this group,[1] is shown in Fig. 2. The supersonic molecular beam conditions used to obtain this spectrum were adjusted to minimize contamination from $(H_2O)_7$ and larger clusters. A spectrum obtained by the Watts group,[3] in which a water-rich gas mixture and high pressure were used, supposedly to favor production of large clusters, is shown in Fig. 3. Since a bolometer was used for the detector, this spectrum contains contributions from clusters of many different sizes. Table I summarizes the beam conditions used to obtain each spectrum.

There are obvious similarities between the three cluster spectra (Figs. 1 - 3). First, there is a broad hump, centered around 3400-3500 cm^{-1}. Second, there is a narrow peak at ~ 3715 cm^{-1}, whose amplitude is about half that of the hump. There are some clear differences too. The sharp dips in Fig. 3 could come from the detection of vibrationally excited monomers, whose O-H stretching bands are near 3657 and 3756 cm^{-1}. Also, the hump in Fig. 3 has much less intensity in the low-frequency (~3200 cm^{-1}) region than the $(H_2O)_6$ and $(H_2O)_{19}$ spectra (Figs. 1,2) show.

IV. Discussion

To explain the features of the cluster spectra, we use the "local mode" description of the O-H stretching vibrations of the water molecule. This model treats the O-H stretches as two weakly coupled, largely independent anharmonic oscillators, and reproduces the 3657 and 3756 cm^{-1} vibrational frequencies of the monomer.[13] The sharp 3715-cm^{-1} band in the cluster spectra is due to the "free" O-H bonds, in which the H atoms are not very near O atoms of other molecules and are not hydrogen bonded. This feature occurs is absent in the liquid and ice spectra; it is believed that there are few free O-H bonds in macroscopic samples of the condensed phases.

Considering the O-H stretch of the H atoms which are not "free" (i.e. <u>are</u> hydrogen bonded) we find a band with a large (300 cm^{-1} or more) red shift from the monomer frequency. The ~ 400 cm^{-1} breadth of this band is supposed to be caused by varying degrees of perturbation from H-bonding, resulting in a range of O-H stretching frequencies. This would occur when n-mers were formed in different stable configurations.[1,8,14] In the case of the dimer, whose structure is accurately known, this feature is sharper and is modeled theoretically, with the use of the RWK2-M potential.[8] However, current calculations with this potential do not reproduce spectra of polymers larger than the trimer, nor of the condensed phases. Since a detailed vibrational analysis of these broad humps is not possible, we proceed to ask simple questions about the clusters: Are they like liquids? Are they like solids? Figure 1 tells us that (a) the liquid spectrum peaks at ~ 3400 cm^{-1}, with half-intensity points around 3150 and 3600 cm^{-1}, and (b) the solid spectrum peaks near 3200 cm^{-1}, with a FWHM ~ 150 cm^{-1}. It is

also known[1,3] that the water dimer's H-bonded O-H stretch band occurs at ~ 3500 cm^{-1}, and is less than 100 cm^{-1} wide. Figures 1 and 2, on the other hand, show the qualitatively different behavior of the $(H_2O)_6$ and $(H_2O)_{19}$ absorptions: roughly uniform intensity between 3200 and 3500 cm^{-1}, with the half-maximum points at 3150 and 3600 cm^{-1}. Although this is different from the condensed-phase spectra, the enhanced absorption around 3200 cm^{-1} compared with the liquid shows that an "ice-like" aspect is present. Evidently the clusters of size $n \geq 6$ are large enough to force some water molecules into local environments which resemble that of ice. On the other hand, they retain some of the structural randomness which is characteristic of liquids and causes many different environments to exist, broadening the absorption spectra. Unfortunately, the temperatures and structures of the clusters are not known. It seems plausible that they are cold and extensively H-bonded, having been supersonically cooled. They could then be considered "frozen" in the inner regions, but with an outer layer of molecules with substantially more freedom (witness the "free O-H" feature at 3715 cm^{-1}). The surface-to-volume ratio, in terms of numbers of monomer subunits, is not very different from 1, and there are many dangling O-H bonds. A study of considerably larger clusters (of size several hundred) should show more definitive tendencies toward liquid or solid spectral features.

The Watts spectrum (Fig. 3) has a hump suggestive of the liquid absorption; it peaks at ~ 3500 cm^{-1} and falls by 1/2 at ~ 3300 and 3600 cm^{-1}. It does not, however, match the liquid spectrum because the falloff at low frequency is too rapid. This behavior is opposite that of Figs. 1 and 2. The spectrum must be dominated by clusters which are

too small to reproduce the liquid absorption spectrum.

With that in mind, we make the following comparison. Figures 1 and 2 show spectra in which a fraction of the clusters was cold enough to "freeze". For example, the medium-sized polymers could form cyclic, rigid structures in their lowest-energy states, but would have looser, more open structures at higher temperatures. Figure 3 is a spectrum of warmer and/or smaller clusters, which are not rigid. Several facts support this view. First, it is difficult to create a molecular beam sample in which large clusters predominate. Our mass-spectrometric assessment of the cluster size distribution shows a rapid "tailing off" with increasing size around n ~ 2-6. Second, absorption features which have been assigned to the dimer[1,3] and trimer[3] coincide closely in frequency with the envelope of Fig. 3. Third, it has been amply demonstrated[11,15] that as the temperature of a liquid sample is raised, its O-H stretching spectrum shows a shift in the intensity distribution: the 3500 cm^{-1} peak gains at the expense of the 3200 cm^{-1} feature. Figure 3 shows this tendency; this type of spectrum would be expected from a warm sample.

V. Conclusion

Differences in IR absorption spectra, the signatures of structure and bonding in a system, are crucial in formulating and testing theories of intermolecular interactions. An important consideration in the analysis of cluster IR spectra is an estimate of the cluster temperatures and size distribution of the sample. We have shown how the use of mass spectrometry in the study of hydrogen-bonded clusters can give information complementary to that obtained without cluster

size selection. The elimination of contributions from small clusters showed that H_2O clusters of size $n \geq 6$ can act as though they are partly "frozen". The realistic simulation of a spectrum should involve a sum over cluster states with different sizes, internal energies, and geometries, and is therefore extremely challenging. Size selection with mass spectrometry can reduce the difficulty somewhat.

Improvements in the technology of cluster research are clearly to be desired. A gentler form of ionization than electron-impact would reduce fragmentation and would allow selective detection of clusters of a particular size. Furthermore, some reliable means of determining the temperature of the clusters would improve the chance of interpreting the spectra in an unambiguous way. We hope that methods will be developed which will give high-resolution spectra of clusters with better-defined sizes, structures, and temperatures. This will aid greatly in the ultimate determination of the interactions between water molecules.

References

1. M. F. Vernon, D. J. Krajnovich, H. S. Kwok, J. M. Lisy, Y. R. Shen, and Y. T. Lee, J. Chem. Phys. 77, 47 (1982).

2. R. H. Page, J. G. Frey, Y. R. Shen, and Y. T. Lee, Chem. Phys. Lett. 106, 373 (1984).

3. D. F. Coker, R. E. Miller, and R. O. Watts, J. Chem. Phys. 82, 3554 (1985).

4. T. Dyke, K. Mack, and J. S. Muenter, J. Chem. Phys. 66, 498 (1977).

5. J. R. Reimers, R. O. Watts, and M. L. Klein, Chem. Phys. 64, 95 (1982).

6. D. F. Coker and R. O. Watts, preprint.

7. D. F. Coker, J. R. Reimers, and R. O. Watts, Aust. J. Phys. 35, 623 (1982).

8. J. R. Reimers and R. O. Watts, Chem. Phys. 85, 83 (1984).

9. J. R. Reimers and R. O. Watts, Chem. Phys. 91, 201 (1984).

10. S. J. Brosnan and R. L. Byer, IEEE J. Quantum Electron. 15, 415 (1979).

11. G. Walrafen, J. Chem. Phys. 47, 114 (1967).

12. M. S. Bergren, D. Schuh, M. G. Sceats, and S. A. Rice, J. Chem. Phys. 69, 3477 (1978).

13. J. R. Reimers and R. O. Watts, Mol. Phys. 52, 357 (1984).

14. K. S. Kim, M. Dupuis, G. C. Lie, and E. Clementi, Chem. Phys. Lett. 131, 451 (1986).

15. T. C. Sivakumar, S. A. Rice, and M. G. Sceats, J. Chem. Phys. 69, 3468 (1978).

Table I. Beam conditions in various experiments.

Figure	Temperature(°C)		seed	total pressure	%	nozzle
	H_2O reservoir	nozzle	gas	(Torr)	H_2O	diam.(μ)
1	80	100	Ar	810	44	70
2	84	125	--	417	100	180
3	160	163	He	8770	52	35

Figure Captions

Fig. 1 O-H stretching region IR VPD spectrum with mass spectrometer tuned to monitor $(H_2O)_{18}H^+$ ions. See Table I for beam conditions. On the same axes are plotted the absorption spectra of H_2O liquid at 40°C [11] and ice Ih at 150°K.[12]

Fig. 2 IR VPD spectrum of $(H_2O)_6$, obtained by Vernon et al.[1] Molecular beam conditions were adjusted for minimum contamination from larger clusters, and mass-spectrometric detection was used. See Table I for beam conditions.

Fig. 3 O-H stretching region IR VPD spectrum obtained by the Watts group with bolometric detection of all beam constituents. Reproduced from Ref. 3 with permission. See Table I for beam conditions.

This page for number sequence only. (Boy is this fun!)

IR absorption spectra of H_2O in solid, liquid, and cluster form

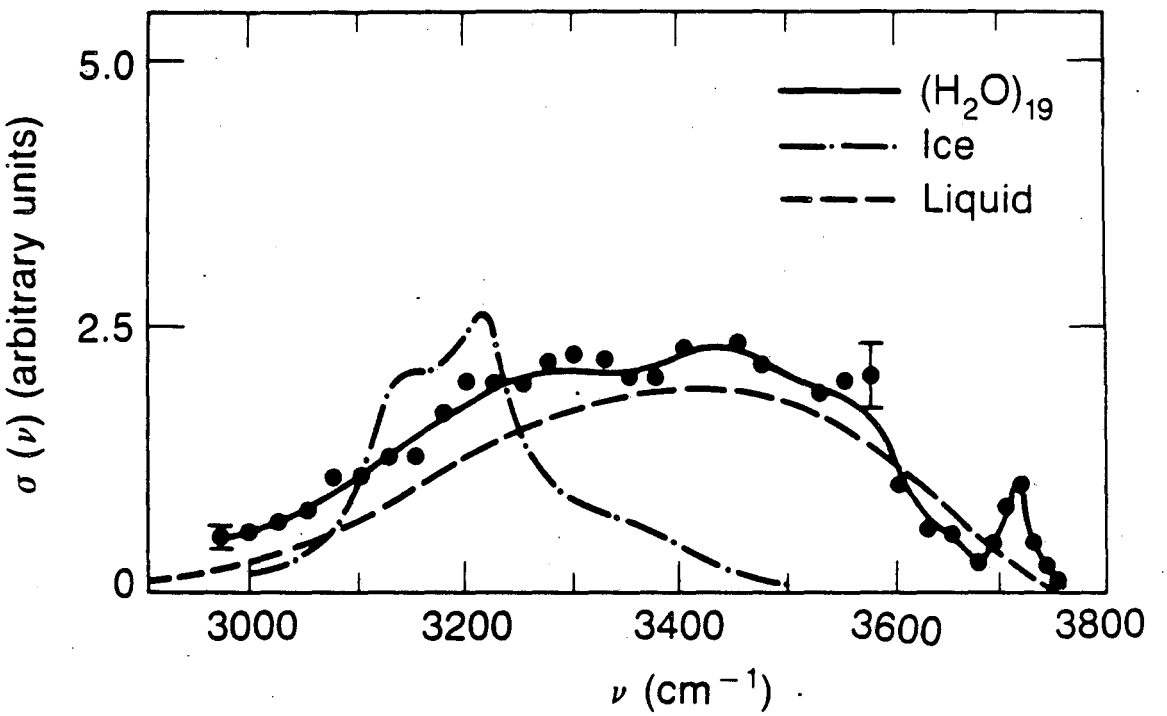

XBL 872-6162

Figure 1.

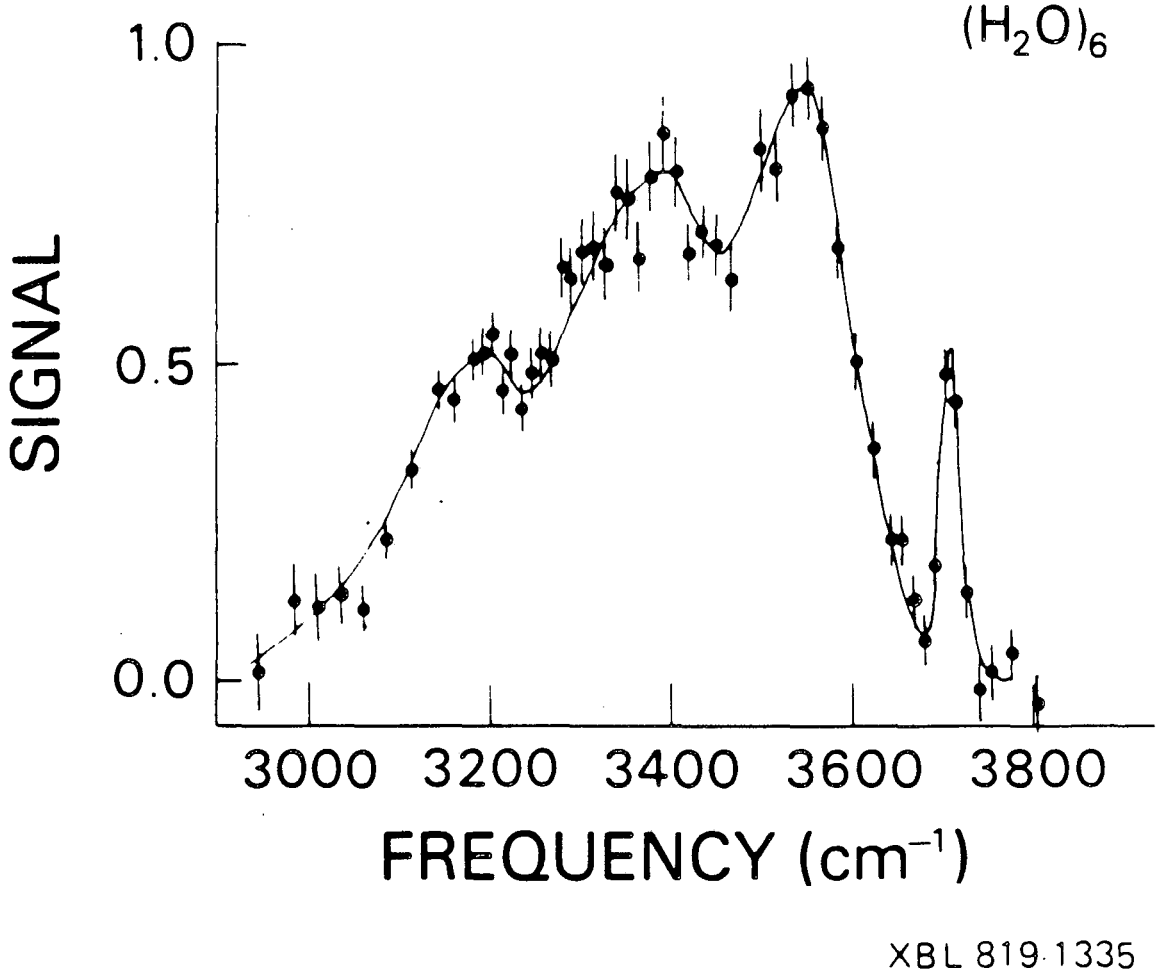
(H2O)6
1.0
0.5
0.0
SIGNAL
3000
3200
3400
3600
3800
FREQUENCY (cm-1)
XBL 819-1335

Figure 2.

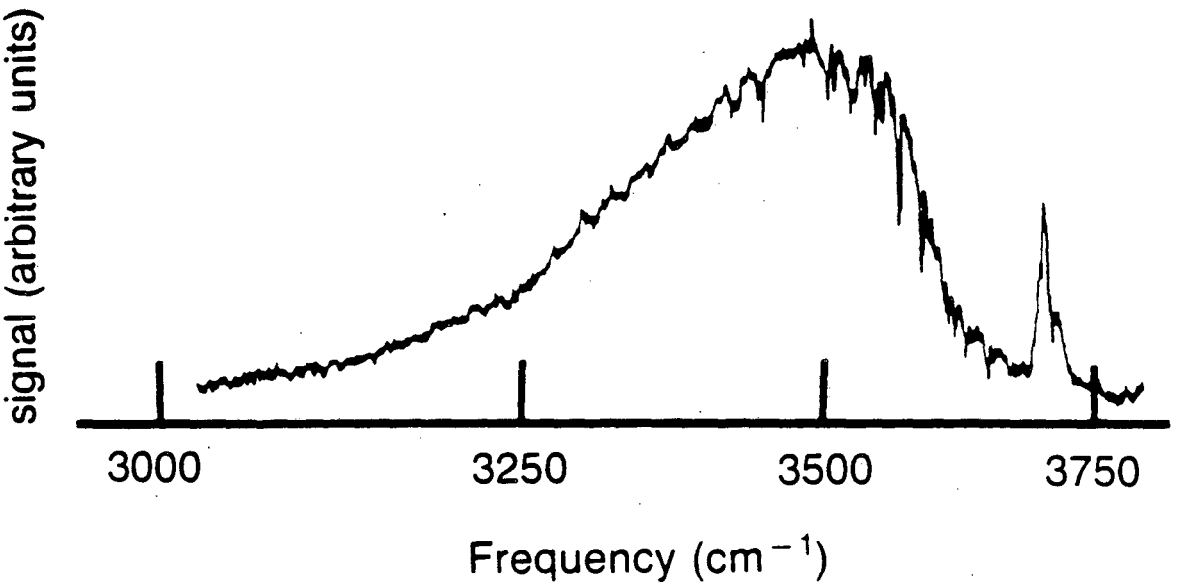

XBL 872-6158A

Figure 3.

III. LOCAL MODES OF BENZENE AND BENZENE DIMER, STUDIED BY INFRARED-ULTRAVIOLET DOUBLE RESONANCE IN A SUPERSONIC BEAM

I. INTRODUCTION

The familiar normal mode model has long been used to describe the vibrations of polyatomic molecules.[1,2] As a zeroth-order description, it works well as long as the anharmonic interactions between vibrational states are weak compared with the spacings between their energy levels. A general vibrational state can then be expressed as a superposition of normal-mode vibrations. But as the total vibrational energy is raised, the number of states, or ways it can be partitioned among the vibrational degrees of freedom grows rapidly. The states may even become so closely spaced that they overlap and form a "quasicontinuum." Nearly-degenerate zeroth-order states become strongly mixed by the anharmonic interactions, so that the normal mode description is inappropriate. In general, each vibrational state is then a complex admixture of many zeroth-order states. The vibrational motion is quite complicated and energy is distributed throughout the molecule.

Local ("bond") modes provide a counterintuitive and fascinating contrast to this behavior. They are vibrational modes with long (hundreds of vibrational periods) lifetimes in which the motion (and energy) are more or less confined to a single bond. They can exist even when they are embedded in a dense manifold of other vibrational modes, sometimes referred to as a "bath."

By studying these "simple" local modes we hope to understand the

vibrational behavior of molecules better. We want to know under what conditions local modes can exist, and what the details of their motions are. An important aspect of this problem is to understand the couplings between the local and other vibrational modes. These couplings are responsible for the structured spectra and decays of local mode vibrations. It is interesting to see how the effects of these perturbations change as the total energy and density of states vary.

A. Local mode model

The local mode description of vibrations was in use by 1936 [3] in order to explain the overtone absorption spectra of polyatomic molecules. Specifically, the study of local modes[4-7] has concentrated on overtones of stretching vibrations of O-H and C-H bonds. Their high fundamental stretching frequencies (above 3000 cm^{-1}) cause them to be far out of resonance with fundamentals involving more massive parts of a molecule, so that local behavior can stand out. In a molecule with identical "oscillators" (O-H or C-H bonds), not all overtones of their stretches are purely local mode vibrations, which implies that in a local mode, <u>all quanta are in a single bond</u>. With only one bond at a time in motion, the pure local mode spectrum of a polyatomic molecule with identical oscillators mimics that of a diatomic molecule. For each mode, the energy levels in the frequently-used Morse potential[8] are

(1) $$E(v_i) = \omega(v_i + 1/2) - x(v_i + 1/2)^2.$$

v_i is the number of stretching quanta in the i^{th} mode, ω is the frequency (~3150 cm^{-1} for a C-H bond in benzene), and x is the anharmonicity (~60 cm^{-1} for such a bond.) If $v = \sum v_i$ quanta are

shared in a molecule with noninteracting identical bond modes, the total energy is given by $E(v) = \sum E(v_i)$. Figure 1 is a sketch of the v = 0-3 manifolds of a generic molecule with at least three identical oscillators. The "pure local mode" states, henceforth referred to simply as the "local modes", are shown with heavy lines. They have a degeneracy equal to the number of identical oscillators, and are the lowest in energy in each manifold by $2(v-1)x$. A perturbation V_{nm} which couples the local mode state to other states can prevent local behavior from occurring; the oscillators would not then be independent. An example of such a perturbation is easy to imagine: in the methane molecule, all the hydrogen atoms are bonded to the same carbon atom. Vibration about the center of mass of one of the C-H bonds causes the carbon atom to move. This shakes the other hydrogen atoms, and hence they are all mutually coupled. As the stretching quantum number is raised, the effect of such a perturbation becomes weaker as the splitting $2(v - 1)x$ between the coupled states is increased. In this description,[5,7] the bonds become nearly independent of one another when $V_{nm} \ll 2(v - 1)x$.

A simple spectroscopic test for local behavior is to (a) see if the local mode overtone transition frequencies fit the diatomic molecule formula Eq. (1) and (b) determine whether the absorption cross sections are proportional to the number of identical oscillators. The first extensive studies of this sort were done with liquids, which handily provided thick enough samples to measure the small cross sections. (Typical cross sections are ~ 10^{-23} cm^2 at v = 5.) There were many such experiments.[9-20] A representative one[15] was done on toluene, which has two kinds of C-H bonds: the aryl C-H bonds attached to the

ring, and the alkyl C-H bonds in the methyl group. The experiment showed that they could be distinguished in the overtone spectrum. The different strengths of these two types of bonds give different "spring constants" and cause the vibrations to have slightly different fundamental frequencies. As predicted by Eq. (1), the aryl-alkyl splitting is an increasing function of v. With other substituted benzenes it was confirmed that the cross sections were indeed proportional to the number of C-H oscillators. Thus far, the local mode model worked well in describing such overtone spectra.

The local mode overtone transitions were always broad in liquid spectra, with features being smeared out to bandwidths of ~ 50 cm^{-1} or more. Such broadening is due to frequent (psec timescale) collisions, and intermolecular forces which perturb the vibrational frequencies. Consequently, only the grossest splittings in the spectra could be resolved, and there was no chance to test detailed theories of weaker perturbations and dynamics.

B. Mode mixing

A pure local mode vibration involves only a single bond, but this is an oversimplification. More realistically, the local mode is perturbed by other vibrational modes; they each take on some of the other's vibrational and optical absorption characteristics. This fact makes the local mode problem especially interesting and challenging. The spectroscopic manifestation of this mode mixing is sketched in Fig. 2, for three different cases. It is realistically assumed that the local mode contains all of the zeroth-order oscillator strength. (Compared with the overtones of the highest-frequency stretches, overtones and combination bands of low-frequency modes have negligible

intensity.) The intensities of the overtone transitions to states $|n\rangle$, where n represents the number of quanta, are proportional to $|\langle n|\mu|0\rangle|^2$, where μ is the electric dipole transition operator. As n is increased, the transition becomes less and less "allowed" and the absorption intensity decreases rapidly. Overtones of high-frequency stretches are degenerate with much higher and much weaker overtones of low-frequency modes. It is typically the case that only the overtones of the high-frequency stretches are visible in the near-infrared and visible spectrum. The pure (unperturbed) local mode's inherent homogeneous linewidth, due solely to radiative decay, is γ_{rad} ($< 10^{-8}$ cm^{-1} for typical oscillator strengths of C-H stretching overtones). In Fig. 2, case (a) describes the coupling of strength $\bar{v}$ between the local mode and a discrete nearly-degenerate mode. Two "eigenstates" result from such a Fermi resonance.[21] They are separated by about $2\bar{v}$, and their mode characters are mixed. This leads to the appearance of two lines in the absorption spectrum. In case (b), the local mode is effectively coupled with a number of nearby states, and consequently, its mode character is distributed into these coupled states. If the density of states is ρ, then the bandwidth of the effectively coupled states is $\Gamma \sim 2\pi|\bar{v}|^2\rho$. As a result, a thicket of sharp lines with a bandwidth of Γ should appear in the absorption spectrum. In the limit when the local modes couples with a continuum of states with $\rho\gamma_{rad} > 1$, case (c) results. The absorption spectrum then shows a single broadened line with a linewidth $\Gamma = 2\pi|\bar{v}|^2\rho$.[21-25] Cases (a) and (c) represent the limits of small and large molecules, respectively, and (b) is the "intermediate case".

At this point we can further clarify what we mean by the term

"local mode", and how we tell when we have found one. The prescription of Fig. 2 tells us that each transition corresponds to an excitation of a mixed state $\psi_n = a_n|LM\rangle + \sum_m b_{nm}|NM_m\rangle$ (LM ≡ local mode; NM ≡ normal mode). In the pure local mode case, $a_n = 1$, $b_{nm} = 0$, and a single transition should be observed, assuming $\langle NM|\mu|0\rangle = 0$. In the more general case, the fraction of local character in the mixed state ψ_n is $|a_n|^2$ and the transition to that state has an oscillator strength proportional to $|\langle\psi_n|\mu|0\rangle|^2 \propto |a_n|^2$. We can say that the spectrum describes a local mode when it contains a line possessing a significant fraction of the oscillator strength of the group of lines (corresponding to a line with a significant value of $|a_n|^2$, say 0.5, for example). This is the definition of a local mode we will adopt.

There is a philosophical point that has been discussed[26] concerning the timescale (and its Fourier transform partner, the energy resolution) of an experiment. The qualitative conclusions regarding the local character of a spectrum often depend on the time or spectral resolution of the spectrum. Consider "plucking" a C-H bond in benzene.[26-31] For a short time, the resulting oscillation looks like C-H stretching. After a long time, the C-H stretch energy is redistributed throughout the molecule and dissipated into heat. So for a short time, the vibration is "local"; if we used a broadband optical system to get the absorption spectrum, we would see a single transition. At long times, the vibration is not local; with a high-resolution system we could detect the many states that are coupled to the local mode. Thus, it is necessary to specify the time or spectral resolution of the experiment when making conclusions from the results about the existence of the local modes.

C. Optical spectroscopy

Through its ability to get absorption spectra like those mentioned above, optical spectroscopy is well suited to searching for evidence of local modes. But success in such an endeavor requires that the good resolution available with optical techniques not be compromised by smearing of the fine structure due to line broadening, as in a liquid.

Better local-mode spectra were obtained from gaseous samples. Fourier transform, photoacoustic, and other spectroscopies have provided highly resolved (better than 0.1 cm^{-1}) local-mode spectra of "small" molecules such as substituted methanes.[32-37] From these spectra it was possible to analyze the Fermi resonances between the local mode state $|v_{stretch}>$, with v C-H stretching quanta, and the state $|(v-1)_{stretch}, 2_{bend}>$, comprising (v - 1) C-H stretching and two C-H bending quanta. The bending frequency, at ~1500 cm^{-1}, is roughly half the stretching frequency of ~3000 cm^{-1}, so that the two states are nearly degenerate. Typical magnitudes of coupling matrix elements of this Fermi resonance are in the tens of cm^{-1}; however, stretch-bend interactions can be as strong as 100 cm^{-1}.

D. Large molecules

Local-mode spectra of small molecules had shown Doppler-limited linewidths of less than 0.01 cm^{-1}. This indicates that the vibrational relaxation in these molecules is rather slow (> 0.5 nsec). The density of vibrational states in small molecules is presumably too small to provide the "quasicontinuum" coupling to the local mode required for faster relaxation. The results on large molecules seemed very different as judged from the local-mode spectra of benzene obtained by Bray and Berry[38] and later by Reddy, Heller, and Berry.[39] Their

spectra, reproduced in Fig. 3, covered the C-H stretching bands of v = 1-9. The v = 2-9 bands showed quasi-Lorentzian lineshapes that were very broad (Γ ~ 50 cm^{-1} FWHM.) Each band, presumably a local-mode band, was assumed to be due to a single transition. The "homogeneous" bandwidth Γ would then correspond to a lifetime τ of ~ 100 fsec. Thus, there is qualitatively a huge contrast between the spectra of large and small molecules. A surprising feature of the results was that the bandwidth did not increase monotonically with the overtone level, but actually peaked at v = 5. A naive application of the Fermi Golden Rule $\Gamma = 2\pi|\bar{v}|^2\rho$ would predict a dramatic increase of Γ with energy, if the coupling $\bar{v}$ were constant. In other words, the decay rate should mirror ρ, the rapidly increasing density of vibrational states. This density of states ranges from $1000/cm^{-1}$ at v = 2 to $10^8/cm^{-1}$ at v = 6 in benzene.[38]

These benzene spectra inspired calculations of local mode dynamics and overtone lineshapes in large molecules.[6,7,26-31,38-54] Lately it has been speculated[50] that a local mode may be effectively coupled to only a few of the many nearly degenerate vibrational states. This would then limit ρ and hence the decay rate. It has also been suggested that local modes may even exist in polymeric solids such as polyacetylene, $(CH)_n$.[51] It, like benzene, has coupled C-H "oscillators", but the number of atoms, and total density of states, are huge. The observation of a C-H stretching local mode in such a system would indeed be interesting.

Serious questions concerning the details underlying the broad spectral envelopes have been raised. It is important to discover whether the large bandwidths are really homogeneous, and if not, what

are the origins of the resolvable features. Spectra of small molecules in the gas phase are inherently easier to resolve because there are fewer vibrational modes. In addition, the smaller moments of inertia yield larger rotational constants (e.g. ~10 cm^{-1} for methane vs. ~0.2 cm^{-1} for benzene.) For large molecules, the resolution of individual rovibrational transitions in regions where vibrational bands overlap is very difficult. Even for a single vibrational band, collisional broadening approaches the ~0.01 cm^{-1} spacing between rovibrational transitions.[55] More sophisticated experiments are needed in order to provide better-resolved overtone spectra of large molecules.

Perry and Zewail studied crystalline benzene[56] and durene[57] (1,2,4,5 tetramethylbenzene) at 1.8°K, hoping to distinguish between homogeneous and inhomgeneous broadening in the v = 5 spectra. In such cold crystals, the molecules should all be in the ground rovibrational state. (Static intermolecular perturbations could occur, however.) In their spectra the ~100 cm^{-1} linewidths of the aromatic C-H stretches were seen to exceed those of the methyl C-H stretches (~25 cm^{-1}). An explanation of this difference was that the aromatic oscillators were more directly coupled to the phenyl ring, which provides a large density of states and facile relaxation pathways. The methyl oscillators, on the other hand, were supposed to act more like isolated methane molecules, with a much sparser manifold of states.

E. Supersonic beams

Cooling a gaseous sample is a guaranteed method of eliminating hot-band absorption and reducing the spectral congestion. Molecules in a cell would condense at low temperature, but can be examined in a supersonic beam, with an effective cooling in the rotational degrees of

freedom. The small density of molecules in the beam makes the overtone absorption measurements difficult. It is, however, possible to detect overtone absorption in a beam by monitoring the products of vibrational predissociation resulting from overtone excitation. Butler et. al.[58] used laser-induced fluorescence to detect the OH radicals producted by predissociation of H_2O_2 from the v = 6 local O-H stretching mode. They also obtained the v = 4 spectrum with resonantly enhanced, stepwise two-photon pumping: the first photon excited the local-mode state and the second photon provided the energy to overcome the dissociation barrier. The v = 4 local mode spectrum showed nearly laser-limited linewidths of ~0.08 cm^{-1}, as expected for a small molecule. But the linewidths in the v = 6 spectrum were ~1.5 cm^{-1}. This was presumably due to an enhanced predissociation rate; the corresponding lifetime would be a few psec.

Tetramethyldioxetane (TMDO) is a suitable choice for overtone absorption studies in a molecular beam because it produces fluorescent products (electronically excited acetone) upon predissociation. West et. al.[59] obtained the v = 5 spectra of the C-H stretch local mode of room-temperature TMDO gas, and gas that had undergone varying degrees of cooling in supersonic expansions. The spectra were dominated by a strong peak with a 90 cm^{-1} width, and appeared to be independent of the degree of cooling provided by the supersonic expansion. This was interpreted as evidence that its single broad peak was due to a single lifetime-broadened transition. Recent experiments by McGinley et. al.[60] on the v = 3-5 bands have given similar results. They found that the v = 4,5 bands have some inherent structure, regardless of the temperature. This structure was interpreted as confirmation that the

hydrogen atoms are not all on equivalent sites, so that their C-H bonds have different vibrational frequencies. The asymmetry of the TMDO molecule causes each methyl group to have more than one characteristic C-H stretching frequency, regardless of the temperature. In addition, the stretch-bend couplings observed in substituted methanes are present in TMDO as well. These Fermi resonances should give rise to structure in the TMDO local mode bands. Although the structure was not completely resolved, it was possible to put an upper limit of 50 cm^{-1} on the homogeneous linewidth of each peak. A limitation of these experiments was the inability to characterize the rotational and vibrational temperatures. No diagnostics were devised for that purpose. Supersonic expansions are known to provide a high degree of rotational cooling, but are rather ineffective in vibrational cooling. Several vibrational states could have been populated in the molecular beams, so that the conclusion on the temperature dependence was not definitive. The origin of spectral broadening was therefore uncertain.

F. Benzene photoacoustic results revisited

It is widely recognized that highly resolved spectra are necessary to provide definitive answers to questions concerning local modes in molecules. Let us consider here in more detail the results of Reddy, Heller, and Berry,[39] henceforth RHB, on benzene in a gas cell using photoacoustic spectroscopy, noting the problems which could have kept them from getting cleanly resolved spectra.

Their spectra are shown in Fig. 3. The resolution was ~3 cm^{-1} at v = 1, ~6 cm^{-1} at v = 2, and ~0.5 cm^{-1} for the higher local mode bands. The overtone spectra were analyzed from the point of view that the strongest peak in each spectrum represented a single vibrational

transition to the local mode state of the manifold. The 25 - 50 cm^{-1} bandwidths of these transitions were thought to be largely due to the lifetime broadening (100-200 fsec.) A picture like Fig. 2(c) was used to explain the results.

On the other hand, the fundamental (v = 1) transitions are known to have long lifetimes[55,61] and very small (< 10^{-8} cm^{-1}) homogeneous linewidths. The fundamental band contains three vibrational transitions as a result of a Fermi resonance between the zeroth-order C-H stretch and two combination modes with C-H bending character. At room temperature, each transition has a "rotational envelope" of 30 cm^{-1} width. This envelope is present in all vibrational spectra of room temperature samples. RHB used a deconvolution procedure to remove the rotational contribution to the observed linewidths of the v > 1 bands. The resulting "homogeneous" widths were then 23 cm^{-1} each for the v = 2,3 bands, and larger for higher overtones.

The presence of more than one non-degenerate vibrational transition in the overtone band would invalidate this deconvolution procedure. At room temperature (kT ~ 200 cm^{-1}), ~40% of the molecules are vibrationally excited by thermal agitation. Excitations of the C-H stretching overtones from the hot levels have frequencies different by a few cm^{-1} from those from the ground state. Furthermore, rovibrational bands whose centers were separated by only a few cm^{-1}, (much less than their rotational bandwidths of 30 cm^{-1}), would be difficult to resolve.

G. Goal

For many years, benzene has been important as a prototypical "large" molecule. Its harmonic vibrational force field has been

analyzed, and serves as a textbook example.[1] It was the subject of early work on vibrational anharmonicity and local modes.[4,10,11] As an ensemble of identical, weakly coupled C-H oscillators it is a superb candidate for a thorough study of local modes. This fact, and the uncertainty in the reported under-resolved spectra of the room-temperature gas are compelling reasons to undertake more incisive study of the local mode spectra. It was our goal to obtain local mode overtone absorption spectra as free of congestion as possible in order to resolve details of the vibrational structure.

This we did by cooling the molecules in a supersonic beam to a rotational temperature of 5°K and using state-selective multilevel saturation spectroscopy[62] to obtain the absorption spectra of molecules in the ground vibrational state. We recorded spectra of the C-H stretching $v = 1$-3 local mode overtone bands of the benzene monomer and dimer. These local mode bands are not composed of single, homogeneously broadened transitions. Instead, many vibration-rotation bands have been resolved. The monomer $v = 2$ band contains at least 25 vibrational transitions, the strongest of which, at 6006 cm^{-1}, has a natural linewidth below 1 cm^{-1}. Similarly, the monomer $v = 3$ band contains at least 5 vibrational transitions; the strongest, at 8827 cm^{-1}, has a natural linewidth less than 3 cm^{-1}. (The $v = 3$ spectrum has a lower signal- to-noise ratio and hence, some weak transitions may have been missed.) The local mode description of the spectra appears to apply increasingly well as the quantum number v is increased.

The dimer spectra are similar in gross appearance to those of the monomer. Fine structure in the $v = 1$ spectrum supports the allegation that the dimer is T-shaped and puts a lower limit of ~3 psec on the

vibrational predissociation lifetime at ~3000 cm^{-1} total energy. Broadening of the rovibrational bands comprising the local mode overtone bands is observed. We interpret this broadening, which increases with vibrational energy, as being a manifestation of "site splitting" of inequivalent C-H bonds.

II. NEW TECHNIQUE

We have used two powerful techniques to reduce spectral congestion and thereby resolve the spectra: cooling of the molecular rotations, and state-selective saturation spectroscopy. Each is discussed in detail below.

A. Cooling

The inhomogeneous width of a rovibrational band is governed by the thermal population distribution in the rotational and vibrational states. Let us consider the rotations first, with a diatomic molecule taken as a simple example.

Lowering the "rotational temperature" has the effect of reducing the width of a vibration-rotation band, as shown in Fig. 4. The rotational Hamiltonian is of the form $E_{rot} = BJ(J + 1)$, where B is the "rotational constant". The Boltzmann factor $\exp(-E_{rot}/kT)$ strongly reduces the distribution above the rotational level J_{max}, at which $E_{rot} \sim kT$. The quadratic dependence of E_{rot} on J implies that $J_{max} \propto \sqrt{T}$. In single photon absorbtion with $\Delta J = \pm 1$ the rotational envelope of a vibrational line appears as a "comb" whose teeth are spaced by 2B (not necessarily resolved), and whose width is roughly $4BJ_{max} \propto \sqrt{T_{rot}}$, where T_{rot} is the "rotational temperature." Our supersonic expansion caused the IR absorption bandwidth of a vibrational transition of benzene to

drop from 30 cm^{-1} (room temperature) to 4 cm^{-1} (T_{rot} = 5°K.)

At room temperature, kT ~ 200 cm^{-1}, and roughly 40% of benzene molecules are not in the ground vibrational state. The presence of these hot molecules in the sample causes inhomogeneous broadening of a C-H stretching band. However, we were able to prevent the "hot" molecules from contributing to our spectra by using state-selective spectroscopy.

B. State selection

Our state-selective three-level saturation spectroscopy scheme used the "inverted Λ" configuration, shown in Fig. 5(a). The essence of state selection is this: a "probe" beam is adjusted to monitor only the population in a chosen subset of the $|g\rangle$ states. The "pump" beam is scanned through the spectral region of interest. Absorption from $|g\rangle$ to $|v\rangle$ causes the ground state population being probed to decrease, and hence, the probe signal. The change in the probe signal versus the pump frequency then gives us the desired absorption spectrum.

Since the laser linewidths are finite, the observed lineshapes are the convolution of the pump and probe lineshapes with the absorption spectra of the selected states:

$$\bar{\alpha}(\omega_{pump}) = \sum_i \iint f_i \alpha_i(\omega')\beta_i(\omega'')I(\omega_{pump} - \omega')I^*(\omega_{probe} - \omega'')d\omega' d\omega''.$$

$\bar{\alpha}(\omega_{pump})$ is the observed absorption spectrum, f_i is the fractional population in the i^{th} quantum (rotational, vibrational) state, α_i is the true absorption spectrum of that state, and β_i is its absorption spectrum. $I(\omega_{pump} - \omega')$ and $I^*(\omega_{probe} - \omega'')$ are the normalized pump

and probe beam lineshapes, respectively. If the probe is so highly resolved that a single quantum state j can be selected, then a spectrum free of congestion from multiple ground states can result. Such a spectrum could have the pump lineshape deconvolved to give the true homogeneous absorption spectrum $\alpha_j(\omega)$.

In Fig. 5(a), we assume that the probe beam has selected 3 states in the $|g\rangle$ manifold. Each of the states can make a transition $|v\rangle \leftarrow |g\rangle$ to the two states in $|v\rangle$. If the pump has a resolution that separates the $|v\rangle$ states but not the $|g\rangle$ states, two peaks (each containing three unresolved lines) should be expected, as shown in Fig. 5(b).

In our experiment, selective probing was accomplished by resonantly-enhanced two-photon ionization (R2PI), using the 260 nm $\tilde{A} \leftarrow \tilde{X}$ transition as the intermediate resonant step [see Fig. 6(a)]. The vibrational bands of this transition have been accurately assigned,[63,64] and even the rotational structure of the vibrational bands has been well analyzed.[65,66] It is therefore possible to selectively probe a particular ground rotational and vibratinal state. Because of our limited probe laser resolution, we were able to proble only a selected group of rotational states in the ground vibrational level.

This electronic $\tilde{A} \leftarrow \tilde{X}$ transition also exists in the benzene dimer; in this case the vibrational assignments have been done[67-69] but the rotational analysis has not. The dimer's structure and moments of inertia, which determine the rotational band-structure, are unknown.[70] The wavelength needed to probe vibrational-ground-state dimers is appreciably different from that used for monomers. This wavelength

difference, together with the use of a mass spectrometer, allowed us to study monomers and dimers separately.

III. EXPERIMENTAL ARRANGEMENT

Figure 7 shows the salient components of our apparatus. Our sample was a supersonic beam formed by passing argon at 200 torr through a -30°C or 0°C bubbler which contained frozen benzene. It proceeded into the 10^{-7} torr experimental chamber via a Lasertechnics[71] LPV pulsed valve equipped with a 0.5 mm diameter nozzle, a region of differential pumping, and a skimmer. Infrared and ultraviolet laser beams were focused and carefully overlapped. They crossed the molecular beam inside a set of ion extraction plates. The pulses of ions generated by R2PI passed through a time-of-flight mass spectrometer (a drift tube) and were detected with a Johnston electron multiplier.[72] Flight times for ions of mass M varied as $\sqrt{M}$. We used gated integrators to average the ion signals for several laser shots.

Independently triggerable pulsed Nd:YAG laser systems[73] generated the tunable UV and IR frequencies required. Each Nd:YAG oscillator-amplifier system could generate 700-mj, 9-nsec, 9394-cm^{-1} pulses at a rate of 10 Hz. This fundamental-frequency output was frequency-doubled or -tripled, as required, in KDP crystals. Light around 38600 cm^{-1} came from a Coumarin 500 dye laser, whose output was frequency-doubled in an automatically-tracked angle-tuned KDP crystal. Infrared light came from mixing of a Nd:YAG laser beam at 9394 cm^{-1} with an IR/red dye laser beam in an automatically-angle-tuned $LiNbO_3$ crystal (WEX-1d[73]), yielding ~ 1 mj/pulse at 3000-3100 cm^{-1} and ~ 5 mj/pulse at 5800-6200 cm^{-1}. We noted experimentally that these

energies were sufficient to saturate the strongest transitions in the v = 1 and v = 2 bands respectively, as predicted with the measured cross sections of RHB. We could obtain ~15-30 mj/pulse at 8700-8900 cm^{-1}, the region of the v = 3 band, by pumping DNDTPC dye[74] with the Nd:YAG fundamental. This was sufficient to pump ~ 10% of the molecules to be probed.

The resolution achieved with our lasers was 1 cm^{-1} in the IR and 0.3 cm^{-1} in the UV. We sometimes increased the UV resolution to better than 0.1 cm^{-1} by using an intracavity etalon in the dye laser, but the output amplitude stability was poor. By using accurately known transitions in neon optogalvanic[75] and methane photoacoustic spectra, we calibrated the laser frequencies to better than 1 cm^{-1}. Benzene transitions occurred at their predicted positions in the UV and v = 1 IR spectra.

A digital computer recorded ion signal levels, scanned laser wavelengths, and actuated a shutter which was used to turn the IR beam on and off. We took special pains to overlap the foci of the IR and UV beams carefully. First we spatially filtered the UV beam with a pair of lenses and a pinhole at the focus between them. This pair of lenses also served as a telescope for adjusting the divergence of the UV beam, whose diameter was ~ 25 mm at the output lens, which had a focal length of 35 cm. We then also installed a telescope in the IR beam to give it an adjustable divergence and increase its diameter to ~ 30 mm at the output lens of the telescope. The alignment procedure was first to adjust the beam divergences to get the foci of the two beams nearly overlapped, then set the UV beam waist to the best location for ion extraction in the molecular beam, and finally readjust the IR beam to

have it well overlapped with the UV beam. The IR light, regardless of its wavelength, proved to be highly effective at fragmenting the mass-78 benzene ions produced by the UV pulse.[76-79] Therefore, to check the beam overlap, we fired the IR pulse just after the UV pulse and used the ion signal from the molecular beam as an indication for the beam overlap. This method is quite sensitive and effective; in our experiment, it was even necessary to attenuate the IR pulse energy to avoid saturation of the ion signal.

For data-taking, a group of rotational energy levels in the monomer or dimer ground vibrational state was selected by tuning the UV probe beam to the proper part of the 6_0^1 band. The R2PI spectrum of this band in the monomer, obtained by pressure-tuning the dye laser with a 0.1 cm^{-1} resolution, is shown in Fig. 6(b). In order to eliminate fluctuations in the probe signal due to time jitter between the UV and IR pulses, the UV probe pulse was delayed by ~ 15-20 nsec with respect to the IR pulse. This guaranteed that the molecules received full IR pumping before being probed. Repopulation of the vibrational ground state could not have occurred in this 15-20 nsec, since the $v = 1$ states have typical lifetimes of msec, and the higher states should have even longer lifetimes.

With the shutter in the IR beam closed, no molecules were pumped. With it open, the ground state population was depleted. Closing and opening the shutter every few seconds thus imposed a modulation on the population of the ground-state molecules and hence, the ion (probe) signal. Recording the modulation amplitude of the probe signal as a function of IR pump frequency gave us the IR absorption spectra.

The IR-pumping-induced modulation is quite small, and we were faced

with the problem of observing an adequate signal-to-noise ratio. Our UV laser had an intensity fluctuation of several percent and an output frequency jitter larger than the $\sim 10^{-4}$ cm^{-1} linewidths of the transitions being probed. (The UV output spectrum presumably consisted of many cavity modes. The intensity distribution among them varied from shot to shot.) Normalization of the ion signal to the laser pulse energy or its square was not effective in reducing the ion signal fluctuation. We desired a normalization technique which would accomodate laser frequency fluctuations as well as an arbitrary dependence of the ion signal on the laser pulse energy.

A two-beam method with identical samples was clearly mandated. We developed such a method by splitting the UV beam into two with similar powers focused on the molecular beam at two separate foci, one overlapping with the IR beam and the other not. Figure 8(a) describes the setup. The diverging UV beam struck a Suprasil flat at ~ 45° incidence. The beam was S-polarized, so that ~ 10% was reflected off the front and back surfaces of the flat, which also served as the combiner for the IR and UV beams. The resulting pair of UV beams was focused at two points separated by 2 mm in the ion-extraction field of the time-of-flight mass spectrometer. The ion flight times from each of the foci to the detector were different because the foci were at different potentials. This made it possible to separate the two ion signals with time-resolved detection by gated integrators. Figure 8(b) is a schematic oscilloscope trace of the ion multiplier's output, showing that benzene ions of mass 78 and 79 [80,81] were nearly resolved in the signal from each focus. The ratio of the ion signals from the IR-pumped UV beam and its unpumped twin gave the fraction of molecules

that had not absorbed IR light. (The ratio was 1 when no molecules absorbed and 0 when they all absorbed.)

This system worked very well in our experiment. R2PI provided well over 10,000 benzene ions/shot when the UV light was tuned to the most intense part of the 6_0^1 band. Each of the the ion signals from the two UV probes fluctuated several percent, but their ratio was constant to a few tenths of a percent, roughly the statistical limit. The resulting increase in the signal-to-noise ratio allowed us to see many weak transitions which would otherwise have been undetectable.

IV. DETAILS OF STATE SELECTION -- CHARACTERISTICS OF UV AND IR SPECTRA

We wished to obtain two types of spectra in this experiment. First, we wanted to locate the vibrational transitions that make up the local mode bands. This we did with fast scans over a broad range around the RHB band centers. During these scans we did not try to resolve rotational structure within each vibration-rotation band. We call these "nonselective spectra". Then we used the state-selective technique to observe the more detailed substructure of the vibrational transitions of a smaller group of rotational states. Since this technique played an important role in our experiment, we give now a more in-depth explanation of its use.

The coarse structure in the $\tilde{A} \leftarrow \tilde{X}$ spectrum of benzene is due to vibrational transitions from thermally populated levels in the $\tilde{X}$ state (at 0, 399, 608 cm^{-1} ...) to levels in the $\tilde{A}$ state. The pure electronic transition is symmetry-forbidden. But the symmetry reduction caused by an e_{2g}-symmetry ("squashing") vibration makes the transition weakly allowed when accompanied by a unit change in the

number of e_{2g} quanta. ν_6 is the e_{2g} mode which makes the transition the strongest, and its rotational behavior has been most thoroughly analyzed. In an attempt to probe the ground vibrational state molecules, we therefore chose the 6_0^1 band. The 6_0^1 designation means that 1 quantum of ν_6 is present in the $\tilde{A}$ state and zero in the $\tilde{X}$ state. As shown in Fig. 6(a), this band occurs at 38608 cm^{-1}. No transitions from the other thermally populated vibrational levels occur at this frequency.

The rotational structure of the 6_0^1 band is quite complicated and has been analyzed by Callomon, Dunn, and Mills.[65] Here we give enough detail to explain the features of our spectra and clarify our method of rotational state selection.

Since we are considering an electric dipole transition, we expect P ($\Delta J = -1$), Q ($\Delta J = 0$), and R ($\Delta J = 1$) branches in the 6_0^1 band. The transition is polarized in the plane of the molecule (perpendicular to the sixfold symmetry axis; see Fig. 9 for a sketch of the relevant axes and angular momenta.) The selection rules on K, which is the projection of $\vec{J}$ on the 6-fold axis, are $\Delta K = -1$ (p sub-branch) or $\Delta K = +1$ (r sub-branch). Consequently, there are altogether six branches of rotational transitions, labeled as ${}^{\Delta K}\Delta J$: ${}^{p}P$, ${}^{p}Q$, ${}^{p}R$, ${}^{r}P$, ${}^{r}Q$, ${}^{r}R$. Their relative intensities for a given ground state depend on the orientation of J with respect to the symmetry axis R, and can be computed from Clebsch-Gordan coefficients. In the limit that J,K >> 1, the ${}^{p}P$ and ${}^{r}R$ branch intensities vary as $(1/2)(1 + K/J)^2$, ${}^{p}Q$,${}^{r}Q$ branch intensities $\sim(1 - K^2/J^2)$, and ${}^{p}R$,${}^{r}P$ branch intensities $\sim(1/2)(1-(K/J))^2$. (Exact rotational transition matrix elements, or Hönl-London factors, are given by Herzberg.[2]) As will be discussed below, J and K tend toward parallel alignment and equal magnitude at low temperatures. This

strongly favors the ^{r}R and ^{p}P branches; the ^{p}R and ^{r}P branches are so weak that they may be neglected, while the ^{p}Q,^{r}Q branches have medium intensity and are close together in frequency.

General trends in the PQR rotational structure can be understood with recourse to a simplified model in which the dependence on K is ignored. In this simple picture, the P branch corresponds to the real ^{p}P branch; the R branch is derived from the ^{r}R branch, and the ^{p}Q,^{r}Q branches are lumped together as the Q branch. The transition frequencies between the ground state with a rotational energy $B''J''(J''+1)$ and the excited state with a rotational energy $B'J'(J' + 1)$ are $\omega = \omega_0 + B'J'(J' + 1) - B''J''(J'' + 1)$. Thus, the P, Q, and R branch transitions are shifted by $(B' - B'')J''^2 - (B' + B'')J''$, $(B' - B'')J''(J'' + 1)$, and $(B' - B'')J'^2 + (B' + B'')J'$, respectively, from ω_0. A sketch of these transition frequencies vs. J" is shown in Fig. 10. Because the molecule is larger in the excited electronic state, we have $B' < B''$. It is seen that the Q branch transitions are closely grouped, slightly to the red of the origin ω_0. The P-branch transitions have their frequency change most rapidly with J". This makes the spacing between transitions from different (J",K") states the largest in the P branch. Therefore, if we want to probe simultaneously as many (J",K") states as possible with the limited probe beam linewidth, we should tune to the Q branch. If we want to probe only a small number of states, we should use the P branch.

The thermal population distribution in the K levels of each J manifold also affects the rotational state selection. For benzene, the more accurate ground-state rotational energy is given by $B''[J''(J'' + 1) - K''^2/2]$. Figure 11 is a sketch of the energy levels in this

situation. When the rotational temperature T_{rot} is low, low-energy states with K" ~ J" are strongly favored in the distribution. This is especially true at large J", where the rotational energy changes rapidly with respect to kT_{rot} when K" ~ J". With only a few K" states populated for each high J" state, and the transition frequencies most widely spaced in the wing of the P branch, the chance to probe only a few (J,K) states is best there.

The above discussion applies equally to the IR vibrational spectra; the ^{P}P, ^{P}Q, ^{r}Q, and ^{r}R branches are also expected. In this case, however, the rotational constants of the ground and excited vibrational states do not differ substantially. With the rotational energy given by $B[J(J + 1) - K^2/2]$, IR transitions from the heavily populated states (J,K~J) would be expected ~ +BJ from the vibrational frequency for the ^{P}Q and ^{r}R branches and ~ -BJ for the ^{r}Q and ^{P}P branches. Here the ^{r}Q,^{P}Q branches overlap the ^{P}P,^{r}R branches because benzene is symmetric with $I_z = 2I_x = 2I_y$. This coincidence disappears when the doubly degenerate nature of the in-plane vibrations is analyzed more completely as follows.

A doubly degenerate harmonic oscillator possesses a "vibrational angular momentum"[2] and the Coriolis coupling between rotation and vibration must be taken into account. The rotational energy is then given by $E_{rot}(J,K,\zeta) = B[J(J + 1) - (K + \zeta)^2/2]$, where ζ is the Coriolis constant with $|\zeta|$ between 0 and 1. Consequently, transitions from the state (J,J) are displaced from ω_o not by $\pm BJ$, but by $\pm B(1 - \zeta)J$ for the ^{r}R, ^{P}P branches and by $\pm B(1 + \zeta)J$ for the ^{P}Q, ^{r}Q branches. For sufficiently high J, these four branches can be well separated, as Fig. 12 with $\zeta = -1/3$ illustrates. The observed IR spectrum clearly

depends on ζ. For example, when $\zeta = 0$, the Q branches are buried under the R and P branches at $\pm BJ$. If $\zeta = -1$, the Q branches coincide at ω_o, and the R and P branches are at $\pm 2BJ$. The Q branches are expected to be weak because of the $(1 - K^2/J^2)$ dependence of their intensities.

All of the above considerations for monomer spectra apply to the dimer, with some modifications. While the C-H vibrational energy level structure of the dimer is not very different from that of the monomer, there is quite an important difference in the characteristics of the rotational states: The energy levels are more closely spaced in the dimer. Without knowing whether its two constituents are able to rotate with respect to each other, it is not possible to state the selection rules for rotational transitions very well. We did not succeed in selecting a small group of rotational states during our study of the dimer. The solution of the dimer's structure and rotational spectrum appears to be a viable research problem in itself.

V. RESULTS

A. UV Probe Spectrum

In our R2PI spectrum of Fig. 6(b) the ^pQ and ^rQ branches are not resolved. The J structure is nearly resolved in the P and R branches. Transitions from different K states provide fine structure which fills in the gaps between the intense lines from (J,K = J) states. We wrote a computer program, modeled after that of Beck et. al.,[66] which calculated the absorption spectrum of the 6_0^1 band. With the rotational temperature as a variable parameter, the calculated spectrum in Fig. 6(c) appears to fit the observed spectrum in Fig. 6(b) quite well. The temperature thus determined was $T_{rot} = 5°K$. This temperature yields

correctly the most intense part of the observed spectrum, but did not accurately represent the distribution in states higher than J" ~ 30. The actual populations in the high-energy states are higher than those predicted from an equilibrium distribution described by T_{rot}. This is fortunate, as part of our experiment relied on probing these high rotational states.

B. Monomer v = 1 Spectrum

Our nonselective scans were performed with the UV laser frequency tuned to the intense Q branch. This gave an ion signal large enough that statistical fluctuations in the ion number were unimportant. We could then obtain a spectrum with a high signal-to-noise ratio even while scanning rapidly. The resulting IR spectra should mimic linear absorption spectra of benzene gas at 5°K. Figure 13(a) shows the spectrum in the fundamental C-H stretching region under these conditions. This is to be contrasted with the fundamental band in Fig. 3. The vibrational bands of our spectrum have a FWHM of 4 cm^{-1}, consistent with T_{rot} = 5°K and the fact that "hot band" transitions are absent. The PQR rotational structure is not resolved because most of the states contributing to the signal have relatively low J values. When the UV laser was tuned to selectively probe only rotational states with high J, the rotational features in the IR spectrum could be observed.

Figure 14 shows the P-R branch splitting in the 3048 cm^{-1} fundamental C-H stretch band under different probing conditions. As the probe frequency moves further out in the wing of the P branch in Fig. 6(b), higher J states are selectively probed, and the P-R branch splitting becomes larger. The spectra are intrinsically broadened

because still a group of rotational states instead of a single one was selected. They are also broadened by the finite pump laser linewidth of 1 cm^{-1}.

To within our error, the heights of the split P and R peaks in Fig. 4 are equal. This is expected since the rotational line strengths in the P and R branches should be about the same when $J >> 1$. By knowing the J values being probed and the splitting of the P-R branches, we can calculate ζ, the Coriolis constant. We find, for the 3048 cm^{-1} band, $\zeta = -0.1 \pm 0.1$, in agreement with the value $\zeta = -.0984 \pm .0023$ found by Pliva.[55]

C. Monomer nonselective spectra

Figures 13(a), (b), and (c) show our nonselective spectra of the v = 1-3 bands, respectively. In the v = 2 spectrum, ~ 25 vibration-rotation bands have been resolved, each with a bandwidth ~4 cm^{-1} as in the v=1 spectrum. Homogeneous broadening and the 4 cm^{-1} rotational envelopes contribute to these widths. Deconvolution shows that the homogeneous broadening is less than ~3 cm^{-1}. Weaker bands have been emphasized by deliberately saturating the largest peak; in an unsaturated spectrum this peak has twice the intensity of its neighbor. The result here indicates that about 10 vibrational transitions are within the envelope of the most intense peak in the v = 2 photoacoustic spectrum of Reddy et al. (Fig. 3).

In our nonselective spectrum of the v=3 local mode band, only four peaks are distincly resolved. The strongest one has a FWHM of 10 cm^{-1}, which could be indicative of a single peak with 4 cm^{-1} rotational structure and ~9 cm^{-1} homogeneous broadening. However, the observed asymmetry suggests that this peak consists of at least two unresolved

vibration-rotation bands, homogeneously broadened by at most a few cm^{-1}. That this is actually the case will be seen later in the results with state selection.

The vibration-rotation transition frequencies we observed in the monomer v = 1-3 bands are listed in Table I. It is interesting to note that the most intense peaks in the v = 2,3 spectra are blue shifted ~ 10 cm^{-1} and ~ 20 cm^{-1}, respectively, from the room-temperature absorption maxima. These shifts are not expected if the only difference between the two sets of spectra is a compression of the rotational envelope of each vibration-rotation band. This implies that the vibrational "hot band" transitions are responsible. The frequency of maximum intensity in the room-temperature spectrum would be between the vibrational band centers of the "hot band" and "cold band".

D. Localization

We can use our nonselective v = 1-3 spectra to assess the tendency toward local-mode behavior. Our criterion for local behavior was that a single transition have the bulk (for example, 50%) of the intensity in a band. A look at the spectra in Fig. 13 and Table I shows that the strongest peak at v = 2 has ~ 1/3 the total intensity of the 50 cm^{-1} band, and that there are many other peaks with appreciable intensities. This is not what we would call a local-mode-type spectrum. But in the v = 3 spectrum, the strongest feature has ~ 2/3 of the total intensity, and only a few other states have significant oscillator strength. This band fits our criterion for local-mode behavior.

We can even get a semi-quantitative feeling for the strengths of the interactions between the local mode and the nearly degenerate

combination mode states. By counting the number of observed vibration-rotation bands and dividing by their frequency span Γ, we can obtain a lower limit on the density of states that are effectively coupled with the local mode. Then we use the prescription of Fig. 2 to estimate the coupling strength, $\bar{v} \sim (\Gamma/2\pi\rho)^{1/2}$. If the C-H stretch local mode decouples from the other vibrational modes, $\bar{v}$ should decrease. As ρ is usually underestimated in this method because of spectral resolution (the overall vibrational density of states of benzene is $\sim 10^3/cm^{-1}$ at $v = 2$ and $\sim 10^5/cm^{-1}$ at $v = 3$), $\bar{v}$ is overestimated.

The $v = 1$ band is a famous case of a "Fermi resonance" between the C-H stretch ν_{20} and the combination modes $\nu_8 + \nu_{19}$ and $\nu_1 + \nu_8 + \nu_{19}$. We use Fig. 2(a) to analyze this situation. From the separation between the peaks we find $\bar{v} = 25\ cm^{-1}$. The $v = 2$ spectrum of Fig. 3(b) can be analyzed with the help of Fig. 2(b). Simple counting of the observed bands gives $\rho \sim 0.2/cm^{-1}$, and the observed width $\Gamma = 30\ cm^{-1}$ leads to a value $\bar{v} \sim 5\ cm^{-1}$. For the $v = 3$ band, in Fig 13(c) we have $\rho \sim 0.3/cm^{-1}$, and $\Gamma \sim 10\ cm^{-1}$, and hence $\bar{v} = 2\ cm^{-1}$. The trend of $\bar{v}$ decreasing from $25\ cm^{-1}$ at $v = 1$ to $2\ cm^{-1}$ at $v = 3$ shows that the "local mode" description becomes increasingly appropriate with increasing v. We note that we actually count only a small number of strongly-coupled states. This is not unreasonable, considering that anharmonic coupling strengths typically depend on the degree of vibrational wavefunction overlap. There is only a small subset of all the modes that has enough "C-H stretching character" to be able to couple strongly with the C-H local mode.

E. State-selective spectra

As described earlier (see Figs. 12, 14), probing in the UV P branch enabled us to put stricter limits on the homogeneous linewidths by selecting only a few rotational states. In the 3048 cm^{-1} v=1 band, where homogeneous broadening was negligible, the P and R branches appeared in our spectra with widths ~ 1 cm^{-1}, limited by our laser linewidth.

Repeating this state-selection procedure on the intense 6006 cm^{-1} peak in the v = 2 band gave again the laser-limited spectral width. Thus, the homogeneous linewidths in the v=2 local mode band are also less than 1 cm^{-1}. Just as in the v = 1 spectrum, the P and R branches had equal intensities and we found $\zeta = -0.1 \pm 0.1$.

State selection of the v = 3 local mode band, with its apparently unresolved vibration-rotation band structure at 8827 cm^{-1}, presented more of a challenge. The 10 cm^{-1} bandwidth suggested that we could only hope to observe selected rotational states whose P and R transitions are separated by more than 10 cm^{-1}. To do so, we had to tune to high J states (J ~ 32) in the UV P branch. The sparse population in these states caused the probe signal to be very weak. We could increase the signal tenfold by warming the benzene reservoir from -30°C, where the saturated vapor pressure of benzene is ~ 2 torr, to 0°C, where it is ~20 torr. This did not substantially increase the rotational temperature of the molecules in the beam, as far as the population in low J states was concerned. The distribution in the high J states is apparently not described by the rotational temperature. (For T_{rot} = 5°K, the equilibrium population distribution would drop to ~ 10^{-8}% at J = 32.)

Figure 15 shows our state-selected v = 3 spectrum. Part (a),

obtained with probing in the UV Q branch, depicts the nonselective spectrum of the intense 8827 cm^{-1} peak. Part (b) shows that if probing is set at J ~ 2 in the UV P branch, the P and R transitions are resolved. With selective UV probing of the J ~ 32 states, three peaks are actually resolved as shown in Fig. 15(c). In order to resolve these peaks better, we tried to select a smaller group of (J,K) states by reducing the UV dye laser linewidth to 0.1 cm^{-1}. The observed spectrum shown in Fig. 15(d) is not very different from that in (c). This suggests that the peak width of 2-3 cm^{-1} could be dominated by homogeneous broadening, but this is an upper limit on the homogeneous linewidth since we realize that the UV probing could still have selected several (J,K) states with J ~ 32.

Our discovery of three peaks in the v = 3 spectrum is anomalous. For each vibrational transition, we expect two nearly equally intense peaks (P and R). Thus, it takes more than one vibrational transition to account for the three peaks in the 8827 cm^{-1} band. On the basis of peak shapes and intensities we suggest that the low-frequency peak consists of overlapping P branch peaks and the two high-frequency peaks come from the R branch.

F. Dimer nonselective spectra

We can get more information about the C-H stretching local modes in benzene by looking at their nonselective spectra in the dimer, shown in Fig. 16(a-c). The v=1 band shows the monomer-like absorptions; The peaks are red-shifted by 1-2 cm^{-1} compared with the monomer spectrum, and they have different relative intensities. An important feature to note is the presence of two new combination bands with only 2 cm^{-1} FWHM at 3014 and 3072 cm^{-1}, presumably arising from van der Waals vibrations

between molecules. We shall postpone the interpretation to a later part in this section.

The spectrum of the v = 2 band of the dimer is quite similar to that of the monomer, except for a ~ 3 cm^{-1} red shift. Our resolution was not sufficient for us to find new peaks arising from the van der Waals interactions between the monomer subunits. We did observe a ~ 1 cm^{-1} broadening [from FWHM = 4 cm^{-1} (monomer) to 5 cm^{-1} (dimer)] on the strong peaks, which was not seen in the v = 1 spectrum. The v = 3 spectrum of the dimer appears to contain a single peak with ~24 cm^{-1} FWHM, red-shifted ~ 4 cm^{-1} from its monomer counterpart.

It is believed that the structure of the benzene dimer is asymmetric. Then site splittings in the C-H stretching frequencies are expected. The spectral broadenings seen in the dimer spectra could be due to the unresolved splittings of the C-H bonds. As the bond motions become more "local" in progressing from v = 1 to v = 3, each C-H bond becomes freer to move independently and experience its own local vibrational potential, and the widths of the vibration-rotation bands should increase.

Let us now consider the v=1 dimer spectrum more carefully, as it has bearing on a couple of long-standing problems. First, there is the question of the vibrational predissociation lifetime. In vibrational predissociation, the C-H stretching vibration decays, imparting some of its energy to the van der Waals bond between the monomers and causing the dimer to dissociate. The strength of the van der Waals bond is estimated to be ~ 900 cm^{-1}; CO_2 laser radiation at 1037 cm^{-1} is observed to fragment the dimers.[82,83] The rates of predissociation have been estimated from the observed homogeneous linewidths. Since

the weak bands at 3014, 3072 cm^{-1} have linewidths of < 2 cm^{-1} before deconvolution of the laser linewidth of 1 cm^{-1}, we conclude that the predissociation lifetime from the 3014 and 3072 cm^{-1} excitations exceeds ~ 3 psec. A similar conclusion has been inferred from experiments with CO_2 lasers at 1037 cm^{-1} [83] and from a lower-resolution study with an optical parametric oscillator.[84] It has been suggested on the basis of higher-resolution (0.1 cm^{-1}) spectra obtained by Miller that the lifetime is actually in excess of ~50 psec.[85]

The structure of the dimer is not really known. Calculations[86] have not resolved the controversy. Studies of the dimer's behavior in the $\tilde{A} \leftarrow \tilde{X}$ transition have led to the conclusions that it is roof-shaped[81] or has the monomers stacked parallel with their centers offset[70] Molecular beam electric resonance (MBER) experiments[87,88] had shown that the dimer has a dipole moment, and its structure was thought to be T-shaped [see Fig. 17(a)]. Our dimer spectrum seems to support this latter contention. Consider molecule A in Fig. 17(a). The weakness of the van der Waals bond between A and B allows this subunit to rotate with only a mild hindrance about the axis 2, without causing rotation of molecule B. Then molecule A is nearly the same as a free monomer, and its spectrum should reflect that. Indeed, the gross features of our monomer and dimer spectra are identical. The effective moment of inertia, the factor that determines the width of a vibration-rotation band, is also unchanged. The intense dimer bands do retain the FWHM of 4 cm^{-1} as observed for the monomer. (The band at 3078 cm^{-1} appears to be perturbed by proximity to the 3072 cm^{-1} peak, and its halfwidth is ambiguous.)

Now consider molecule B. C-H stretching motion oriented along 2 is

coupled with stretching of the van der Waals bond, also in the $\hat{z}$ direction. Combination bands formed by these two vibrations must therefore exist. This explains the presence of the bands at 3014 and 3072 cm^{-1}, which could result from the 3047 cm^{-1} C-H stretches accompanied by the loss and gain, respectively, of one van-der-Waals stretching quantum. An energy level diagram of these transitions is presented in Fig. 17(b). It is assumed that the van der Waals bond strengths for the ground and excited states are 33 and 25 cm^{-1}, respectively. The average shift of the combination bands from the 3047 cm^{-1} band is 29 cm^{-1}. Considering that in a molecular beam, the "vibrational temperature" often considerably exceeds the "rotational temperature", it is reasonable that van der Waals stretching modes in the C-H stretching ground state are populated. Figure 17(b) also indicates that a transition at 3039 cm^{-1} is expected. The shoulder at 3040 cm^{-1}, on the intense 3047 cm^{-1} band, could very well be this transition.

The final problem is to explain the small (2 cm^{-1} vs. 4 cm^{-1}) bandwidth of the 3014 and 3072 cm^{-1} combination bands. The width of the rotatinal envelope of a vibrational transition is $\sim 4BJ_{max} \propto \sqrt{B}$, where B is the rotational constant, inversely proportional to the effective moment of inertia. The rotation associated with C-H stretching of molecule B is about the axis $\hat{k}$, shown in Fig. 17(a), and the entire dimer tumbles. The moment of inertia for this rotation is more than 6 times that of a free monomer[88] and the corresponding rotational constant B would be less than one-sixth of its monomeric value. This would cause the "rotational envelope" to shrink, to about 1.6 cm^{-1} vs. the width of 4 cm^{-1} from the rotation of a monomer. With

our 1 cm^{-1} laser resolution, the combination bands would then be observed as having a width just under 2 cm^{-1}. An elegant experiment in which the rotational structure in the spectrum of a dimer of aromatic molecules was actually resolved was done on s-tetrazine ($C_2N_4H_2$) by Haynam et. al.[89]

G. Results summarized

At this point a brief recapitulation of our interpretations of our results is in order. The room temperature linear absorption spectra of the C-H stretching local mode bands clearly do not reveal their true vibrational structure. Our state-selective technique has brought to light the fact that the homogeneous linewidths are less than 1 cm^{-1} in the v=2 band and ~2-3 cm^{-1} in the v=3 band, so that vibrational lifetimes are <u>at least</u> a few psec in the v = 2,3 local mode bands. This is at odds with the subpicosecond lifetimes deduced from broad (~100 cm^{-1}) room temperature spectra. As the number of C-H stretching quanta is increased, the "local mode" model appears to become more appropriate in describing the spectra. The T-shaped benzene dimer leads us to expect site splitting of the C-H vibrations. This causes broadening of the observed vibration-rotation bands in the local mode spectra of the dimer. The tendency toward local behavior as the number of C-H stretch quanta is increased is also manifested in the dimer spectra as an increase in the overtone bandwidth.

V. DISCUSSION

A. More Sophisticated Models of State Mixing

State mixing is a key element in calculations of molecular dynamics and spectra when anharmonic couplings are present. Thus far, we have

used a crude model, as described with Fig. 2, to provide a reference point for viewing the local modes. In this model, the coupling $\bar{v}$ is equally strong between the local mode and all the other modes, whose density is ρ. Our use of this model was very empirical: by looking at our spectra we estimated ρ by counting the observed vibration-rotation bands and dividing by Γ, the overall bandwidth of the bands. The value of Γ was estimated visually. This interpretation is in the spirit of Fig. 2(b). We have ignored the fact that the total density of states is actually far greater. Calculations[38] show that this density is ~ $10/cm^{-1}$ at the energy of 1 C-H stretching quantum (v = 1), ~ $10^3/cm^{-1}$ at v = 2, and ~ $10^5/cm^{-1}$ at v = 3. From our spectra we had estimated that ρ ~ $0.04/cm^{-1}$ at v = 1, ~ $0.2/cm^{-1}$ at v = 2, and ~ $0.3/cm^{-1}$ at v = 3.

This forces the conclusion that not all states are equally strongly coupled to the local mode state. Intuitively, this is expected; states whose motions have little resemblance to C-H stretching will have only small wave function overlap, and hence small coupling with the local mode. Sibert et al.[26] used more than one "tier" of states, to take into account the different degrees of coupling with the local mode, as shown in Fig. 18. In this multitier model, C-H stretching states $|v_{CH}\rangle$ with v quanta are coupled strongly to the "first tier" of states $|(v-1)_{CH},2_N\rangle$, which have v-1 C-H stretching quanta and two quanta in "normal" vibrations ν_{N1} and ν_{N2}. These "first tier" states are then coupled to "second tier" states $|(v-2)_{CH},4_N\rangle$, and so on. Inclusion of more than three tiers is theoretically possible, but computationally difficult.

Coupling matrix elements are of the form $\langle v_{CH}|H_{LN}|(v-1)_{CH},2_N\rangle$,

where H_{LN} is the perturbation Hamiltonian between the "local" (C-H) and "normal" modes. Fermi resonances can occur between $\langle v_{CH}|$ and $\langle (v-1)_{CH}, 2_N|$ if $\nu_{CH} \sim \nu_{N1} + \nu_{N2}$. H_{LN} has its origins in anharmonic kinetic coupling in the model of Sibert. A harmonic potential is of the form

$\sum_{i,j} (g_{ij}p_ip_j + f_{ij}q_iq_j)$, where p's and q's are conjugate momenta and positions, respectively. Anharmonic terms used by Sibert et. al. were of the $g_{ijk}p_ip_jp_k$ sort; one of the indices represents the C-H stretch, and the other two represent normal modes. Many kinetic couplings exist; an important one is the stretch-bend coupling, illustrated in Fig. 19. As the C-H bond is stretched, the "effective mass" (or moment of inertia) of the bending motion increases. This lowers the frequency of the bending, lessening the amount of energy in bending motion. The nearly 2:1 frequency ratio of stretching to bending mode makes this coupling between $|v_{CH}\rangle$ and $|(v-1)_{CH}, 2_{bend}\rangle$ resonantly enhanced.

Magnitudes of the matrix elements of H_{LN} are about 25 cm^{-1} for the strongly coupled states. This sets the scale of the breadth of a local mode band. Weakly-coupled and far-off-resonance states can be ignored. For example, first tier states with $\nu_{N1} + \nu_{N2}$ more than ~ 50 cm^{-1} away from ν_{CH} are often not effectively coupled to the local mode unless the matrix element of H_{LN} is in the tens of cm^{-1}.

The perturbed local mode wave function is then given by

$$\sum_n a_n|\psi_n\rangle.$$

where $|\psi_n\rangle$, in a three-tier calculation of $|6_{CH}\rangle$, is of the form of $|6_{CH}, 0_N\rangle$, $|5_{CH}, 2_N\rangle$, $|4_{CH}, 4_N\rangle$, or $|3_{CH}, 6_N\rangle$. In Sibert's three-tier

calculation, ~ 150 terms were included. The absorption spectrum $\Sigma(\omega)$ is expressed as

$$\Sigma(\omega) = \sum_n |\langle v_{CH}|\psi_n\rangle|^2 \delta(\frac{E_n}{\hbar} - \omega);$$

such a "stick spectrum" is shown in Fig. 20.

The bandwidths of the v = 5-7 local modes of benzene calculated by Sibert et al. to be ~ 50 cm^{-1}, are not very different from the RHB experimental values. Such a width is, however, quite large compared with our 10 cm^{-1} bandwith of the v = 3 band. If the local mode behavior persists with increasing v, we would expect the experimental v > 3 band envelopes not to exceed 10 cm^{-1} in width. This would contradict the theoretical results. To be certain, spectra for the v = 1-3 bands should be calculated using Sibert's model.

There are two obvious shortcomings in Sibert's model which could be remedied. First is the neglect of anharmonic potential (as opposed to kinetic) coupling, of the form of $f_{ijk}q_iq_jq_k$. This was justified on the basis of small anharmonic terms in the vibrational force field calculated by Pulay et al[90], but has not been experimentally verified. The second is the omission of cubic couplings (kinetic or potential, represented by terms $g_{ijkl}p_ip_jp_kp_l$ and $f_{ijkl}q_iq_jq_kq_l$ in the Hamiltonian) of the form $\langle v_{CH}|H_{LN}|(v-1)_{CH},3_N\rangle$. They could be significant as, for example $|1_{CH}\rangle$ (ν_{20}) is nearly degenerate and effectively coupled with a $|3_N\rangle$ state composed of the normal modes ν_1, ν_6, and ν_{19} of benzene.

We have discussed here one of the most widely known theories for the local mode spectra and dynamics of benzene. It is unique in that

it predicts the detailed vibrational structure of a local mode overtone band. Other theories simply calculate the width of such a band.[47-49] They are much more statistical in nature; average densities of states and average coupling matrix elements can be used in the calculations. They do not predict detailed absorption spectra that could be compared with our results. Furthermore, since they are parameterized to agree with the room-temperature experimental bandwidths of RHB, the results predictably contradict our experimental finding.

B. Modifications to theories

It is generally difficult to calculate the local mode overtone absorption spectrum of a large, anharmonic molecule. If one used the normal-mode picture to calculate an IR spectrum for the C-H stretching overtones of benzene from combinations of C-H stretching fundamentals, three bands would be expected[44] in the $v = 2$ (6000 cm^{-1}) region. [Fundamental C-H stretches occur in a_{1g}, b_{1u}, e_{2g}, and e_{1u} symmetries. Only three pairwise combinations of these fundamentals can give the IR-active e_{1u} symmetry.] If the IR-active Fermi triad at $v = 1$ is taken into account, seven bands[91] instead of three should show up. These numbers fall far short of the ~ 25 bands we actually observed at $v = 2$. Surely there are other couplings which have yet to be included to account for such a spectrum. The approach of Sibert et al. seems to be appropriate, if modifications can be made to include cubic couplings and potential as well as kinetic anharmonicity. Inclusion of potential anharmonicity will require improvement of the benzene intramolecular vibrational force field. The results of our experiment, listed in Table I, can provide part of the requisite input data concerning line frequencies and intensities for the calculation. Raman and other

studies of the vibrations would help to refine the values of the anharmonic coupling constants.

Realistic calculations of room temperature spectra must include contributions from "hot" molecules. This would require an understanding of anharmonic frequency shifts and the change in local mode absorptions induced by low-frequency vibrations in the hot molecules.

C. Other experiments at similar total vibrational energies

Previous experiments on benzene have given results similar to ours when the question of homogeneous linewidths vs. total vibrational energy was addressed. The two-photon absorption study of the vibration-assisted $\tilde{A} \leftarrow \tilde{X}$ transition by Aron et. al.[92] on molecules in a supersonic beam showed that the lifetime broadening of the vibrational state at 6000 cm^{-1} in the excited $\tilde{A}$ state is less than ~ 3 cm^{-1}. Another molecular beam experiment by Chernoff et. al.[93] used vibrational-assisted fluorescence from the $\tilde{A}$ state to study vibrational states up to ~ 10,000 cm^{-1} in the electronic ground state $\tilde{X}$. The results showed that homogeneous broadening of the fluorescent lines was limited to at most 5 cm^{-1}. In both of these experiments, most of the vibrational energy appeared in the totally symmetric, ~1000 cm^{-1} "breathing mode". They suggest that this mode is only weakly coupled with other modes, since the molecule does not change its shape as the carbon ring expands and contracts.

D. Future studies

Our experiments coud be repeated with better laser sources. Nanosecond laser pulses with transform-limited linewidth (~ .001 cm^{-1}) and good amplitude stabilty are obtainable. Their application could

allow single (J,K) state selection, and hence a better resolution of the vibrational transitions in the local mode bands as well as a more reliable determination of the homogeneous broadening. This would facilitate a better spectral analysis and lifetime estimates.

Studies of overtone transitions in vibrationally hot molecules would give insight into the nature of the anharmonic coupling between the C-H overtones and the low-frequency modes. This could be achieved by using a warmer sample and selectively probing the UV "hot band" transitions. It should then be possible to see how the room-temperature spectra are composed.

Of course, it is desirable to extend the study to higher overtone bands ($v = 4, 5, \ldots$). To do so with our technique would require development of a tunable laser in the near IR - visible range with large pulse energies (hundreds - thousands of mj), because of the rapid decrease of the absorption cross section with increasing v, as described in Fig. 3. The peak intensity should, however, be sufficiently low in order to avoid nonlinear optical processes that may yield spurious signals, such as multiphoton electronic transitions and stimulated Raman scattering.

It is also desirable to obtain similar overtone spectra on substituted molecules. The vibrational analyses of molecules have traditionally included the spectroscopy of an entire family of isotopically substituted molecules. Substitution of an atom is a convenient, controlled, and predictable way to make slight shifts in the frequencies of a few modes. This greatly facilitates assignment of transitions in nearly-degenerate modes. When the symmetry is lowered, it also causes some formerly forbidden transitions to become weakly

allowed. In this case the study of deuterated benzenes[91,94,95] is mandated. The coupling between stretches of C-H and C-D bonds is expected to be quite weak, since the frequencies differ by ~1000 cm^{-1}. If couplings between identical bonds were the major hindrance to local behavior, then the local mode is be expected to appear at a lower level of excitation in partially deuterated benzene than in benzene-h_6. On the other hand, stretch-bend coupling might not be affected much. The experiments of RHB did include extensive spectroscopy of deuterated and other substituted benzenes. Their experiments should, however, be repeated in a cold molecular beam using the state-selective technique.

E. Related problems

There are several research problems on polyatomic molecular vibrations that are related to this work. Calculations of the force fields[90,91,94,95] rely on spectroscopic data on frequencies and intensities of various vibrational transitions. Determination of the anharmonic force constants has typically been extremely difficult, and has largely been theoretical, without experimental confirmation. Our spectra provide some data to check the calculations on benzene. Likewise, the availability of a benzene dimer spectrum will facilitate calculations of the intermolecular potential.[86] Our observation of the combination bands with the van der Waals modes is especially advantageous in that respect. It is the next best thing to finding the frequencies of the van der Waals modes themselves.

Vibrational relaxation has received considerable attention in many circumstances. It is an important factor affecting IR stepwise multiphoton excitation and dissociation. A frequent claim has been that vibrational energy randomization is so rapid that the weakest bond

in a molecule is always the first to break, independent of which vibrational mode is initially excited. Energy drain out of the excited mode via vibrational relaxation is faster than the excitation of the mode. With the local mode, however, if the psec lifetimes we observed were to persist up to the dissociation level, selective bond breaking might still be possible with psec IR multiphoton pumping.

VII. CONCLUSION

We have reported on what we believe to be the first high-resolution, state-selective study of local modes in a large molecule -- benzene. The technique we used was a combination of rotational cooling in a supersonic beam expansion and multilevel, state-selective saturation spectroscopy. There is no doubt that the room-temperature local mode overtone spectra of large molecules previously published have had inhomogeneous congestion. Broad "rotational envelopes" and "hot bands" appear to be the culprits. Linear absorption measurements on room-temperature samples simply cannot uncover the wealth of detail which is present in the spectra.

Many suspected but heretofore undetected perturbations between the local and other vibrational modes obviously occur. Judging from the appearances of the overtone spectra of the monomer and dimer, we conclude that the "local mode" description of the benzene C-H stretches applies to $v \geq 3$. Perturbation matrix elements change from ~ 25 cm^{-1} at $v = 1$ to ~ 2 cm^{-1} at $v = 3$. Our linewidth measurements show that the lifetimes of the C-H stretching vibration exceed a few psec, even at a total energy of ~8800 cm^{-1}. This is in accordance with lifetime data on other vibrational modes of benzene excited to similar

energies. In the absence of direct lifetime measurements of the local mode states, these lifetime estimates based on the measured linewidths are likely to be only a lower bound.

All in all, we believe that a new perspective on vibrational relaxation rates and local mode behavior may be called for. Our results on the local modes of the prototypical large molecule paint a picture different from the earlier one the experimentalists have sometimes believed in, and the theorists have strived to explain. In that context it appears that the model of Sibert et. al.[26] has much merit in its approach. However, as their calculation has not included the local mode bands we have studied, we appeal to the theorists to renew their efforts.

Our measurements of the C-H stretching spectra of the benzene dimer could help to resolve questions concerning its intermolecular potential, structure, and vibrational predissociation lifetime. They support the hypothesis that the dimer is T-shaped. New lines around the C-H stretching fundamental band have been observed which show that the van der Waals stretching frequency is - 30 cm^{-1}. Certainly, the dimer's vibrational predissociation lifetime is in excess of a few psec at 3000 cm^{-1} vibrational energy.

References

1. E. B. Wilson, Jr., J. C. Decius, and P. C. Cross, Molecular Vibrations (McGraw-Hill, New York, 1955).

2. G. Herzberg, Molecular Spectra and Molecular Structure. II. Infrared and Raman Spectra of Polyatomic Molecules (Van Nostrand Reinhold, New York, 1945).

3. R. Mecke, Z. Physik 101, 405 (1936).

4. B. R. Henry, Accounts of Chemical Research 10, 207 (1977).

5. M. S. Child and R. T. Lawton, Faraday Discussions of the Chemical Society 71, 273 (1981).

6. M. L. Sage and J. Jortner, Advances in Chemical Physics 47, part I, 293 (1981).

7. M. S. Child and L. Halonen, Advances in Chemical Physics 57, 1 (1984).

8. P. M. Morse, Phys. Rev. 34, 57 (1929).

9. R. J. Hayward and B. R. Henry, J. Mol. Spectrosc. 57, 221 (1975).

10. B. R. Henry and W. Siebrand, J. Chem. Phys. 49, 5369 (1968).

11. R. J. Hayward and B. R. Henry, J. Mol. Spectrosc. 46, 207 (1973).

12. R. L. Swofford, M. E. Long, and A. C. Albrecht, J. Chem. Phys. 65, 179 (1976).

13. M. S. Burberry, J. A. Morrell, A. C. Albrecht, and R. L. Swofford, J. Chem. Phys. 70, 5522 (1979).

14. N. Yamamoto, N. Matsuo, and H. Tsubomura, Chem. Phys. Lett. 71, 463 (1980).

15. R. J. Hayward and B. R. Henry, Chem. Phys. 12, 387 (1976).

16. W. R. A. Greenlay and B. R. Henry, J. Chem. Phys. 69, 82 (1978).

17. O. S. Mortensen, B. R. Henry, and M. A. Mohammadi, J. Chem. Phys.

75, 4800 (1981).

18. B. R. Henry, A. W. Tarr, O. S. Mortensen, W. F. Murphy, and D. A. C. Compton, J. Chem. Phys. 79, 2583 (1983).

19. M. K. Ahmed and B. R. Henry, J. Phys. Chem. 90, 1081 (1986).

20. M. S. Burberry and A. C. Albrecht, J. Chem. Phys. 71, 4631 (1979).

21. E. Fermi, Z. Physik 71, 250 (1931).

22. M. Bixon and J. Jortner, J. Chem. Phys. 48, 715 (1968).

23. F. Lahmani, A. Tramer, and C. Tric, J. Chem. Phys. 60, 4431 (1974).

24. K. F. Freed and A. Nitzan, J. Chem. Phys. 73, 4765 (1980).

25. K. F. Freed and A. Nitzan, in Energy Storage and Redistribution in Molecules, J. Hinze, ed. (Plenum, New York, 1983).

26. E. L. Sibert III, W. P. Reinhardt, and J. T. Hynes, J. Chem. Phys. 81, 1115 (1984); Chem. Phys. Lett. 92, 455 (1982).

27. E. L. Sibert III, W. P. Reinhardt, and J. T. Hynes, J. Chem. Phys. 81, 1135 (1984).

28. P. J. Nagy and W. L. Hase, Chem. Phys. Lett. 54, 73 (1978).

29. D.-H. Lu, W. L. Hase, and R. J. Wolf, J. Chem. Phys. 85, 4422 (1986).

30. K. L. Bintz, D. L. Thompson, and J. W. Brady, J. Chem. Phys. 85, 1848 (1986); Chem. Phys. Lett. 131, 398 (1986).

31. P. R. Stannard and W. M. Gelbart, J. Phys. Chem. 85, 3592 (1981).

32. H.-R. Dübal and M. Quack, J. Chem. Phys. 81, 3779 (1984).

33. G. J. Scherer, K. K. Lehmann, and W. Klemperer, J. Chem. Phys. 81, 5319 (1984).

34. G. A. Voth, R. A. Marcus, and A. H. Zewail, J. Chem. Phys. 81, 5494 (1984).

35. J. W. Perry, D. J. Moll, A. Kuppermann, and A. H. Zewail, J. Chem.

Phys. 82, 1195 (1985).

36. J. E. Baggott, H. J. Clase, and I. M. Mills, J. Chem. Phys. 84, 4193 (1986).

37. A. Campargue and F. Stoeckel, J. Chem. Phys. 85, 1220 (1986).

38. R. J. Bray and M. J. Berry, J. Chem. Phys. 71, 4909 (1979).

39. K. V. Reddy, D. F. Heller, and M. J. Berry, J. Chem. Phys. 76, 2814 (1982).

40. G. A. Voth and R. A. Marcus, J. Chem. Phys. 82, 4064 (1985).

41. K. N. Swamy and W. L. Hase, J. Chem. Phys. 84, 361 (1985).

42. G. A. Voth, J. Phys. Chem. 90, 3624 (1986).

43. M. E. Kellman, J. Phys. Chem. 87, 2161 (1983).

44. L. Halonen, Chem. Phys. Lett. 87, 221 (1982).

45. G. M. Korenowski and A. C. Albrecht, Chem. Phys. 38, 239 (1979).

46. D. F. Heller, Chem. Phys. Lett. 61, 583 (1979).

47. D. F. Heller and S. Mukamel, J. Chem. Phys. 70, 463 (1979).

48. S. Mukamel and R. Islampour, Chem. Phys. Lett. 108, 161 (1984).

49. V. Buch, R. B. Gerber, and M. A. Ratner, J. Chem. Phys. 81, 3393 (1984).

50. S. Mukamel, J. Phys. Chem. 88, 832 (1984).

51. R. Bruinsma, K. Maki, and J. Wheatley, Phys. Rev. Lett. 57, 1773 (1986).

52. M. L. Sage and J. Jortner, Chem. Phys. Lett. 62, 451 (1978).

53. T. Uzer, Chem. Phys. Lett. 110, 356 (1984).

54. B. R. Johnson, R. T. Skodje, and W. P. Reinhardt, Chem. Phys. Lett. 112, 396 (1984).

55. J. Pliva and A. S. Pine, J. Mol. Spectrosc. 93, 209 (1982).

56. J. W. Perry and A. H. Zewail, J. Chem. Phys. 80, 5333 (1984).

57. J. W. Perry and A. H. Zewail, J. Phys. Chem. 86, 5197 (1982).

58. L. J. Butler, T. M. Ticich, M. D. Likar, and F. F. Crim, J. Chem. Phys. 85, 2331 (1986); J. Chem. Phys. 85, 6251 (1986) (erratum).

59. G. A. West, R. P. Mariella, Jr., J. A. Pete, W. B. Hammond, and D. F. Heller, J. Chem. Phys. 75, 2006 (1981).

60. E. S. McGinley and F. F. Crim, J. Chem. Phys. 85, 5741 (1986).

61. G. M. Stewart and J. D. McDonald, J. Chem. Phys. 78, 3907 (1983).

62. Y. R. Shen, The Principles of Nonlinear Optics (John Wiley & Sons, New York, 1984), p.227.

63. T. A. Stephenson, P. L. Radloff, and S. A. Rice, J. Chem. Phys. 81, 1060 (1984).

64. G. H. Atkinson and C. S. Parmenter, J. Mol. Spectrosc. 73, 20 (1978).

65. J. H. Callomon, T. M. Dunn, and I. M. Mills, Phil. Trans. Roy. Soc. London, Ser. A 259, 499 (1966).

66. S. M. Beck, M. G. Liverman, D. L. Monts, and R. E. Smalley, J. Chem. Phys. 70, 232 (1979).

67. J. B. Hopkins, D. E. Powers, and R. E. Smalley, J. Phys. Chem. 85, 3739 (1981).

68. P. R. R. Langridge-Smith, D. V. Brumbaugh, C. A. Haynam, and D. H. Levy, J. Phys. Chem. 85, 3742 (1981).

69. K. H. Fung, H. L. Selzle, and E. W. Schlag, J. Phys. Chem. 87, 5113 (1983).

70. K. S. Law, M. Schauer, and E. R. Bernstein, J. Chem. Phys. 81, 4871 (1984).

71. Lasertechnics Inc., Albuquerque, New Mexico.

72. Johnston Laboratories, Towson, Maryland.

73. Quanta-Ray (Spectra-Physics, Inc.), Mountain View, California.

74. Exciton Chemical Co., Inc., Dayton, Ohio.

75. J. R. Nestor, Applied Optics 21, 4154 (1982).

76. A. P. Simonov, G. A. Abakumov, V. T. Yaroslavtzev, V. A. Lundrev, and E. A. Fedorov, Laser Chem. 5, 275 (1985).

77. B. S. Freiser and J. C. Beauchamp, Chem. Phys. Lett. 35, 35 (1975).

78. H. H.-I. Teng and R. C. Dunbar, J. Chem. Phys. 68, 3133 (1978).

79. N. B. Lev and R. C. Dunbar, Chem. Phys. Lett. 84, 483 (1981).

80. K. G. Owens and J. P. Reilly, J. Opt. Soc. Am. B2, 1589 (1985).

81. K. O. Börnsen, H. L. Selzle, and E. W. Schlag, J. Chem. Phys. 85, 1726 (1986).

82. I. Nishiyama and I. Hanazaki, Chem. Phys. Lett. 117, 99 (1985).

83. R. D. Johnson, S. Burdenski, M. A. Hoffbauer, C. F. Giese, and W. R. Gentry, J. Chem. Phys. 84, 2624 (1986).

84. M. F. Vernon, J. M. Lisy, H. S. Kwok, D. J. Krajnovich, A. Tramer, Y. R. Shen, and Y. T. Lee, J. Phys. Chem. 85, 3327 (1981).

85. R. E. Miller, private communication.

86. M. Schauer and E. R. Bernstein, J. Chem. Phys. 82, 3722 (1985).

87. K. C. Janda, J. C. Hemminger, J. S. Winn, S. E. Novick, S. J. Harris, and W. Klemperer, J. Chem. Phys. 63, 1419 (1975).

88. J. M. Steed, T. A. Dixon, and W. Klemperer, J. Chem. Phys. 70, 4940 (1979).

89. C. A. Haynam, D. V. Brumbaugh, and D. H. Levy, J. Chem. Phys. 79, 1581 (1983).

90. P. Pulay, G. Fogarasi, and J. E. Boggs, J. Chem. Phys. 74, 3999 (1981); P. Pulay, J. Chem. Phys. 85, 1703 (1986).

91. S. Brodersen and A. Langseth, Mat. Fys. Skr. Dan. Vid. Selsk. 1,

1 (1956).

92. K. Aron, C. Otis, R. E. Demaray, and P. Johnson, J. Chem. Phys. 73, 4167 (1980).

93. D. A. Chernoff, J. D. Myers, and J. G. Pruett, J. Chem. Phys. 85, 3732 (1986).

94. S. N. Thakur, L. Goodman, and A. G. Ozkabak, J. Chem. Phys. 84, 6642 (1986).

95. A. G. Ozkabak, L. Goodman, S. N. Thakur, and K. Krogh-Jespersen, J. Chem. Phys. 83, 6047 (1985); J. Chem. Phys. 85, 2346 (1986) (erratum).

Table I. Fundamental and overtone transitions observed in the benzene molecule.

frequency (cm^{-1})	intensity (arb. units)	remarks
v = 1		
3048 ± 0.5	5	"ν_{20}"
3079	4	"$\nu_1 + \nu_6 + \nu_{19}$"
3101	6	"$\nu_8 + \nu_{19}$"
v = 2		
5865 ± 1	1	
5873	1	
5878	1	
5882	2	
5899	3	
5908	2	
5926	4	
5934	8	
5947	6	
5957	4	
5967	2	
5974	5	
5980	5	
5987	6	
5993	2	
6001	12	
6006	25	saturated (intensity is 17 in Fig. 13)
6018	7	
6025	3	
6035	1	
6042	2	
6051	2	
6064	2	
6113	2	
6126	1	
6135	1	
6145	1	
6156	2	
6162	2	
6171	1	
v = 3		
8806 ± 2	1	
8827	6	unresolved bands
8854	1	
8878	1	

FIGURE CAPTIONS

Fig. 1. $v = 0$-3 manifolds in a molecule with at least 3 identical bonds which can share the v quanta. Each bond i has the Morse-oscillator energy levels $E(v_i) = \omega(v_i + 1/2) - x(v_i + 1/2)^2$. The "local mode" state has all quanta in the same bond and is the lowest in each manifold by $2(v-1)x$, and is shown with a heavy line. V_{nm} is the perturbation between the local mode and next nearest states. "Local" behavior can occur when $V_{nm} << 2(v - 1)x$.

Fig. 2. Modifications to the absorption spectrum of a local mode (assumed to possess all the zeroth-order oscillator strength) when it is coupled to (a) one state (i. e. "Fermi resonance"); (b) several states; (c) a continuum. In each case, $\bar{V}$ is the magnitude of the perturbation matrix element between the local mode and the other states, and γ_{rad} is the radiative decay rate of the local mode.

Fig. 3. C-H stretch overtone absorption spectra of room temperature benzene gas, reprinted from Ref 39 with permission. Spectral assignments in terms of the number of C-H stretching quanta appear in the upper-right-hand corner of each panel, along with $\bar{\nu}_o$, the positions (in cm^{-1}) of the band centers or maxima. Dashed lines indicate deconvolved spectral features, and horizontal double arrows identify FWHM bandwidths. The 30 cm^{-1} room-temperature rotational envelope is seen in the $v = 1$ spectrum, known to be composed of unresolved sharp lines. Other authors have used these spectra to estimate "homogeneous" linewidths of $v \geq 2$ bands.

Fig. 4. Effect of cooling on the rotational state distribution and width of the rotational envelope of a diatomic rovibrational band. ω_{vib} is the vibrational frequency of the transition, and B is the rotational constant (inverse moment of inertia.) Cooling depopulates the higher J" ground states, shrinking the band, whose width is proportional to $\sqrt{T}$.

Fig. 5. Three-level saturation spectroscopy ("inverted Λ") scheme. (a) ω_{probe}, tuned to resonance with the $|e\rangle \leftarrow |g\rangle$ transition, measures the population in three states belonging to $|g\rangle$. ω_{pump} induces transitions from $|g\rangle$ to $|v\rangle$, the states being studied. The depletes the population being probed, and diminishes the probe signal. Scanning ω_{pump} with ω_{probe} fixed gives the $|v\rangle \leftarrow |g\rangle$ spectrum. (b) Resulting spectrum; six lines occur (3 $|g\rangle$ states each have transitions to 2 $|v\rangle$ states) but are not completely resolved.

Fig. 6. (a) "Inverted Λ" double resonance scheme, as applied to benzene. Only vibrational-ground-state molecules are probed with resonantly-enhanced two-photon ionization (R2PI) via the $\tilde{A} \leftarrow \tilde{X}$ 6_0^1 transition at 38608 cm^{-1}. Other thermally populated vibrational levels which contribute to a linear absorption spectrum are present at 399, 608, 674, and 707 cm^{-1}. Overtone pumping decreases the population of electronic-ground-state molecules, decreasing the probe (ion) signal. Molecules which are not in the vibrational ground state engage in "hot band" overtone transitions but do not contribute to the observed spectrum. (b) High resolution R2PI spectrum of the 6_0^1 band showing P ($\Delta J = -1$), Q ($\Delta J = 0$), and R ($\Delta J = +1$) bands. (c)

Simulated spectrum of the 6_0^1 band. The rotational temperature is determined to be 5°K. $J'' \leq 8$ levels have the largest populations.

Fig. 7. Diagram of experimental apparatus. Overlapped, tunable, focused IR (pump) and UV (probe) laser beams intersect the pulsed molecular beam between a set of ion extraction plates. The ion signal is mass-resolved and detected with a Johnston electron multiplier. A digital computer scans the IR wavelength, chops the IR laser beam, and records spectra.

Fig. 8. Dual Beam Technique for eliminating laser-induced fluctuations in the proble signal. (a) Apparatus: P - source of diverging input beam. SS - beam splitter (Suprasil flat.) L - lens. Ff, Fb - foci of beams from front and back of beam splitter. P - ion extraction plates. E - extraction field. The beamsplitter forms the UV beam diverging from point P into two parallel, non-paraxial beams. The lens focuses them at different points in the ion extraction field. Ion flight times to the detector differ for the two foci. (b) Schematic oscillogram of ion multiplier output showing that the ion signals from the two foci are well separated, and that masses 78 and 79 are nearly resolved.

Fig. 9. Angular momenta of benzene and selection rules for the $\tilde{A} \leftarrow \tilde{X}$ and C-H stretching transitions, which are both polarized in the plane of the molecule. (They are "perpendicular" transitions.) K is the projection of $\vec{J}$ on the symmetry axis.

Fig. 10. (a) Symmetric top transition frequencies in the P ($\Delta J = -1$), Q ($\Delta J = 0$), and R ($\Delta J = +1$) branches vs. J", the ground state

angular momentum. The K" dependence has been suppressed. The excited state rotational constant B' is less than B", the ground state constant. This causes a quadratic dependence of ω on J", as occurs in the $\tilde{A} \leftarrow \tilde{X}$ transition in benzene. The spacing between transitions is greatest in the P branch. The rotational distribution "cuts off" at Jmax. (b) The mapping of transitions from state J_0 onto the absorption spectrum.

Fig. 11. Energies of (J,K) rotational levels in benzene. The rotational Hamiltonian is $E(J,) = B[J(J + 1) - K^2/2]$. States with K = 0 have $E_{rot} = BJ^2$; states with K = J, the lowest in each J manifold, have $E_{rot} = BJ^2/2$. At low temperatures, the states with K ~ J are most highly populated.

Fig. 12. Composite spectra of a single vibration-rotation band obtained with state-selective three-level saturation spectroscopy. Different groups of rotational states are probed in each case, and the pump frequency is scanned. (a) Probe is tuned to UV Q branch. Nearly all (J,K) states contribute to the probe signal. There are four intense branches: ^{P}P, ^{r}Q, ^{P}Q, and ^{r}R. (b) Angular momentum of probe population is increased, and branches begin to be resolved. (c) Probe population has high angular momentum J. Positions of the four IR branches depend on ζ, the Coriolis constant. In this example $\zeta \sim -1/3$. Observed linewidths always exceed ~1 cm^{-1}, the convolution of the pump and probe linewidths, even if a single state is probed.

Fig. 13. Nonselective spectra of benzene monomer overtone transitions to (a) v=1, (b) v=2, and (c) v=3. Absorption is in arbitrary

units. Frequencies of band maxima (band center for v=1) in cm^{-1} are indicated. Error bars indicate the amplitude of the noise.

Fig. 14. Rotational-state-selective probing of the fundamental (v=1) 3048 cm^{-1} band. P and R branches are observed to separate as J" is increased in (a) through (d). FWHM linewidths of these branches are ~1 cm^{-1}, the lower limit with our system resolution of 1 cm^{-1}. Error bars indicate the amplitude of the noise.

Fig. 15. Spectra of 8827 cm^{-1} intense v=3 peak with different rotational state selection conditions. The noise level in each spectrum is indicated with an error bar. (a) Q branch probing of the majority of the rotational states significantly populated in the molecular beam. (b) Probing a group of states with J ~ 27. (c) Probing a group of states with J ~ 32. (d) Repeat of (c) with UV dye laser in high resolution (0.1 vs. 0.3 cm^{-1}) mode. Three peaks (two overlapping P branches and two R branches) are observed, showing that the peak in part (a) contains at least two vibrational transitions.

Fig. 16(a-c) Nonselective spectra of benzene dimer overtone transitions, as in Fig. 3. (a) v = 1 features at 3014 and 3072 cm^{-1} are combination bands with ~30 cm^{-1} van der Waals stretch motions. The shoulder at 3040 cm^{-1} could be the "hot band" predicted to appear at 3039 cm^{-1}. (b,c) v = 2,3 dimer bands are broadened with respect to those of the monomer. This would occur if the C-H bonds were not identical in the

dimer.

Fig. 17. T-shaped benzene dimer. (a) Structure of dimer. Molecule A is nearly a monomeric free rotor about the $\hat{z}$ axis. The rotation of molecule B about its sixfold axis $\hat{R}$ is strongly hindered by the van der Waals bond. The moment of inertia associated with the dimer's tumbling motion is several times the monomer's. van der Waals stretching is relative motion of A and B along the $\hat{z}$ axis. (b) Transitions observed and predicted around the 3047 cm^{-1} band. The van der Waals stretching frequency is 33 cm^{-1} in the ground state and 25 cm^{-1} in the vibrationally excited state. Observed features at 3014 and 3072 cm^{-1} are combination bands. The band at 3039 cm^{-1} is predicted to occur and is weakly observed as a shoulder on the 3047 cm^{-1} band. See Fig. 16(a) for the spectrum.

Fig. 18. Three tier scheme of Sibert et. al. for calculating local mode spectra and dynamics. The pure C-H stretching local mode is anharmonically coupled to combination vibrations involving normal modes. Fermi resonance couples one C-H stretch quantum with two normal mode quanta. The $v = 6$ local mode state and the first two tiers of normal modes are shown. "First tier" states $|5_{CH}, 2_N\rangle$ are as calculated; "second tier" states $|4_{CH}, 4_N\rangle$ are schematic. Further tiers are not displayed.

Fig. 19. Stretch-bend interaction, resulting in coupling between local and normal modes in benzene. Changing the C-H bond length s modifies the "effective mass" of the bending motion β. This

changes the amount of energy in bending motion, so that the stretch and bend are coupled.

Fig. 20. Stick spectra calculated with the three tier model for the v = 5, 6, and 9 local mode bands. Sticks in the spectrum represent redistribution of the local mode's oscillator strength into the normal modes. Spectral envelope widths agree roughly with room-temperature data (Fig. 3.)

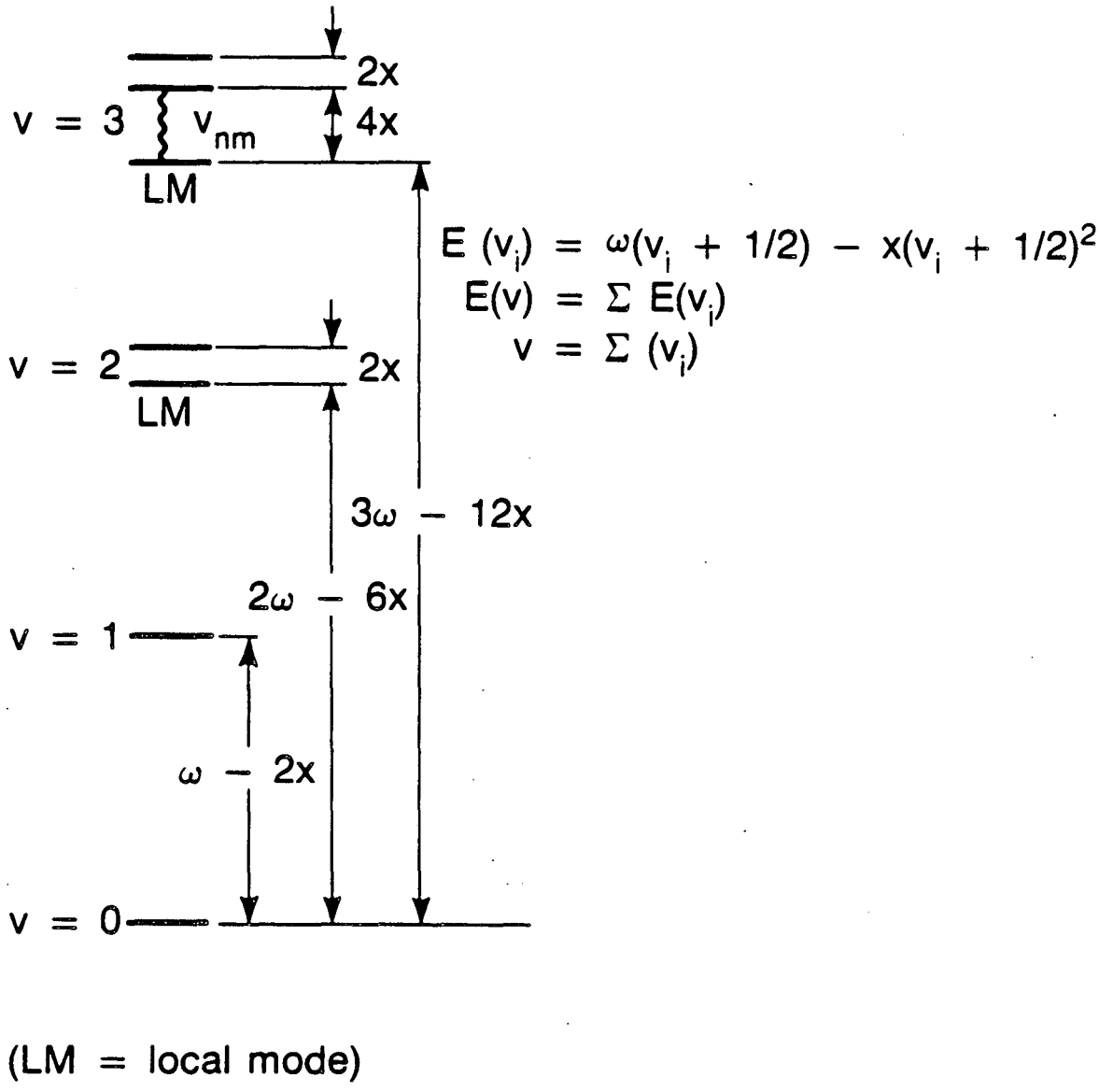

XBL 872-6134

Figure 1.

Crude model of local mode coupling with other modes

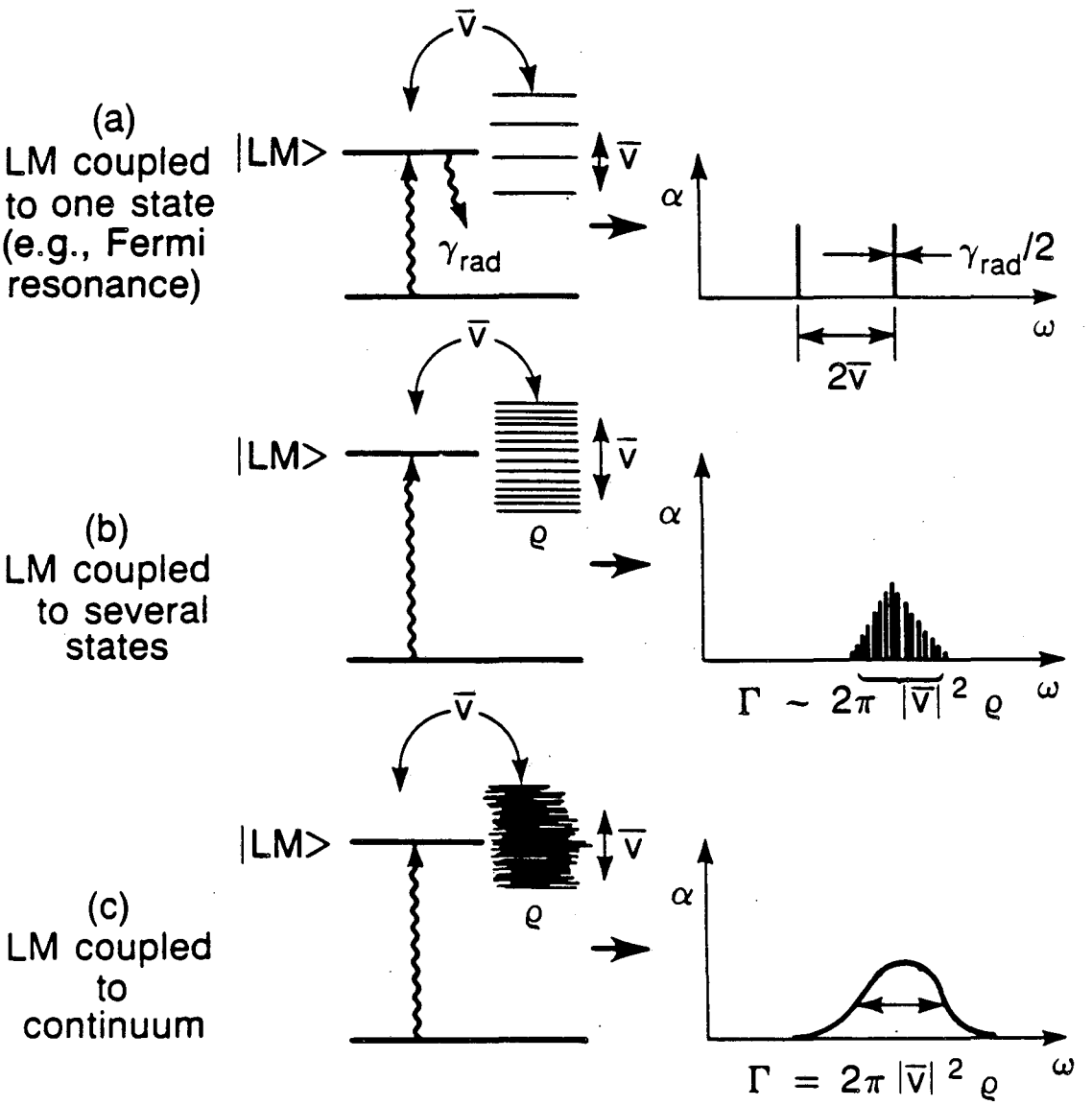

XBL 872-6163

Figure 2.

Room temperature absorption spectra of benzene gas

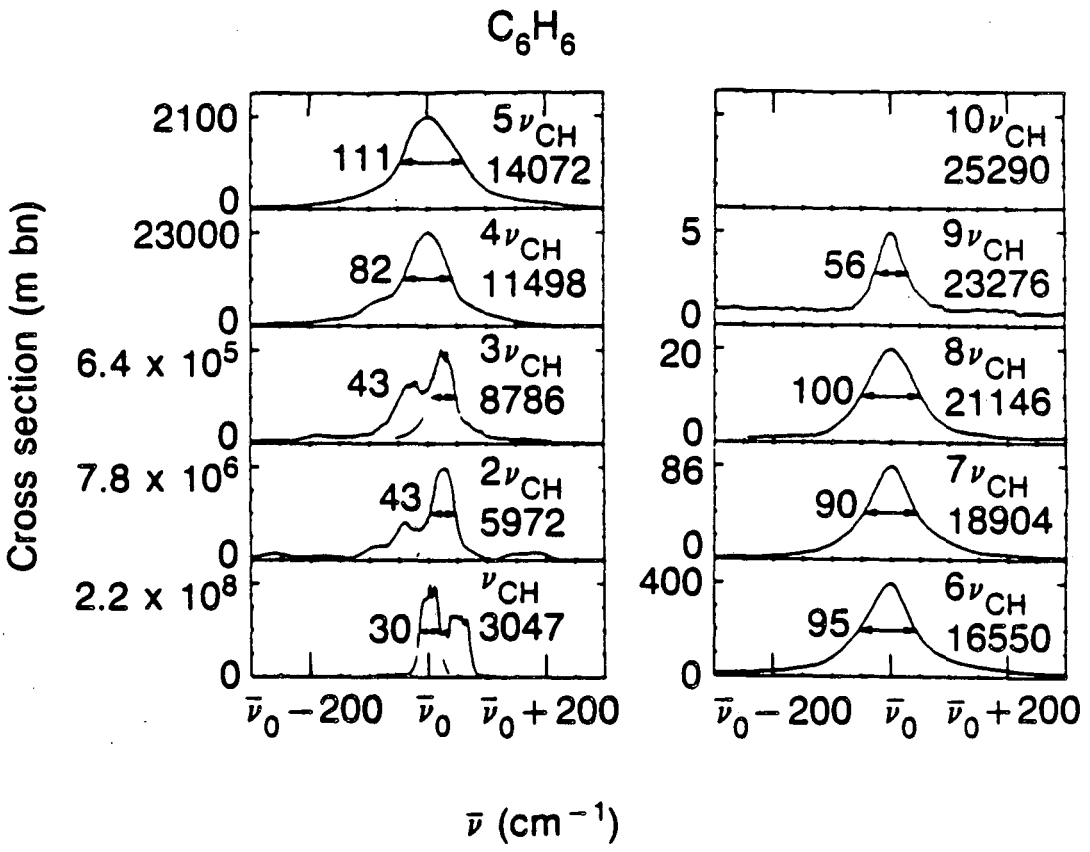

XBL 872-6150

Figure 3.

Diatomic vibration — rotation band at different temperatures

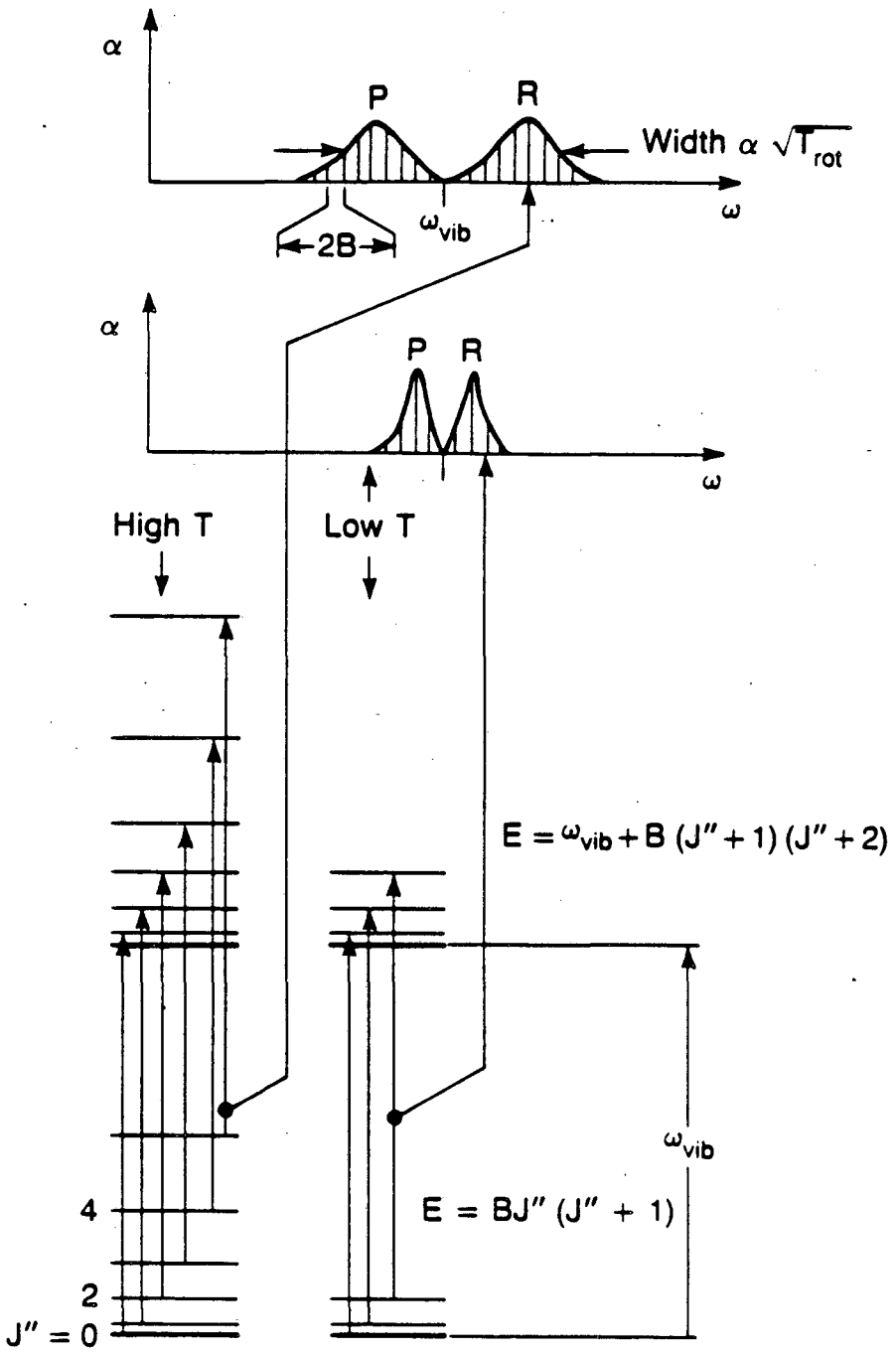

XBL 872-6126

Figure 4.

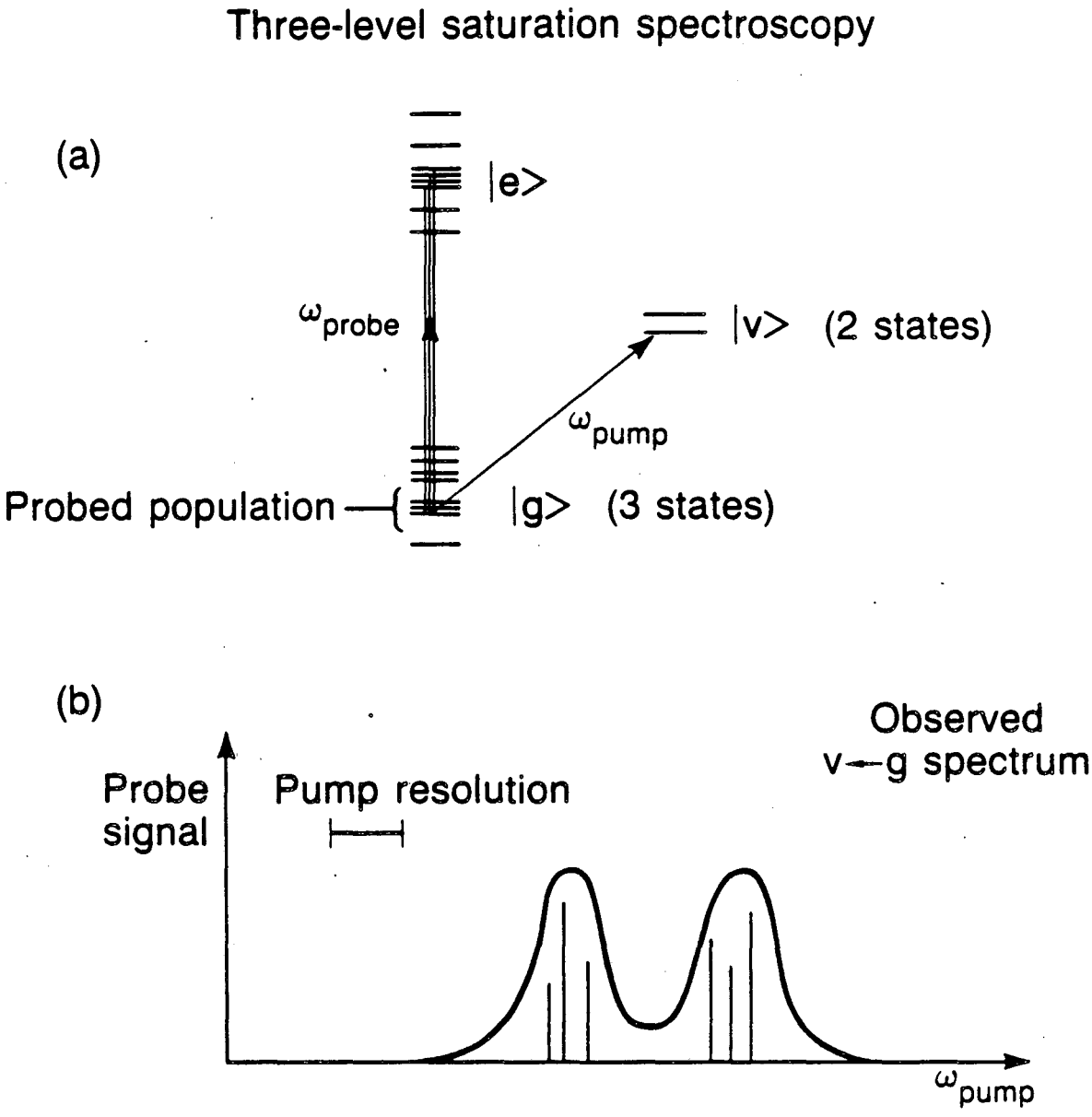

Figure 5.

XBL 872-6128

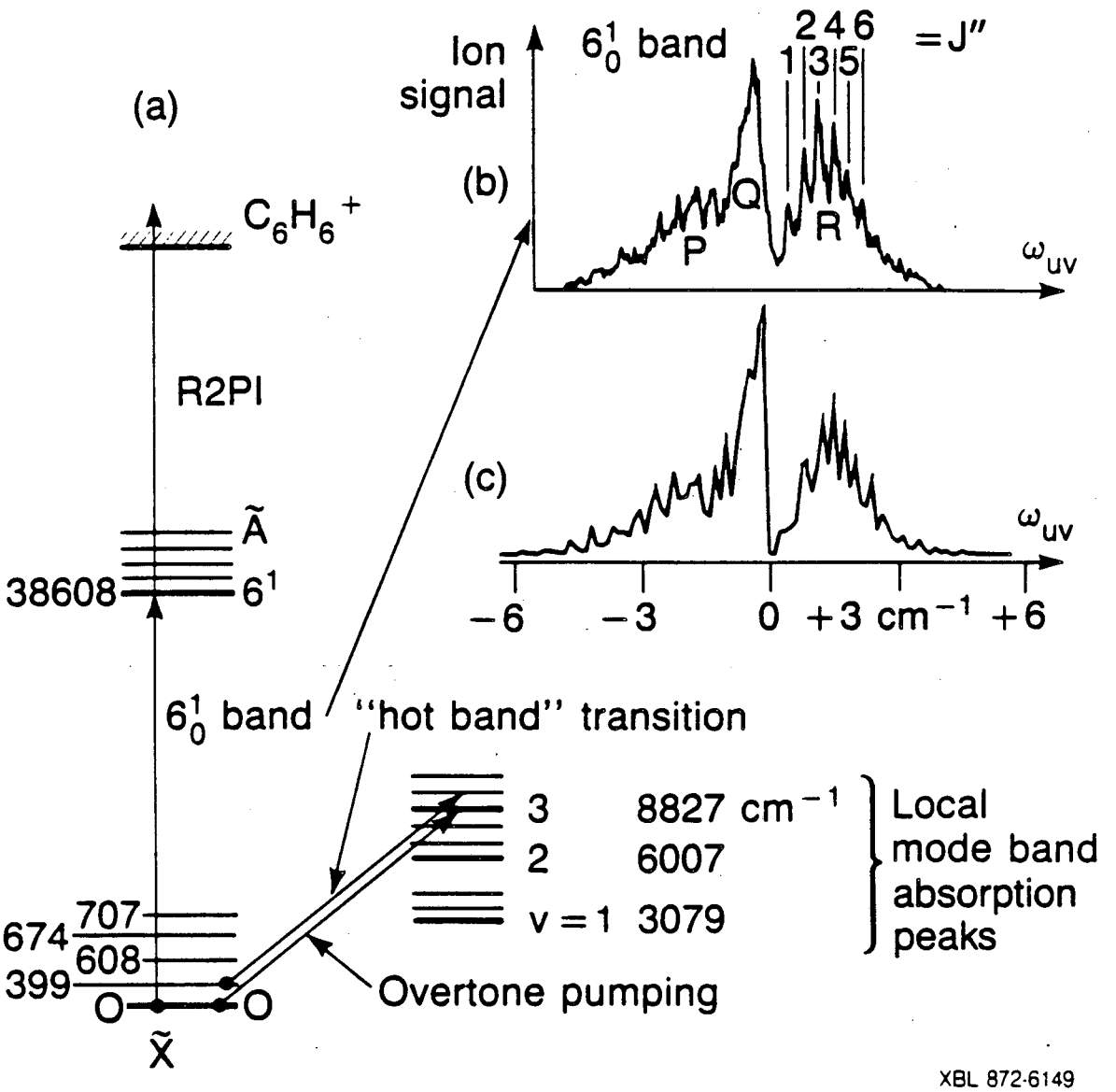
Implementation of three-level saturation spectroscopy
(a)
$C_6H_6^+$
R2PI
$\tilde{A}$
38608
6^1
6_0^1 band
"hot band" transition
674
707
608
399
O
O
$\tilde{X}$
Overtone pumping
3
8827 cm^{-1}
2
6007
v = 1
3079
Local mode band absorption peaks
Ion signal
(b)
6_0^1 band
1 3 5
2 4 6
=J"
P
Q
R
ω_{uv}
(c)
ω_{uv}
−6
−3
0
+3 cm^{-1}
+6
XBL 872-6149

Figure 6.

Experimental Arrangement

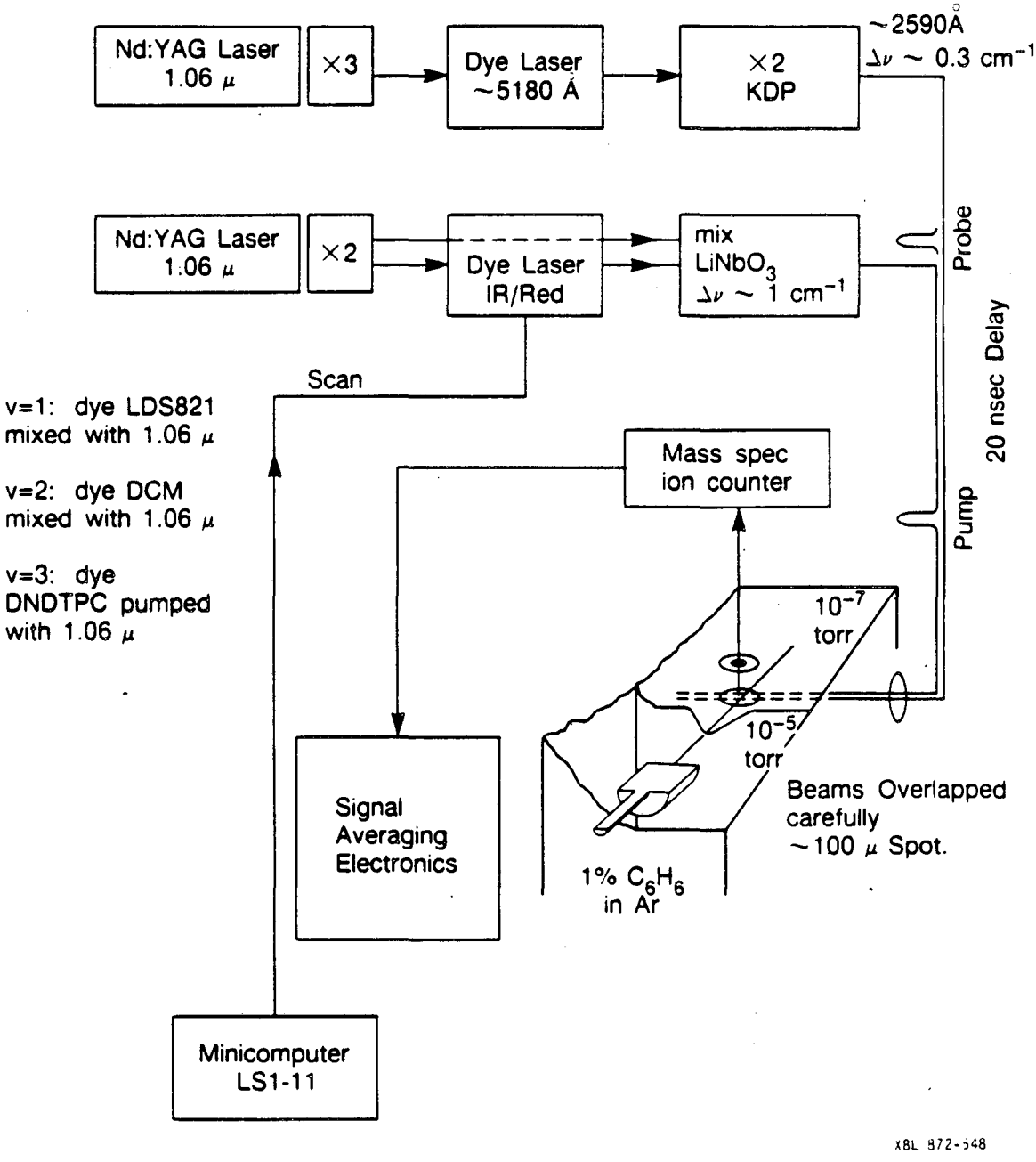

Figure 7.

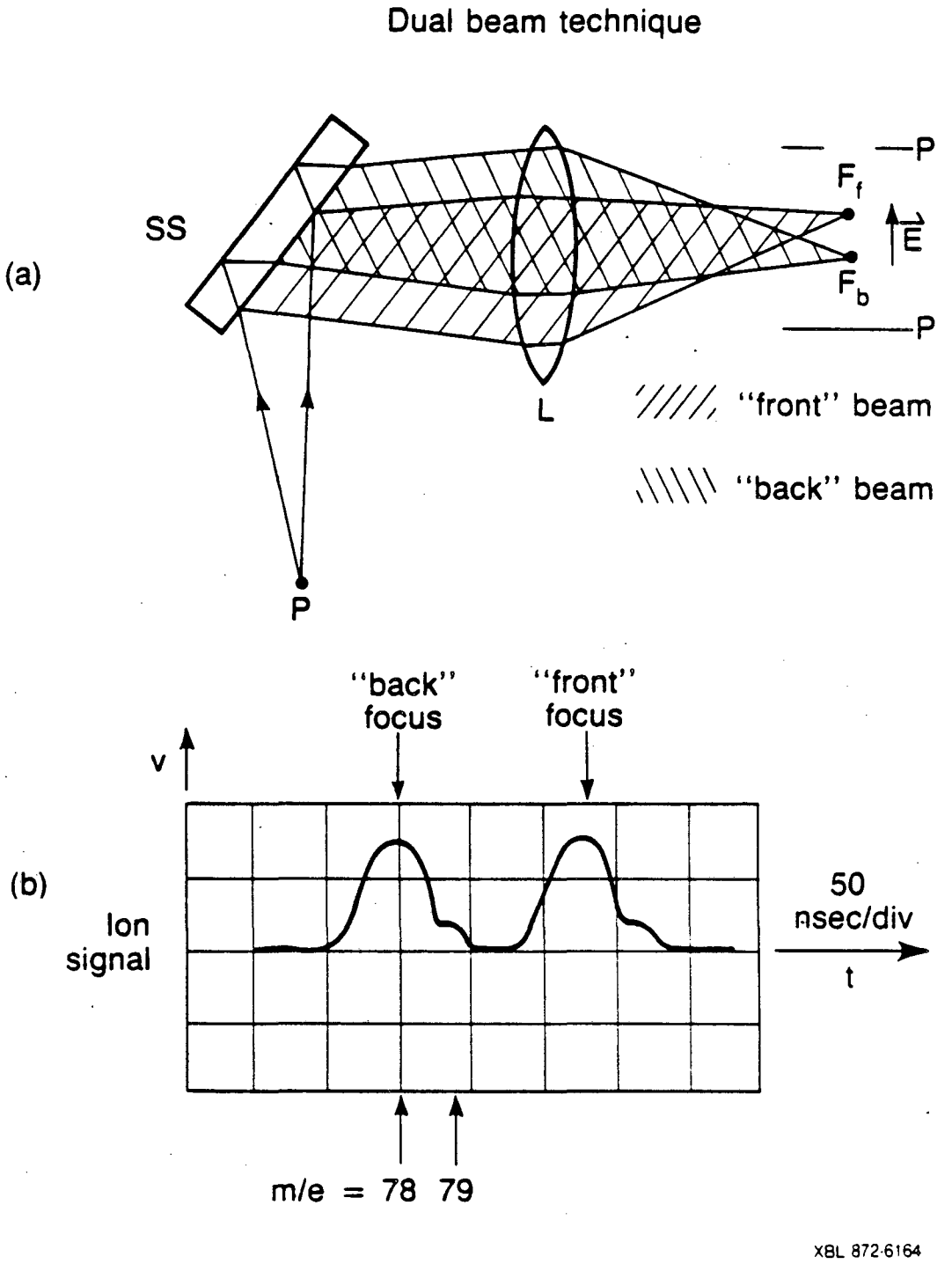
Dual beam technique
(a)
SS
P
F_f
F_b
P
P
L
E
"front" beam
"back" beam
(b)
"back" focus
"front" focus
v
Ion signal
50 nsec/div
t
m/e = 78 79
XBL 872-6164

Figure 8.

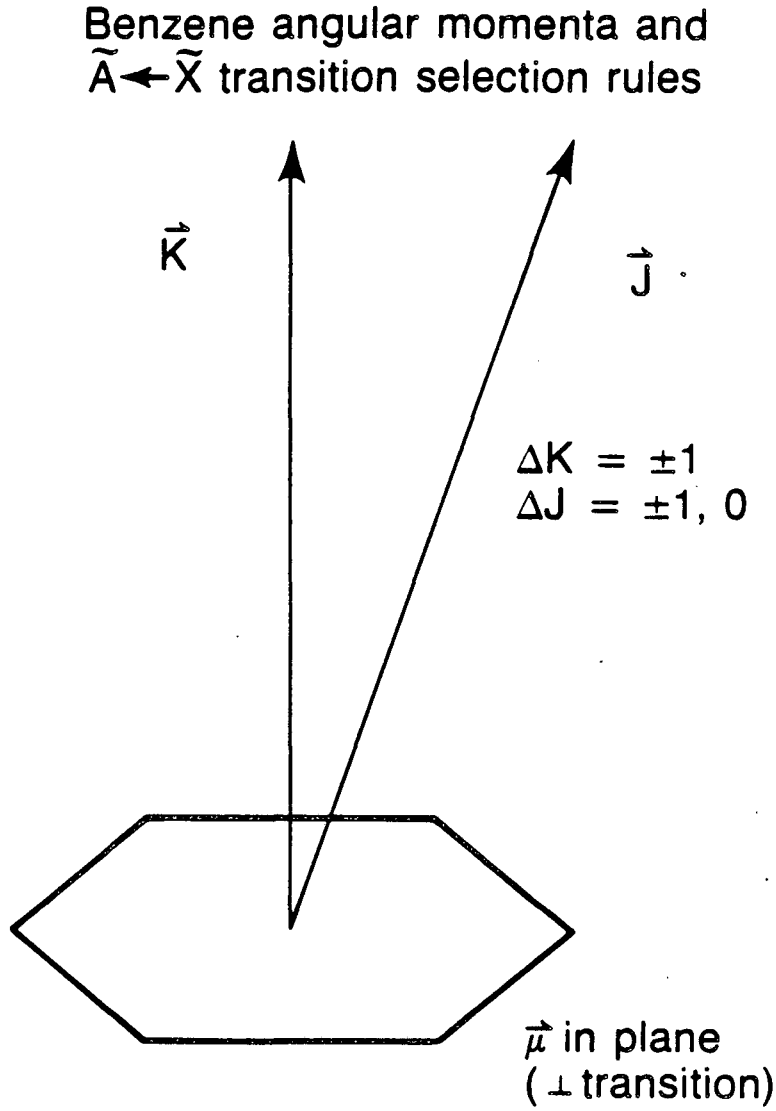
Benzene angular momenta and
$\tilde{A} \leftarrow \tilde{X}$ transition selection rules
$\vec{K}$
$\vec{J}$
$\Delta K = \pm 1$
$\Delta J = \pm 1, 0$
$\vec{\mu}$ in plane
($\perp$ transition)
XBL 872-6129

Figure 9.

Rotational structure of "symmetric top" electronic transition; B′ < B″

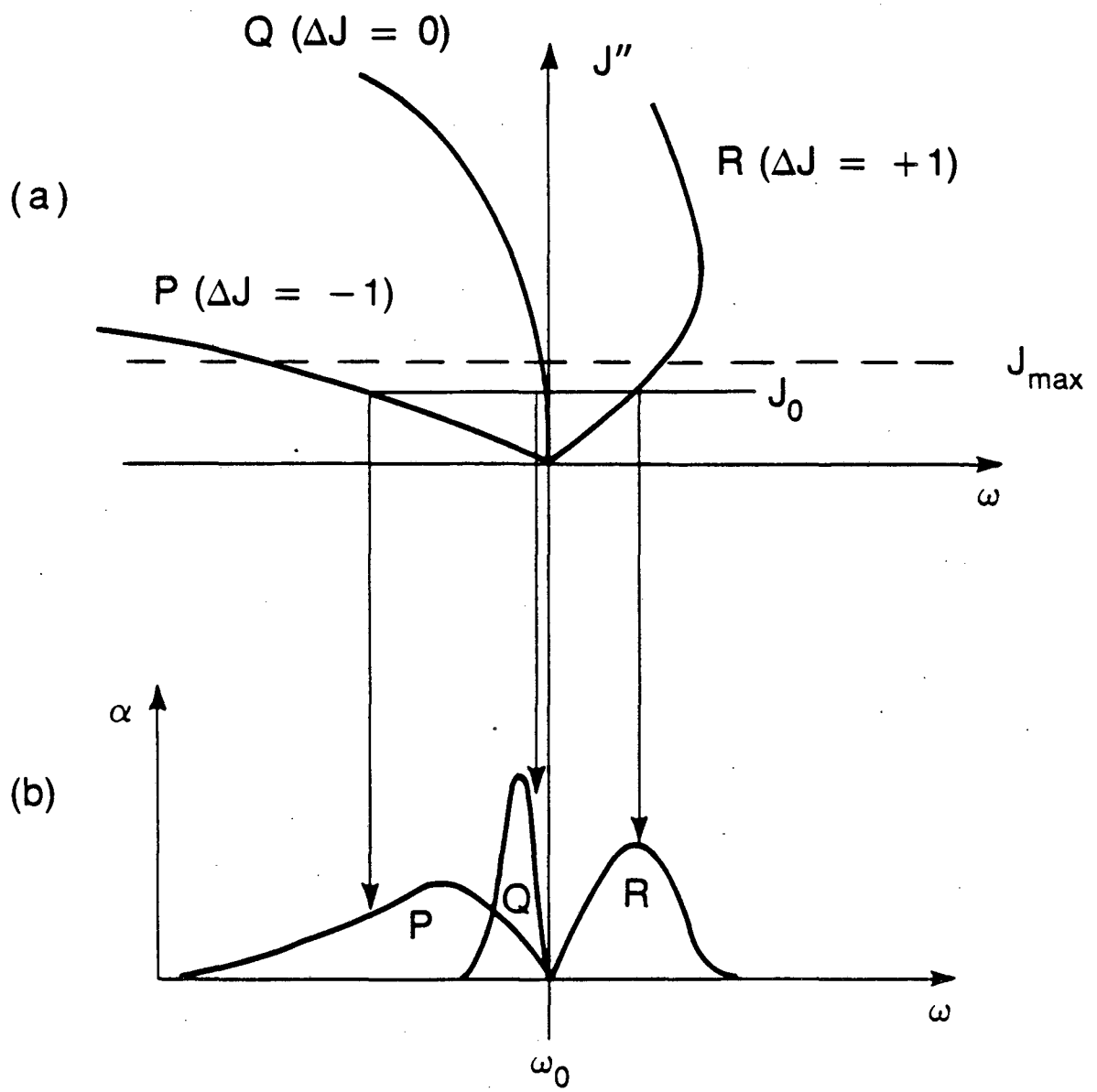

XBL 872-6130

Figure 10.

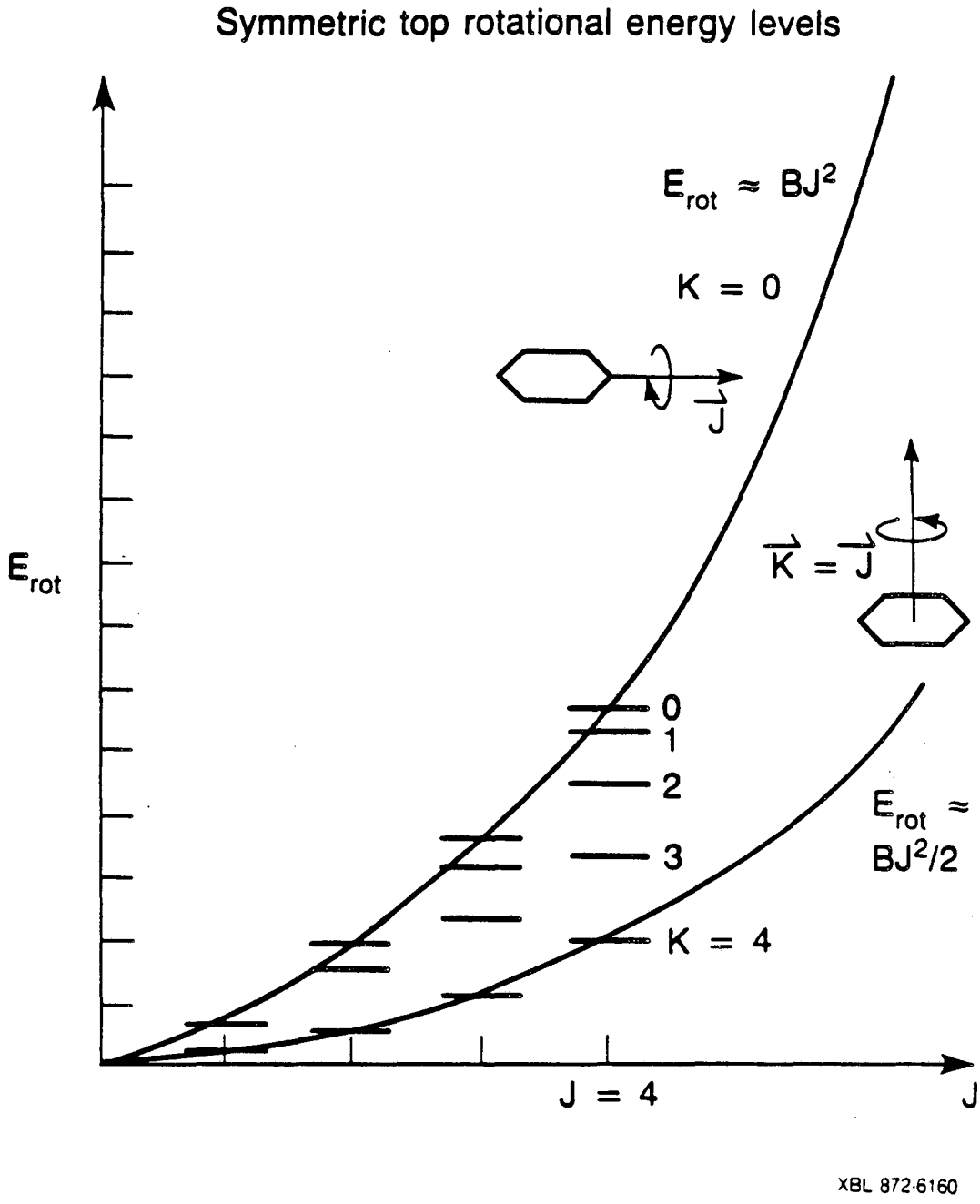
Symmetric top rotational energy levels
$E_{rot} \approx BJ^2$
K = 0
J
E_{rot}
$\vec{K} = \vec{J}$
0
1
2
3
K = 4
$E_{rot} \approx BJ^2/2$
J = 4
J
XBL 872-6160

Figure 11.

Evolution of state-selective 3-level saturation spectroscopy spectrum of a single vibrational band as different rotational states are probed

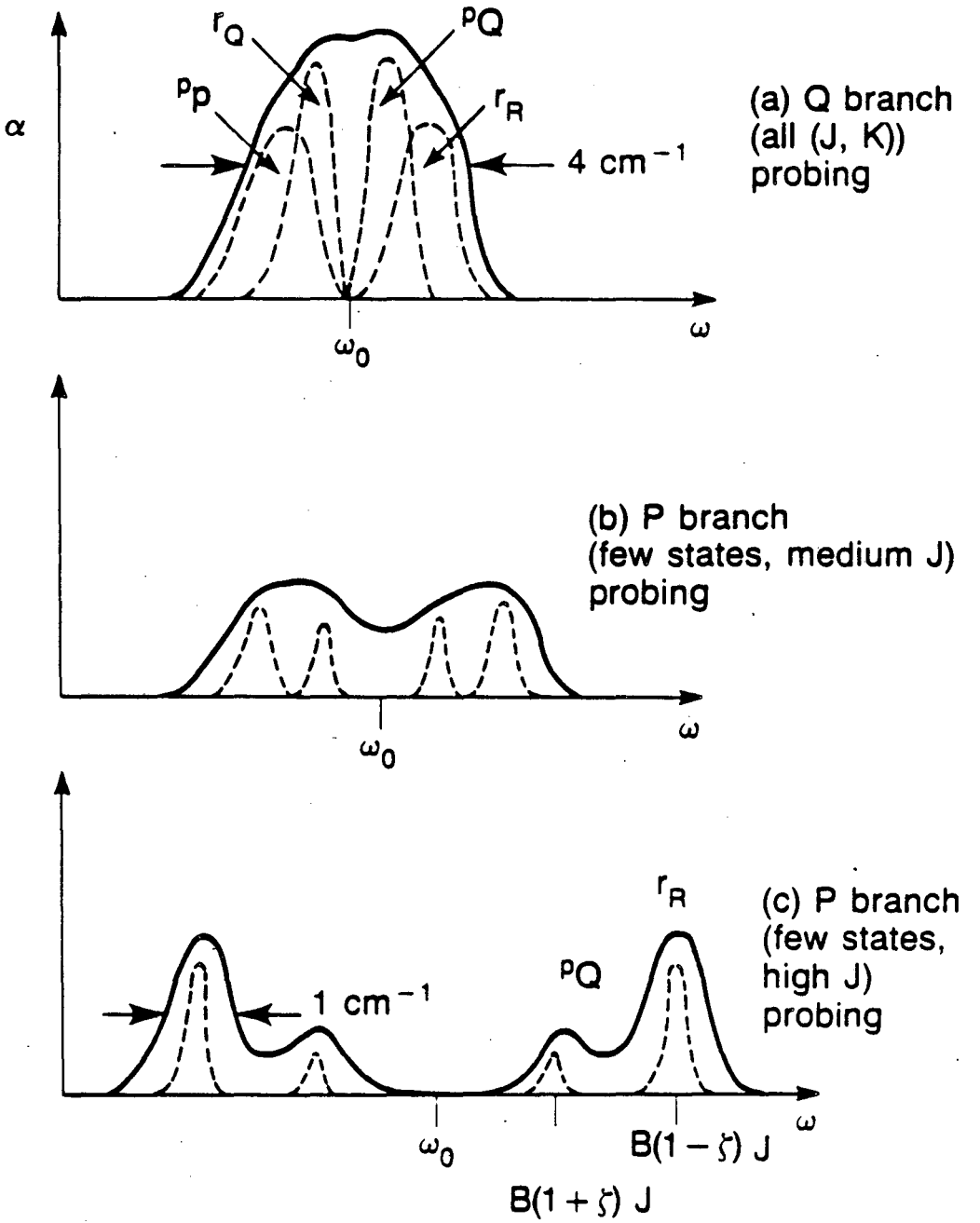

Figure 12.

XBL 872-6133

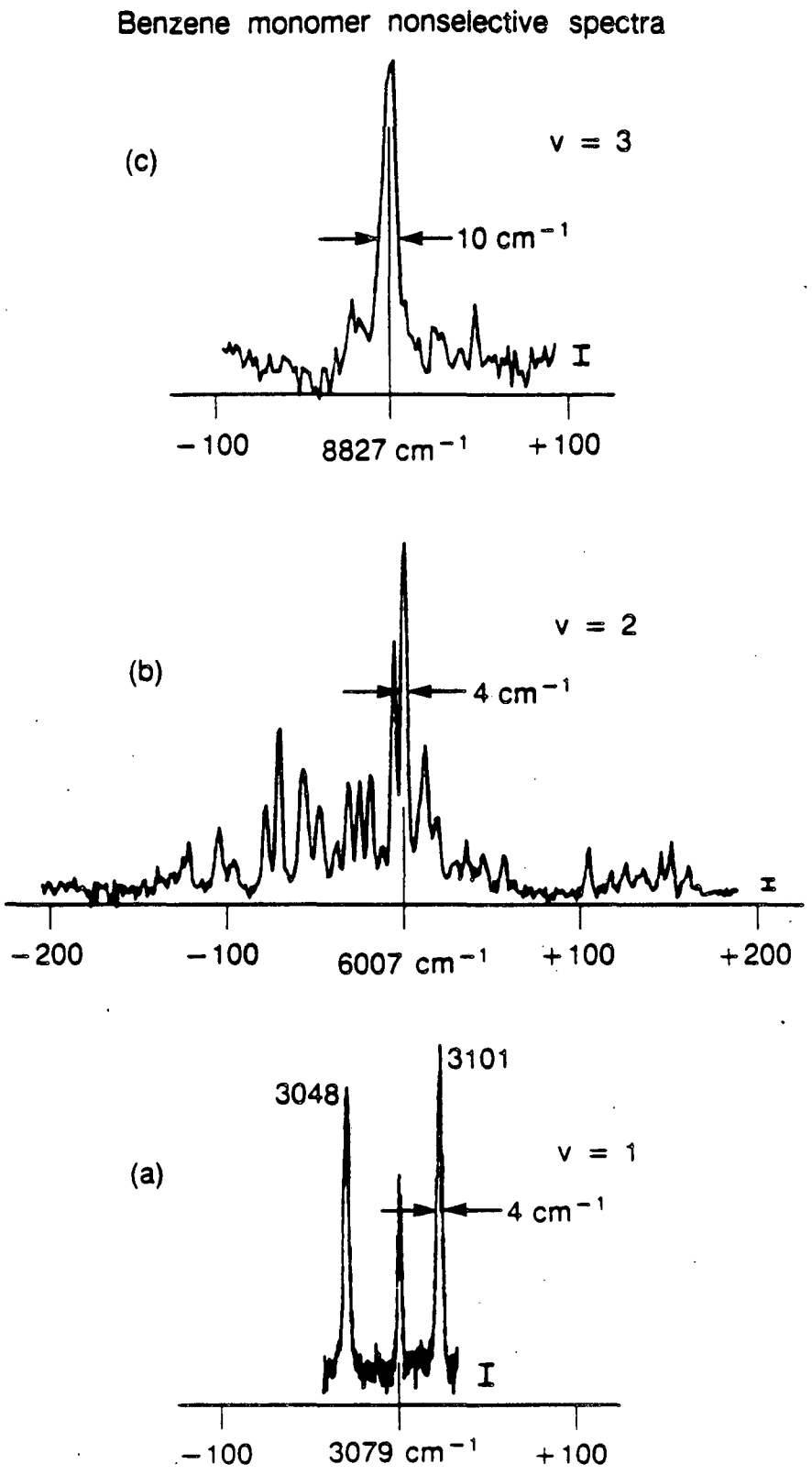

XBL-872-6146

Figure 13.

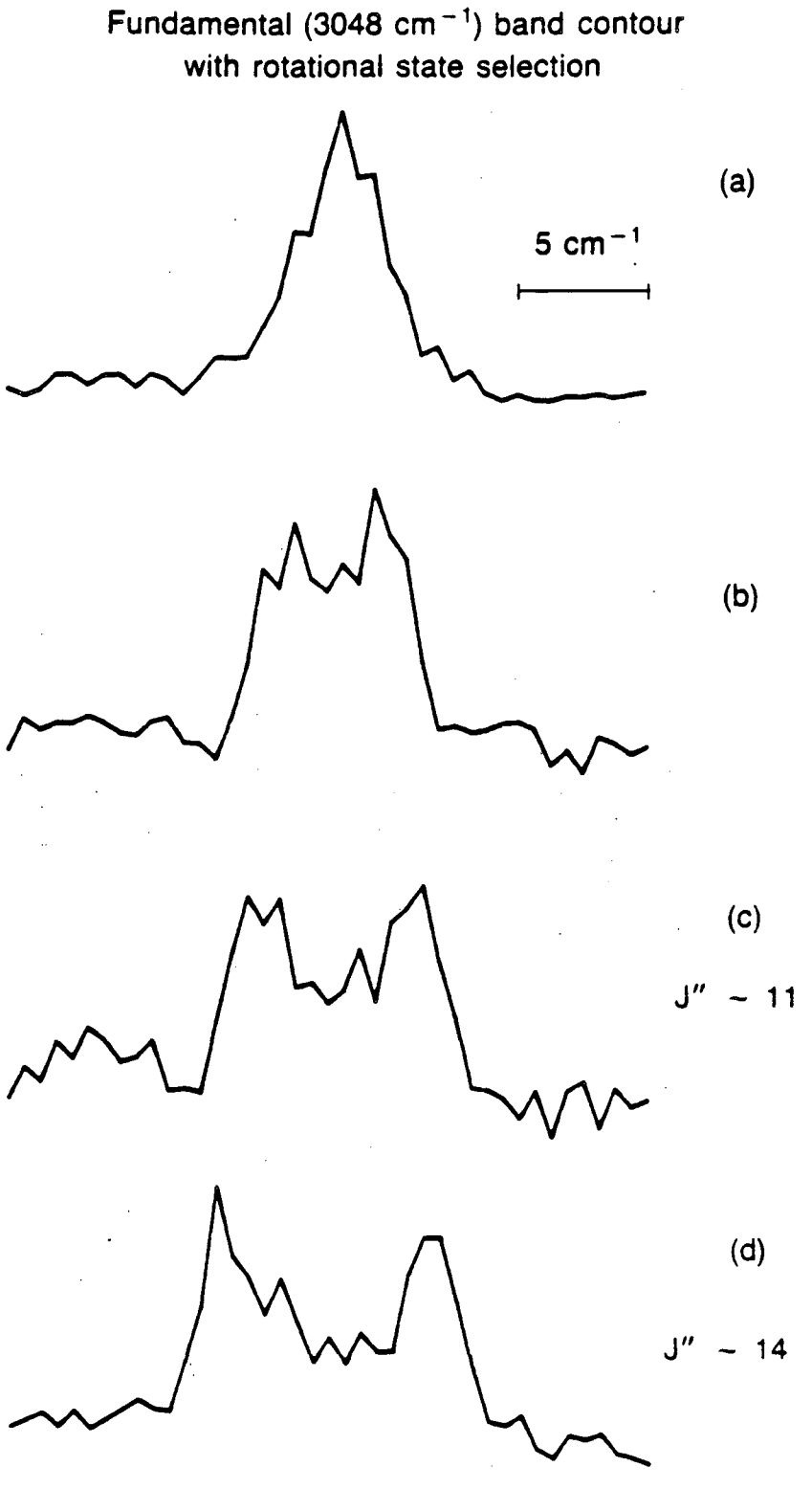
Fundamental (3048 cm^{-1}) band contour
with rotational state selection
(a)
5 cm^{-1}
(b)
(c)
J" ~ 11
(d)
J" ~ 14
XBL 872-6169

Figure 14.

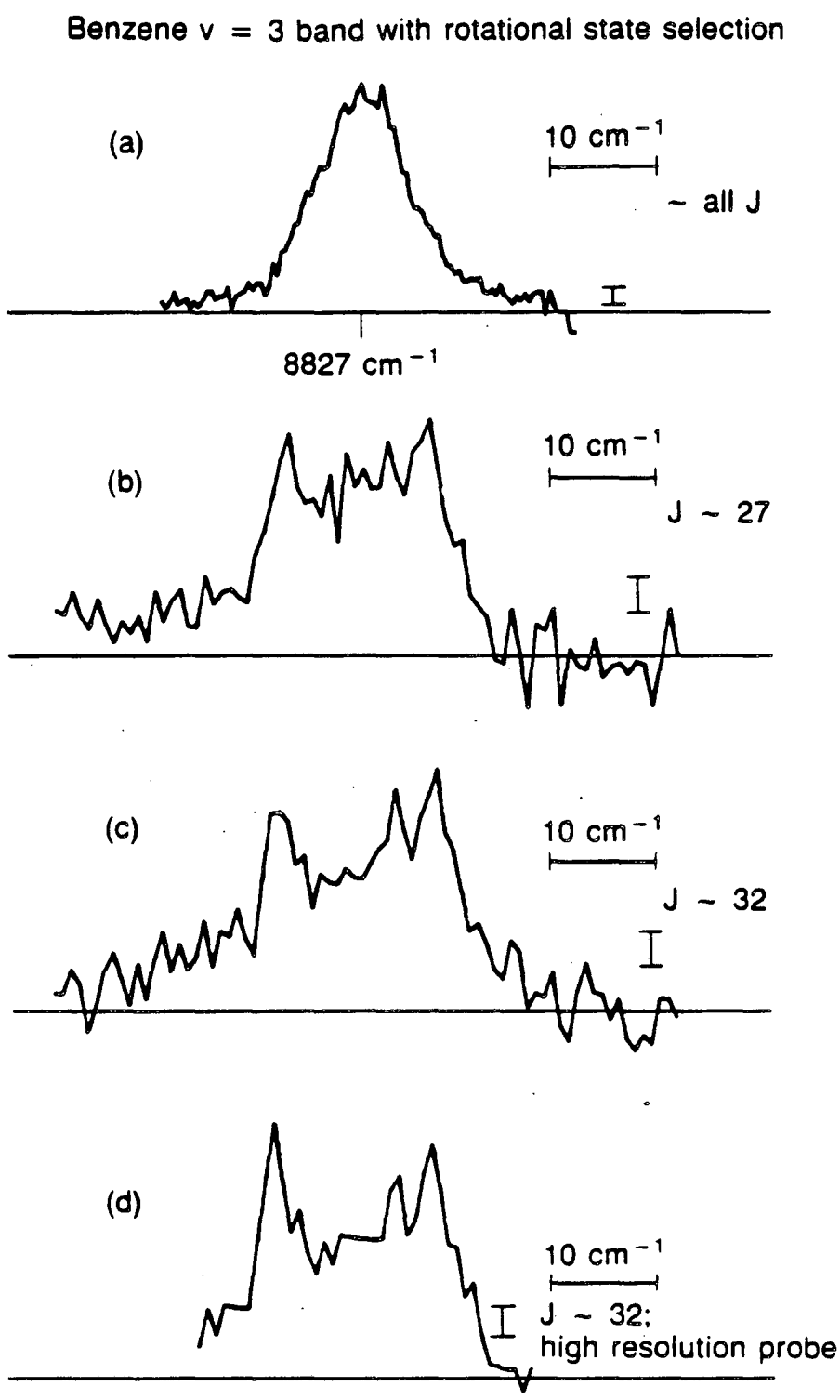
Benzene v = 3 band with rotational state selection
(a)
10 cm⁻¹
~ all J
8827 cm⁻¹
(b)
10 cm⁻¹
J ~ 27
(c)
10 cm⁻¹
J ~ 32
(d)
10 cm⁻¹
J ~ 32;
high resolution probe
XBL 872-6131

Figure 15.

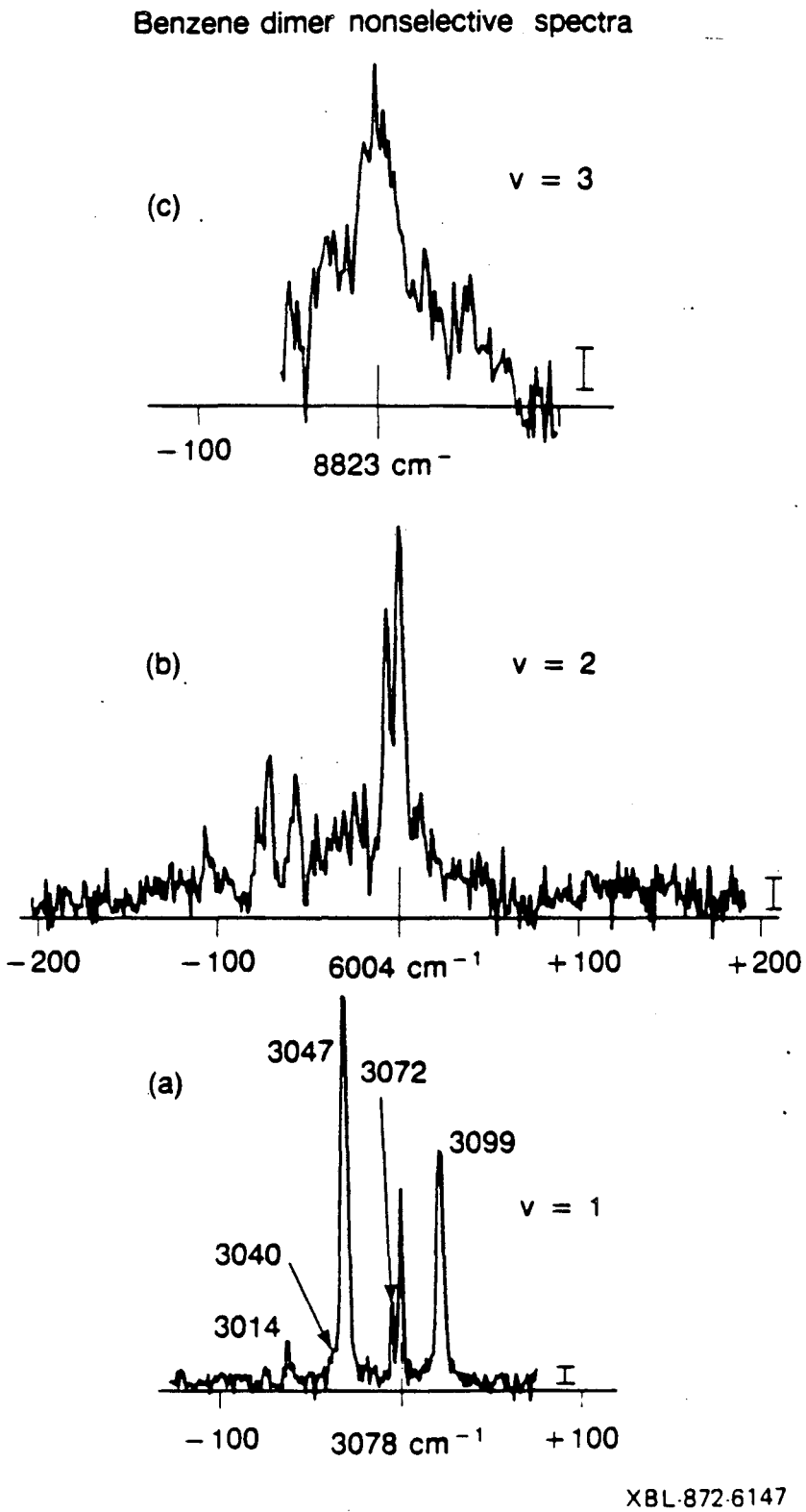
Benzene dimer nonselective spectra
(c)
v = 3
−100
8823 cm⁻
(b)
v = 2
−200
−100
6004 cm⁻¹
+100
+200
(a)
3047
3072
3099
v = 1
3040
3014
−100
3078 cm⁻¹
+100
XBL-872-6147

Figure 16.

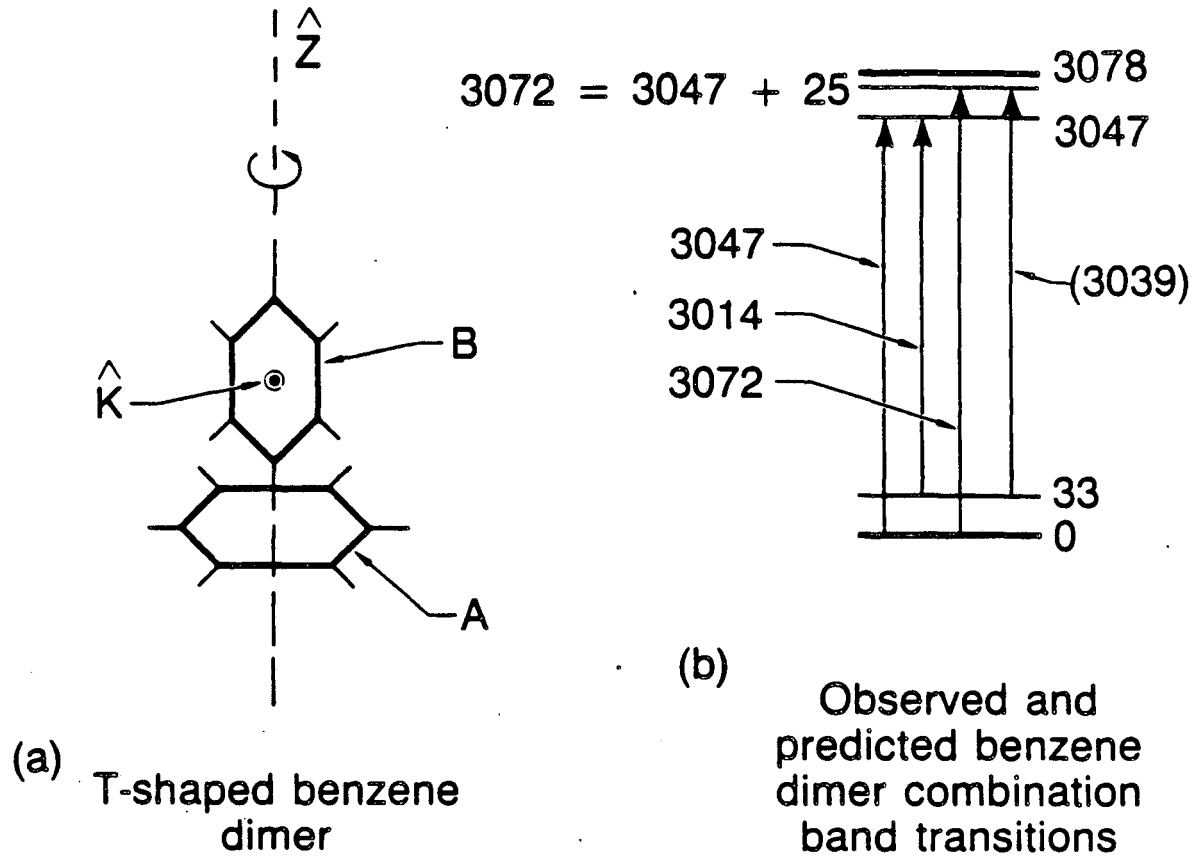
Ẑ
B
K̂
A
(a)
T-shaped benzene dimer
3072 = 3047 + 25
3078
3047
3047
3014
3072
(3039)
33
0
(b)
Observed and predicted benzene dimer combination band transitions
XBL 872-6120

Figure 17.

Three tier coupling scheme of Sibert et al.

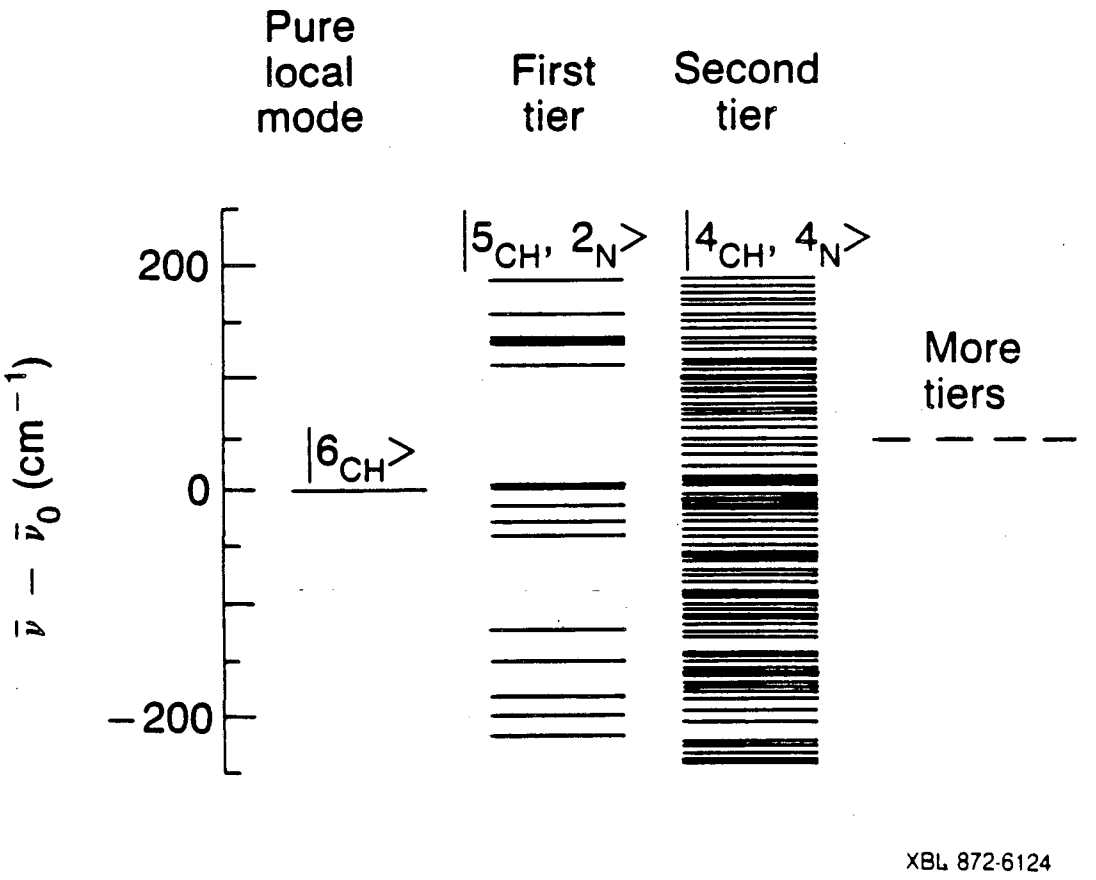

Figure 18.

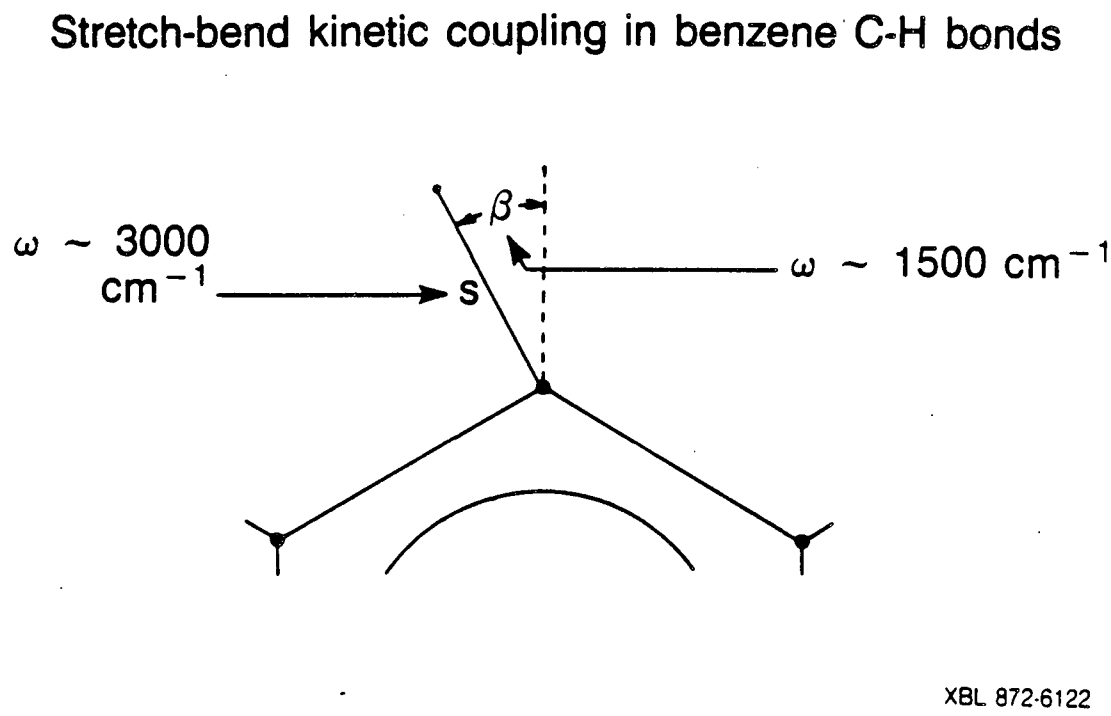
Stretch-bend kinetic coupling in benzene C-H bonds
ω ~ 3000
cm⁻¹
s
β
ω ~ 1500 cm⁻¹
XBL 872-6122

Figure 19.

Local-mode overtone transition
stick spectra of Sibert et al.

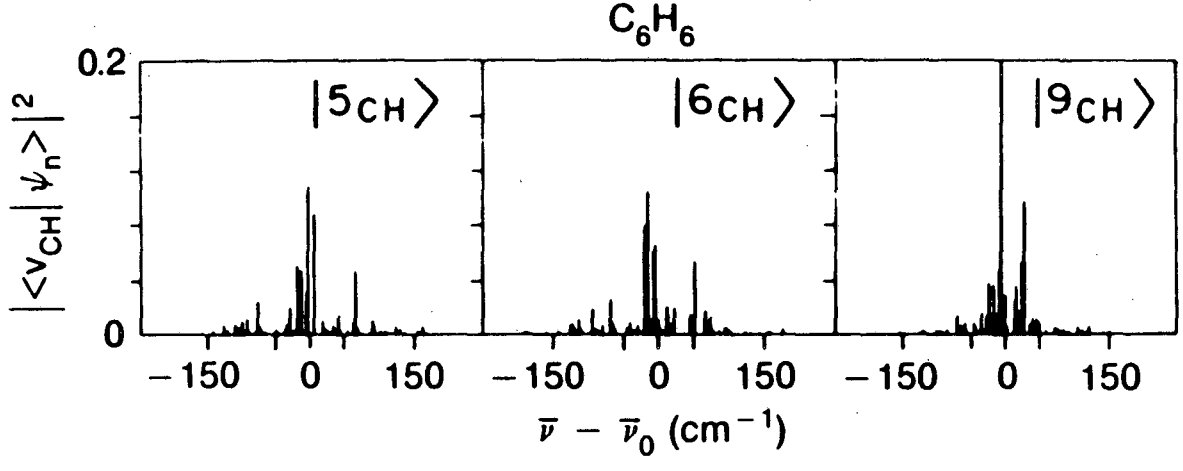

Figure 20.

XBL 872-6121

IV. INFRARED-ULTRAVIOLET DOUBLE RESONANCE STUDIES OF BENZENE MOLECULES IN A SUPERSONIC BEAM

I. INTRODUCTION

It is quite an ambitious project to describe in detail the interatomic interactions that are manifested as chemical bonds in polyatomic molecules. After all, many electrons move in the complicated potential of the atomic nuclei, and they experience mutual repulsions as they do so. Theoretical construction of an exact total molecular wavefunction is therefore unrealistic. In the attempt to explain the nature of chemical bonds, modern models are derived from phenomenological, intuitive approaches which employ approximate electronic wavefunctions, or molecular orbitals. The simplification allows one to rationalize intramolecular forces in terms of orbital overlap, bonds angles, and bond order (e.g. single or double). Furthermore, the strongest forces can usually be explained by considering pairwise interactions between atoms which are bonded to each other. For example, one could imagine stretching or bending a particular C-H bond in a molecule while leaving all other bonds in their (supposedly only slightly changed) equilibrium positions.

Of course, knowing the masses and geometrical arrangement of the atoms in a molecule, it is possible to use a given model of the intramolecular forces to determine the normal modes and vibrational frequencies. Experimental measurements of a molecule's vibrational spectrum can often find the frequencies to better than 0.1%, and are an extremely sensitive test of a proposed force field. In fact, vibrational spectroscopy and the study of force fields have

traditionally been intimately related endeavors.

The use of digital computers to perform ab initio calculations of intramolecular potentials, and to refine empirical force fields, has facilitated the theoretical modeling of molecules of ever-increasing size. In fact, the status quo is such that even the 12-atom benzene molecule, C_6H_6, has recently been the subject of detailed ab initio[1,2] and empirical[3-9] calculations. This is extremely significant because benzene is a textbook[10] "large molecule" and evidences many of the physics exhibited in large molecules such as symmetry, Fermi resonance, vibration-rotation coupling, and radiationless transitions. Its high degree of symmetry makes possible a reduction in the number of independent force constants used to parameterize its potential. Compared with an arbitrary 12-atomic molecule, a much more intuitive picture exists relating the vibrational spectrum and the force field. The symmetry also forbids the appearance of some vibrational modes in the infrared absorption or Raman spectra, and guarantees that no mode can appear in both. (IR- and Raman-active modes have opposite parities, and vibrational parity is well defined in benzene.) This simplifies the spectra and allows clear interpretations and assignments of the observed modes.

Accordingly, the work on benzene has been quite extensive. In 1934 Wilson[11] calculated the normal coordinates and correctly assigned most of the modes observed in the infrared and Raman spectra. His system of numbering the modes, used in this article, is firmly entrenched in the literature, but is unfortunately different from the logical system of Herzberg.[12] His simple parameterization of the potential included only 6 force constants: 4 for the in-plane motions and 2 for the

out-of-plane motions. A popular textbook on molecular vibrations[10] included more details concerning general techniques of vibrational analyses and included a chapter using benzene as an example. The study of slightly altered (e.g. deuterated, $C_6H_nD_{6-n}$) benzene molecules, which have predictably perturbed normal modes and frequencies, has also been exhaustively performed.[4,13] This has added greatly to the spectroscopic data base useful in refining force constants. High-resolution techniques have been used to measure the detailed rotational structure of some vibrational bands: IR absorption[14-16] and Raman[17-19] studies have given accurate values of moments of inertia and vibration-rotation interaction constants. Overlapping bands which have mutual perturbations (Fermi resonance) have also been probed.[20,21]

These spectroscopic experiments have been accompanied by harmonic force field parameterizations of successively increasing accuracy and sophistication. A prototypical, empirical fit by Whiffen[7] has been improved upon by Duinker and Mills,[8] Kydd,[9] and lately Ozkabak et al.[3] However, the ab initio calculations by Pulay, Fogarasi, and Boggs[1] does not predict the force constants which have been deduced from the empirical fit to experimental data. Evidently there is still more work to be done, both to improve ab initio calculations, and to prove that empirical fits are correct.

Although the spectroscopic characterization of the fundamental vibrations of benzene in its ground ($\tilde{X}$) state is fairly complete experimentally, the same cannot be said of the first excited ($\tilde{A}$) state, since the frequencies of some modes are not yet known. Vibrational modes in the $\tilde{A}$ state have typically been studied by examining the vibrational structure associated with the $\tilde{A} \leftarrow \tilde{X}$ transition. Just as in

the IR and Raman studies of the $\tilde{X}$ state, the $\tilde{A} \leftarrow \tilde{X}$ transition is governed by the molecular symmetry. This will be discussed more fully in the Results section of this paper. For now it is sufficient to know that the $\tilde{A} \leftarrow \tilde{X}$ transition involves excitation of one of the delocalized π electrons into a π^* state, and that the transition is symmetry-forbidden in the electric-dipole approximation. It becomes slightly allowed with the aid of a vibrational excitation (of the correct symmetry); in other words it is "vibronically induced". The effect of the vibration is to mix the $\tilde{A}$ state slightly with a higher state to which transitions <u>are</u> allowed from the $\tilde{X}$ state.

Naturally, the first spectra were obtained with direct absorption techniques; features in these spectra were plentiful and difficult to assign conclusively. The use of the fluorescence technique by Knight, Parmenter, and Schuyler[22] gave detailed information in the form of fluorescence spectra from selected vibrational levels in the $\tilde{A}$ state. With the $\tilde{X}$ state levels (final states) already largely understood, this made it possible to infer much more securely the vibrational characteristics of the emitting level in the $\tilde{A}$ state. A series of papers by Atkinson and Parmenter[23,24] is devoted to improving and summarizing the analyses of the $\tilde{A} \leftarrow \tilde{X}$ spectrum up to about 1978. At that time, direct absorption and related measurements had only provided $\tilde{A}$ state assignments of 11 of benzene's 20 vibrational modes. (There are 30 modes, but 10 are doubly degenerate.)

The application of lasers to the problem led to significant progress because multiphoton transitions, which require high light intensities, could now be investigated. This meant that the selection rules were different for different vibrational modes active in

"inducing" a two-photon as opposed to a one-photon transition. Even a three-photon $\tilde{A} \leftarrow\!\!\!\leftarrow\!\!\!\leftarrow \tilde{X}$ spectrum has been reported.[25] It has been analyzed to give the assignment of an $\tilde{A}$ mode. The two-photon fluorescence excitation studies in benzene gas[26-34] permitted confirmation of the mechanism of the two-photon transition and an analysis of the laser polarization dependence of its vibrational bandshapes. (In contrast with linear absorption spectra, bandshapes observed with multiphoton transitions depend strongly on vibrational symmetry and laser polarization.) Even more detailed polarization studies were made with a two-photon fluorescence-excitation experiment on a benzene crystal at 4.2°K.[35] With these two-photon transitions, 4 more vibrational modes in the $\tilde{A}$ state were assigned and analyzed, with 4 left to be determined. Referring to Fig. 1, the frequencies of modes 3, 12, 13, and 20 in the $\tilde{A}$ state have not yet been measured.

Just as in the studies of the $\tilde{X}$ state, additional useful information about the $\tilde{A}$ state is gained by studying isotopically substituted molecules. This work, undertaken largely by the Goodman group[36-39] is, however, not complete, and is perhaps not of great utility until more is known about C_6H_6 itself.

Naively, one would think that one- and two-photon spectroscopy should give access to all <u>gerade</u> and <u>ungerade</u> modes in the $\tilde{A}$ state. How do we account for the fact that 4 of 20 modes have not been detected? First, it is not enough to consider only the <u>g/u</u> aspect of the symmetry. The symmetry of benzene is so high that 3 of these unobserved modes are of symmetry classes not allowed in $\tilde{A} \leftarrow \tilde{X}$ transitions with one photon or 2 photons of the same frequency. The last unobserved mode, a C-H stretching mode, is symmetry-allowed in

two-photon transitions but is simply too weak to be observed. Remembering that the $\tilde{A} \leftarrow \tilde{X}$ transition occurs only when the carbon ring π orbitals are perturbed, we expect that vibrations which are effective in "squashing" the ring will be best at inducing $\tilde{A} \leftarrow \tilde{X}$ excitation. The C-H stretches are largely decoupled from the ring, and do not change its shape much. The π clouds sandwiching the carbon ring are largely unaffected by motions which stretch the C-H σ bonds. Even if they are weakly present in a spectrum, features due to C-H stretches are likely to be masked by strong combination bands nearby.

II. NEW TECHNIQUE

As part of an experiment to study overtones of C-H stretches in the benzene molecule,[40] we developed a straightforward technique which gave access to several previously unobserved vibrational levels in the $\tilde{A}$ state of benzene. As a result we were able to determine frequencies of two hitherto unobserved modes (3 and 20) and confirm the assignment of a third (19), which has been a subject of controversy. Our assignments also support Pliva's analysis[41] of the fundamental C-H stretch associated with the $\tilde{X}$ state of benzene. Furthermore, our results have led us to re-examine previous spectroscopic data and assignments and suggest that the C-H stretching modes in the $\tilde{X}$ and $\tilde{A}$ states may not be as different as we thought.

A schematic diagram depicting our IR + UV two-photon excitation of the C-H stretching vibrations in the $\tilde{A}$ state is shown in Fig. 2(a). In this paper we use the standard spectroscopic notations ν_i'', ν_i' to denote the frequency of the i^{th} vibrational mode in the ground ($\tilde{X}$) and excited ($\tilde{A}$) states, respectively. The label $i_m j_n \ldots$ ($i^m j^n \ldots$) describes

vibrational levels in the ground (excited) electronic state with m quanta of mode i, n quanta of mode j, etc. The transition frequency between the states $i_m j_n$ and $i^k j^\ell$ is compactly described as $i^k_m j^\ell_n$. Also, here we invent the notation CH_m (CH^m) to indicate a generic IR-active C-H stretching mode with m quanta in the $\tilde{X}$ ($\tilde{A}$) state. In Fig. 2, we assume (not true in the case of benzene) for simplicity that the zero-vibration UV transition 0^0_0 is allowed. The CH^1_0 transition is weak or forbidden. But there is nothing to prevent the CH^1_1 transition, which is actually just the 0^0_0 transition with the C-H stretching mode as a spectator. To excite the molecule to CH^1, we can first create the CH_1 population with IR excitation at $\nu_{IR} = \nu''_{CH}$ followed by UV excitation at $\nu_{UV} = CH^1_1$. The excited-state C-H stretching frequency is given by $\nu'_{CH} = \nu''_{CH} + CH^1_1 - 0^0_0$.

Readers who are familiar with polyatomic electronic spectra will recognize that this is a logical extension of the procedure of analyzing "hot bands". Vibrational levels whose energies are below ~ 1000 cm^{-1} have significant thermal populations; their fractional Boltzmann populations at room temperature are at least e^{-5} ~ 1%, since kT ~ 200 cm^{-1}. It is not necessary to use a laser to pump populations into these levels. The thermal populations of C-H stretching states at ~ 3000 cm^{-1} are however extremely small at room temperature.

Let us now see how one goes about getting an IR-UV double resonance spectrum. We fix the IR frequency at ν''_{CH} and turn the IR light beam alternately on and off so that the CH_1 population is modulated. Then we expect to see an enhanced absorption at CH^1_1, and a diminished absorption at 0^0_0. The spectrum we expect in this simple example is shown in Fig. 2(b); the modulated UV absorption vs. ν_{UV} is sketched.

In this example $\nu'_{CH} > \nu''_{CH}$, so that $CH_1^1 > 0_0^0$. Also, the intensity ΔI_{CH} of the double-resonance signal is often less than ΔI_0, that of the ground-state depletion signal, for the following reasons. First, the Franck-Condon factor $|\langle CH^1|CH_1\rangle|^2$ could be less than 1, since the mode ν'_{CH} may be somewhat different from the mode ν''_{CH}. After all, the force constants are different in the two electronic states. Second, when pulsed lasers are used with a time delay between the IR and UV, there is a chance for the population in the CH_1 state to relax to other levels. We assume that radiative decay is negligible because radiative lifetimes are often long compared to IR-UV laser pulse delays. Third, the IR light could also excite the transition $CH_2 \leftarrow CH_1$, especially if it is intense enough to pump $CH_1 \leftarrow 0_0$ efficiently, and remove a fraction of the population in CH_1.

In our experiment we used a supersonic molecular beam as the sample. UV absorption measurements on such a "thin" sample are difficult. Our way around that difficulty was to use resonantly-enhanced two-photon ionization (R2PI), which gave an ion signal proportional to the absorption experienced by the laser beam at ν_{UV}. Molecules which have been resonantly excited to levels in the $\tilde{A}$ state are nonresonantly ionized by photons from the same beam pumping the $\tilde{A} \leftarrow \tilde{X}$ transition. The ion signal is proportional to the $\tilde{A}$ state population and is easy to detect and measure.

While an experiment such as this could be done with a static gas sample, the use of a supersonic molecular beam has an important advantage. With proper supersonic expansion, the molecules in the beam are "rotationally cold", with their rotational state distribution roughly described by a temperature $T_{rot} \sim 5°K$. The width of the

"rotational envelope" associated with each vibrational band is greatly reduced, from ~ 30 cm^{-1} at T_{rot} ~300 °K to ~ 4 cm^{-1} at ~ 5°K. As a result, spectra which are horribly congested at room temperature take on a much more "sparse" appearance. This both increases the signal strength and makes both the IR and UV spectra easier to analyze. With given IR and UV laser bandwidths less than 1 cm^{-1}, only a fraction of the ground state rotational distribution is excited to the CH_1 state and detected with the CH_1^1 transition. This fraction increases as the laser bandwidths overlap a larger portion of the rotational envelope.

III. EXPERIMENTAL

Figure 3 shows the salient components of our apparatus. Our sample was a supersonic beam formed by passing argon gas at 200 torr through a -30°C bubbler which contained frozen benzene. It proceeded into the 10^{-7} torr experimental chamber via a Lasertechnics[42] LPV pulsed valve equipped with a 0.5 mm diameter nozzle, a region of differential pumping, and a skimmer. Infrared and ultraviolet laser beams were loosely focused, and overlapped. They crossed the molecular beam inside a set of ion extraction plates. The ions generated by R2PI passed through a time-of-flight mass spectrometer and were detected with a Johnston electron multiplier.[43] We used a gated integrator to accumulate the ion signal for several laser shots.

Independently triggerable pulsed Nd:YAG laser systems[44] generated the tunable UV and IR frequencies required. Each laser could generate 700-mj, 9-nsec, 9394-cm^{-1} (1.06 μm) pulses at a rate of 10 Hz. The frequency-doubled output of one laser was used to pump a dye laser with LDS 698 or LD 700 [45] dye, to yield an output around 14000 cm^{-1}. This

dye laser output was frequency-doubled in an automatically-tracked, angle-tuned KDP crystal and the resulting UV light was mixed with the fundamental Nd:YAG laser beam in yet another KDP crystal to give the ~ 38000 cm^{-1} UV frequency we actually used. The frequency-doubled output of the other Nd:YAG laser was used to pump another dye laser with LDS 821 [45] dye to yield an output around 12400 cm^{-1}. This dye laser output was mixed with the fundamental Nd:YAG laser beam in an automatically-angle-tuned $LiNbO_3$ crystal to generate an IR beam of ~1 mj/pulse at 3000-3100 cm^{-1}. This energy was sufficient to saturate the IR transitions, as expected on the basis of reported cross sections.[13] The resolution achieved with our lasers was 1 cm^{-1} in the IR and in the UV. The laser frequencies were calibrated to better than 1 cm^{-1} by measuring the accurately known spectral lines of neon with optogalvanic spectroscopy[46] and those of methane with photoacoustic spectroscopy.

A digital computer recorded ion signal levels, scanned laser wavelengths, and actuated a shutter which was used to turn the IR beam on and off every few sec. Our Nd:YAG pump lasers had a relative timing jitter of several nsec. In order to eliminate jitter-induced fluctuations in the R2PI signal, we made sure that the pump (IR) pulse always led the probe (UV) pulse. This guaranteed that the molecules received the complete dose of infrared light before being probed. A relative delay of ~15-20 nsec in triggering the UV laser with respect to the IR laser was sufficient. Repopulation of the vibrational ground state in ~ 20 nsec was insignificant, since the 3000-cm^{-1} states have radiative lifetimes of the order of msec.

A chopper operating at 0.3 Hz was used to turn the IR beam on and off. With the shutter in the IR beam closed, no molecules were

pumped. With it open, the ground state population was depleted, and the CH_1 population was enhanced. Chopping the IR beam with the shutter thus imposed a modulation on the populations of the ground-state and the CH_1 state, and hence the ion (probe) signal. With the UV light fixed to ionize ground-state molecules, the amplitude of the probe signal modulation vs. IR frequency gave us the anticipated IR absorption spectra. On the other hand, fixing the IR excitation to create a population in a given mode and scanning the UV laser yielded the IR-UV double resonance spectra.

IV. RESULTS

Our presentation of the results will be in three stages: first we will display R2PI spectra of portions of the $\tilde{A} \leftarrow \tilde{X}$ band as they appear without IR excitation. We will explain the characteristics of this electronic transition insofar as they pertain to this experiment. Second, we will show an IR spectrum of the fundamental C-H stretching vibrations, and describe a previous interpretation of its features. Finally, a series of spectra related to the IR-induced UV transitions will be presented. The analysis section of this paper is devoted to explaining the observed new spectral features.

A. R2PI Spectra

Our R2PI spectra, involving resonant transitions around 6_1^0 and 6_0^1 in the absence of infrared excitation, are shown in Figs. 4(a) and (b), respectively. The "rotational temperature" was determined to be ~ 5 °K and the "vibrational temperature" ~ 200 °K. Figure 4(c) is a corresponding energy level diagram illustrating these resonant transitions. It contains detail of hot bands and vibrational angular

momentum splittings but does not include some weak transitions also observed in the R2PI spectra. The 0_0^0 transition around 38086 cm^{-1} is forbidden and hence was not observed. The spectral assignments are those derived from the recent molecular beam work of Stephenson et al.;[47] assignments not provided in that work are taken from the earlier study by Atkinson and Parmenter.[23] The reader who wishes to understand the minutiae of the $\tilde{A} \leftarrow \tilde{X}$ spectrum is advised to consult these references.

It is seen that the 6_0^1 transition, saturated in our spectrum, is the dominating feature. It is at least 20 times more intense than the neighboring 16_0^2 band. Before we move on, let us briefly review the symmetry, mechanism, and bandshapes associated with transitions of the sort $6_n^{n\pm1}1_\chi^\pi$.

There are many symmetry operations in the benzene molecule, and the notation used to describe the wavefunctions accordingly has several elements: a letter, a numerical subscript, and the usual g (gerade) or u (ungerade) subscript to indicate the parity. Figure 1 is a picture of the normal modes of benzene with their symmetry designations. We use capital letters to represent electronic wavefunctions and lower-case letters for vibrational functions. The overall symmetry of a vibronic state is the product of the electronic and vibrational symmetries. Letters A, B, and E describe wavefunctions of different symmetries with respect to rotation about the sixfold symmetry axis. Following the phase convention of Atkinson and Parmenter,[24] a $2\pi/6$ rotation about this axis is equivalent to multiplying the wavefunction by a phase factor $e^{-i\theta}$, with $\theta = 0$ for A, and π for B functions, as can be seen in Fig. 1. For the doubly degenerate modes E the $2\pi/6$

rotation causes a phase change of $2\pi/6$ in the wavefunction for the E_1 modes and $4\pi/6$ for the E_2 modes. When applied to the A and B states, the subscript 1 or 2 indicates even or odd behavior with respect to a rotation of π about an axis containing two carbon atoms.

The following multiplicative properties then apply:[10] $g \cdot g = u \cdot u = g$; $g \cdot u = u$. For A and B states, 1 and 2 behave analogously: $1 \cdot 1 = 2 \cdot 2 = 1$; $1 \cdot 2 = 2$. For the rotational symmetry, $A \cdot A = B \cdot B = A$; $A \cdot B = B$, $A \cdot E_1 = E_1$, $A \cdot E_2 = E_2$, $B \cdot E_1 = E_2$, and $B \cdot E_2 = E_1$. Also, $E_1 \cdot E_1 = E_2 \cdot E_2 = A_1 + A_2 + E_2$; $E_1 \cdot E_2 = B_1 + B_2 + E_1$.

Descriptive names have been applied to several of the modes. For example, ν_1 (a_{1g}), in which the molecule expands and contracts uniformly, is the "breathing" mode. ν_2 is the C-H stretching analog to ν_1, which is more a C-C stretching mode. The e_{2g} modes ν_6 - ν_9 tend to "squash" the molecule into a two-fold symmetric shape. Similarly, a threefold-symmetric "squashing" of the molecule occurs when b_{2u} modes are excited. e_{1u} vibrations cause the sets of carbon and hydrogen atoms to "slosh" with respect to each other, and produce a varying electric dipole moment which is the source of the infrared activity of these modes.

The selection rules for the electronic transition are found by evaluating the matrix element of the dipole moment operator $\langle \tilde{A} | \vec{\mu} | \tilde{X} \rangle$. It is simply a number, whose value cannot change when a symmetry operation is performed on the product $\tilde{A}\vec{\mu}\tilde{X}$. The only symmetry species whose members are invariant with respect to all symmetry operations is A_{1g}. Therefore, the symmetry of $\langle \tilde{A} | \vec{\mu} | \tilde{X} \rangle$ must be A_{1g} in order for the matrix element to be nonzero. This symmetry is equal to the product of the symmetries of $\tilde{A}$, $\vec{\mu}$, and $\tilde{X}$. We already know that the symmetry

species of $\tilde{A}$ and $\tilde{X}$ are B_{2u} and A_{1g}, respectively. Also, the in-plane dipole moment of $\vec{\mu}$ has E_{1u} symmetry. It is readily checked that $B_{2u} \cdot E_{1u} \cdot A_{1g} = E_{2g}$, not A_{1g}, so the $\tilde{A} \leftarrow \tilde{X}$ transition is formally forbidden. However, as the molecule vibrates, its electronic wavefunction is no longer purely B_{2u} in the $\tilde{A}$ state, or A_{1g} in the $\tilde{X}$ state. The electric dipole moment matrix element $\langle\mu\rangle = \langle\tilde{A}|\vec{\mu}|\tilde{X}\rangle$ can be expressed with the perturbation expansion

$$\langle\mu\rangle = \langle\mu\rangle|_o + \sum_i \frac{\partial\langle\mu\rangle}{\partial Q_i}\Big|_o Q_i + \sum_{i,j} \frac{\partial^2\langle\mu\rangle}{\partial Q_i \partial Q_j}\Big|_o Q_i Q_j + \ldots$$

In this (Herzberg-Teller) expansion, the Q's represent normal coordinates and the constants are evaluated at the equilibrium geometry. The overall symmetry of each of the terms involving derivatives of $\langle\mu\rangle$ is the product of the symmetries of $\langle\mu\rangle|_o$ and the normal modes Q. We have just shown that $\langle\mu\rangle|_o$ has E_{2g} symmetry and that its magnitude is zero. In order to obtain A_{1g} symmetry for the derivative terms of $\langle\mu\rangle$, it is therefore necessary for Q_i (or Q_iQ_j) to have e_{2g} symmetry.

In this context, ν_6 is by far the most effective vibration that can induce the $\tilde{A} \leftarrow \tilde{X}$ transition because it squashes the ring the most. To zeroth order, the $\tilde{A} \leftarrow \tilde{X}$ spectrum is described by the selection rule $\Delta v_6 = \pm 1$. In the following, we will only be concerned with transitions involving $\Delta v_6 = \pm 1$.

Qualitatively, the $\tilde{A} \leftarrow \tilde{X}$ transition promotes a C-C π-bonding electron into an antibonding (π^*) state. The strength of the bonds holding the ring together is weakened, and the ring expands; this can be considered as setting the molecule into motion in the ν_1 mode. In

fact, the strongest features in the $\tilde{A} \leftarrow \tilde{X}$ spectrum are the $6_0^1 1_0^n$ transitions, where n ranges from 0 to about 4. These transitions are spaced by $\sim \nu_1' = 923\ cm^{-1}$. Interestingly, the states with 1 quantum of ν_1 in the $\tilde{X}$ and $\tilde{A}$ states are nearly orthogonal, and the intensity of a transition such as $6_0^1 1_1^1$ is at least 10 times smaller than 6_0^1 or $6_0^1 1_1^m$, where m = 0,2,3.[48] The forces which prevent out-of-plane motion are also much weaker in the $\tilde{A}$ state than in the $\tilde{X}$ state; frequencies of some out-of-plane modes are roughly half their $\tilde{X}$ state values. These out-of-plane normal modes (4, 5, 10, 11, 16, and 17) therefore have considerably different displacements in the two states. Within one or the other of the two electronic states, the vibrational modes have the usual orthonormal properties: $\langle i_m | i_k \rangle = \delta_{mk}$ and $\langle i_m j_n | i_k j_\ell \rangle = \delta_{mk}\delta_{n\ell}$, etc. Between the two states, the orthonormality is lost: $\langle i^m | i_k \rangle \neq \delta_{mk}$. Overlap integrals (Franck- Condon factors) such as $|\langle 16^1 17^1 | 0_0 \rangle|^2$ can then have appreciable values, and we have just mentioned that $|\langle 1^1 | 1_1 \rangle|^2 \ll 1$.

When we look at the spectrum of the 6_0^1 region we see that there are "hot bands" of the sort $6_0^1 16_1^1$ displaced to the red of the 6_0^1 band by $\nu_{16}'' - \nu_{16}' \sim 161\ cm^{-1}$. Here, the population in the 16_1 level is merely serving as another "ground state" for the 6_0^1 transition. If we did not know the value of ν_{16}' but knew ν_{16}'', we could find it from the relation $6_0^1 16_1^1 = 6_0^1 + \nu_{16}' - \nu_{16}''$.

A subtlety which pertains to our experiment is the shape of the rotational envelope of each band; it depends on the nature of the vibrational transition. When only one quantum of a degenerate vibration is involved, the band consists of a single peak, or a peak with a notch in the center if the resolution is sufficient to separate

the P and R branches. Examples of this are the 6^9_1, $6^9_1 1^1_0$, and 6^1_0 bands, which have identical shapes. But when two or more quanta of degenerate vibrations are present, as in the 6^2_1 band at ~38520 cm^{-1} (Fig. 4b), the situation is more complex because the vibrations interact to produce a spectroscopically-observed splitting. (The weak $6^9_1 1^2_0$ band is masked by the 6^2_1 band.)

The presence of "vibrational angular momentum" can lift the degeneracy. The energy of a vibrational level is

$$E(v) = \sum_i \omega_i v_i + \sum_{i,j} x_{ij} v_i v_j + \sum_{i,j} g_{ij} \ell_i \ell_j . \qquad (1)$$

ω_i is the harmonic frequency of mode i, x_{ij} is the anharmonicity between modes i and j, and g_{ij} is yet another anharmonic constant responsible for the energy dependence on the vibrational angular momentum quantum numbers ℓ_i, ℓ_j. When v_i quanta are present in a degenerate mode, ℓ_i can have the values v_i, $v_i - 2$, $v_i - 4$, ... - v. Figure 5(a) illustrates the effect of the vibrational angular momentum term $g_{ii}\ell_i^2$ on the energy levels. Other contributions to the energy are ignored because they don't depend on the vibrational angular momentum. Allowed ($\Delta\ell = \pm 1$) transitions are sketched. Only one final state energy is accessible from $\ell'' = 0$ (e.g. 6_0) states, but when $|\ell''| = 1$, two final state energies ($|\ell'| = 0,2$) are possible; their separation is $4g'_{ii}$. Figure 5(b) represents the 6^1_0 and 6^2_1 bands schematically, showing the $4g' = 7$ cm^{-1} splitting in the latter. Observed bandshapes are helpful in assigning transitions.

B. IR Spectra

The IR vibrational spectrum of benzene can be obtained by fixing

the UV light at the 6_0^1 frequency and scanning the IR excitation. When the IR frequency is resonant with a transition to a vibrational state, population is removed from the 0_0 level and a dip in the R2PI ion signal results. Our spectrum in the region of the C-H stretching vibration obtained by this technique is shown in Fig. 6. There is only one infrared-active C-H stretching mode as predicted by the normal mode analysis, namely, ν_{20}. In the ground $\tilde{X}$ state, two combination modes have nearly the same frequency as the C-H stretch ν''_{20}, and are therefore in Fermi resonance with ν_{20}. They are anharmonically coupled with ν_{20} and each other, and have the e_{1u} symmetry. Three transitions are then observed, corresponding to the absorption peaks at 3048, 3079, and 3101 cm^{-1}. These transitions are originated from ν''_{20}, $\nu''_8 + \nu''_{19}$, and $\nu''_1 + \nu''_6 + \nu''_{19}$, respectively. The energy level diagram in Fig. 7 depicts how the levels shift due to anharmonic coupling. Because of the coupling, the new levels have mixed character. To avoid confusion, we label them a", b", and c". Upon analysis of the double-resonance spectra, it will be possible to say what the dominant character of each level is. Each level can now serve as a ground state for UV transitions to levels in the $\tilde{A}$ state, so that more $\tilde{A}$-state vibrational levels can be examined. This and the chance to unravel the details of the C-H stretching Fermi resonance add a new dimension to the already interesting challenge of finding ν'_{20}.

C. IR-UV Double Resonance Spectra

We obtained double-resonance signals via each of the states a", b", and c", in both the 6_1^0 and 6_0^1 regions. This was done by fixing the IR excitation to pump the desired level and scanning the UV frequency. Opening and closing the shutter in the IR beam modulated the

populations of molecules in the ground and excited vibrational states. The modulation was thus also imposed on the R2PI signals, and its UV frequency dependence was the information we desired. The spectra we present are actually the ion signals observed with the IR excitation on, minus the signals with it off. Thus all the features are due, in some way, to IR pumping.

Because the IR-excited levels a", b", and c" all have mixed character, it is expected that many transitions should exist in the UV spectra. The level $|a''\rangle$, for example, is actually $\alpha|20_1\rangle + \beta|8_1 19_1\rangle + \gamma|1_1 6_1 19_1\rangle$, with $\alpha^2 + \beta^2 + \gamma^2 = 1$, and $|\langle 20^1|a''\rangle|^2 \sim \alpha^2$, $|\langle 8^1 19^1|a''\rangle|^2 \sim \beta^2$, and $|\langle 1^1 6^1 19^1|a''\rangle|^2 \sim \gamma^2$. We assume that the Fermi resonance is quite different in the $\tilde{A}$ state with very different coefficients α, β, and γ. Then $|\langle b'|a''\rangle|^2 \neq 0$, etc. The picture in Fig. 2 (the double-resonance scheme) can be modified to reflect the state mixing: the CH_1 level then includes a", b", and c", and the CH^1 level splits into a', b', and c'. Accordingly, each (a", b", or c") in the $\tilde{X}$ state level could have transitions to three different $\tilde{A}$ state levels. A sketch of this situation is shown in Fig. 8(a). Note that since the doubly resonant transitions start from the common ground level state, $\nu_{IR} + \nu_{UV}$ for the transitions depends only on the energies of the final states. Thus, the UV transitions from the $\tilde{X}$ levels to a particular final state can be readily identified if the UV spectra are presented with the horizontal axes lined up to represent the <u>sum</u> of the IR and UV frequencies, as shown in Fig. 8(b). We have not included in Fig. 8(b) features due to depletion of the 0_0 level. Also, it is assumed that the strongest transitions come from $\langle a''| \rightarrow \langle a'|$, $\langle b''| \rightarrow \langle b'|$, and $\langle c''| \rightarrow \langle c'|$ because $|\langle a'|a''\rangle|^2 \gg |\langle a'|b''\rangle|^2$, etc. The top UV spectrum is

expected when the IR excitation pumps the a" transition, the middle spectrum is obtained with the b" level populated, and the bottom spectrum shows transitions from the c" state.

Our observed IR-UV double resonance spectra, arranged in the fashion of Fig. 8(b), are presented in Figs. 9 (for the 6_1^0 region) and 10 (for the 6_0^1 region). Because more transitions are actually present and depletion of the ground level population can give rise to additional features, the spectra appear more complicated, but can still be well understood after analysis following the approach outlined above, as we shall see.

In the R2PI spectra (Figs. 4ab) obtained with no IR excitation, each peak comes from a thermally populated $\tilde{X}$ vibrational level which can potentially be depleted by IR excitation. By looking at the dips in the double-resonance spectra (Figs. 9,10) one can see which of the thermal levels have their populations depleted by IR pumping at $\nu_{a"}$, $\nu_{b"}$, and $\nu_{c"}$. The dips in the spectra of Figs. 9 and 10 are labelled according to their ground state vibrational levels. Peaks, on the other hand, are assigned and labeled according to their final state identities. It is seen that, in addition to depopulating 0_0, the IR excitations also depopulated the 11_1 and 16_1 levels. This is because the hot-band excitations of the a", b" and c" modes from 11_1 and 16_1 also occur at $\nu_{a"}$, $\nu_{b"}$, and $\nu_{c"}$, respectively. The 6_1 level was depopulated by $\nu_{a"}$ and $\nu_{c"}$ excitations, but not by $\nu_{b"}$ excitation. The latter happens because the hot-band excitation $b"6_1 \leftarrow 6_1$ has a frequency red-shifted by ~ 3 cm^{-1} from the ground-state excitation $b" \leftarrow 0_0$.[49] In Fig. 10, at the peak of the 6_0^1 transition, the detector was saturated by the huge ion signal whether the IR excitation was on or

off, but at the wings of the peak, the detctor was able to record the IR-induced change in the 0_0 population, thus giving rise to a pair of dips.

We shall now try to account for all of the strong features, and a few of the weak ones, in the analysis.

V. ANALYSIS

The presence of the C-H stretching Fermi triad is fortuitous and fascinating. Through it we have access, with double resonance, to a great many vibrational levels in the $\tilde{A}$ state. None of these levels has been previously detected, and we have a chance to determine the frequencies of the modes which make up the combination levels a', b', c'. Since we will be using the values of several vibrational frequencies in our transition assignments and calculations of newly-determined frequencies, we present in Table I an up-to-date list of the known frequencies in the $\tilde{X}$ and $\tilde{A}$ states. Some of these are known very accurately, having been determined with high-resolution laser spectroscopy. Others have been deduced in 1956 by Brodersen and Langseth[13] or estimated from observations of slightly-allowed transitions in benzene derivatives with lower symmetry. We have cited original sources of the vibrational frequency determinations and give the frequencies to the nearest 0.1 cm^{-1} if they are so reliably known. Suspicious or indirectly determined frequencies are enclosed in parentheses.

Our plan for analyzing the double-resonance spectra (Figs. 9 and 10) uses a modified version of the model of Fig. 8; the main difference is that appropriate selection rules for the benzene $\tilde{A} \leftarrow \tilde{X}$ vibronic

transition are implemented. This model will account for most of the transitions, identify their upper states, and give the values of hitherto unknown vibrational frequencies (ν_3', ν_{19}' and ν_{20}'). Observed transitions which are not predicted by the model will then be assigned. Minor spectral features arising from hot bands will be identified. Finally, the "characters" of each of the a", b", and c" states comprising the C-H stretching Fermi triad will be assessed.

The first goal is to assign the UV transitions from the IR-excited levels a", b", and c". From earlier spectroscopic analysis,[13] it is known that a", b", and c" are mixtures of the 20_1, $8_1 19_1$, and $1_1 6_1 19_1$ states, as indicated in Fig. 7. For the benzene $\tilde{A} \leftarrow \tilde{X}$ UV transitions, the selection rules discussed in Sec. IV.A. require $\Delta v_6 = \pm 1$ and $\Delta v_1 =$ any integer, but $v_1' = v_1'' = 1$ would lead to a weak transition because of the small Franck-Condon factor. The upper states would be a', b', and c'. Thus, transitions from a", b", c" to a', b', c' (which are mixtures of 20^1, $8^1 19^1$, and $1^1 6^1 19^1$) shown in Fig. 8(a) are not allowed. We therefore consider only the ν_6-vibration-assisted transitions in the 6_0^1 and 6^9 regions. Figure 11 describes those upper states in $\tilde{A}$ that we believe we have observed in our spectra in Figs. 9 and 10. We assume in Fig. 11 that state mixing due to anharmonic vibrational coupling is not appreciable so that the states in $\tilde{A}$ retain more or less their pure mode character. This is largely vindicated by the analysis, as we shall see.

Figure 11(a) depicts the UV transitions in the 6_0^1 region with $\Delta v_6 = 1$ and $\Delta v_1 = 0$. Since the initial states involve 20_1, $8_1 19_1$, and $1_1 6_1 19_1$, the final states are thus $6^1 20^1$, $6^1 8^1 19^1$, and $1^1 6^2 19^1$. Figure 11(b) shows the transitions in the 6^9 region. The only final state

that can be reached from a", b", and c" with $\Delta v_6 = -1$ and $\Delta v_1 = 0$ is $1^1 19^1$. Coincidentally, the $6^2 19^1$ state is near $1^1 19^1$, and is accessible via a $\Delta v_6 = +1$, $\Delta v_1 = -1$ transition.

The energy levels in Fig. 11 are plotted as a function of the total energy $\nu_{IR} + \nu_{UV}$, which can be identified with the frequency scale of Figs. 9 and 10, except for a 0° constant offset. Energies of these vibrational levels in the excited electronic state can now be expressed in terms of the vibrational frequencies of ν_1', ν_6', ν_9', ν_{19}', and ν_{20}'. The first three are known from previous spectroscopic work (see Table I), thus allowing ν_{19}' and ν_{20}' to be determined from our spectra.

Figure 11 also shows splittings of the levels associated with $v_6' = 2$ and $v_6' = v_8' = 1$, due to the presence of vibrational angular momentum (see Fig. 5 and accompanying discussion). Theoretically, splittings could also be induced by vibrational angular momenta associated with modes 19 and 20. However, since these modes mainly involve motion of the H atoms, they cause little distortion of the carbon ring and hence have small vibration-rotation interactions. We can therefore ignore the resulting small splittings.

The transitions which are predicted from the selection rules to be strongest are shown in Fig. 11 by heavy lines. In the manner of Fig. 8(b), each final level can be identified with a trio of vertically-aligned peaks in Fig. 9 or Fig. 10, corresponding to IR excitations of the three states a", b", and c". Beginning with the 6φ region (Fig. 9), we can identify, from a frequency estimate, the intense peak at $E_{vib} = 2445$ cm^{-1} as the $6^2 19^1$ level. It is a doublet, as predicted, and the splitting is ~ 9 cm^{-1}, roughly in agreement with the 7 cm^{-1} splitting predicted in the model of Fig. 5. The $1^1 19^1$ level is

expected to appear as a weak singlet at ~ 120 cm^{-1} to the red of the $6^2 19^1$ doublet. Indeed, it appears, at $E'_{vib} \approx 2330$ cm^{-1} in Fig. 9.

Continuing into the 6^1_0 region (Fig. 10), the peak at $E'_{vib} \approx 3430$ cm^{-1} should correspond to the $6^1 8^1 19^1$ final level. It should appear as a doublet, as most clearly discerned in the a" spectrum in Fig. 10. Since the value of the vibrational angular momentum coupling constant $g'_{6,8}$ in Eq. (1) is not known, the magnitude of the splitting is not predicted.

Thus the energies of $1^1 19^1$, $6^2 19^1$ and $6^1 8^1 19^1$ are found. Only that of $6^1 20^1$ is yet to be found. There are <u>two</u> relatively intense peaks at $E'_{vib} \approx 3580$ and 3618 cm^{-1} in each spectrum in Fig. 10. They have a nearly <u>constant intensity ratio</u> of ~ 2, and must correspond to two related final states. Since both appear in the neighborhood of $6^1 20^1$, and are optically accessible via $\Delta v_6 = +1$ transitions, we postulate that they arise from a Fermi resonance between $6^1 20^1$ with another level (either $6^1 13^1$ or $6^1 8^1 14^1$). These levels are not noticeably split by vibrational angular momenta.

With the positions of the $1^1 19^1$ and $6^2 19^1$ combination levels secured, it is now possible to determine the frequency ν'_{19} by knowing ν'_1 and ν'_6. We consider two different approximations, both ignoring anharmonic shifts of levels involving ν'_{19}: (a) $\nu'_{19} = 1^1 19^1 - 1^1 = (1^1 19^1 - 0^0) - \nu'_1 = 2330\ cm^{-1} - 923\ cm^{-1} = 1407\ cm^{-1}$ and (b) $\nu'_{19} = 6^2 19^1 - 6^2$. In the latter case, the 6^2 state has two vibrational angular momentum components, $\ell' = 0$ and $\ell' = 2$. From the relation $E(v) = \Sigma\, \omega_i v_i + \Sigma\, x_{ij} v_i v_j + \Sigma\, g_{ij} \ell_i \ell_j$, with $\omega'_6 = 519.0\ cm^{-1}$, $x'_{6,6} = 0.7$ cm^{-1}, and $g'_{6,6} = 1.7\ cm^{-1}$,[24] we obtain $6^2\ (\ell' = 0) - 0^0 \approx 1041\ cm^{-1}$ and $6^2\ (\ell' = 2) - 0^0 \approx 1048\ cm^{-1}$. We then find $\nu'_{19} = 6^2 19^1 - 6^2 = 2443 -$

1041 cm^{-1} = 1402 cm^{-1} for $\ell' = 0$ and ν'_{19} = 2452 - 1048 = 1404 cm^{-1} for $\ell' = 2$. The averaged value of ν'_{19} determined from all these estimates is 1405 cm^{-1}, in fair agreement with Hochstrasser's recent assignment[35] of ν'_{19} = 1400 cm^{-1}, from a two-photon-induced fluorescence spectrum of a benzene crystal at 4.2°K, considering that the gas-to-crystal shift can easily exceed ~ 10 cm^{-1}.

The frequency of ν'_{19} can be used with the value of ν'_6 and ν'_8 to predict the position of the $6^1 8^1 19^1$ level: E'_{vib} = = $\nu'_6 + \nu'_8 + \nu'_{19}$ = 3442 cm^{-1}. This is ~ 12 cm^{-1} higher than the observed position at E'_{vib} = 3430 cm^{-1}; an anharmonic shift due to interactions between the three modes ν'_6, ν'_8 and ν'_{19} could easily account for the difference.

We now wish to deduce ν'_{20} from the doublet we have assigned to be associated with $6^1 20^1$. The final states of the doublet are believed to originate from $6^1 20^1$ and another state (either $6^1 13^1$ or $6^1 8^1 14^1$) to which the transitions from a", b", and c" have zero intensity. If W is the coupling matrix element between $6^1 20^1$ and the other state, ΔE_o and ΔE the energy separations between the two states before and after taking into account the coupling, respectively, and R is the intensity ratio of the two observed peaks, then Daunt and Shurvell[50] have shown that

$$\frac{W}{\Delta E} = \frac{\sqrt{R}}{R + 1} ,$$

$$\frac{\Delta E_o}{\Delta E} = \frac{R - 1}{R + 1} .$$

The more intense peak is associated with the perturbed $6^1 20^1$ state.

Using these equations with the observed $\Delta E = 38\ cm^{-1}$ and R = 2, we find $\Delta E_o = 13\ cm^{-1}$ and $W = 18\ cm^{-1}$. Therefore, the original decoupled states should have vibrational energies of $E'_{vib} = (1/2)[(3618 + 3580) \pm 13] = 3605$ and $3592\ cm^{-1}$. The former is the vibrational energy of the decoupled $6^1 20^1$ state, and we find $\nu'_{20} = 6^1 20^1 - 6^1 = (6^1 20^1 - 0^0) - \nu'_6 = 3605\ cm^{-1} - 521\ cm^{-1} = 3084\ cm^{-1}$. A possibility for the perturbing state is $6^1 8^1 14^1$. A harmonic prediction of its position is $E'_{vib} = \nu'_6 + \nu'_{18} + \nu'_{14} = 3607\ cm^{-1}$; anharmonicity would make the actual position lower, and closer to the $E'_{vib} = 3592\ cm^{-1}$ location of the decoupled perturber. The $6^1 20^1$ and $6^1 8^1 14^1$ levels have the same symmetry and can interact; note that 20^1 (e_{1u}) and $8^1 14^1$ ($e_{2g} \cdot b_{2u} = e_{1u}$) also can interact. Another possibility for the perturber is $6^1 13^1$ ($e_{2g} \cdot b_{1u} = e_{1u}$) which can interact with $6^1 20^1$ ($e_{2g} \cdot e_{1u} = b_{1u} + b_{2u} + e_{1u}$) by symmetry. The frequency ν'_{13} would be $3592 - 521 = 3071\ cm^{-1}$. This is quite different from the value - $3160\ cm^{-1}$ predicted by Robey[5] and Krogh-Jespersen.[6]

In Figs. 9 and 10, we notice that the c" spectra (Figs. 9, 10) have 3 extra peaks at $E'_{vib} = 2477$, 3402, and $3522\ cm^{-1}$. They must arise from UV transitions from the c" state, but we seem to have already exhausted all possibilities. Recently, however, Pliva[41] has shown, experimentally and theoretically, that the C-H stretching fundamental region actually contains a Fermi tetrad instead of the triad a", b", and c". It is believed that the original c" state is nearly degenerate with $3_1 6_1 15_1$ and hence the two states mix and create two new states c''_1 and c''_2 at ~ $3101\ cm^{-1}$ with only $1\ cm^{-1}$ separation between them [see Fig. (12)]. The a" and b" states are, however, sufficiently far away not to be affected by $3_1 6_1 15_1$. In our IR excitation, because of the

limited laser resolution c_1'' and c_2'' were always simultaneously excited.

If we accept this picture of Pliva, the assignment of the extra peaks in the c" spectra would be straightforward. They should be ν_6-assisted $\tilde{A} \leftarrow \tilde{X}$ transitions, and must therefore involve the following final states $3^1 15^1$ for $v_6 = -1$, $3^1 6^2 15^1$ for $\Delta v_6 = +1$, and $1^1 3^1 15^1$ for $\Delta v_6 = -1$ and $\Delta v_1 = +1$. These transitions have similar Franck-Condon factors and hence nearly equal intensities. The transition to $3^1 6^2 15^1$ ought to display a doublet or complex bandshape due to the presence of more than one vibrational angular momentum (ℓ') level in the $3^1 6^2 15^1$ final state. These expectations are completely fulfilled. We can indeed assign peaks in the c" spectra of Figs. 9 and 10 as transitions from c" to $3^1 15^1$ at $E'_{vib} = 2477\ cm^{-1}$, to $1^1 3^1 15^1$ at $E'_{vib} = 3402\ cm^{-1}$, and to $3^1 6^2 15^1$ (which has a complex bandshape; its high-frequency "notch" is assumed to be the band center) at $E'_{vib} = 3522\ cm^{-1}$.

The mode frequency ν_3' can now be determined, knowing $\nu_1' = 923\ cm^{-1}$, $\nu_{15}' = 1150\ cm^{-1}$, and $\nu_6' = 521\ cm^{-1}$ from Table I. From $E'_{vib} = 2477\ cm^{-1}$ for $3^1 15^1$, we deduce $\nu_3' = 1327\ cm^{-1}$; from $E'_{vib} = 3402\ cm^{-1}$ for $1^1 3^1 15^1$, $\nu_3' = 1328\ cm^{-1}$; and from $E'_{vib} = 3522\ cm^{-1}$ for $3^1 6^2 15^1$, $\nu_3' \sim 1330\ cm^{-1}$. Since the first value should be least affected by the neglect of anharmonic corrections to the total vibrational energy, it is the preferred one. Thus we pick $\nu_3' = 1327\ cm^{-1}$.

All the peaks in the double resonance spectra of Figs. 9 and 10 whose IR transitions originated from 0_0 level, have now been assigned. The remaining peaks can be associated with double resonances originating from some IR hot bands. Recalling that the 11_1 and 16_1 levels are thermally populated (see Sec. IV), we expect that the IR-UV double resonance transitions to $6^2 19^1 11^1$ and $6^2 19^1 16^1$ should also

appear in the spectrum of Fig. 9. Their positions are predicted to have shifted by ~ -160 cm^{-1} from the transitions to $6^2 19^1$, as estimated from Table I or the separation between 6_0^1 and the $6_0^1 11_1^1$/ $6_0^1 16_1^1$ features in Fig. 4(b). Figure 9 shows that there is indeed a weak doublet in the b" spectrum at E''_{vib} = 2280,2288 cm^{-1}, which is 163 cm^{-1} lower than the intense $6^2 19^1$ doublet at E'_{vib} = 2243,2252 cm^{-1}.

Relative intensities of the different peaks in the double-resonance spectra give information about the state mixing in the C-H stretching Fermi tetrad. For example, the relative intensities of the transitions from a", b", and c" to $6^1 8^1 19^1$ are determined by the squared matrix elements $|\langle 6^1 8^1 19^1|\mu|a''\rangle|^2$, etc. These in turn are proportional to the Franck-Condon factors $|\langle 8^1 19^1|a''\rangle|^2$ etc., because ν_6 is responsible for inducing the transition but ν_8 and ν_{19} are not. Also, because ν'_8 and ν'_{19} differ only slightly from ν''_8 and ν''_{19}, respectively, their mode displacements must be similar in the two electronic states. The relation $|\langle 8^1 19^1|8_1 19_1\rangle|^2 \sim 1$ then holds. This in turn implies that $|\langle 8^1 19^1|a''\rangle|^2 \sim |\langle 8_1 19_1|a''\rangle|^2$. Then, the fact that the $6^1 8^1 19^1$ signal is largest from the a" state indicates that a" has more of the character of $8_1 19_1$ than b" or c".

Similarly, a" is found to have more ν''_{20} character than b" or c" because the a" spectrum has the biggest $6^1 20^1$ peaks. Following the same line of argument, we find b" has the most $6_1 1_1 19_1$ character (contradicting the early assignment of b" in the literature[12]). $c''_{1,2}$ contains a substantial admixture of $\nu''_3 + \nu''_6 + \nu''_{15}$, but also has contributions to its makeup from 20_1, $8_1 19_1$, and $1_1 6_1 19_1$.

Knowledge of the $\nu''_1 + \nu''_6 = \nu''_{19}$ "parentage" of the b" state is also useful in explaining the observed 3 cm^{-1} shift between b"6_1 + 6_1 and b"

← 0_0 as described at the end of Sec. IV. This occurs because b" has most of the ν_6'' character in the Fermi tetrad, and hence its anharmonic frequency shift due to interaction with 6_1 is the largest. It is known that anharmonic interaction with in a mode is usually larger than that between modes. None of the a", b", or c" levels contains ν_{11}'' or ν_{16}'', so no appreciable shift of a", b", or c" is expected to be induced by interaction with ν_{11}'' or ν_{16}''.

This completes the analysis of the spectra. Since it was a long process, replete with detail, we summarize now the main points.

1. With IR excitation around 3000 cm^{-1} we have selectively created populations in the a", b", and $c_{1,2}''$ states. These states, which are in Fermi resonance, are derived from the zeroth-order states ν_{20}'', ν_8'' + ν_{19}'', ν_1'' + ν_6'' + ν_{19}'', and ν_3'' + ν_6'' + ν_{15}''.

2. We have observed UV transitions from each of these levels, and thereby managed to get a rough estimate of the makeup of each. Pliva's[41] analysis, which asserts that the b" state most nearly resembles ν_1'' + ν_6'' + ν_{19}'', is confirmed. Also, the presence of ν_3'' + ν_6'' + ν_{15}'' in the c" level, but not in the other levels, is unambiguously proven.

3. We have evaluated the mode frequencies of ν_3', ν_{19}', and ν_{20}' in the excited electronic $\tilde{A}$ state, heretofore undetermined in gas-phase studies. They are ν_{19}' = 1405 cm^{-1}, ν_3' = 1327 cm^{-1}, and ν_{20}' = 3084 cm^{-1}.

4. We have detected the possible existence of an $\tilde{A}$ state Fermi resonance which splits the $6^1 20^1$ level. The coupling state could be $6^1 8^1 14^1$ or $6^1 13^1$. If the latter is the case, it would give ν_{13}' a frequency of ~ 3071 cm^{-1}.

VI. DISCUSSION

A. Review of in-plane force field problem

The new frequency assignments provide new insight into the chemical bonding and vibrational behavior of benzene in its $\tilde{A}$ ($^1B_{2u}$) state, and serve as a test of recently calculated force fields. We shall show that current $\tilde{A}$ state force fields may have been calculated with incorrect vibrational frequencies as input data. For this purpose, assignments of $\tilde{A}$ state C-H stretching frequencies will be critically reviewed: Our goal is to arrive at a self-consistent picture of the C-H stretches in the $\tilde{X}$ and $\tilde{A}$ states. Before discussing the implications of the new data, let us recall how the vibrational frequencies and force fields are related, with the in-plane modes of benzene as an example.

There are two standard ways to express the intramolecular vibrational potential energy of a molecule: in terms of "valence" (internal) coordinates and valence forces, and alternatively in terms of "symmetry" coordinates and symmetry force constants. The two approaches are related by a linear coordinate transformation.

Figure 13 is a picture of a benzene molecule with its internal coordinates for planar motions labeled. In this picture, S_i and β_i represent stretching and bending of the i^{th} C-H bond, and t_i represents stretching of the i^{th} C-C bond. α_i describes deviation of the C-C-C bond angle of the i^{th} node from its equilibrium value of 120°. With this description of the coordinates, the potential energy in the harmonic approximation is expressed as $V = \sum V_{ij} r_i r_j$, where the r_i's are generalized displacements in the internal coordinates. There are 44 distinct, nonzero valence force constants v_{ij}, but in his early work Wilson[11] used only the four diagonal ones representing C-C stretching,

C-H stretching, C-H bending, and C-C-C bond bending, and neglected the others.

In terms of symmetry coordinates, the potential in the harmonic approximation is

$$V = \sum_{ij} F_{ij} q_i q_j, \qquad (2)$$

where the q_i's are generalized displacements in the symmetry coordinates. For example, q_2 describes the totally-symmetric C-H-stretch coordinate $1/\sqrt{6}\ (S_1 + S_2 + S_3 + S_4 + S_5 + S_6)$. The same symmetry argument that was used to find selection rules on the transition dipole moment $\langle \tilde{A} | \vec{\mu} | \tilde{X} \rangle$ applies here: V should not change under a symmetry operation. For this to be true, only terms in which the product $q_i q_j$ is of the totally-symmetric (a_{1g} in benzene) class can contribute. $F_{ij} = 0$ unless q_i and q_j are of the same symmetry class; in other words, vibrations of different symmetries are non-interacting. If the kinetic energy T of the vibrations is written as $T = \sum_{ij} m_{ij} q_i q_j$, the same symmetry argument applies. Figure 14 shows how the $\underline{F}$ and $\underline{m}$ strices look for the in-plane vibrations. Normal mode frequencies and expansions in terms of symmetry coordinates are obtained by solving the secular equation $|\underline{F} - 4\pi^2\nu^2\underline{m}| = 0$. Since the $\underline{F}$ and $\underline{m}$ matrices are block-diagonal, the many equations can be solved one symmetry block at a time. With the eigenvalues ν known experimentally, and the $\underline{m}$ matrix known from the structure and mass distribution of the molecule, the F_{ij}'s can be determined. For example, $F_{2,2}$ is the force constant associated with the totally symmetric pure C-H stretch q_2. The <u>observed</u> totally-symmetric "C-Hstretch" ν_2, at 3074 cm^{-1}, largely

involves motion in the q_2 coordinate, but has a slight C-C stretch component (q_1) as well. Conversely, the totally-symmetric "C-C stretch" ν_1 (993 cm^{-1}), is mostly q_1, but contains a bit of q_2. $F_{2,2}$, therefore, depends greatly on ν_2, and slightly on ν_1.

It is hoped that through force constant fitting, and ab initio calculation, one could obtain the valence force constants V_{ij} that would describe the chemical bonds. Naively, finding the valence force constants proceeds in the following manner: the normal mode frequencies are used with the secular equation(s) to find the normal coordinates and symmetry force constants F_{ij}. A linear transformation is then used to find V_{ij} from F_{ij}.

An obstacle in determining the force constants is in the fact that the input data is often insufficient. Consider the example of the 14 in-plane modes of benzene, of which 7 are degenerate. Spectroscopically, we may obtain from measurements the 14 vibrational frequencies of the modes, and 7 Coriolis constants (ζ) constants of the 7 degenerate modes. Thus, there are a total of 21 input data, but from Fig. 14, the number of nonvanishing force constants F_{ij} for the 14 in-plane modes is 26, which exceeds the number of data. The force field is thus underdetermined.

For example, considering the a_{1g} symmetry block in Fig. 14, one would have only ν_1 and ν_2 to determine 3 force constants $F_{1,1}$, $F_{2,2}$, and $F_{1,2}$. There are alternative sets of solutions in such a case, and the choice between them is guided by chemical intuition. Normally the smaller value of $F_{1,2}$ is chosen because according to the molecular orbital theory, different electrons in the C-C (ν_1) and C-H (ν_2) bonds hardly interact. Occasionally the choice between the alternative

solutions is controversial; for example, the discussion concerning the value of $F_{14,15}$ for benzene began roughly two decades ago[8] and still continues.[2]

The corresponding valence force constants for the in-plane vibrations have been discussed by Duinker and Mills;[8] there are 33 of them. Even if the 26 in-plane symmetry force constants F_{ij} are correctly found, they are expressed as linear combinations of the 33 valence force constants V_{ij}. The cause of the disparity in the number of force constants in the symmetry and valence force fields is that some of the valence force constants are associated with motions in redundant (or "null") symmetry coordinates.[10,51] As an illustration, sufficient valence force constants exist to express the resistance to simultaneous opening up of all C-C-C bond angles α. The symmetry coordinate for this motion is $1/\sqrt{6}\ (\alpha_1 + \alpha_2 + \alpha_3 + \alpha_4 + \alpha_5 + \alpha_6)$. But since benzene is ring-shaped, the constraint $\Sigma\ \alpha_i = 0$ makes motion in this coordinate impossible. This does not imply that any of the valence force constants describing carbon ring bending are zero: they simply are not independent. Many of the 33 valence force constants are routinely assigned null values on the basis of intuition, but as experimental data become more plentiful and calculations get more sophisticated, that approach loses its appeal.[3] The problem of providing enough data to determine a force field can in principle be solved by spectroscopic measurements on isotopically- substituted benzenes, which have the same chemical bonds and valence forces, but different normal modes and vibrational frequencies. Such a fully determined force field has recently been published[3] for the ground ($\tilde{X}$; $^1A_{1g}$) state of benzene, resulting from a fit to 244 experimental data

on various substituted benzenes. It is not in agreement with predictions[2] from ab initio calculations.

For future reference, Table II is a list of the in-plane modes, their experimental $\tilde{X}$ and $\tilde{A}$ state frequencies, and their $\tilde{A}$ state values calculated in 1977 by Robey and Schlag[5] and in 1984 by Krogh-Jespersen et al.[6] Both of the calculations are fits to experimental data. The Robey-Schlag field has salient errors in its prediction of ν_3' and ν_8', neither of which was known at the time. (Nor was ν_{12}', ν_{13}', or ν_{20}'!) With 17 valence force parameters, their force field reproduced the 8 known vibrational frequencies and two known Coriolis constants. The average error was only ~ 0.33%. Important spectroscopic developments occurred around and after the time of their work, causing the force field to be re-examined by Krogh-Jespersen et al. Especially relevant were the determinations of ν_{19}' and ν_8'. A description of these experiments follows.

B. Review of recent experiments

This section describes progress in finding two specific $\tilde{A}$ state vibrational frequencies, namely, ν_{19}' and ν_8'. Several experiments with two-photon excitation have been done, resulting in many reports of ν_{19}', predicted to be a mode that can induce the $\tilde{A} \leftrightarrow \tilde{X}$ transition. The first value, 1560 cm^{-1}, was found by Hochstrasser et al.,[26] who were actually observing the 14_0^1 band. Bray et al.[27] later found a distinct, weak peak near this 14_0^1 band and called it 19_0^1 with ν_{19}' = 1586 cm^{-1}. Friedrich and McClain[28] revised this to ν_{19}' = 1579 cm^{-1}. Wunsch et al.[29,30] pointed out that this extra peak was actually a rotational branch of the 14_0^1 band and managed to find ν_{19}' = 1213 cm^{-1} in C_6D_6. Lombardi et al.[34] also found ν_{19}' = 1209 cm^{-1} in C_6D_6; they estimated

that $\nu'_{19} = 1330\ cm^{-1}$ in C_6H_6. However, it seems to us that the isotopic product rule[10] $\nu_{18D}\nu_{19D}\nu_{20D}/\nu_{18H}\nu_{19H}\nu_{20H} = (m_H/m_D)\sqrt{(M_D/M_H)}$ could have been used to estimate this frequency more accurately. (The capital M's represent the total masses of the isotopic molecules.) $\nu'_{20H,D}$ was not known, but with the reasonable assumption that $\nu'_{20} = \nu_{20}$ and knowing $\nu'_{18D} = 758\ cm^{-1}$, $\nu'_{19D} = 1209\ cm^{-1}$, and $\nu'_{18H} = 922\ cm^{-1}$, one gets $\nu'_{19H} = 1430\ cm^{-1}$, an answer nearly in agreement with the 1405 cm^{-1} value we have obtained. Wunsch et al.[32] correctly surmised that $\nu'_{19} \sim 1410\ cm^{-1}$, and that the 19^1_0 band was buried under the intense $14^1_0 16^1_1$ band at 1408.0 cm^{-1}.[33] In spite of the fact that this latter band appears to be very sharp and narrow in the molecular beam spectrum of Sur et al.,[33] its width at the 10% height is ~ 6-7 cm^{-1}. It is therefore conceivable that the $14^1_0 16^1_1$ and 19^1_0 bands coincide. Hochstrasser et al.[35] also found $\nu'_{19} = 1400\ cm^{-1}$ in a 4.2°K benzene crystal. But since this last work, Aron et al.[52] and Sur et al.[33] have found reason to support the 1330 cm^{-1} value of Lombardi et al.[34] To solve the controversy, we suggest that a high-resolution two-photon $\tilde{X} \leftarrow \tilde{A}$ absorption spectrum around $E'_{vib} = 1410\ cm^{-1}$ should be obtained in a very cold molecular beam. By suppressing th $14^1_0 16^1_1$ peak via cooling, the 19^1_0 may become more distinct.

The ν'_8 frequency had long been sought, since as an e_{2g} mode ν_8 can induce the one-photon $\tilde{A} \leftarrow \tilde{X}$ transition. The 8^1_0 transition was discovered in 1983 by Otis et al.[25] by using three-photon fluorescence excitation spectroscopy. The assignment was confirmed by the one-photon absorption spectroscopy measurement of Muller and Knight,[53] and the final value $\nu'_8 = 1516\ cm^{-1}$ was obtained from the molecular beam spectrum of Stephenson et al.[47] This accurately determined value of ν'_8

made it worthwhile to revise the earlier force field calculations.

C. New force field

Still using 17 valence force constants, Krogh-Jespersen et al.[6] recently were able to improve on the Robey-Schlag force field. Whereas Robey and Schlag had used input data from two isotopic benzenes C_6H_6 and C_6D_6, Krogh-Jespersen et al. used frequency from six molecules C_6H_6, s-$C_6H_3D_3$, p-$C_6H_4D_2$, p-$C_6H_2D_4$, m-$C_6H_4D_2$, and C_6H_5D.

The value $\nu_{19}' = 1347\ cm^{-1}$, obtained by them from analyzing the work of Aron et al.[52] is unfortunately incorrect (our value is $1405\ cm^{-1}$). It is not stated whether ν_{19}' was observed in the other five benzenes they studied. An iterative technique was used, in which force constants were adjusted so that calculated vibrational frequencies agreed best with the experimental data. Their calculated ν_{19}' value of $1359\ cm^{-1}$ is the only salient disagreement with current data on C_6H_6. The errors in ν_3' and ν_8' as determined by the Robey-Schlag field have been removed, but there is now an error in ν_{19}'. There is as yet no force field that reproduces all known vibrational frequencies correctly.

In order to show how difficult it is to determine a force field, we give a picture of the effects of the use of an incorrect vibrational frequency. This will motivate a reassessment of the "big picture" of the $\tilde{A}$-state in-plane vibrational frequencies. A good starting point is to consider the nominally C-H bending modes (3, 9, 15, and 19). Of these, ν_3, a pure C-H bending mode (see Fig. 1) is unique in being the only one of its (a_{2g}) symmetry class. This means that the symmetry force constant $F_{3,3}$ is uniquely defined. If the C-H bonds were non-interacting, the diagonal C-H bending (valence) force constant would also be known accurately; it would be a multiple of $F_{3,3}$.

Unfortunately, this is not the case; the recent parameterizations of the potential have included small but non-negligible off-diagonal interactions between bending motions on different C-H bonds. $F_{3,3}$ depends on these interactions.

The C-H bending valence force constant is of major importance in determining the frequencies of the four modes 3, 9, 15, and 19. These frequencies also depend on constants which describe ortho-, meta-, and para-type interactions between C-H bends on sites separated by one, two, or three carbon atoms. Also, ν_3 is the only mode which is purely C-H bending. The other three (ν_9, ν_{15}, and ν_{19}) are admixtures with the C-C stretching modes (ν_8, ν_{14}, and ν_{18}) of their respective symmetries. This means that the C-C stretching diagonal force constant and off-diagonal ortho-, meta-, and para-interactions come into play in determining their frequencies. Changes in the values of the C-C stretching force constants also affect the geometries and frequencies of the C-C stretching modes 1, 8, 14, and 18. As a result, the C-H bending and C-C stretching valence force constants and mode frequencies are all strongly interdependent. When a force field is fitted to experimental frequencies, a change in one of the frequencies necessitates a change in a large number of valence force constants and hence the frequencies of the other modes. Clearly a force field can be "poisoned" if a single incorrect datum is employed in the calculation.

D. New perspective on $\tilde{A}$ state vibrations

Evidently it is wise to regard the calculated $\tilde{A}$ state force fields as one obtained from computer-optimized, underdetermined parameterizations which are not absolutely trustworthy. In that spirit, the assignments of the C-H stretching frequencies are

questioned, with the goal of providing a qualitative, self-consistent picture of benzene's $\tilde{A}$ state vibrations. Our new data are helpful in this task.

In the molecular orbital description of the $\tilde{A} \leftarrow \tilde{X}$ transition, a π electron in the carbon ring makes a $\pi^* \leftarrow \pi$ bonding-to-antibonding transition. The carbon ring weakens, and the C-C bond length increases from 1.3974(10) A to 1.4319(9) A, a lengthening of .0345(15) A.[31] Therefore, the carbon ring is easier to squash, twist, and stretch, as evidenced by the reductions in normal mode frequencies upon going from $\tilde{X}$ to $\tilde{A}$. This happens for all the out-of-plane modes, the "C-C-C angle-bending" (squashing) vibrations ν_6 and ν_{12}, and the "C-C stretches" ν_1, ν_8, and ν_{18}.

The nominally C-C stretching mode, ν_{14}, shows on the other hand a frequency <u>increase</u> of 260 cm^{-1}! Calculation of the frequency of this mode has always been problematic. Mikami and Ito[54] explain the observation by the argument that in the ground ($\tilde{X}$) state, its symmetry force constant and frequency are lower than those predicted by simple estimates. Their reasoning is this: In the $\tilde{X}$ state, C-C bond distortion with b_{2u} symmetry forces the other bonds of the molecule to rearrange into the "Kekule structure", in which the C-C bonds are alternately single and double. This conformation, with the double bonds shorter than the single ones, is supposed to be relatively more stable (low-energy), so that the molecule is more susceptible to such a deformation. The b_{2u} vibrational frequency is thereby lowered. The same argument does not apply to the $\tilde{A}$ state because there are not enough bonding electrons for three double bonds. Simulating this effect in model force fields is, however, difficult.[2]

The C-H σ bonds should not be strongly affected by the $\tilde{A} \leftarrow \tilde{X}$, $\pi^* \leftarrow \pi$ transition because their σ electrons are not part of the π cloud.[54] We expect that the C-H bending force constant could appear to be slightly less in the $\tilde{A}$ state than in the $\tilde{X}$ state, because bending a C-H bond also tends to cause some C-C stretching motion in the weakened carbon ring. This effect can be important in the normal mode analysis because the C-C stretching and C-H bending frequencies at 1000-1500 cm^{-1} are not widely separated: Many modes in that region have mixed C-C stretch/C-H bend characteristics. The C-H stretches, at ~ 3000 cm^{-1}, are however much more decoupled, and their force constants should be largely unaffected.

In addition to determining the 0.035 A increase in the C-C bond length caused by the $\tilde{A} \leftarrow \tilde{X}$ transition, Lombardi et al.[31] found that the C-H bond length change was zero, with an uncertainty of 0.005 A. Thus the C-H bond strength is expected to be about the same in the $\tilde{X}$ and $\tilde{A}$ states. Compared to the changes in the frequencies of the C-C stretching modes in going from $\tilde{X}$ to $\tilde{A}$ we have already mentioned, reductions in the "C-H bending" frequencies of ν_3, ν_9, ν_{15}, and ν_{19} should be rather small. Indeed, Table I shows that the "pure" bending mode ν_3 decreases by ~ 20 cm^{-1}; ν_9 goes down ~ 30 cm^{-1}, ν_{15} does not change, and ν_{19} loses ~ 80 cm^{-1}. The average reduction of these mode frequencies only amounts to ~ 2.5%.

Now we look at the C-H stretches ν_2, ν_7, ν_{13}, and ν_{20}. In the $\tilde{X}$ state their frequencies all fall within a 20 cm^{-1} range. Since the C-H bond strength is nearly unaffected by electronic excitation in the carbon ring, the C-H stretching modes in the $\tilde{A}$ state are expected to be about the same as in the $\tilde{X}$ state. Table I shows that ν_7 increases by

only 20 cm^{-1} in the $\tilde{A}$ state. The 3077 cm^{-1} assignment of ν_7' is reliable because, as an e_{2g} mode, the ν_7-assisted $\tilde{A} \leftarrow \tilde{X}$ transition should be easily detectable. Also, there are no other strong transitions near the 7_0^1 band. Therefore, the assignment is unambiguous. The values of ν_{20}'' (3065 cm^{-1}) and ν_{20}' (3084 cm^{-1}) also show a ~ 20 cm^{-1} difference. The small increase in the C-H stretching frequencies caused by the $\tilde{A} \leftarrow \tilde{X}$ transition is explained as follows: The $\pi^* \leftarrow \pi$ transition makes the π electrons in the C-C bonds repel each other slightly and shift into the C-H bonds, thereby strengthening them and increasing the C-H stretching frequency.

The 3130 cm^{-1} value of ν_2' assigned by Atkinson and Parameter[23] appears to be 56 cm^{-1}, instead of ~ 20 cm^{-1}, higher than ν_2''. This makes the assignment questionable. Mikami[54] has suggested that the 3130 cm^{-1} vibration in the $\tilde{A}$ state may actually correspond to the $2\nu_{14}$ mode: $2\nu_{14}$ has a_{1g} symmetry, the energy is almost exactly correct, and the Franck-Condon factor $|\langle 14^2|0_0\rangle|^2$ is nonzero because mode 14 has different frequencies and spatial wave functions in the $\tilde{X}$ and $\tilde{A}$ states. In their extensive analysis of the $\tilde{A} \leftarrow \tilde{X}$ absorption spectrum, Atkinson and Parmenter[24] had found ν_2' through identification of a progression which they assigned as $6_0^1 2_0^1 1_0^n$, where n ranges from 0 to 4. However, there is a slightly weaker progression 41 cm^{-1} lower. The lowest-frequency member occurs at 41700 cm^{-1}. If <u>this</u> were called $6_0^1 2_0^1$, we would have $\nu_2' = 6^1 2^1 - 0^0 - \nu_6' = 3093$ cm^{-1}. Since no assignment was proposed for these transitions, we suggest that <u>they</u> could be the $6_0^1 2_0^1 1_0^n$ bands, and claim that $\nu_2' = 3093$ cm^{-1}. This value fits into the new picture and is ~ 20 cm^{-1} higher than ν_2'' at 3074 cm^{-1}.

Finally we consider ν_{13}', unobserved to date because of its b_{1u}

symmetry. Force field calculatins by Robey and Schlag, and by Krogh-Jespersen et al., put ν'_{13} at ~ 3160 cm^{-1}. However, this may not be reliable as the force field which yields this number has been constrained to reproduce what we believe to be an incorrect value of ν'_2. Being a C-H stretching mode, it seems likely that ν'_{13} is also ~ 20 cm^{-1} higher than ν''_{13}, or ν'_{13} = 3077 cm^{-1}. This is about the value it would need to have to cause a Fermi resonance between the $6^1 20^1$ and $6^1 13^1$ levels, as we speculated in the Analysis section.

Here, we have determined the frequency (ν'_{20}) of one of the four $\tilde{A}$ state C-H stretches. It and the other reliably-assigned mode frequency (ν'_7) are both ~ 20 cm^{-1} higher than their $\tilde{X}$ state values. This fact has led us to scrutinize previous spectroscopic work and propose a reassignment of the frequency of a third C-H stretch (ν'_2), so that its behavior also follows the same pattern. It also allows us to predict the frequency of the fourth C-H stretch (ν'_{13}) to be ~ 80 cm^{-1} lower than the force field calculations suggest. It would now be worthwhile to repeat the force field fitting with these augmented data and altered frequency assignments.

VII. CONCLUSION

We have used the powerful, elegant double-resonance technique to study a prototype large molecule (benzene) cooled in a supersonic expansion. The thorough work which has already been done on the $\tilde{X}$ vibrations and the $\tilde{A} \leftarrow \tilde{X}$ transition of benzene allowed us to make decisive assignments of several IR-pumping-induced UV transitions. With these assignments we were able to confirm, in a qualitative way, Pliva's analysis of the C-H stretching Fermi tetrad in the $\tilde{X}$ state.

Also, we provided a determination of the gas-phase value of ν'_{19}, the IR-active C-H bend, and the first observation in the $\tilde{A}$ state of ν_3, the "C-H libration", and of ν_{20}, the IR-active C-H stretch. The values of these frequencies are found to be $\nu'_{19} = 1405\ cm^{-1}$, $\nu'_3 = 1327\ cm^{-1}$, and $\nu'_{20} = 3084\ cm^{-1}$.

Observation of a Fermi resonance with the $6^1 20^1$ level led us to speculate that $\nu'_6 + \nu'_{20}$ could be perturbed by $\nu'_6 + \nu'_8 + \nu'_{14}$, or $\nu'_6 + \nu'_{13}$. If the latter were the case, it would determine the unobserved ν'_{13} frequency as ~ 3071 cm^{-1}.

A qualitative consideration of the valence forces at work in $\tilde{A}$-state benzene impelled us to assert that the C-H bonds are largely unaffected by the $\tilde{A} \leftarrow \tilde{X}$ transition. C-H stretching frequencies ν_2, ν_7, ν_{13}, and ν_{20} should increase uniformly by ~ 20 cm^{-1} in the $\tilde{A}$ state. ν_7 and ν_{20} fit this pattern. The longstanding assignment of ν'_2, the totally symmetric C-H stretch, does not. A review of the data of Atkinson and Parmenter[24] supports our suspicion that ν'_2 is really ~ 3093 cm^{-1}, 20 cm^{-1} above the $\tilde{X}$-state value. In this context, ν_{13}, the unobserved IR- and Raman-inactive b_{1u} C-H stretch could very well have a value of ~ 3070-3080 cm^{-1}.

The $\tilde{A}$ state force fields of Robey and Schlag[5] and Krogh-Jespersen et al.[6] do not reproduce our experimental results and disagree with our qualitative analysis of the benzene molecule in its first excited state. Our analysis shows that the $\tilde{A}$ state resembles the $\tilde{X}$ state to a higher degree than was thought. Fitting of force fields should be easier when the more realistic vibrational frequencies we now have are used as input data.

Even with new vibrational frequencies, the data are insufficient to

completely determine a force field. Now that it is widely recognized[3] that a large spectroscopic data base is required for the attainment of a plausible fit, we hope that our technique, and variants of it, will be espoused in the quest for accurate data on hard-to-observe modes. There are several ways in which this could proceed: (1) Study of the selectively deuterated benzenes, as has been done in the $\tilde{X}$ state, would provide extremely useful data on normal modes, frequencies, and assignments. (2) Higher resolution (~ .001 cm^{-1}) lasers could give well-resolved rotational structure, leading to the determination of vibration-rotation interaction (Coriolis) constants. These constants can be used as input data for force-field refinement calculations. (3) Different optical transitions could be employed: namely, (a) many IR-active modes in the ~ 1000 cm^{-1} region could be pumped with a CO_2 laser. (b) Raman pumping instead of IR pumping could be used to populate different $\tilde{X}$ state modes, as demonstrated by Esherick and Owyoung.[21] (c) The second step of the double-resonance excitation could be done with multiphoton transitions instead of single photon transitions. This would allow different $\tilde{A}$ levels to be studied, and would present the opportunity for polarization-dependence studies of transitions in the new modes. Clearly, there are many possibilities, each of which can lead to interesting information about the excited states of aromatic molecules.

A thorough understanding of the first excited state of a simple phenyl system could prove useful in several situations. Vibrations and their anharmonicity are thought to be important in mediating radiationless transitions. Radiationless decay is not thoroughly characterized in either the $\tilde{X}$ or $\tilde{A}$ states of benzene. Also, the

electronic properties of phenyls help to determine the qualities of many molecules of photophysical and photochemical interest. For example, phenyl rings form the basis of many (e.g. laser) dyes. Enhancements in lasing efficiency and photochemical stability could perhaps be engineered with better knowledge of excited-state geometries and forces.[55-57]

We are confident that the step we have taken toward understanding $\tilde{A}$ ($^1B_{2u}$)-state benzene better will encourage further calculations and spectroscopic inquiries.

References

1. P. Pulay, G. Fogarasi, and J. E. Boggs, J. Chem. Phys. 74, 3999 (1981).

2. P. Pulay, J. Chem. Phys. 85, 1703 (1986).

3. A. G. Ozkabak, L. Goodman, S. N. Thakur, and K. Krogh-Jespersen, J. Chem. Phys. 83, 6047 (1985).

4. S. N. Thakur, L. Goodman, and A. G. Ozkabak, J. Chem. Phys. 84, 6642 (1986).

5. M. J. Robey and E. W. Schlag, J. Chem. Phys. 67, 2775 (1977).

6. K. Krogh-Jespersen, R. P. Rava, and L. Goodman, J. Phys. Chem. 88, 5503 (1984).

7. D. H. Whiffen, Phil. Trans. Roy. Soc. London, Ser. A 248, 131 (1955).

8. J. C. Duinker and I. M. Mills, Spectrochim. Acta 24A, 417 (1968).

9. R. A. Kydd, Spectrochim. Acta 27A, 2067 (1971).

10. E. B. Wilson, J. C. Decius, and P. C. Cross, Molecular Vibrations, (McGraw-Hill, New York, 1955).

11. E. B. Wilson, Phys. Rev. 45, 706 (1934); 46, 146 (1934).

12. G. Herzberg, Molecular Spectra and Molecular Structure. II. Infrared and Raman Spectra of Polyatomic Molecules (Van Nostrand, Princeton, NJ, 1945).

13. S. Brodersen and A. Langseth, Mat. Fys. Skr. Dan. Vid. Selsk. 1, (1) 1 (1956); 1, (7) 1 (1959).

14. J. Pliva and A. S. Pine, J. Mol. Spectrosc. 93, 209 (1982).

15. J. Pliva and J. W. C. Johns, Can. J. Phys. 61, 269 (1983).

16. J. Pliva and J. W. C. Johns, J. Mol. Spectrosc. 107, 318 (1984).

17. B. P. Stoicheff, Can. J. Phys. 32, 339 (1954).

18. A. B. Hollinger and H. L. Welsh, Can. J. Phys. 56, 974; 1513 (1978).

19. H. B. Jensen and S. Brodersen, J. Raman Spectrosc. 8, 103 (1979).

20. D. L. Snavely, V. A. Walters, S. D. Colson, and K. B. Wiberg, Chem. Phys. Lett. 103, 423 (1984).

21. P. Esherick, A. Owyoung, and J. Pliva, J. Chem. Phys. 83, 3311 (1985).

22. A. E. W. Knight, C. S. Parmenter, and M. W. Schuyler, J. Am. Chem. Soc. 97, 1993; 2005 (1975).

23. G. H. Atkinson and C. S. Parmenter, J. Mol. Spectrosc. 73, 20 (1978).

24. G. H. Atkinson and C. S. Parmenter, J. Mol. Spectrosc. 73, 31; 52 (1978).

25. C. E. Otis, S. G. Grubb, K. S. Haber, and A. C. Albrecht, Chem. Phys. Lett. 102, 145 (1983).

26. R. M. Hochstrasser, J. E. Wessel, and H. N. Sung, J. Chem. Phys. 60, 317 (1974).

27. R. G. Bray, R. M. Hochstrasser, and H. N. Sung, Chem. Phys. Lett. 33, 1 (1975).

28. D. M. Friedrich and W. M. McClain, Chem. Phys. Lett. 32, 541 (1975).

29. L. Wunsch, H. J. Neusser, and E. W. Schlag, Chem. Phys. Lett. 31, 433 (1975).

30. L. Wunsch, H. J. Neusser, and E. W. Schlag, Chem. Phys. Lett. 38, 216 (1976).

31. J. R. Lombardi, R. Wallenstein, T. W. Hänsch, and D. M. Friedrich, J. Chem. Phys. 65, 2357 (1976).

32. L. Wunsch, F. Metz, H. J. Neusser, and E. W. Schlag, J. Chem. Phys. 66, 386 (1977).

33. A. Sur, J. Knee, and P. Johnson, J. Chem. Phys. 77, 654 (1982).

34. J. R. Lombardi, D. M. Friedrich, and W. M. McClain, Chem. Phys. Lett. 38, 213 (1976).

35. R. M. Hochstrasser, C. M. Klimcak, and G. R. Meredith, J. Chem. Phys. 70, 870 (1979).

36. S. N. Thakur and L. Goodman, J. Chem. Phys. 78, 4356 (1983).

37. R. P. Rava, J. G. Philis, K. Krogh-Jespersen, and L. Goodman, J. Chem. Phys. 79, 4664 (1983).

38. L. Goodman and R. P. Rava, Advances in Laser Spectroscopy, Vol. 1, 21 (Heyden and Son, Philadelphia, 1982).

39. L. Goodman and R. P. Rava, Advances in Chemical Physics, I. Prigogine and S. A. Rice, eds.,Vol. 54, 177 (Wiley & Sons, New York, 1983).

40. R. H. Page, Y. R. Shen, and Y. T. Lee, to be published.

41. J. Pliva, private communication.

42. Lasertechnics, Inc., Albuquerque, New Mexico.

43. Johnston Laboratories, Towson, Maryland.

44. Quanta-Ray (Spectra-Physics, Inc.), Mountain View, California.

45. Exciton Chemical Co., Inc., Dayton, Ohio.

46. J. R. Nestor, Appl. Opt. 21, 4154 (1982).

47. T. A. Stephenson, P. L. Radloff, and S. A. Rice, J. Chem. Phys. 81, 1060 (1984).

48. C. S. Parmenter, K. Y. Tang, and W. R. Ware, Chem. Phys. 17, 359 (1976).

49. R. H. Page, unpublished results.

50. S. J. Daunt and H. F. Shurvell, J. Mol. Spectrosc. 62, 373 (1976).

51. B. Crawford and J. Overend, J. Mol. Spectrosc. 12, 307 (1964).

52. K. Aron, C. Otis, R. E. Demaray, and P. Johnson, J. Chem. Phys. 73, 4167 (1980).

53. D. J. Muller and A. E. W. Knight, J. Phys. Chem. 88, 3392 (1984).

54. N. Mikami and M. Ito, J. Chem. Phys. 64, 3077 (1976).

55. M. Rinke, H. Güsten, and H. J. Ache, J. Phys. Chem. 90, 2661; 2666 (1986).

56. G. A. Reynolds and K. H. Drexhage, J. Org. Chem. 42, 885 (1977).

57. B. Kopainsky, P. Qiu, W. Kaiser, B. Sens, and K. Drexhage, Appl. Phys. B 29, 15 (1982).

Table I. Compilation of benzene $\tilde{X}$ ($^1A_{1g}$) and $\tilde{A}$ ($^1B_{2u}$) frequency assignments.

Mode[b]	$\tilde{X}$ (cm^{-1})[c]	Ref.[a]	$\tilde{A}$ (cm^{-1})[c]	Ref.[a]
1 (2)	993.1	HW	923.0	AP
2 (1)	3073.9	HW	(3130.1)[g]	AP
3 (3)	(1350)[d]	BL	1327 ± 3[hd]	
4 (8)	(707)[d]	BL	365	KPS
5 (7)	(990)[d]	BL	744.6	AP
6 (18)	608.1	HW	521.4	AP
7 (15)	(3056.6)[e]	HW	3077.2	KPS
8 (16)	1600[f]	EOP	1516	SRR
9 (17)	1177.8	HW	1147.7	AP
10 (11)	(847.1)[e]	HW	580.7	AP
11 (4)	674.0	SWCW	515-518[d]	AP
12 (6)	(1010)[d]	BL		
13 (5)	(3057)[i]	BL		
14 (9)	1309.8	TGO	1570.0	SKJ
15 (10)	1148.5	TGO	1149.9	SKJ
16 (20)	398.8	AP	237.5	AP
17 (19)	(967)[d]	BL	717.4	SKJ
18 (14)	1038.3	PJ	919.7	SKJ
19 (13)	1484.0	PJ	1405 ± 3[hd]	
20 (12)	3065[f]	PP; SWCW; BL	3084 ± 5[hfd]	

[a] AP means Atkinson and Parmenter[23]
BL means Brodersen and Langseth[13]
HW means Hollinger and Welsh[18]
EOP means Esherick, Owyoung, and Pliva[21]
SWCW means Snavely et al.[20]
TGO means Thakur, Goodman, and Ozkabak[4]
PJ means Pliva and Johns[15,16]
PP means Pliva and Pine[14]
SRR means Stephenson, Radloff, and Rice[47]
SKJ means Sur, Knee, and Johnson[33]
KPS means Knight, Parmenter, and Schuyler[22]

[b] Wilson numbering; Herzberg numbering in parentheses

[c] Quoted to the nearest 0.1 cm^{-1}; uncertain values in parentheses

[d] Derived from combination band analysis

[e] Uncertainty is > 0.1 cm^{-1}

[f] Deperturbed value; mode is in Fermi resonance

[g] Reassigned in this work to - 3093 cm^{-1}

[h] This work

[i] Estimate from isotopic product and sum rules

Table IIa. $\tilde{X}$ and $\tilde{A}$ state frequencies of in-plane modes.

Mode	Symmetry	Observed (cm^{-1})		Robey-Schlag[5]	Krogh-Jespersen et al.[6]
		$\tilde{X}$	$\tilde{A}$		
1	a_{1g}	993	923	923	921
2	a_{1g}	3074	~3093[a]	3129	3111
3	a_{2g}	1350[b]	1327 ± 3[c]	1246	1320
6	e_{2g}	608	521	519	526
7	e_{2g}	3057	3077	3100	3092
8	e_{2g}	1600[d]	1516	1454	1521
9	e_{2g}	1178	1148	1147	1145
12	b_{1u}	1010		936	928
13	b_{1u}	3057[e]		3159	3167
14	b_{2u}	1310	1570	1567	1572
15	b_{2u}	1149	1150	1150	1148
18	e_{1u}	1038	920	921	930
19	e_{1u}	1484	1405 ± 3[c]	1407	1359
20	e_{1u}	3065[d]	3084 ± 5[cd]	3081	3061

[a] Reassignment from AP[23] value of 3130 cm^{-1}
[b] Deduced from analysis of combination bands in IR spectra
[c] This work
[d] Deperturbed value; mode is part of a Fermi resonance
[e] Estimated from isotopic product and sum rules

Table IIb. $\tilde{X}$ and $\tilde{A}$ state frequencies of out-of-plane modes.

(For footnotes see Table IIa)

Mode	Symmetry	Observed (cm^{-1})		Robey-Schlag[5]
		$\tilde{X}$	$\tilde{A}$	
4	b_{2g}	707[b]	365	365
5	b_{2g}	990[b]	745	750
10	e_{1g}	847	581	585
11	a_{2u}	674	515-518	514
16	e_{2u}	399	238	239
17	e_{2u}	967[b]	717	712

FIGURE CAPTIONS

Figure 1. Normal modes and their symmetries in benzene. Exact atomic displacements may be different in the $\tilde{X}$ and $\tilde{A}$ states.

Figure 2. (a) Two-photon (IR-UV double resonance) route to C-H stretches (CH^1) in the $\tilde{A}$ state. IR pumping populates the CH_1 state, and the CH_1^1 transition excites the CH^1 level. In this example the C-H stretching frequency is larger in the excited state: $\nu'_{CH} > \nu''_{CH}$. (b) Spectrum observed; IR is tuned to pump CH_1. The change in UV absorption vs. UV frequency with IR pumping turned on is sketched. The population in 0_0 is depleted and that in CH_1 is increased. The 0_0^0 transition probes the depletion, and the CH_1^1 transition is the double resonance which allows determination of ν'_{CH}.

Figure 3. Experimental apparatus which includes tunable IR (pump) and UV (probe) sources, a pulsed supersonic molecular beam of benzene seeded in argon, ion extraction and detection, and control electronics. The IR beam around 3000 cm^{-1} excites C-H stretches and is chopped with a beam flag. The UV laser frequency is scanned in order to find new $\tilde{A}$ state vibrational levels. Benzene UV transitions are detected with resonantly-enhanced two-photon ionization (R2PI.)

Figure 4. (a) Resonantly-enhanced two-photon ionization (R2PI) spectrum in the vicinity of the 6_1^0 band. (b) R2PI spectrum near the 6_0^1 band, which is extremely saturated in this scan. (c) Energy level diagram with vibrational angular momentum splitting and thermally excited levels. All transitions in this picture have $\Delta v_6 = \pm 1$.

Figure 5. Effect of vibrational angular momentum on UV transitions involving doubly-degenerate modes (e.g. ν_6). The vibrational angular momentum quantum number ℓ_i takes on the values v_i, $v_i - 2$, ... $-v_i$. For mode i, the energy shift due to vibrational angular momentum interactions is $g_{i,i}\ \ell_i^2$. The selection rule on ℓ during an optical transition in which $\Delta v = \pm 1$ is $\Delta\ell = \pm 1$. (a) Energy levels and allowed transitions of the different ℓ components. (b) Splitting of 4 g' observed in transitions from $\ell'' = 1$ states. In benzene, $g'_{6,6} = 1.7$ cm^{-1}, so the 6^2_1 splitting is ~ 7 cm^{-1}. The 6^1_0 and 6^1_1 transitions are not split.

Figure 6. IR spectrum of C-H stretching region, obtained with the UV laser tuned to 6^1_0. The 3101-cm^{-1} peak is an unresolved doublet. Our a", b", c" labeling of the peaks reflects the fact that zeroth-order names (ν''_{20}, $\nu''_8 + \nu''_{19}$, $\nu''_1 + \nu''_8 + \nu''_{19}$) are inappropriate because of mode mixing.

Figure 7. Energy level diagram of the C-H stretching Fermi triad. The traditional assignment of each observed level (a",b",c") is written above the level corresponding to its zeroth-order "parent".

Figure 8. (a) UV transitions beginning from mixed, IR-pumped levels. No transitions are forbidden, because the ground-state vibrational levels are mixed differently from the excited-state ones. As the heavy lines show, the most intense transitions are those which retain the ground-state vibrational "character." (b) Double-resonance spectra aligned with respect to total (IR + UV) energy. Transitions to common

final states are vertically aligned. Only peaks are shown; in general, dips (see Fig. 1b) are present also. Frequencies of modes 3, 19, and 20 are deduced from these spectra, as is the presence of the $3_1 6_1 15_1$ state in the c" level.

Figure 9. Double resonance spectra around 6_1^0. Dips in the spectra (e.g. 6_1) are assigned according to the ground-state population that caused them. Labels next to peaks are our assignments of the final vibrational states. Frequencies of modes 3, 19, and 20 are deduced from these spectra, as is the presence of the $3_1 6_1 15_1$ state in the c" level.

Figure 10. As in Figure 9, for the 6_0^1 region.

Figure 11. Upper states in double resonance transitions. The selection rules $\Delta v_6 = \pm 1$, Δv_1 = anything, have been used to find the final states accessible in the 6_1^0 region, and the 6_0^1 region. The lower states are a", b", and c" (the mixed 20_1, $8_1 19_1$, and $1_1 6_1 19_1$ levels). In this figure, the heavy lines show the most intense transitions. Those with $v_1' = v_1'' = 1$ have small Franck-Condon factors, and are shown with fainter lines. Levels with $v_2' = 2$ or $v_6' = v_8' = 1$ have a vibrational angular momentum splitting, producing a doublet. The $1^1 6^2 19^1$ level, shown with dashed lines, is outside the energy range we scanned. The $6^2 19^1$ and $1^1 19^1$ levels are separated by $2\nu_6' - \nu_1' \approx 120$ cm^{-1}. Likewise, the $6^1 8^1 19^1$ level is $\nu_8' - \nu_6' \approx 995$ cm^{-1} above the $6^2 19^1$ level.

Figure 12. Benzene C-H stretching Fermi tetrad, according to Pliva's analysis and confirmed by us. $\nu_3'' + \nu_6'' + \nu_{13}''$ is only mixed into the 3101-cm^{-1} level, and $\nu_1'' + \nu_6'' + \nu_{19}''$ is now in the middle.

Figure 13. C_6H_6 in-plane valence (internal) coordinates. S_i represents stretching the i^{th} C-H bond, t_i indicates stretching the i^{th} C-C bond, α_i denotes deviation from 120° of the C-C-C bond angle at the i^{th} node, and β_i describes bending of the i^{th} C-H bond.

Figure 14. Block-diagonal symmetry force constant matrix of in-plane modes. Vibrational modes of different symmetries do not interact in the harmonic approximation, so each symmetry gets its own small submatrix. This reduces the number of force constants used, compared with the valence-force description of the potential.

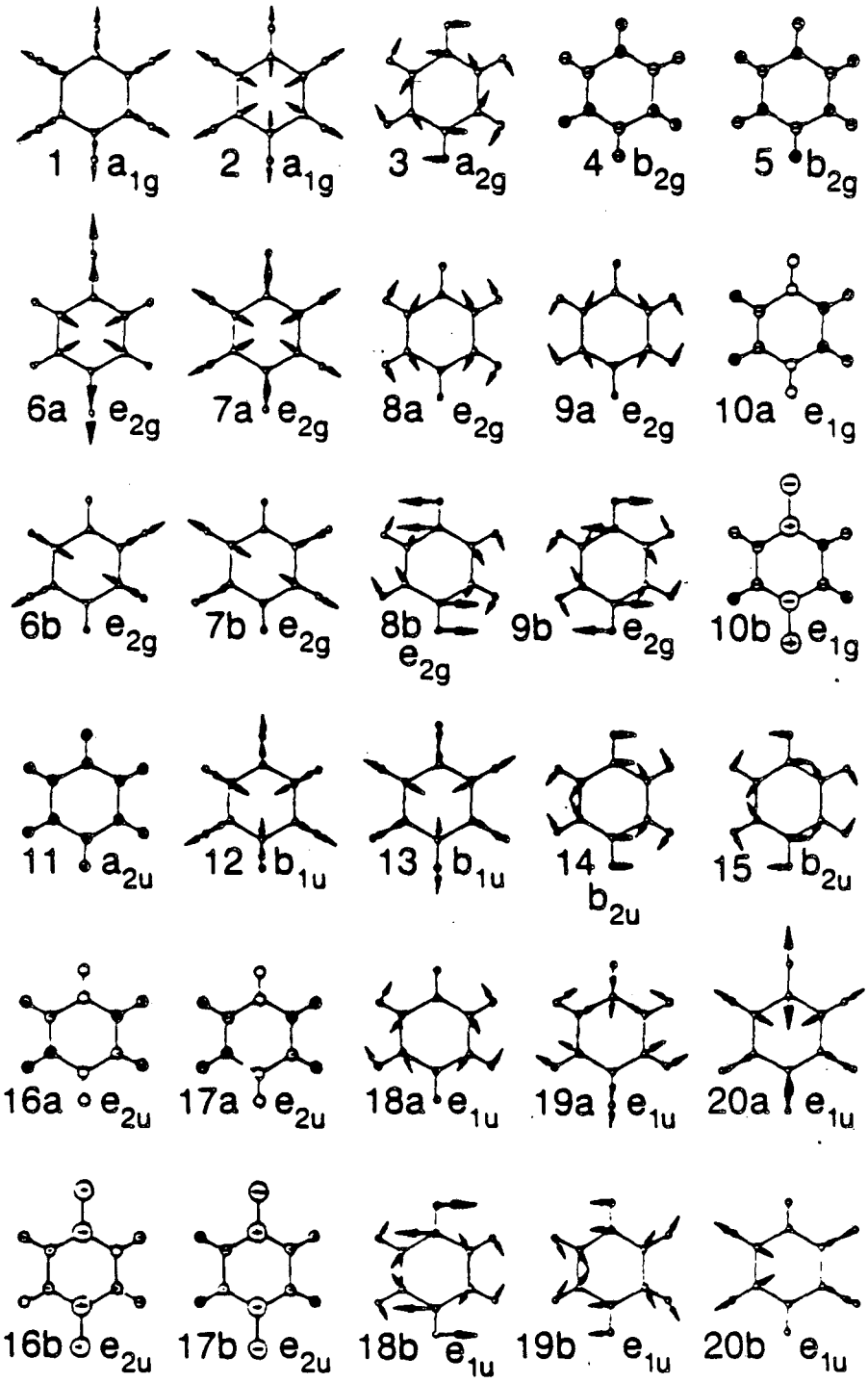

Normal modes of Benzene (Wilson's numbering)

Figure 1.

XBL 872-6153

IR-UV double resonance

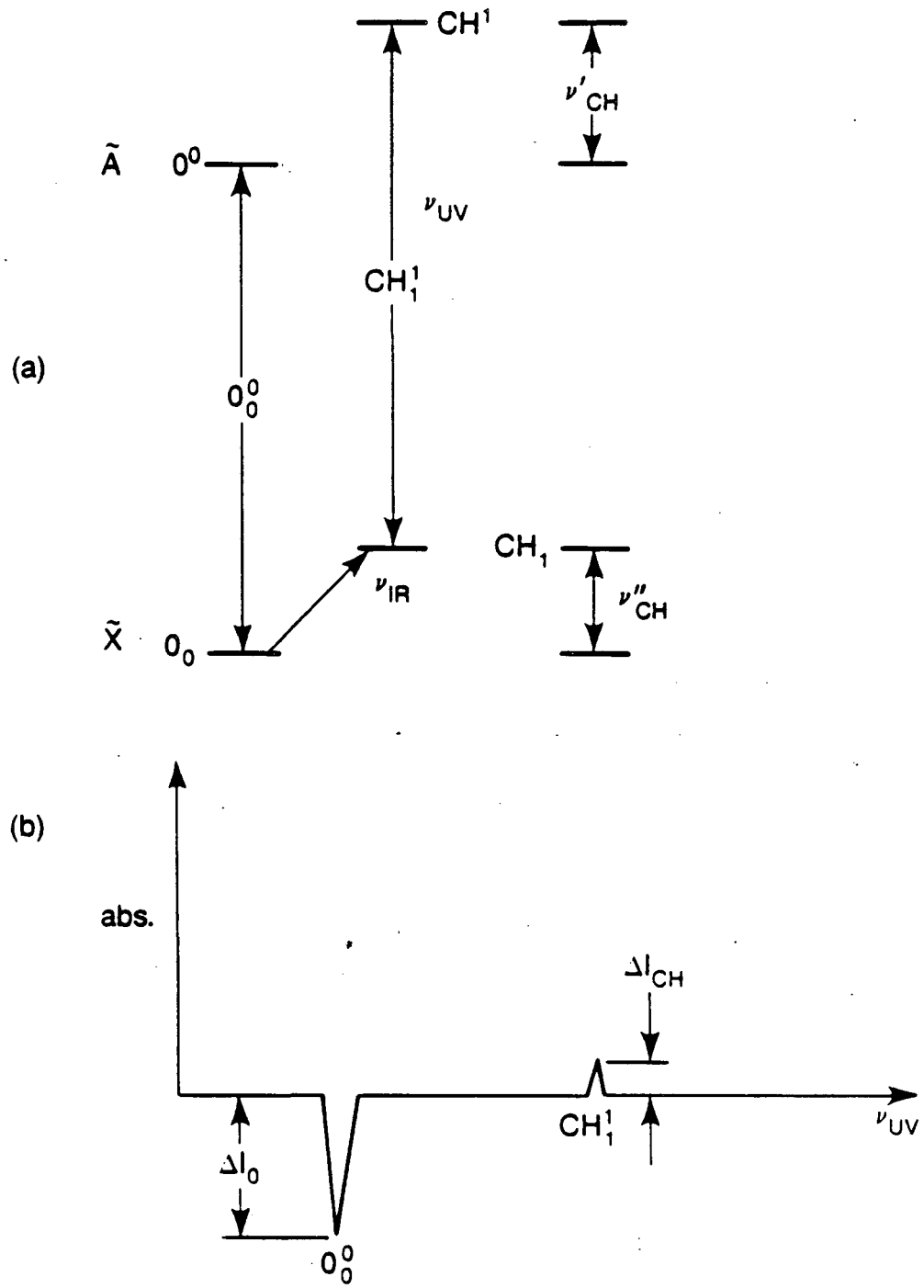

Figure 2.

XBL-872-6190

Experimental apparatus for obtaining IR-UV double resonance spectra

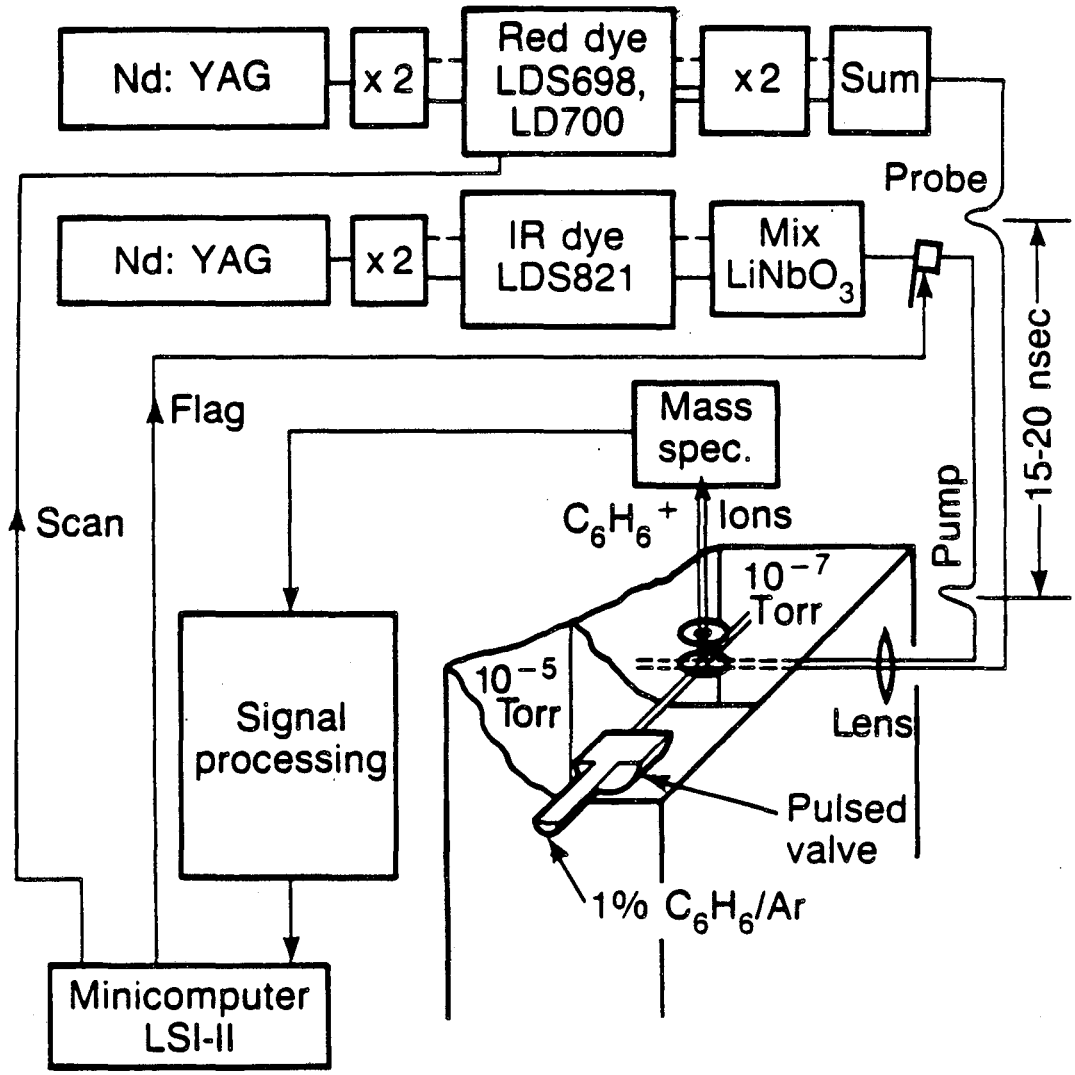

XBL 872-6183

Figure 3.

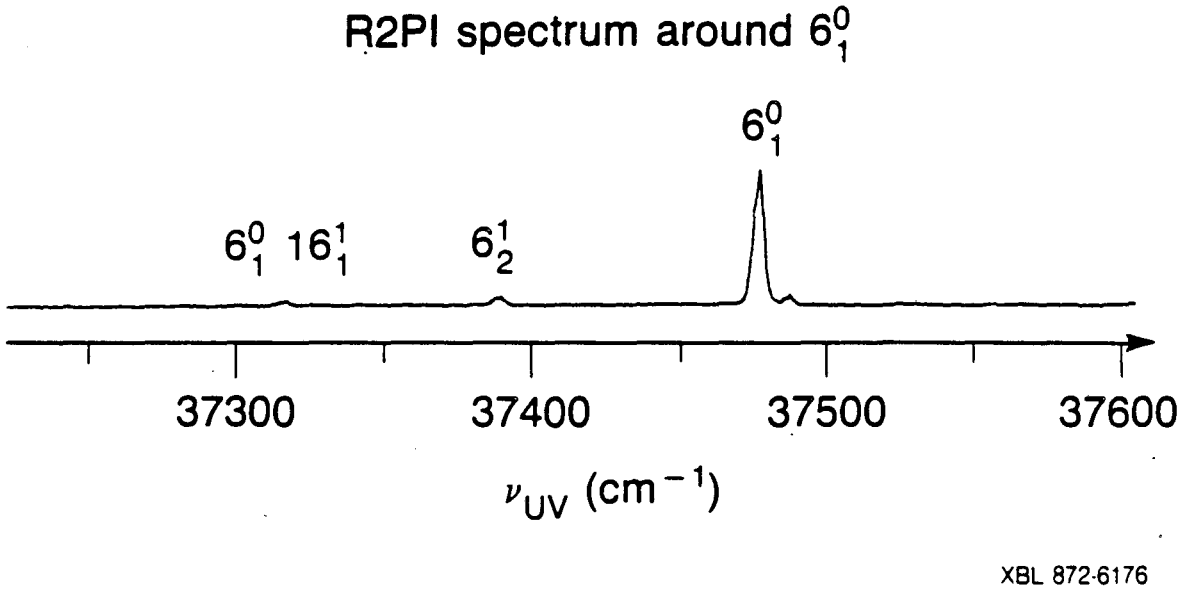

XBL 872-6176

Figure 4(a).

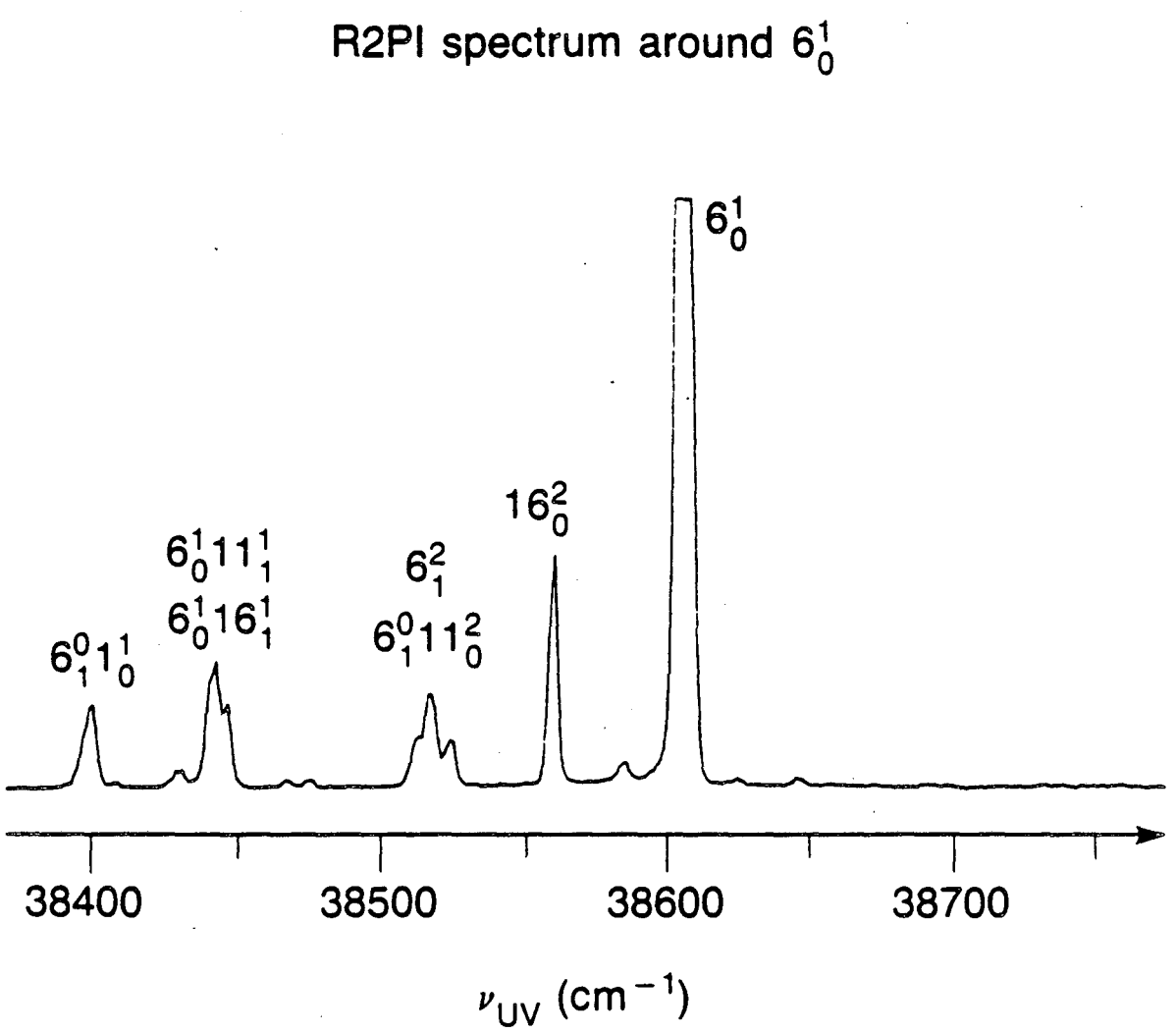

XBL 872-6175

Figure 4(b).

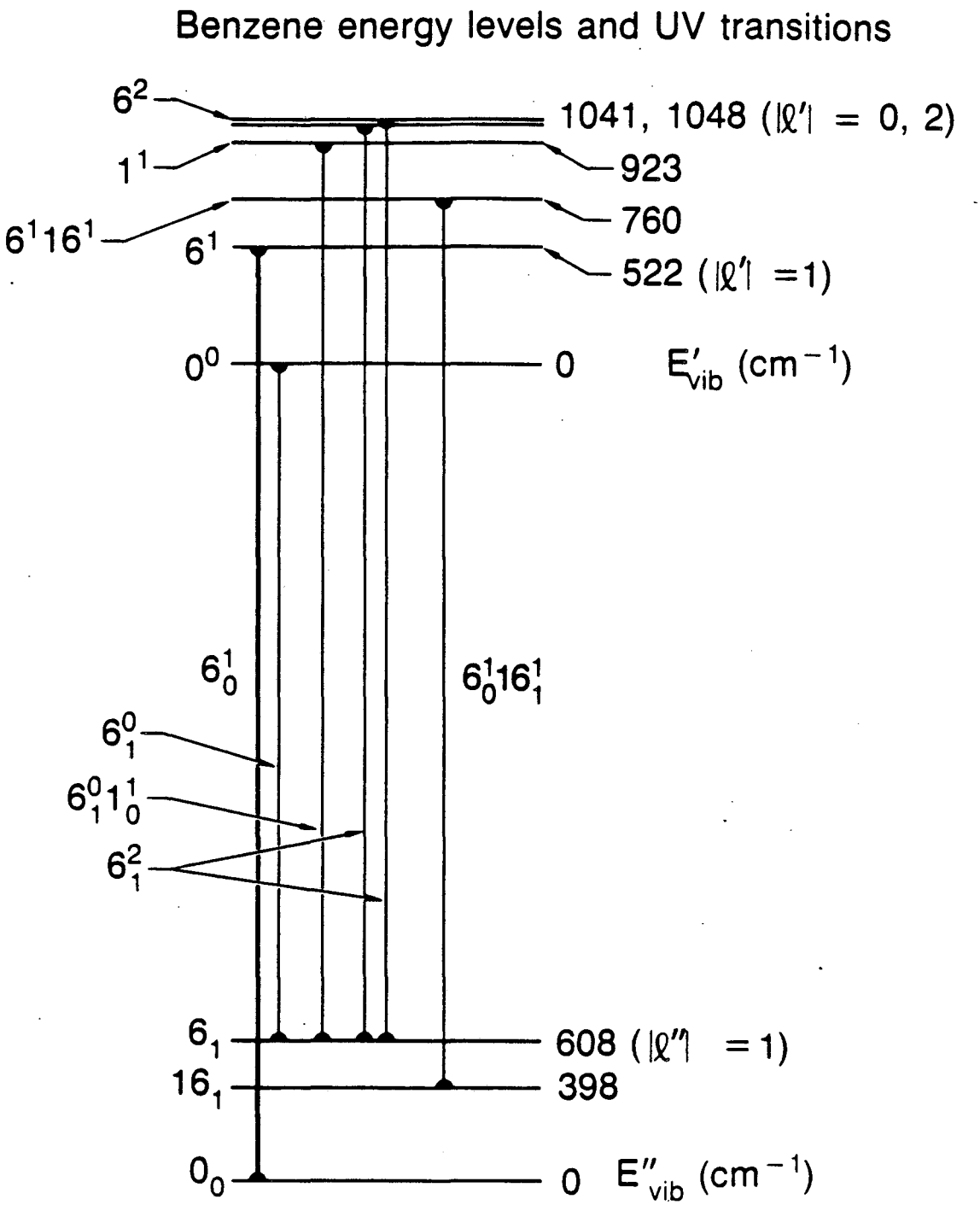

XBL 872-6119

Figure 4(c).

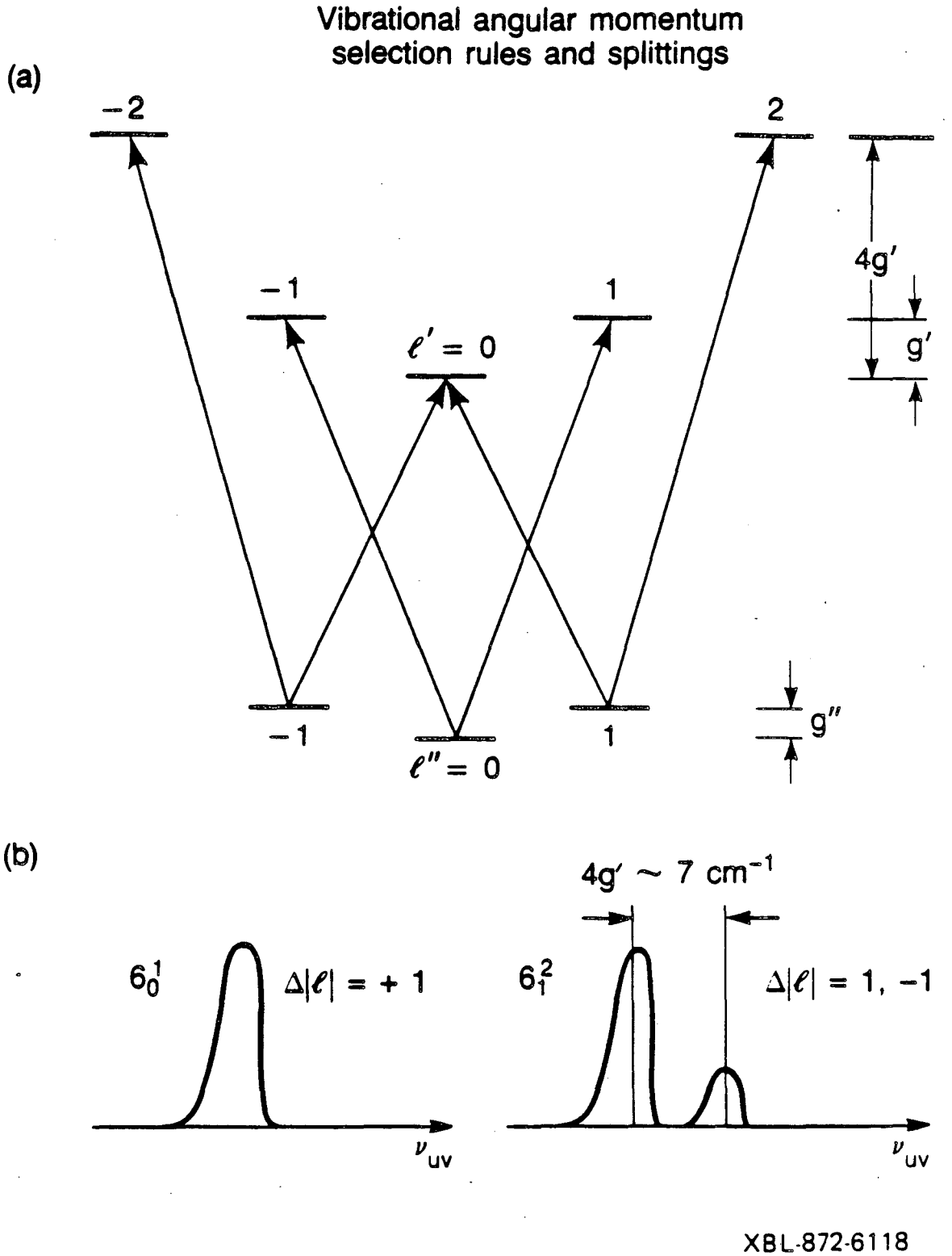
Vibrational angular momentum
selection rules and splittings
(a)
−2
2
4g′
−1
1
ℓ′ = 0
g′
−1
1
g″
ℓ″ = 0
(b)
4g′ ~ 7 cm⁻¹
6¹₀
Δ|ℓ| = + 1
6²₁
Δ|ℓ| = 1, −1
ν_uv
ν_uv
XBL-872-6118

Figure 5.

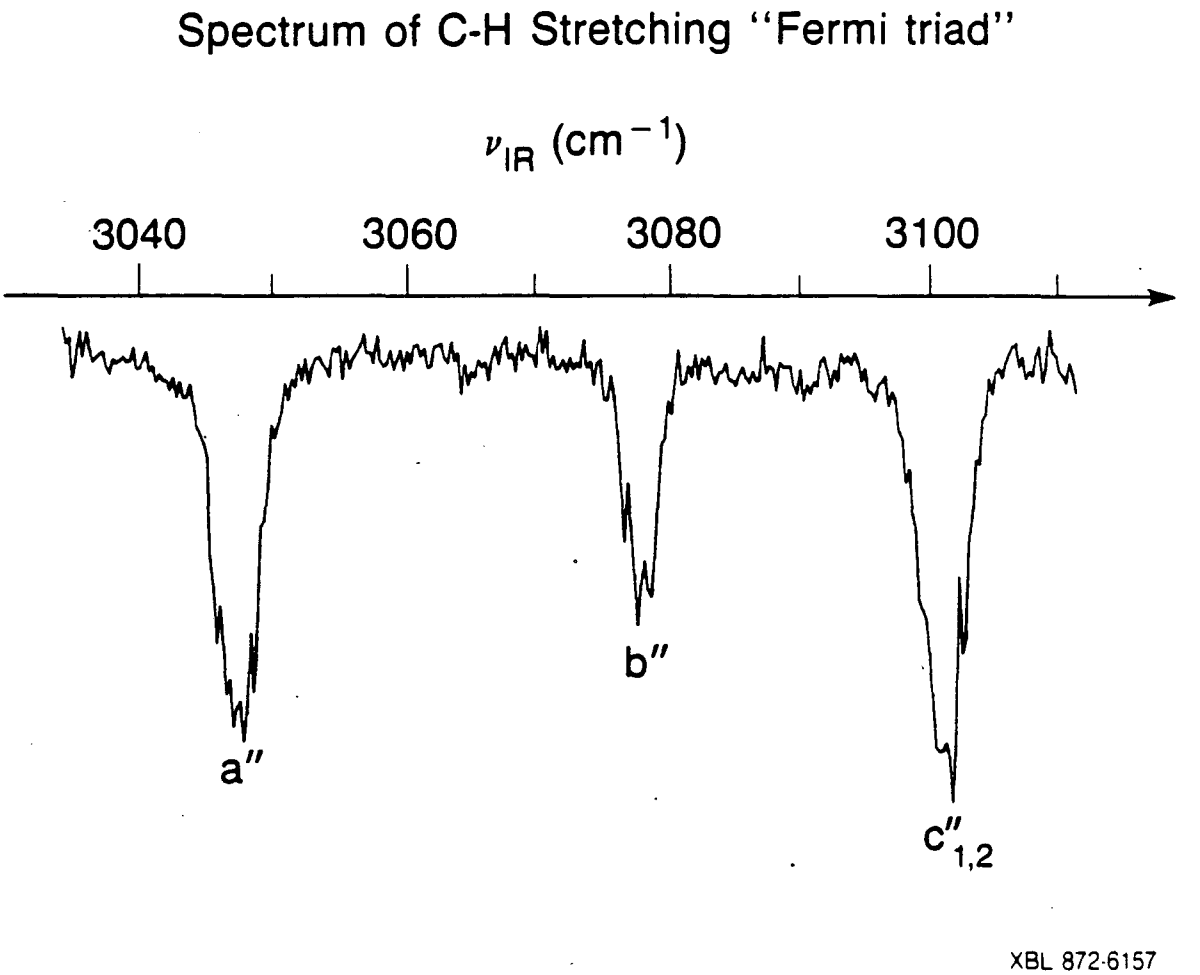
Spectrum of C-H Stretching "Fermi triad"
ν_{IR} (cm^{-1})
3040
3060
3080
3100
a″
b″
c″$_{1,2}$
XBL 872-6157

Figure 6.

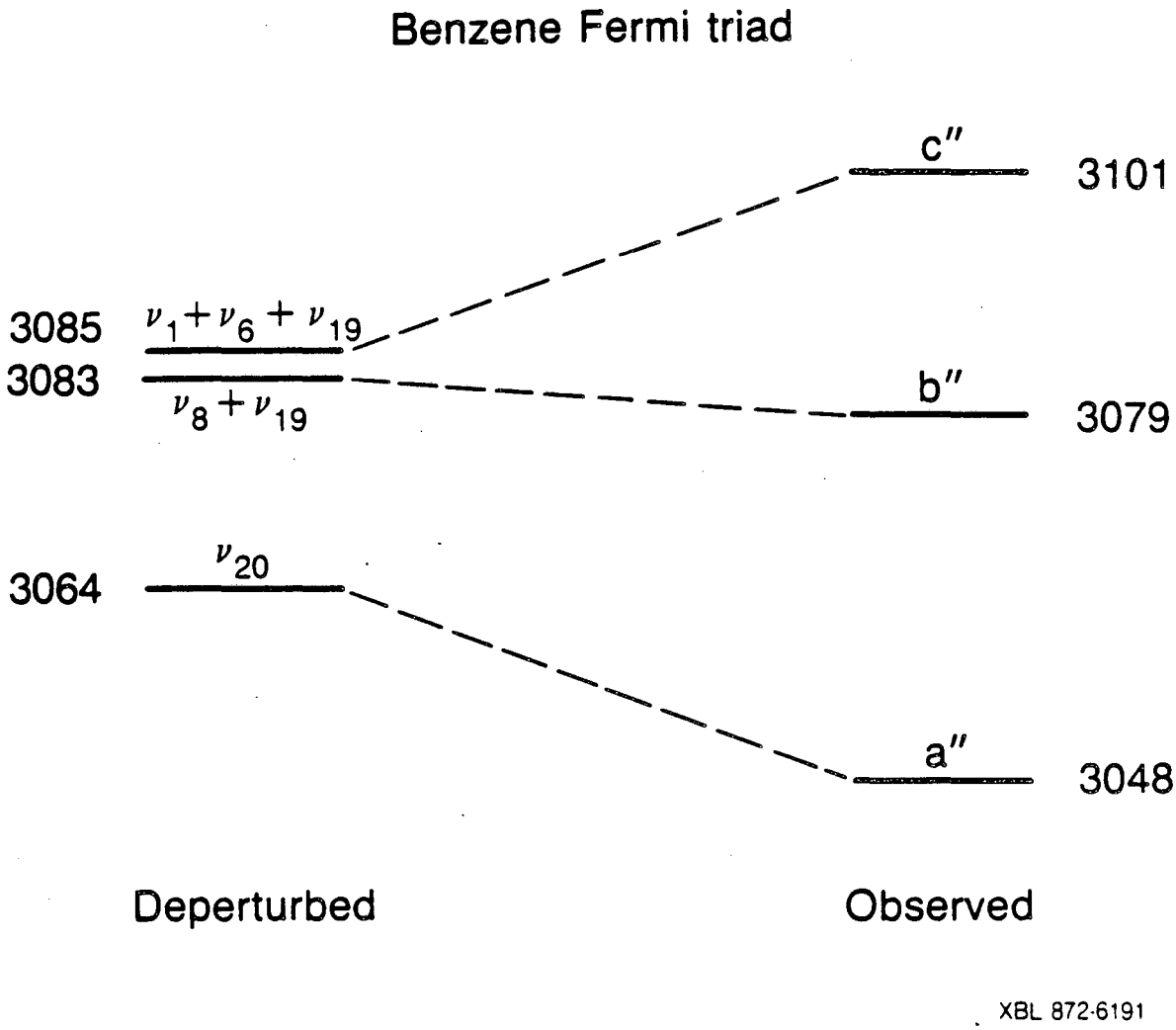
Benzene Fermi triad
c″
3101
3085
$\nu_1+\nu_6+\nu_{19}$
3083
$\nu_8+\nu_{19}$
b″
3079
3064
ν_{20}
a″
3048
Deperturbed
Observed
XBL 872-6191

Figure 7.

Allowed transitions from mixed levels

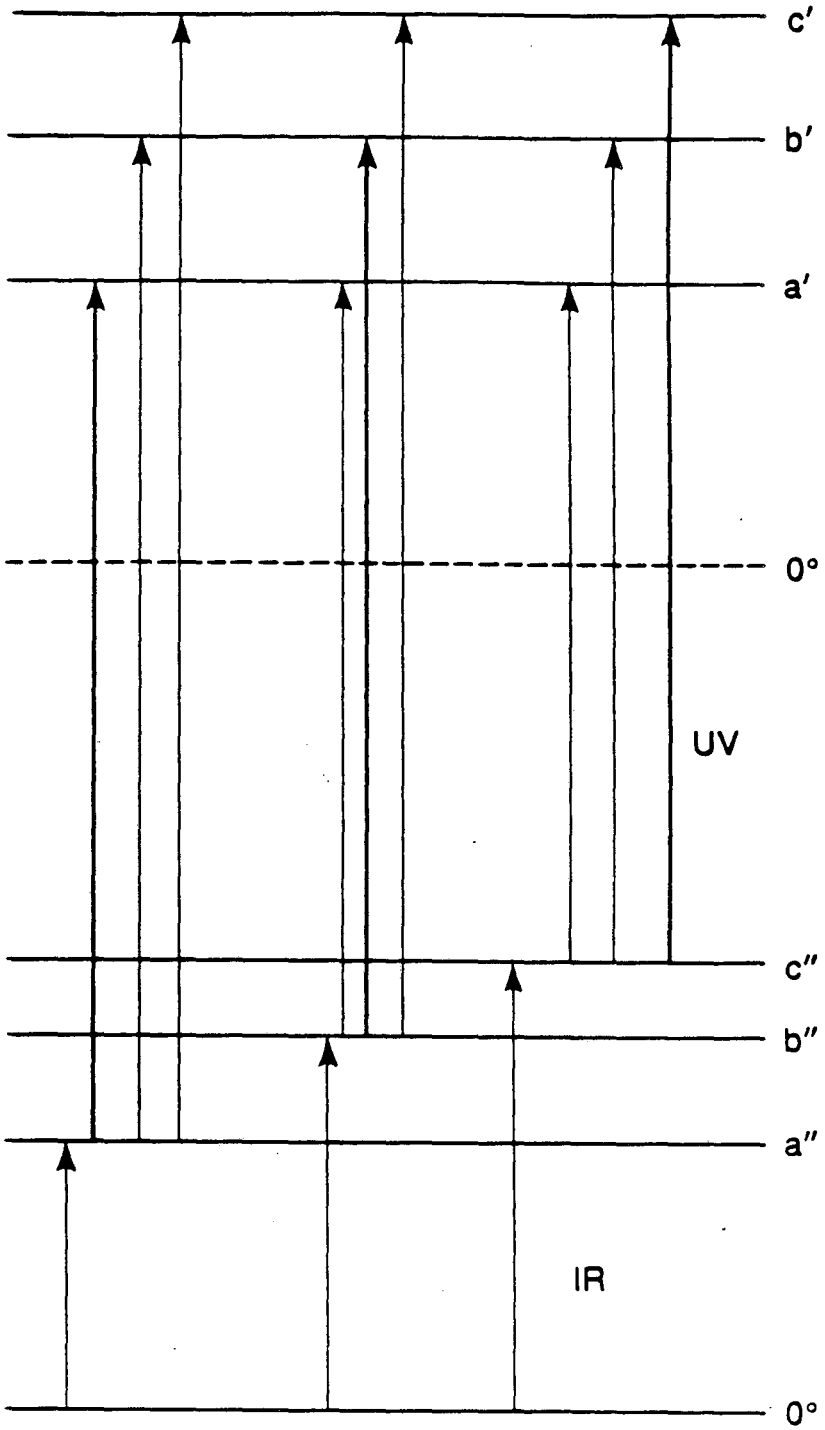

Figure 8(a).

XBL 872-6182

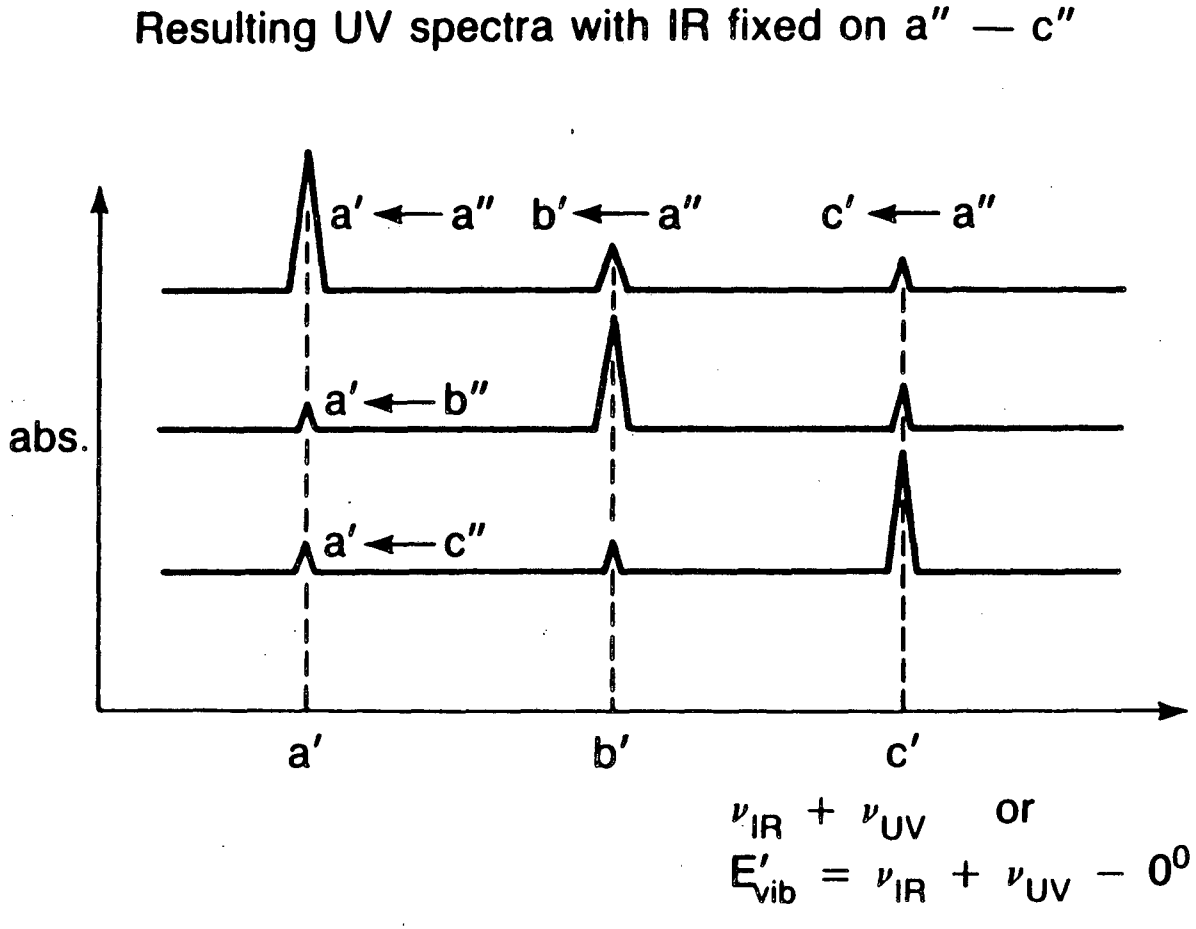

Figure 8(b).

XBL 872-6180

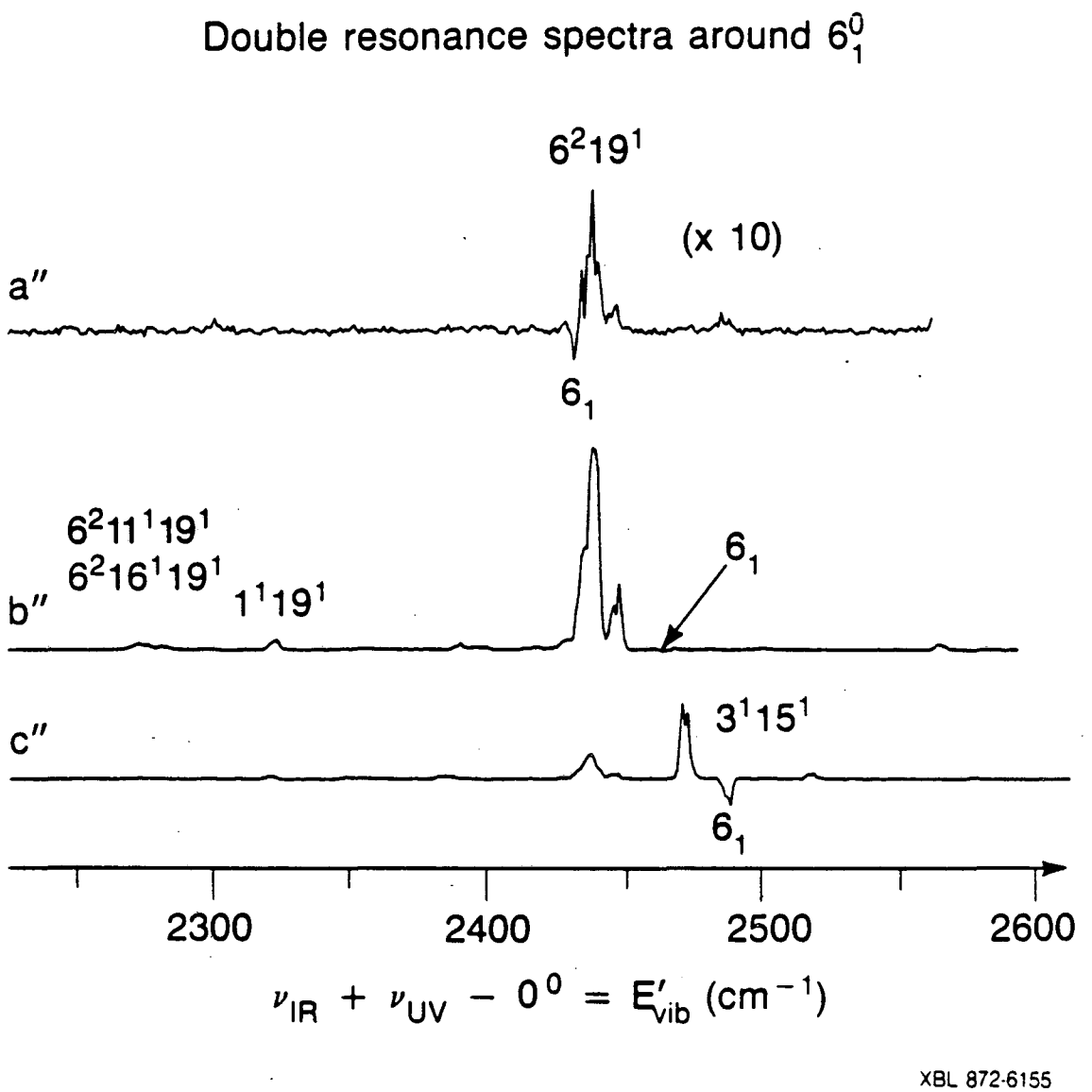
Double resonance spectra around 6_1^0
$6^2 19^1$
(x 10)
a″
6_1
$6^2 11^1 19^1$
$6^2 16^1 19^1$
$1^1 19^1$
b″
6_1
$3^1 15^1$
c″
6_1
2300
2400
2500
2600
$\nu_{IR} + \nu_{UV} - 0^0 = E'_{vib}$ (cm^{-1})
XBL 872-6155

Figure 9.

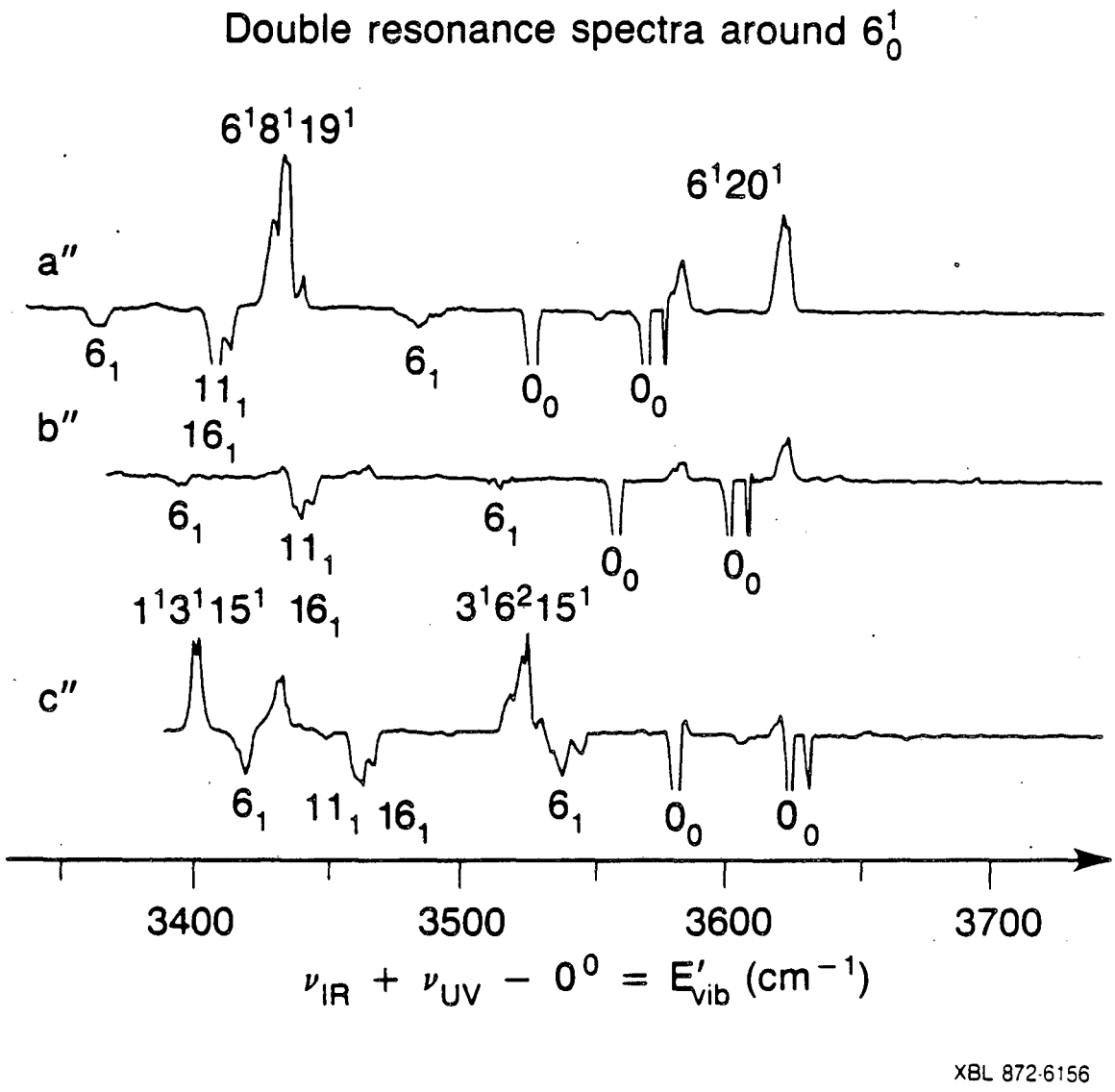
Double resonance spectra around 6_0^1
$6^1 8^1 19^1$
$6^1 20^1$
a″
6_1
11_1
6_1
0_0
0_0
b″
16_1
6_1
11_1
6_1
0_0
0_0
$1^1 3^1 15^1$ 16_1
$3^1 6^2 15^1$
c″
6_1 11_1 16_1
6_1
0_0
0_0
3400
3500
3600
3700
$\nu_{IR} + \nu_{UV} - 0^0 = E'_{vib}$ (cm^{-1})
XBL 872-6156

Figure 10.

Upper States in Double Resonance Transitions

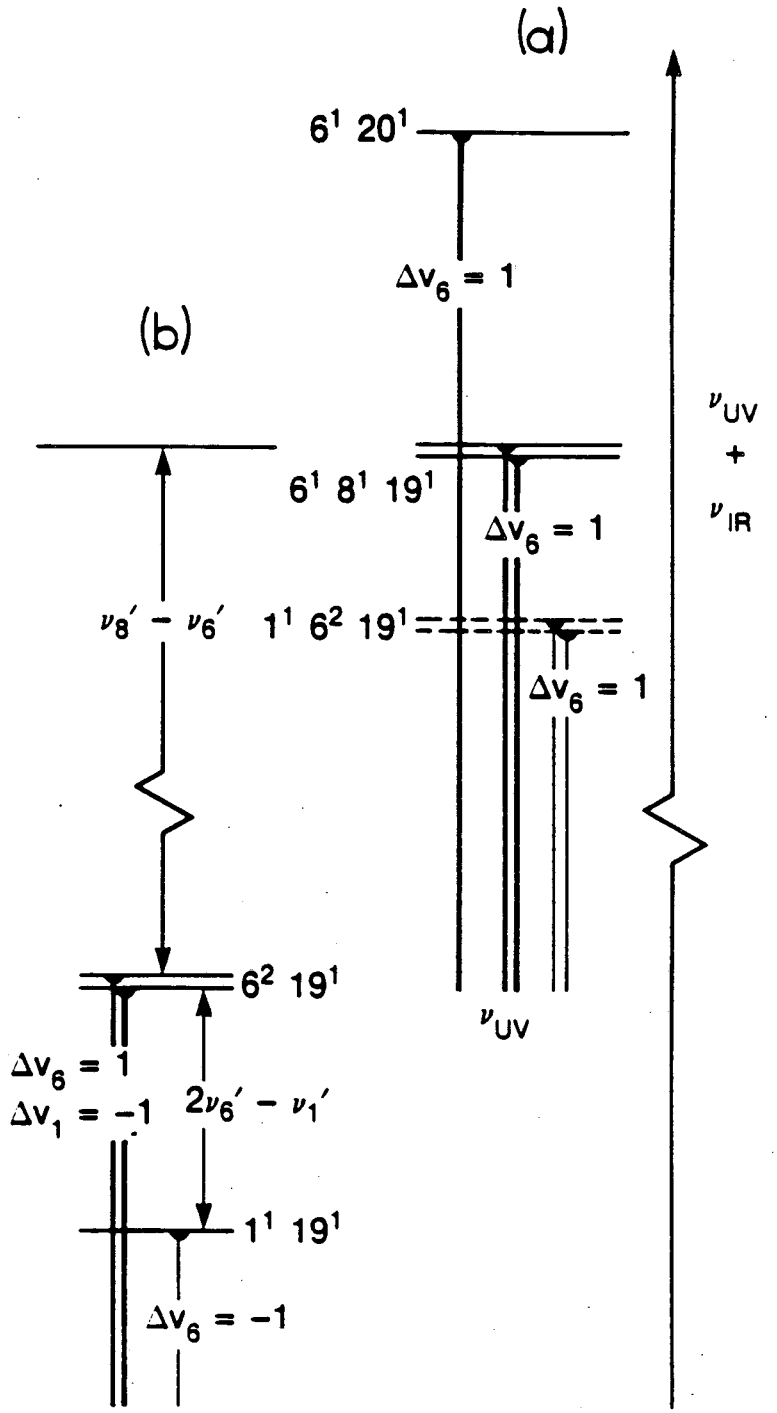

XBL 874-7668

Figure 11.

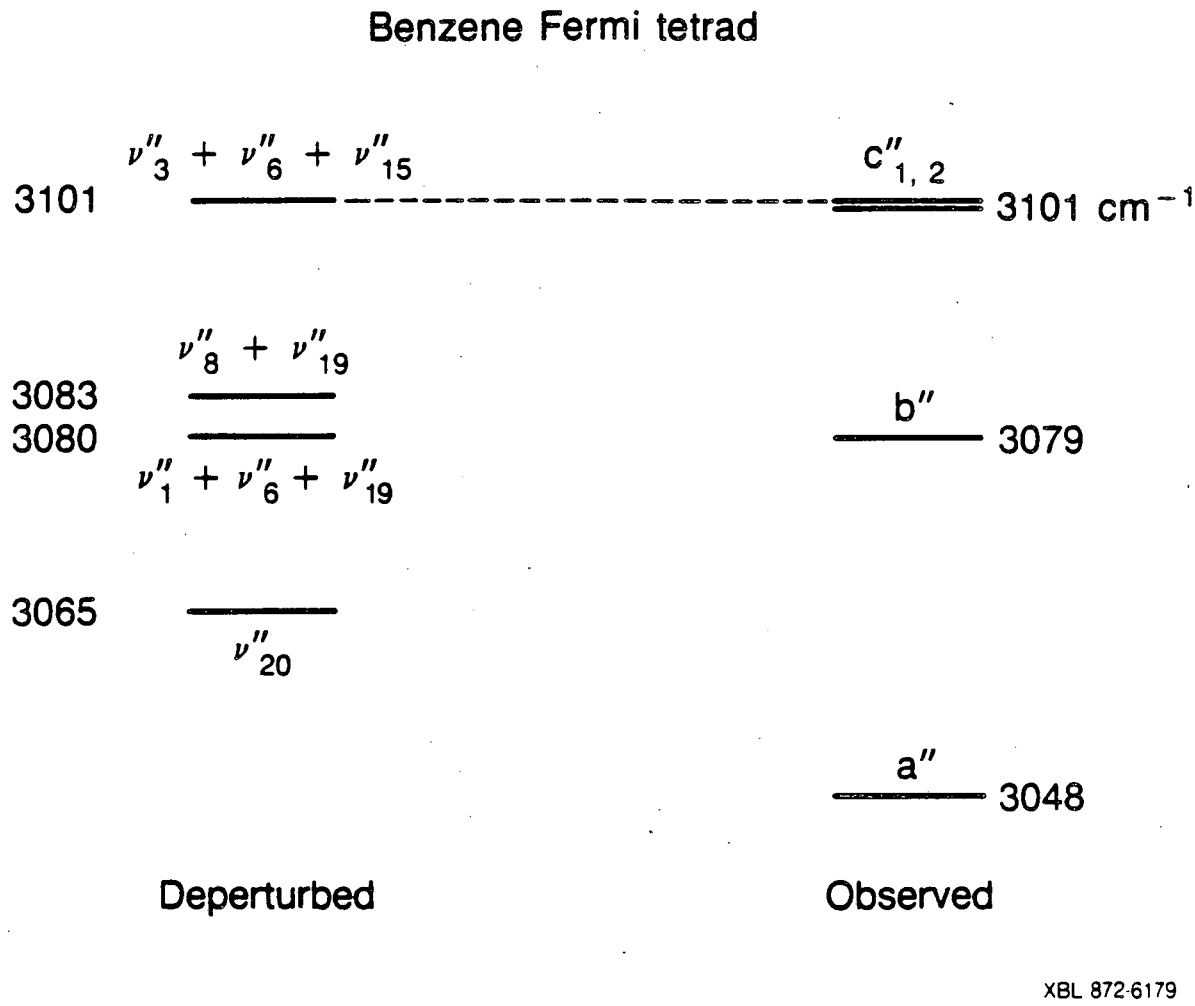
Benzene Fermi tetrad
$\nu''_3 + \nu''_6 + \nu''_{15}$
3101
$c''_{1,2}$
3101 cm^{-1}
$\nu''_8 + \nu''_{19}$
3083
3080
$\nu''_1 + \nu''_6 + \nu''_{19}$
b″
3079
3065
ν''_{20}
a″
3048
Deperturbed
Observed
XBL 872-6179

Figure 12.

C_6H_6 in-plane valence coordinates

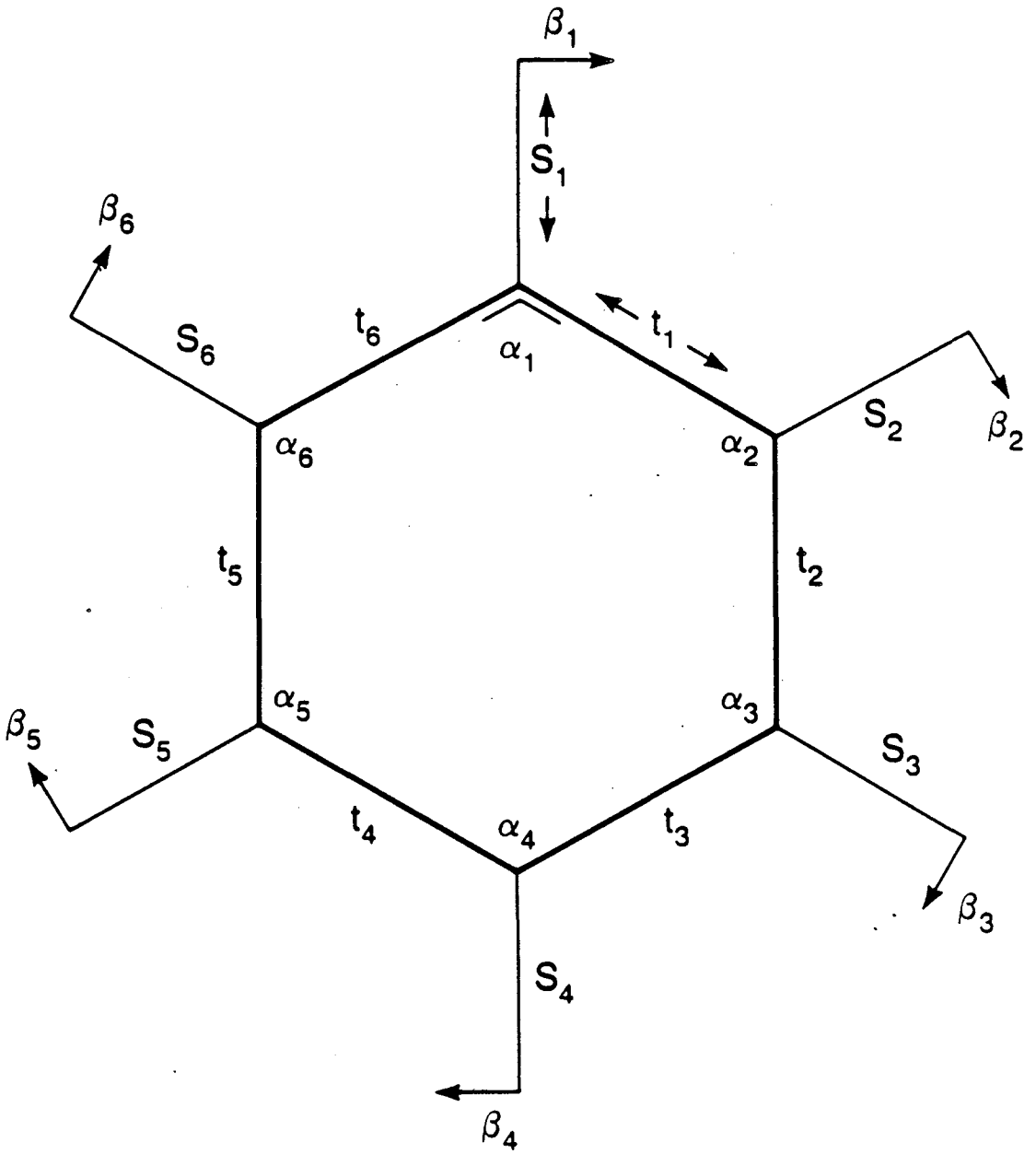

XBL 872-6178

Figure 13.

Block diagonal in-plane symmetry force constant matrix

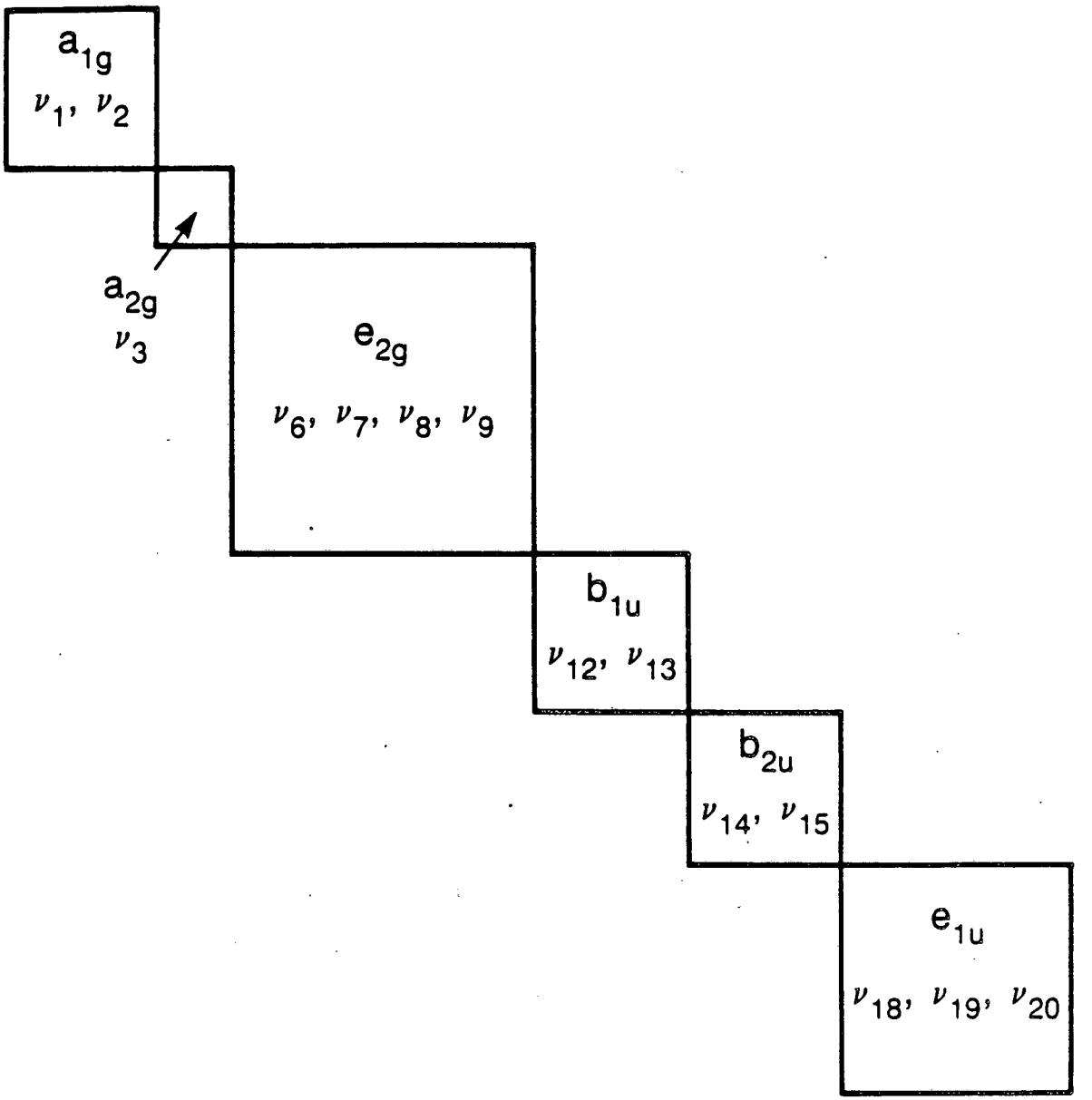

XBL 872-6181

Figure 14.

V. FREQUENCY TRIPLING INTO THE 720-1025 A REGION WITH PULSED FREE JETS

I. Introduction

Many atoms and molecules have excited states in the 10-20 eV (1200 A - 600 A) range, and multiple decay channels (autoionization and predissociation, for example) from those states. Access to these states can best be gotten via optical transitions induced by short wavelength radiation. Traditionally the helium discharge lamp has been used as the light source for this region,[1] and more recently, the synchrotron radiation source is widely used. However, these two sources do not have sufficient resolution and brightness for high resolution studies and for selective excitation of these states. In general, such studies require a broadly tunable, coherent source with high resolution (better than 1 part in 10^6 is desirable). In this article we will describe a coherent source which is continuously tunable between 904 and 1024 A, and line tunable to 720 A. It employs the method of frequency tripling in a pulsed free jet of gas. A comparison of the relative tripling efficiencies as a function of frequency for the gases Ar, Kr, Xe, CO, and N_2 is reported. A major point of this report is to show that even with a relatively simple laser setup, intense, widely tunable XUV light can be generated without gaps in the tuning range.

A goal in the construction of this source was to keep it simple, reliable, and relatively inexpensive. This limits the source to the technique of frequency tripling, which is done with a single tunable laser. The alternative method of four-wave mixing requires at least

two tunable lasers. The techniques of frequency tripling, and, more generally, four-wave mixing, are well-established, and their theory and experiment have recently been reviewed by Vidal.[2]

There are several constraints on the medium used for tripling into the windowless XUV region below 1040 Å. First, it must have a significant nonlinearity $\chi^{(3)}$. Second, it cannot have strong absorption at the input (ω) or output (3ω) frequencies. Third, if the medium completely encloses the focal region, the dispersion $n(3\omega) - n(\omega)$ must be negative in order to have phase matching.[3] Finally, some form of differential pumping must be used to isolate the tripling gas from the remainder of the experimental apparatus.

The inert gases Ar, Kr, and Xe, the molecular gases CO, N_2, and H_2, and mercury metal vapor have all been shown to be useful tripling media in different frequency ranges.[4-12] Several different approaches were devised to tackle the differential pumping requirement. These included the use of pinholes,[4-6,8] gas-dynamic windows,[7] capillary array windows,[9] rotating slits,[10] and pulsed valves.[11,12] Of these approaches, the use of pulsed valves is especially advantageous for two reasons. First, the small duty cycle of the pulsed valve's opening gives a small gas flow that eases the pumping requirements. Second, the small thickness of the well-defined gas jet keeps the jet from enclosing the focal region, eliminating the need for negative dispersion. Also, the generation of XUV light can be performed in the same chamber in which the experiment is to be conducted. Self-absorption at 3ω is restricted to the region of the gas jet. Switching of the tripling gas takes only a few minutes. Thus, tripling in a pulsed jet is our choice for the construction of an XUV source.

There have been several reports on relative efficiencies of XUV generation by four-wave mixing. However, a comprehensive comparison of frequency tripling efficiencies for different media has not been reported. This paper reports on measurements of the relative tripling efficiency vs. input frequency for five commonly used gases (Ar, Kr, Xe, CO, and N_2). We hope it will serve as a user's guide to the generation of continuously-tunable XUV light by frequency tripling.

II. Experimental

Figure 1 illustrates the experimental setup. The near UV laser light was focused into the gas jet provided by a pulsed valve (Newport BV-100), with a 1 mm aperture. The valve was supported by an x-y-z translation stage for fine alignment of the gas pulse with the laser focus. During the gas pulse, the density at the nozzle exit was on the order of several tens of Torr.[11] A sleeve with two ~ 5 mm diameter holes for laser beam passage surrounded the valve and jet; it led to a cone which was connected to a 6 inch diameter cryopump (Varian VK-12). This differential pumping arrangement reduced the chamber background pressure from ~ 10^{-4} Torr to ~ 10^{-6} Torr with the valve running. The UV and XUV beams passed through a set of ion extraction optics 15 cm from the nozzle of the pulsed valve. A beam of molecules to be studied also passed through the ion extractor. This sample beam was delivered by a second pulsed valve (Lasertechnics LPV); the expanding gas was skimmed on its way to the intersection with the XUV beam.

The XUV intensity was measured by recording the photoionization of propylene, C_3H_6. This molecule has a low ionization potential (below 10 eV) so that it can be ionized by light with wavelengths shorter than

1200 A. It also has a rather wavelength-independent photoionization cross section.[13] Ions were extracted through a quadrupole mass filter, and detected by a Johnston electron multiplier. A gated integrator averaged the ion signal for several laser shots at each setting of the dye laser wavelength.

The propylene source and ion detector regions were separated from the main experimental chamber by differential walls. The pressure in the molecular beam source region was ~ 10^{-4} Torr; the main chamber, pumped by two 6 inch diffusion pumps, was at ~ 10^{-6} Torr, and the detector region was below 10^{-8} Torr.

Our Quanta-Ray Nd:YAG laser system included a dye laser and KDP crystals for frequency-doubling its output to 2700-3100 A, and crystals for subsequently mixing with the 10642 A residual beam (the Nd:YAG fundamental) to obtain wavelengths as short as 2160 A. The resolution of the dye laser was ~ 0.3 cm^{-1}, and the linewidth of the Nd:YAG fundamental was ~ 1 cm^{-1}. Dielectric coated, nondispersive optics were used to separate the doubled dye laser output (2710-3070 A) from the dye laser fundamental, so scanning the XUV down to 900 A without beam walk was possible. But the higher-frequency UV output (down to 2160 A), was separated from the other beams with a Pellin-Broca prism, which was quite dispersive. The beam walk was substantial. Thus we did not scan continuously when using the shorter-wavelength UV beam. Instead, we measured the relative tripling efficiencies below 900 A at various atomic and molecular two-photon resonances. Standard laser dyes (all from Exciton) Sulforhodamine 640, Rhodamine 640, Kiton Red 620, Rhodamine 610 Perchlorate, Rhodamine 590, and Fluorescein 548 were used without further purification. Figure 2 shows the dye laser visible

output powers obtained when running the pump laser at 10 Hz. The frequency-doubled power was roughly 15% of the visible power, and the pulsewidth was nominally 5 nsec.

The near UV power was recorded with a Molectron J3-05 pyroelectric joulemeter equipped with a Schott UG-11 filter to reject the small amount of visible light present. Wavelength calibration was accomplished by comparing the observed frequencies of resonantly-enhanced two-photon ionization ($3\omega + \omega$) signals in H_2 with the published positions of the XUV (3ω) transitions of H_2.[14]

The visible wavelength was scanned in steps of 1 A (i.e. 1/6 A in the XUV). The near UV power and XUV intensity (propylene ion signal) were recorded simultaneously. The ion signal was then normalized to the cube of the UV power to give $P(3\omega)/P^3(\omega)$. Intensities obtained with different laser dyes were calibrated against each other in the overlapping wavelength region. The dispersion of the optical system caused the focal spot to drift slightly with respect to the gas jet. This led to systematic error in the intensity distribution of the tripling spectra, somewhat biased against the longest-wavelength side.

Assessment of the systematic and random errors in our measurements led us to conclude that for a given wavelength, the relative tripling efficiencies of the various gases we had measured were quite accurate. On the other hand, for a given gas, the scale factor could be in error by a factor of three between the high- and low-frequency ends of the spectrum.

III. Results

Figures 3-7 show the $P(3\omega)/P^3(\omega)$ spectra in the 1024-904 A region

for the gases Ar, Xe, Kr, CO, and N_2. The nozzle stagnation pressures used with the tripling gas pulsed valve were: 1 atm for Kr and Xe, 2.5 atm for CO, and 5 atm for Ar and N_2. (Note that the pressure for optimum XUV generation depends on the wavelength; we will consider this later.) The fine structure in the Ar spectrum shows the typical amplitude fluctuation after averaging for 30 laser shots. As discussed in the Experimental section, continuous scanning was only possible in the wavelength region above 900A. Table I lists two-photon (2ω) resonance transitions through which XUV outputs below 900 A were obtained.

Marinero et al.[15] had reported an XUV output of 7×10^9 photons/shot when tripling to 1013.4 A in Ar. Their UV energy and pulsewidth were comparable to ours. In our figures, $P(3\omega)/P^3(\omega) = 100$ corresponds to $\sim 5 \times 10^9$ XUV photons out for 10 mj UV in. At our stated energy (10 mj $\sim 1.5 \times 10^{16}$ photon), this represents a conversion efficiency $P(3\omega)/P(\omega)$ of $\sim 10^{-6}$. Equivalently, the peak power of the XUV output is on the order of a Watt.

IV. Discussion

An understanding of the origins of the features observed in the tripling spectra can lead to efficient optimization of the XUV output. Such an optimization includes choosing the best gas and adjusting its density. In general, the XUV output depends on $\chi^{(3)}$ via the relation $P(3\omega) \propto N^2|\chi^{(3)}|^2 P^3(\omega)$; N is the number density and $\chi^{(3)}$ is the third-order nonlinear electric susceptibility per atom (molecule). $\chi^{(3)}$ in turn contains electric dipole matrix elements between many different states. Computation of $\chi^{(3)}$ as a function of ω is possible in

principle. Miles and Harris[16] have performed the calculations for alkali metal atoms, which have hydrogen-like wave functions and easily evaluated matrix elements. In practice, it is necessary to determine $\chi^{(3)}$ experimentally by measuring the tripled output as a function of wavelength under well-controlled conditions of gas density, laser power, and laser beam quality. When the behavior of $\chi^{(3)}$ is dominated by a transition which is nearly at resonance with ω, 2ω, or 3ω, a simple picture can be used to provide an explanation for the appearance of the tripling spectrum. (For a thorough discussion of resonant contributions to $\chi^{(3)}$, the reader is referred to the book by Hanna et al.[17])

In the argon spectrum (Fig. 3), no sharp features are observed. Since ω_{XUV} (= 3ω) is situated between strong transitions at 1048-1065 A (3p - 4s', 4s) and at ~ 867-880 A (3p - 5s, 5s', 3d, 3d'), the broad null at ~ 930 A is presumably due to destructive interference in the contributions to $\chi^{(3)}$ from the two groups of resonances. The fact that the medium is not lossy in this entire region means that a higher gas flow could enhance the XUV output by increasing the macroscopic susceptibility $N\chi^{(3)}$.

The xenon spectrum (Fig. 4) shows a very different behavior. Each feature observed has a correspondence with an absorption peak in the autoionizing Rydberg series (5p - ns', nd').[1,18] More specifically, each minimum in the XUV output coincides with a maximum in the single-photon absorption spectrum, where the exponential absorption coefficient is ~ 6/Torr-mm. Evidently the exponential loss due to absorption in several Torr-mm of gas overcompensates the enhancement in $\chi^{(3)}$ that occurs when 3ω is resonant with an allowed transition. As

the Rydberg states become closer together in energy when the wavelength approaches the series limit at 924 A, the XUV signal undergoes weaker, more rapid oscillations in intensity. This is in accordance with the proposition that the averaged oscillator strength distribution $df/d\omega$ is continuous at the convergence of a Rydberg series. $P(3\omega)/P^3(\omega)$ attains its continuum value at the 924 A convergence; the slight increase at ~ 907 A is probably an artifact due to normalization. We note that because the gas density strongly affects the amount of XUV attenuation that occurs, the relative heights of the peaks and dips in this spectrum change with nozzle stagnation pressure and the operating condition of the pulsed valve. Electronic adjustment of the valve opening amplitude and timing with respect to the UV pulse are rapid and effective ways to optimize the XUV output at a given wavelength.

The Kr spectrum (Fig. 5) is an intermediate case, whose analysis is more complicated than the Ar and Xe spectra. Overlapping $4p \rightarrow ns$ and $4p \rightarrow nd$ Rydberg series which converge to the ground and first excited states of the Kr^+ ion are present, and give resonances at 3ω. As in the Xe spectrum, each transition gives a strong absorption when 3ω is exactly on resonance and an enhancement at neighboring wavelengths. The 3ω resonances are sharp because the scanned region of 3ω is below the ionization level at 886 A. At wavelengths near and below 886 A, the spectrum should appear qualitatively similar to that of Xe (Fig. 4).

The use of molecules for frequency tripling in pulsed jets has been demonstrated by Rettner et al.,[19] who analyzed the rotational structure of a two-photon resonance in detail. They showed how the appearance of the XUV output around 985 A, enhanced by the CO A ($v' = 2$) $\leftarrow$ X ($v'' = 0$) band at 1478 A, changed as the distance between the pulsed valve's

nozzle and the laser focus was increased. The spectral change was induced by the rotational cooling that occurs during a supersonic expansion. As more molecules become simultaneously resonant with 2ω, the effective value of N (the number density) increases, and the XUV output is markedly increased. Our results (Fig. 6) were obtained with the laser focussed at a small distance from, and almost touching the nozzle. The molecules were thus not very cold. In our experience, the peak XUV signal could be increased by a substantial factor by optimizing the distance between nozzle and laser focus. Variation of the rotational temperature can be used to optimize the tripled output, but clearly this does not apply to atoms.

Two-photon resonances with other vibrational levels in the CO A $^1\Pi$ state have been identified at ~ 1006, 963, 946, 928, and 911 A and are labeled in Fig. 6. We have not assigned other features; many 3ω resonances could occur in this region. Several Rydberg electronic states should be present, each with vibrational structure. It is interesting to note that some of the features (e.g. at ~ 954 A) are much "smoother" than others. This characteristic has also been seen in the spectra of Hellner and Lukasik.[8] The likely cause is that the upper level contributing to a "smooth" resonance is predissociative, causing individual rovibronic transitions to become appreciably broadened. Predissociative states are known to exist in CO above ~ 89000 cm^{-1}.[20]

N_2 (Fig. 7), which is isoelectronic with CO, is also a useful tripling medium. (Air, with 80% N_2, has also been used as a tripling medium!) Indeed, its tripling efficiency to 930.7 A is the largest of any gas we have studied in the 904-1024 A range, and it could be

increased further by adjusting the nozzle-to-focus distance. As in the case of CO, there are many peaks in its spectrum. Two-photon resonances in the a $^1\Pi_g$ (v' = 1,2) states occur at output wavelengths of ~ 945 and ~ 925 Å. No attempt has been made to identify all the observed features.

Our spectra show that continuously tunable XUV light can be obtained between 1024 and 904 Å by using only Ar and Xe. However, greater intensity at specific wavelengths can be obtained by using the other gases. Also, intense radiation can be generated at wavelengths as low as 720 Å by taking advantage of two-photon resonances.

While our results are extremely useful, there are clear avenues for extension of the XUV generation capability. An obvious goal is to tune continuously below 900 Å. Our particular system is limited in this regard by using 532-nm light to pump the dye laser, making the shortest visible wavelength available to be ~ 540 nm. The laser power below 540 nm obtainable by pumping with 355-nm light from a Nd:YAG system is much lower; an excimer-pumped dye laser would be better at providing blue light for getting to the 700-900 Å range. Another limitation is the inability of the efficient KDP frequency-doubling crystals to work below ~ 260 nm. The new β-barium borate crystal shows good promise to remove this difficulty.[21,22]

Additionally, XUV output could be increased in many cases by providing a denser gas jet. The attainable gas flow (for a 1 mm diameter nozzle) has been limited by the restricted opening distance of the valve's poppet. An improved pulsed valve recently constructed in our laboratory[23] promises to provide quite a large improvement by employing a piezoelectric transducer with a large travel.

V. Conclusion

We have described an XUV source with many desirable attributes. It is comparatively simple and inexpensive and requires only one tunable laser. The output is widely tunable and is sufficiently intense that double-resonance studies are feasible. Greater than 10^{10} photons/sec in a narrow bandwidth is achievable using standard (commercial) laser sources. Convenience and reliability are key attributes. Changing the tripling gas and its density can be done very rapidly, and alignment of the laser beam for efficient XUV generation is likewise quite simple. Use of a pulsed valve as the provider of the nonlinear medium means that the gas consumption and background pressure are small, so that an experiment and this XUV generation apparatus can coexist in the same vacuum chamber. In our setup, the tripling jet and sample beam are only ~ 15 cm apart, and the background pressure is only 10^{-6} Torr.

We have applied our XUV source in several experiments. The output around ~ 1000 A is ideal for exciting the low-frequency transitions in H_2. We have succeeded in detecting small H_2 concentrations with high sensitivity by using resonantly-enhanced two-photon ionization.[23] Also, the ability to create a large population of excited H_2 molecules allowed us to study the H_2 gerade states around 122,000 cm^{-1} by double-resonance.[24] We have already reported on a study of the H^+H^- ion-pair continuum whose threshold is at ~ 140,000 cm^{-1}.[25]

The high light intensity is useful in high-resolution spectroscopic studies of dilute (molecular beam) samples. We have obtained photoionization spectra of H_2O and D_2O in the 1000-900 A range.[26] The molecules were supersonically cooled and the resolution, limited by the

dye laser, was ~ 2 cm^{-1}. The ion signal was large enough to give a good signal-to-noise ratio with only a few seconds of averaging time at each frequency. This allowed us to acquire the spectra in a couple of days, which would not have been possible with other existing XUV sources. Previously undetected Rydberg series appear in the high-resolution spectra of the cold molecules. A narrower-linewidth dye laser could be used to obtain XUV spectra of molecular beam samples with Doppler-limited resolution.

References

1. J. A. R. Samson, Techniques of Vacuum Ultraviolet Spectroscopy (Pied Publications, Lincoln, Nebraska, 1969).
2. C. R. Vidal, in Tunable Lasers (Topics in Applied Physics, Vol. 59) (Springer, Heidelberg, 1986).
3. G. C. Bjorklund, IEEE J. Quantum Electron. 11, 287 (1975).
4. R. Hilbig and R. Wallenstein, IEEE J. Quantum Electron. 17, 1566 (1981).
5. R. Hilbig and R. Wallenstein, Opt. Commun. 44, 283 (1983).
6. R. Hilbig, A. Lago, and R. Wallenstein, Opt. Commun. 49, 297 (1984).
7. H. Pummer, T. Srinivasan, H. Egger, K. Boyer, T. S. Luk, and C. K. Rhodes, Opt. Lett. 7, 93 (1982).
8. L. Hellner and J. Lukasik, Opt. Commun. 51, 347 (1984).
9. P. R. Herman and B. P. Stoicheff, Opt. Lett. 10, 502 (1985).
10. K. D. Bonin and T. J. McIlrath, J. Opt. Soc. Am. B 2, 527 (1985).
11. A. H. Kung, Opt. Lett. 8, 24 (1983).
12. J. Bokor, P. H. Bucksbaum, and R. R. Freeman, Opt. Lett. 8, 217 (1983).
13. J. A. R. Samson, F. F. Marmo, and K. Watanabe, J. Chem. Phys. 36, 783 (1962).
14. I. Dabrowski and G. Herzberg, Can. J. Phys. 52, 1110 (1974).
15. E. E. Marinero, C. T. Rettner, R. N. Zare, and A. H. Kung, Chem. Phys. Lett. 95, 486 (1983).
16. R. B. Miles and S. E. Harris, IEEE J. Quantum Electron. 9, 470 (1973).
17. D. C. Hanna, M. A. Yuratich, and D. Cotter, Nonlinear Optics of Free Atoms and Molecules, Springer series in Optical Sciences,

vol. 17 (Springer, Berlin, 1979).

18. J. Berkowitz, Photoabsorption, Photoionization, and Photoelectron Spectroscopy (Academic Press, New York, 1979).

19. C. T. Rettner, E. E. Marinero, R. N. Zare, and A. H. Kung, J. Phys. Chem. 88, 4459 (1984).

20. P. H. Krupenie, The Band Spectrum of Carbon Monoxide, NSRDS-NBS 5 (U.S. Government Printing Office, Washington, D.C., 1966).

21. K. Kato, IEEE J. Quantum Electron. 22, 1013 (1986).

22. C. Chen, B. Wu, A. Jiang, and G. You, Sci. Scinica B28, 235 (1985).

23. T. Trickl, private communication.

24. R. H. Page, R. J. Larkin, A. H. Kung, Y. R. Shen, and Y. T. Lee, unpublished results.

25. A. H. Kung, R. H. Page, R. J. Larkin, Y. R. Shen, and Y. T. Lee, Phys. Rev. Lett. 56, 328 (1986).

26. R. H. Page, R. J. Larkin, Y. R. Shen, and Y. T. Lee, to be published.

Table I. Two-photon resonant lines for tripling below 900 A.

Gas	Transition	Two-photon resonance (cm^{-1})	XUV wavelength A	UV energy (mj)	Relative intensity (a.u.)
Xe	$5p \rightarrow 6p(5/2)_2$	78120	853.4	(not measured)	
	$\rightarrow 6p(3/2)_2$	79213	841.6	(not measured)	
	$\rightarrow 6p(1/2)_0$	80119	832.1	0.5	1.7
	$\rightarrow 7p(5/2)_2$	88352	754.6	3.2	0.4
	$\rightarrow 7p(3/2)_2$	88687	751.7	2.6	0.4
	$\rightarrow 7p(1/2)_0$	88843	750.4	3.1	0.9
	$\rightarrow 6p'(1/2)_2$	89163	747.7	4.0	2.2
	$\rightarrow 6p'(1/2)_0$	89861	741.9	4.5	10.
	$\rightarrow 8p(5/2)_2$	92222	722.9	3.2	0.3
	$\rightarrow 8p(3/2)_2$	92371	721.7	3.0	0.2
	$\rightarrow 8p(1/2)_0$	92556	720.3	1.8	1.4
Kr	$4p \rightarrow 5p(5/2)_2$	92308	722.2	3.1	1.8
CO	$\tilde{X}(v''=0) \rightarrow \tilde{B}(v'=0)$	86917	767.0	2.7	4.4
	$\rightarrow \tilde{B}(v'=1)$	89000	749.1	3.5	1.8
	$\rightarrow \tilde{C}(v'=0)$	91919	725.3	3.6	8.9

Figure Captions

Fig. 1 Apparatus for XUV generation with a pulsed free jet. Near UV light (ω) is focused into the tripling jet, which is surrounded by a sleeve which directs the gas toward a cryopump. The XUV (3ω) beam is collinear with the input beam (ω), and crosses a supersonic molecular beam of sample gas. Photoions are extracted, mass filtered, and counted. Differential walls (not shown) support the skimmer and enclose the mass filter/ion detector. The peak pressure in the jet is tens of Torr, and the background pressure in the ion extraction region is ~ 10^{-6} Torr.

Fig. 2 Visible power output vs. wavelength for the dyes Sulforhodamine 640, Rhodamine 640, Kiton Red 620, Rhodamine 610, Rhodamine 590, and Fluorescein 548.

Fig. 3 Normalized XUV output vs. wavelength obtained with argon. With our intensity scale, a $P(3\omega)/P^3(\omega)$ value of 100 corresponds to roughly 5×10^9 XUV photons/laser shot when the laser pulse energy is ~ 10 mj.

Fig. 4 As in Fig. 3, for xenon.

Fig. 5 As in Fig. 3, for krypton.

Fig. 6 As in Fig. 3, for carbon monoxide. Parentheses enclose vibrational assignments of some two-photon (2ω) resonances.

Fig. 7 As in Fig. 6, for nitrogen.

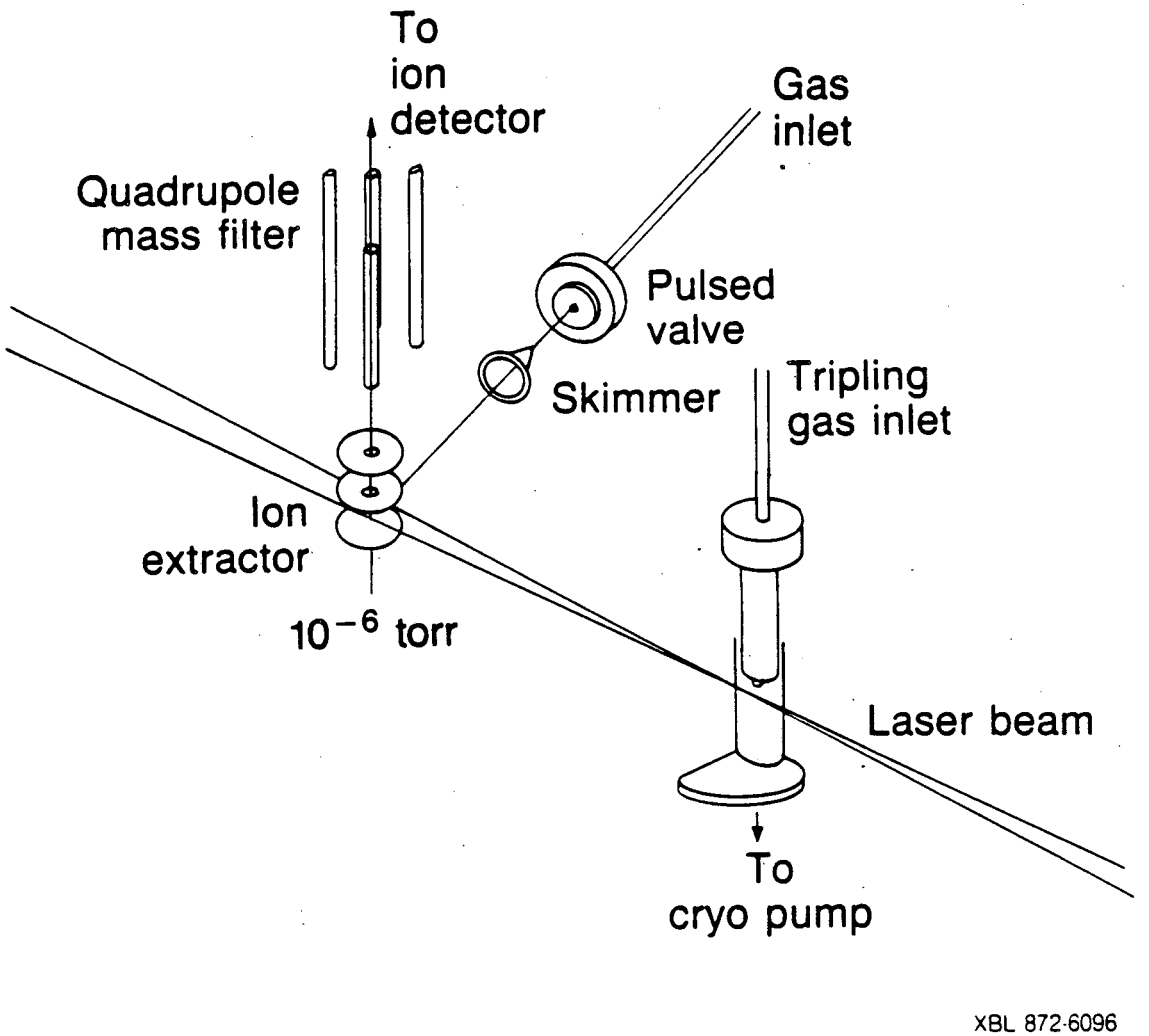
XUV generation apparatus
To
ion
detector
Gas
inlet
Quadrupole
mass filter
Pulsed
valve
Skimmer
Tripling
gas inlet
Ion
extractor
10^{-6} torr
Laser beam
To
cryo pump
XBL 872-6096

Figure 1.

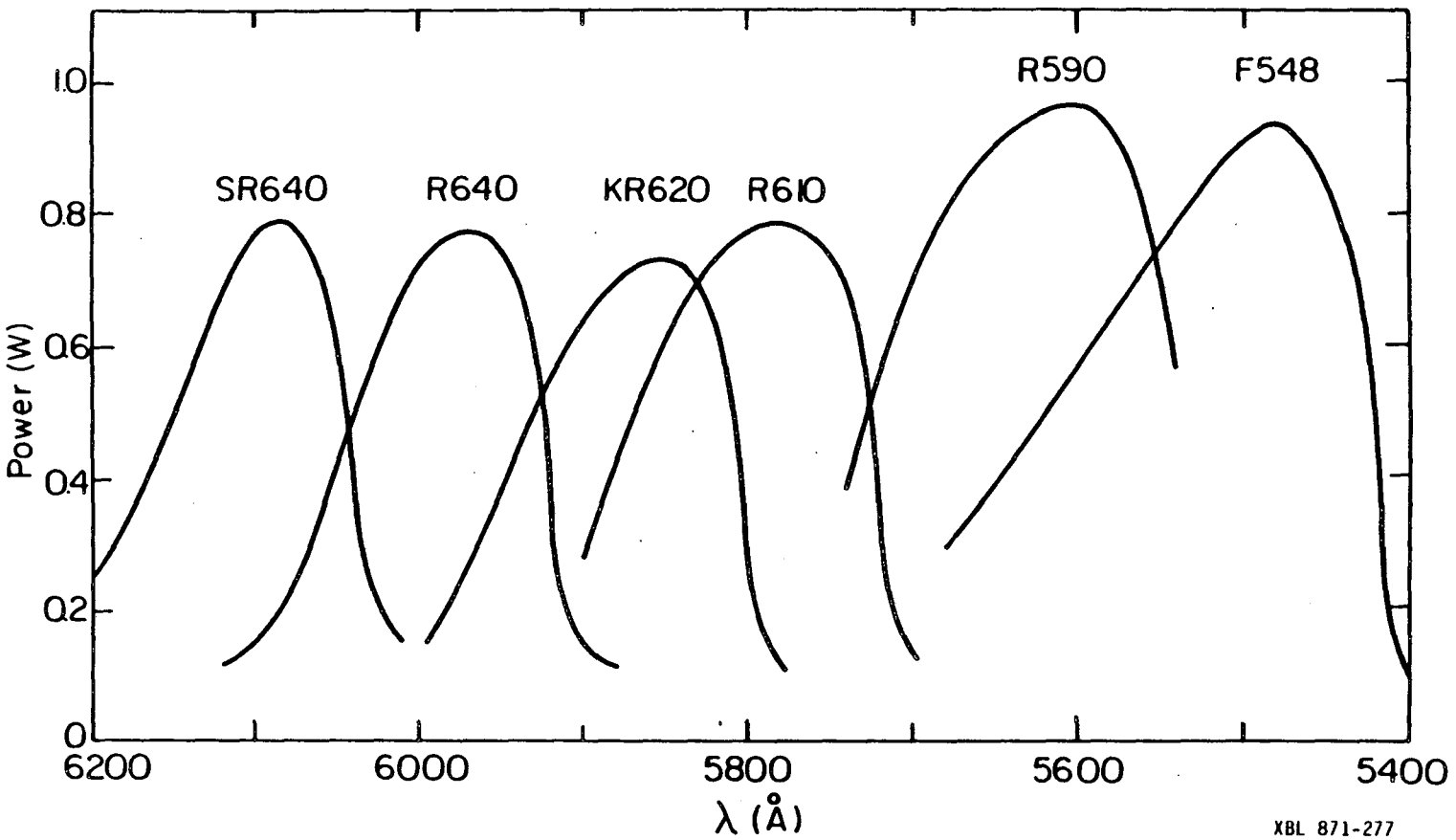
R590
F548
SR640
R640
KR620
R610
1.0
0.8
0.6
0.4
0.2
0
Power (W)
6200
6000
5800
5600
5400
λ (Å)
XBL 871-277

Figure 2.

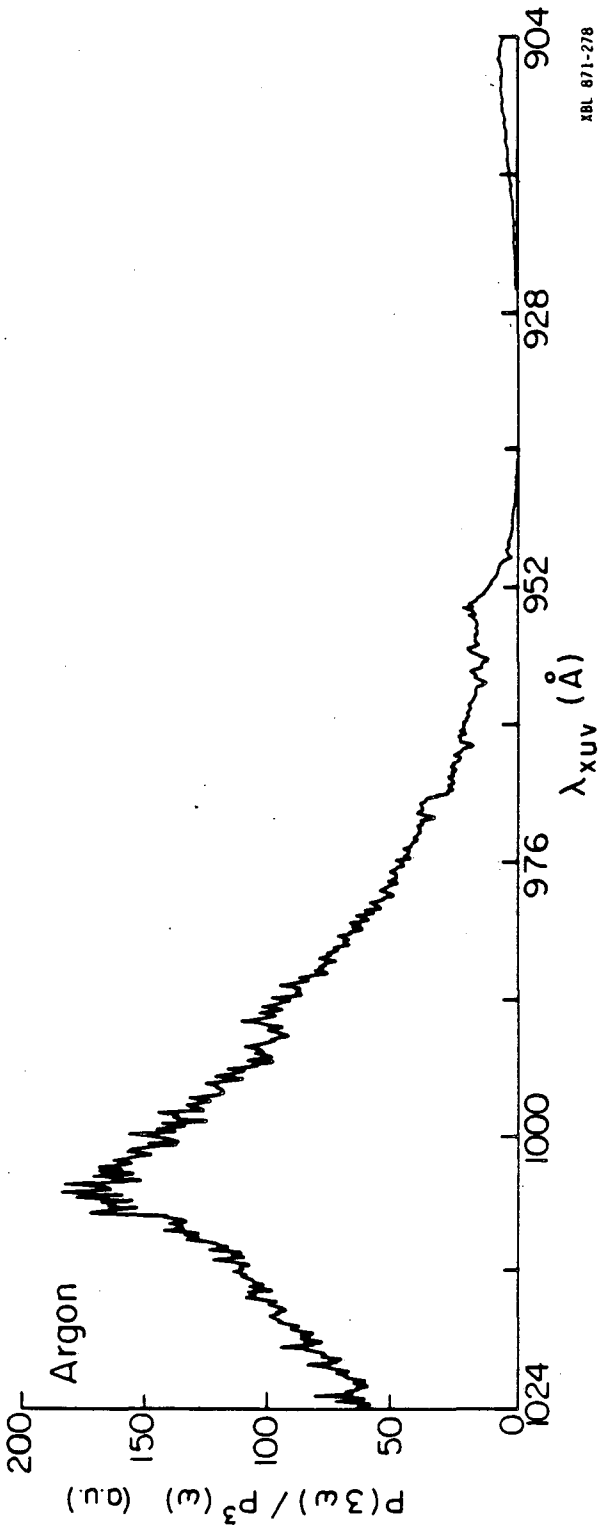
Argon
P(3ω) / P³(ω) (a.u.)
200
150
100
50
0
1024
1000
976
952
928
904
λXUV (Å)
XBL 871-278

Figure 3.

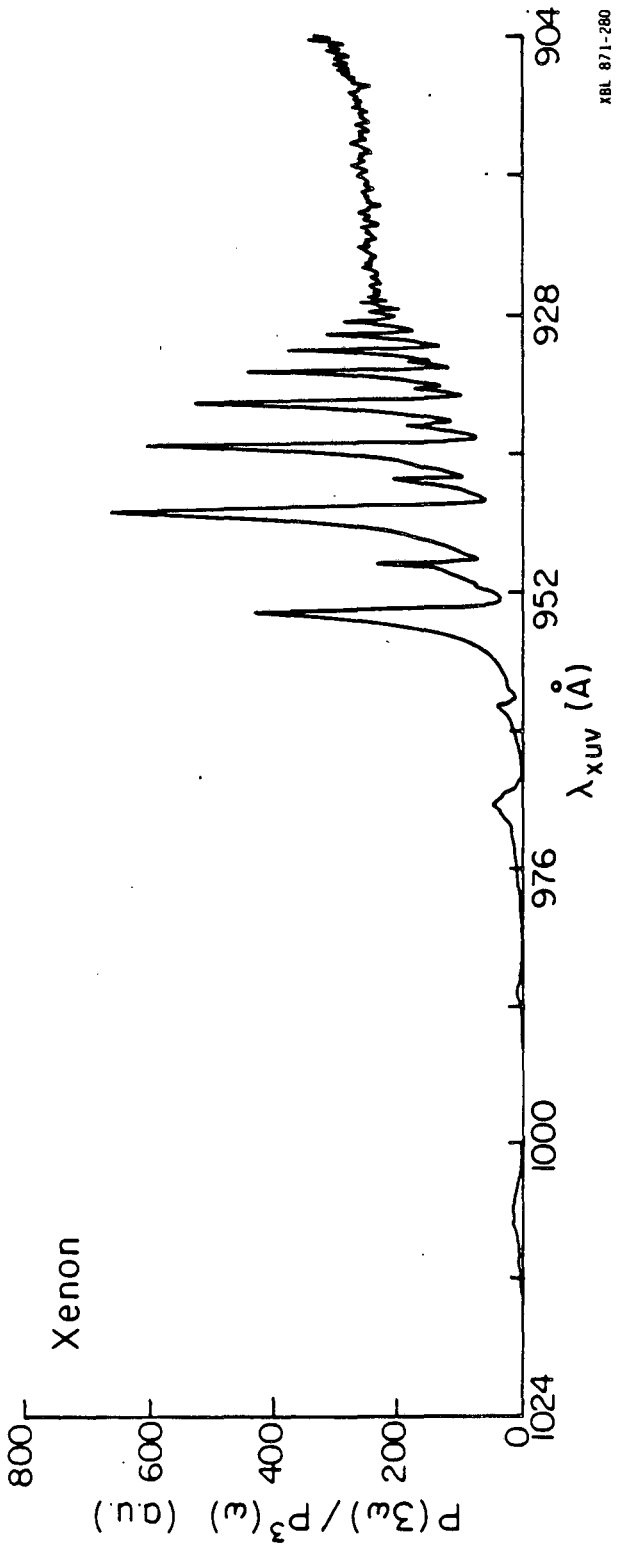
Xenon
800
600
400
200
0
1024
1000
976
952
928
904
λ_{XUV} (Å)
$\Gamma(^3\Sigma_u^-) / P^3(\epsilon)$ (a.u.)
XBL 871-280

Figure 4.

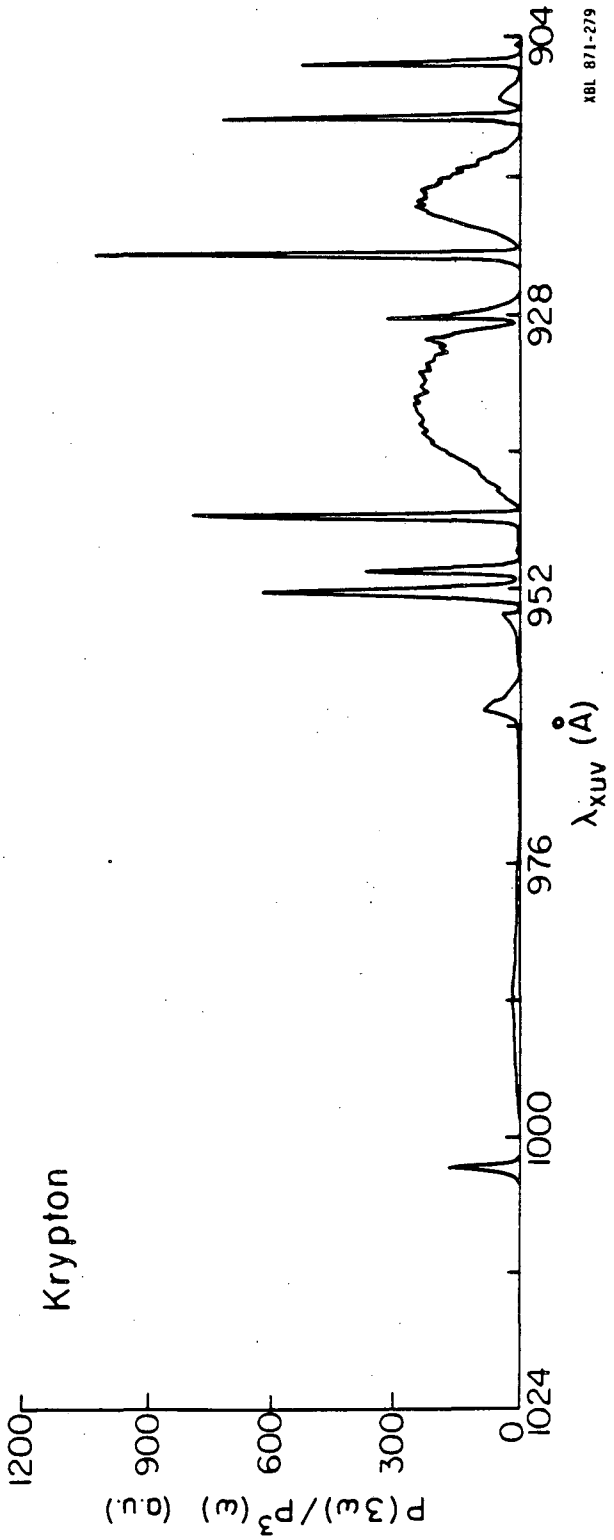
Krypton
P(3ω)/P³ (ε) (a.u.)
1200
900
600
300
0
1024
1000
976
952
928
904
λXUV (Å)
XBL 871-279

Figure 5.

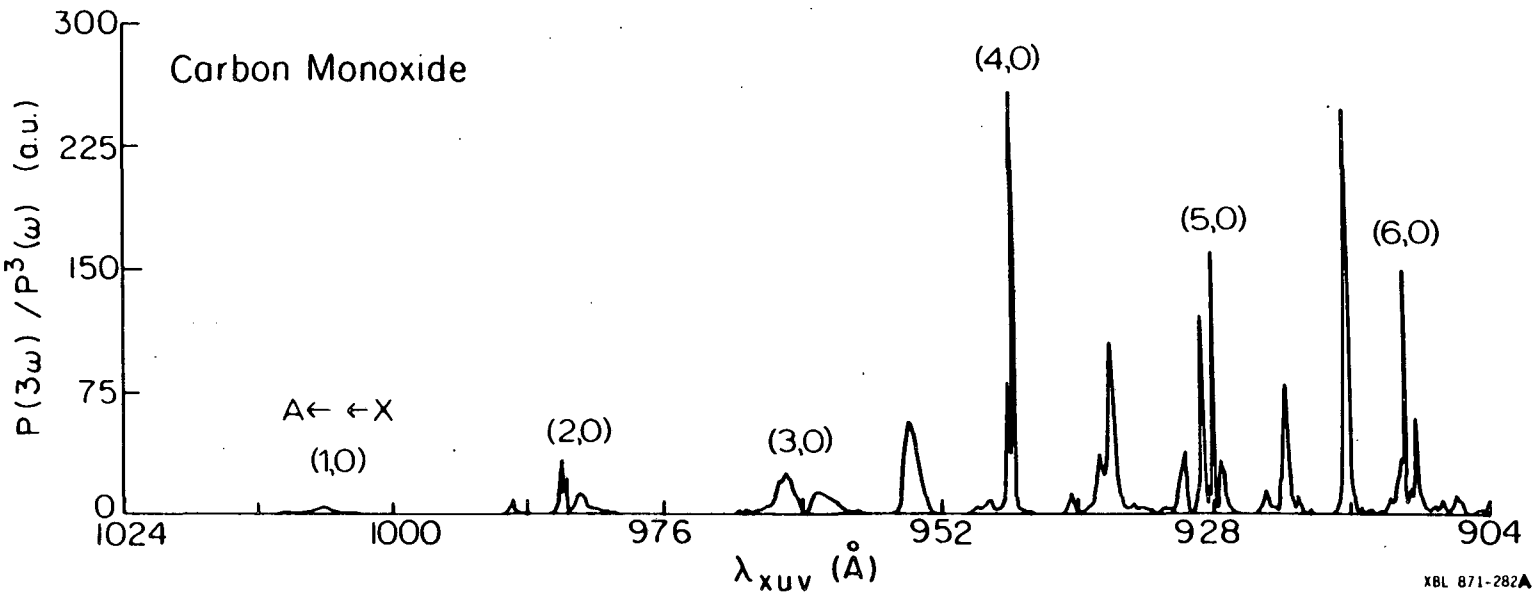
Carbon Monoxide
300
225
150
75
0
P(3ω) / P³(ω) (a.u.)
A← ←X
(1,0)
(2,0)
(3,0)
(4,0)
(5,0)
(6,0)
1024
1000
976
952
928
904
λxuv (Å)
XBL 871-282A

Figure 6.

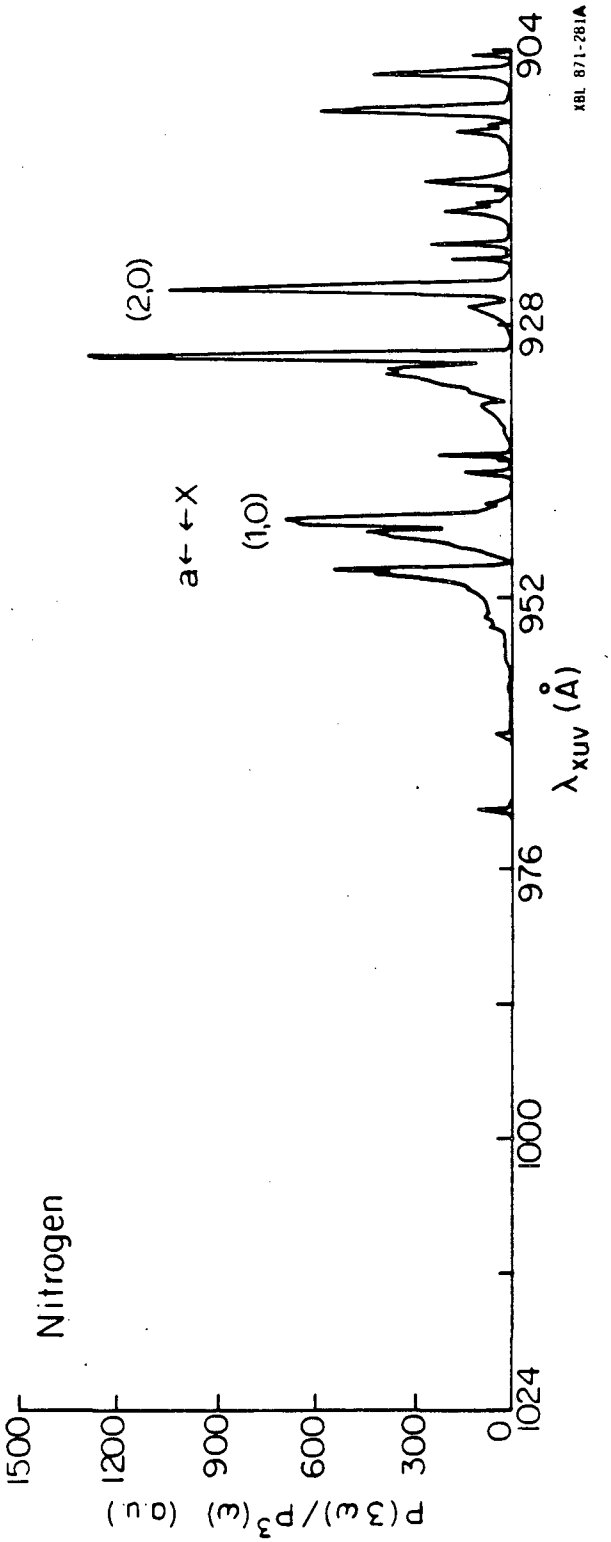
Nitrogen
$P(3\omega)/P^3(\omega)$ (a.u.)
1500
1200
900
600
300
0
1024
1000
976
952
928
904
λ_{XUV} (Å)
a ← ← X
(1,0)
(2,0)
XBL 871-281A

Figure 7.

VI. HIGH RESOLUTION PHOTOIONIZATION SPECTRUM OF WATER MOLECULES IN A SUPERSONIC BEAM

I. INTRODUCTION

There has been a fair amount of effort spent in analyzing the electronically excited states of the water molecule. At present, there is at least a semiquantitative understanding of some of water's excited states, derived from about 50 years' worth of research. But there is also much that is not known, especially concerning the region above ~ 80000 cm^{-1}, where many excited states exist.

The electronic transitions of water are all in the vacuum ultraviolet (VUV; 2000-1000 A) and extreme ultraviolet (XUV; below 1000 A) regions. A study done by Price[1] detected several absorption bands below the IP (ionization potential) and a pair of Rydberg series converging to it. References to other early works are found in papers by Katayama et al.[2] and Wang et al.[3] As spectroscopic resolution was improved, it became possible to look for rotational fine structure in the electronic transitions. Most of the bands were seen to be rather diffuse, leading to the conclusion that their corresponding excited states were rapidly predissociated. Notable exceptions, in which detailed rotational analyses were performed, were the bands at 1240 A [4] and 1115 A.[5] Vibrational structure built on the intense transitions at 1219 and 1240 A was resolved and analyzed[6] to give values for two of the three vibrational frequencies (ν_1 and ν_2) in the electronically excited states. A simple force-constant model was then used, and is still routinely used, to estimate the value of ν_3, the asymmetric O-H stretch.

There are many transitions of interest near and above the ionization threshold at ~ 980 A, lower in wavelength than the "LiF cutoff" at ~ 1040 A. Windowless XUV (below 1000 A) techniques are required to study these transitions. In recent years, it has become possible to study resolved absorption features in the XUV region, including Rydberg series converging to the ionization potential. An important work on H_2O and D_2O was done at medium (~ 50 cm^{-1}) resolution by Katayama, Huffman and O'Bryan[2] and gave quantitative absorption and photoionization cross sections between 580 and 1050 A. They discovered some prominent, structured features around 960 A due to autoionizing states, which they studied at higher resolution. The transitions to these states had significant (few cm^{-1}) linewidths and have consistently been interpreted as a progression in the bending mode ν_2, excited when the molecule snaps from a bent ground state into a quasi-linear excited-state structure. The rotational structure of these autoionizing states has so far not been analyzed, and even the number of bending quanta ν_2 in each state is not reliably known.

With a monochromator as the resolution-determining element, intensity (signal level) and resolution are competing variables. This has prevented the acquisition of well-resolved spectra with laboratory light sources. The higher intensity synchrotron light sources have recently been used in obtaining high-resolution (few cm^{-1}) absorption spectra. Studies by Ishiguro et al.,[7] Gurtler et al.,[8] and Connerade et al.[9] have shown detailed fine structure in many bands below the ionization potential. Mayhew[10] has carried out a study of the Rydberg series converging to the IP, with a resolution of better than 1 cm^{-1}. In spite of this, a detailed rotational analysis has not been

forthcoming, because the Rydberg region with n, the principal quantum number, above ~ 6 is quite congested. There are several overlapping Rydberg series, and each of these has vibrational and rotational structure. The use of high optical resolution does not eliminate this serious congestion. Another problem is that the N_2 molecule has intense absorption lines in this spectral region, and even a slight contamination causes artifacts in absorption spectra.

While Rydberg series below the IP are difficult to study, those above it are no easier: An intense continuum absorption often obscures the weak, discrete lines. To date the autoionizing Rydberg series have not been detected above n ~ 6.

Some information concerning Rydberg series can come from studies of the ionic states to which they converge. In fact, the H_2O^+ ion has been rather well studied. Photoelectron spectra[11-13] have shown the vibrational structure in the $\tilde{X}$, $\tilde{A}$, and $\tilde{B}$ states of the ion. As a result, the ion's geometry in each of these states is roughly known. In the $\tilde{X}$ (ground) state, H_2O^+ has a bent structure much like ground-state H_2O, but it is nearly linear in its $\tilde{A}$ (first excited) state. This fact causes the bending motion to be qualitatively different in the $\tilde{X}$ and $\tilde{A}$ states. In a linear molecule, the vibrational angular momentum interacts with the electronic angular momentum. The interaction, known as the Renner-Teller effect,[14-16] is rather strong in H_2O^+ and has a pronounced effect on the vibronic band structure. The unusual bandshapes characteristic of the Renner-Teller perturbation have long been noted in photoelectron spectra[11-13] and recently displayed with improved resolution by Reutt et al.,[13] who used a supersonic molecular beam of water in their photoelectron spectrometer.

The rotationally resolved emission spectrum of the visible $\tilde{A} \rightarrow \tilde{X}$ transition of H_2O^+ was minutely analyzed by Lew.[17] His determination of the geometries and vibrational frequencies in the ion's $\tilde{X}$ and $\tilde{A}$ states was facilitated by the results from photoelectron spectroscopy, and because of his much better resolution and subsequent rotational analysis, his results have considerably greater accuracy.

Studies of the decay mechanisms of electronically-excited water are helping to complete the picture of its behavior. Fluorescence quantum yields have been measured by Lee and Suto.[18] Dutuit et al.[19] have done an experiment in which fluorescence from the predissociation products H and OH ($\tilde{A}$, $\tilde{B}$) was measured. Their wavelength-resolved fluorescence excitation spectra, obtained over a wide energy range, give very detailed information concerning the predissociation characteristics of the upper states corresponding to individual absorption features. Coupled with the photoionization branching ratio,[2,20] the dissociation and fluorescence quantum yields form a rather thorough catalog of the fates of the individual excited states.

The recent use of the multiphoton ionization (MPI) technique[21-24] has given access to states which do not have electric-dipole transitions from the ground state. When lasers are used, the resolution can be extremely high, so that an accurate rotational analysis is to be expected unless individual rovibronic transitions are so diffuse that they overlap. In fact, the MPI technique has been used to measure homogeneous linewidths of several transitions, with the conclusion that the excited states around 80000 cm^{-1} are predissociated in a manner that depends on the final rotational state.[22-24] Thus far, multiphoton techniques have not been used to study final states above

about 85000 cm^{-1}, but it will be possible to do so when the appropriate lasers are developed.

The effort to deal theoretically with the excited states of water has also been quite extensive. A fairly comprehensive summary of this work is given in an article by Diercksen et al.,[25] who calculated absorption and ionization spectra. They included electric-dipole allowed final-state orbitals of angular momentum up to 2 (i.e. d orbitals). An "unabashedly empirical" approach was taken by Wang et al.,[3] who attempted to provide a consistent explanation of the known absorption spectra and excited states of water. They did not perform ab initio calculations of energy levels and spectra.

While many features of the water spectrum are basically understood, many details remain to be investigated. Notably, many researchers[3,7,10] do not agree on the assignments and symmetries of the Rydberg series around the IP. Also, the prominent features between the first ($\tilde{X}$) and second ($\tilde{A}$) IP's have not been quantitatively analyzed. A recent work[7] has included a large table of observed transitions, with many unassigned bands. Some means of simplifying the complex spectral region near the IP would clearly be helpful.

We have been able to make some progress in this direction. By using the photoionization technique, we have effectively rejected some absorption features which cause dissociation but not ionization. Autoionization features are then selectively studied. Furthermore, we have used a supersonic expansion to cool the water molecules. The smaller number of ground rotational states populated reduces the number of observed transitions dramatically, and shrinks the "rotational envelope" observed on each electronic transition. As a result, the

spectrum becomes much clearer and is more easily interpreted. Finally, we have used the third-harmonic generation (THG) technique to generate the requisite XUV light. This has given us an intense source with good (~ 1.5 cm^{-1}) resolution, making features with small linewidths retain their prominence in the spectra, and allowing us to determine homogeneous linewidths.

Our technique has given us high-quality spectra of H_2O^+ and D_2O^+ in which we have detected two vibrationally autoionizing Rydberg series. From these we derive a new estimate of the ionization potential. Also, we have displayed very intense, well-defined autoionization features which are due to the bending progression in the quasi-linear state. We have done a rotational analysis of some of these bands and determined the vibrational quantum numbers of all of them. This has allowed us to find the electronic origin of the state. Our analysis contradicts earlier assignments of Ishiguro[7] and Wang[3] and will be useful in testing theoretical calculations of energy levels.

II. EXPERIMENTAL

Figure 1 is a schematic diagram of the components inside our vacuum chamber. For clarity, walls which isolate differentially pumped regions are not shown. Our supersonic sample beam was formed by passing Ne through H_2O or D_2O at 0°C, and admitting the mixture to the beam source region via a Lasertechnics LPV pulsed valve. Its nozzle of 1 mm dia. was ~ 15-20 mm from the 1.25 mm dia. skimmer. With the beam source running at 10 pulses per second, the background pressures in the source and experimental region were ~ 10^{-5} and ~ 10^{-7} torr, respectively; the skimmer provided the only gas leak between the two

regions, which had separate pumping facilities. The molecular beam intersected the laser beam between a set of ion extraction plates. Photoions were extracted and sent through a differentially pumped (~ 10^{-9} torr) quadrupole mass filter. This filter was normally run in the high-transmission time-of-flight mode, since the ion signals were created in ~ 5 nsec bursts 10 times a second. With all ions getting roughly the same kinetic energy, the flight times varied roughly as $\tau \propto \sqrt{M}$. We used a Daly-style ion detector with a Johnston electron multiplier, and had ion counting capability.

We used a pulsed free jet[26] as the medium for frequency tripling into the 1000-900 A region. As a windowless system was required, we installed the differentially-pumped pulsed free jet source (Newport Research BV-100) in the same vacuum chamber in which the sample beam was to be ionized. A sleeve/cone arrangement directed the pulse of tripling gas to a separate cryopump. The sleeve had two apertures a few mm in diameter through which the near UV laser beam to be tripled passed. The collinear UV and XUV beams intersected the molecular beam in the ion extraction region. The experimental chamber pressure rose to only ~ 10^{-6} torr when the tripling gas pulsed valve was running. For best XUV generation, it was necessary to adjust the position of the laser focus in the tripling gas jet. This was done by moving the pulsed valve on an XYZ translation stage, rather than disturb the relative alignment of the laser and sample beams. We were able to cover the entire 1000-900 A region continuously by using Ar and Xe as the tripling gases. A more detailed account of our setup, and XUV generation efficiencies obtained with different tripling gases, will be published elsewhere.[27]

Our near UV laser source was a conventional system based on a Nd:YAG laser. A Quanta-Ray DCR-1 laser whose output was frequency-doubled pumped a PDL-1 dye laser. In this experiment we used the dyes Kiton Red 620, Rhodamine 610 Perchlorate, Rhodamine 590, and Fluorescein 548, all obtained from Exciton. The light from the dye laser was frequency-doubled in an automatically tracked KDP crystal (Quanta-Ray WEX-1). Starting with a 1.06 μ fundamental pulse energy of nominally 700 mj, our tunable near UV pulse energies were on the order of 10 mj. Running the laser at 10 pulses per second and with an easily achieved XUV conversion efficiency of at least 10^{-7}, the average XUV photon flux would be above 10^{10}/second. Our XUV bandwidth was ~ 1 1/2 cm^{-1}, giving our source a significantly higher spectral density, compared with other laboratory (i.e. discharge) sources. According to Radler and Berkowitz,[28] a discharge lamp/monochromator combination usually gives ~ 10^9 photon/sec in a 30 cm^{-1} bandwidth in this wavelength region. The dye laser wavelength was calibrated with an uncertainty of ~ ± 0.5 cm^{-1} by observing the optogalvanic effect[29] in an argon-filled voltage-regulator tube. XUV generation multiplied the dye laser frequency by 6, so our quoted XUV frequencies are uncertain to ~ 3 cm^{-1}.

A practical problem in our experiment was that the XUV intensity was quite frequency-dependent, due to resonances in the tripling gas. Also, the various stages of frequency conversion increased the laser's amplitude jitter and caused a pulse-to-pulse fluctuation of ~ 50% in the number of ions produced. In order to solve both of these problems, some sort of XUV intensity normalization was required. An extremely convenient (but not perfect) normalization technique was to include

some C_2H_2 in with the H_2O sample. With the mass spectrometer in the time-of-flight mode, and two separately delayed gated integrators, we measured the H_2O^+ and $C_2H_2^+$ signals separately. For a given ionizing wavelength, the ratio of these two signals was independent of changes, whatever the cause, in the XUV intensity: It depended only on the relative photoionization cross sections of the two molecules. Thus, this ratio can be used with the known C_2H_2 photoionization efficiency curve to find the photoionization efficiency spectrum of H_2O. In the region we studied, the XUV wavelength was less than 990 A and far below the C_2H_2 IP at 1088 A, and there is not known to be any intense fine structure in its ionization cross section.[30] There is, however, a gradual modulation in the cross section, which was imposed on our spectrum. The results we report here concern sharp resonances in the water molecule and are not noticeably affected by this phenomenon.

An extremely advantageous aspect of the use of mass-resolved ion detection was that stray signals from N_2, O_2, and other gases were eliminated. The masses we were measuring were 18 (H_2O^+), 20 (D_2O^+) and 26 ($C_2H_2^+$) amu. The ion signals at these masses disappeared when the pulsed valve supplying either the sample or the tripling gas was turned off. This was proof that our H_2O^+ and D_2O^+ signals were due only to XUV excitation.

A personal computer ran the wavelength scans and recorded the averaged $H_2O^+/C_2H_2^+$, H_2O^+, and optogalvanic frequency calibration signals. Depending on the detail we were trying to observe, the dye laser wavelength was incremented by 0.1 A or 0.05 A for each data point, and the averaging time constant was either 3 or 10 seconds. As will be seen in our spectra, the signal-to-noise ratio was quite good.

A crucial variable in the working of our experiment was the quality (rotational temperature) of the molecular beam generated in the supersonic expansion, as Fig. 2 shows. In it are spectra obtained from two different scans of the threshold region for ionizing H_2O. Part (a) is typical of a warm (~ room temperature) sample of gas. Such a sample would be produced when the pulsed valve was working poorly or when the sample backing pressure was increased from 200 torr (our normal operating pressure) to 800 torr. In the latter case, the density of gas in the skimmer region may have been so great that the expansion became turbulent, with the result that the molecules were not rotationally cooled. In part (b), a spectrum obtained under normal operating conditions is shown. As will be shown later, the "rotational temperature" of the H_2O molecules was reduced to ~ 50°K, and it is clear that their rotational state distribution has substantially collapsed. Whereas a rovibronic band is hundreds of cm^{-1} wide at room temperature, in our beam spectra the analogous "rotational envelope" is evidently only a few cm^{-1} in breadth. It should be noted that all the sharp features in both parts (a) and (b) are real and not noise. Also, in spite of the fact that the ionization thresholds cannot be rigorously identified, the threshold is seen to appear ~ 200 cm^{-1} higher for the cold molecules, as would be expected: They do not contain as much rotational energy which can contribute to ionization. A closer look at the threshold, obtained with even better signal-to-noise ratio, is provided in Fig. 3. Part (a) is a spectrum of room-temperature gas which was leaked into the chamber, so that its temperature was accurately known to be ~ 300°K. Part (b) is the analogous cold-molecule spectrum.

III. BACKGROUND INFORMATION

This section exists for the purpose of describing the pertinent details of the electronic spectroscopy of molecules with C_{2v} symmetry. It includes descriptions of some molecular orbitals, rotational selection rules for electric-dipole transitions, and nuclear spin statistics. All of these topics are involved in the analysis of our spectra.

In its ground state, water has C_{2v} symmetry. The molecule lies in a plane, a second plane bisects the molecule, and the intersection of the two planes is the C_2 axis. The symmetry operations are rotation about the C_2 axis and reflection through the two perpendicular planes. Even or odd behavior of a function upon rotation of the molecule by π about the C_2 axis is denoted by the letter a or b, respectively. The subscript 1 or 2 tells whether the function is even or odd with respect to reflection through the bisecting plane. In this notation, and in order of increasing energy, the ground state of water is described in the molecular orbital picture as $(1a_1)^2(2a_1)^2(1b_2)^2(3a_1)^2(1b_1)^2$. A zeroth-order breakdown into atomic orbitals connects the $1a_1$ and $2a_1$ orbitals with oxygen 1s and 2s electrons. The $1b_2$ and $3a_1$ orbitals come from hydrogen 1s electrons bonded with the oxygen $2p_y$ and $2p_z$ electrons in the molecular plane. Finally, the oxygen $2p_x$ lone pair, sticking out of the molecular plane, is the $1b_1$ orbital, which contributes little to bonding. The overall symmetry of the ground state is $^1A_1$.

The two outermost (highest-energy) orbitals are the ones excited in this experiment. Sketches of their oxygen 2p parents are given in Fig.

4(a). Ionization at threshold corresponds to removal of a $1b_1$ nonbonding electron. This causes the HOH angle to increase ~ 5° and the O-H bonds to lengthen ~ 0.04 Å. Removal of a $3a_1$ H-O-H bonding electron creates the ion's $\tilde{A}$ state, which is quasi-linear.

In the electric dipole approximation, the only forbidden transitions are $a_1 \leftrightarrow a_2$ and $b_1 \leftrightarrow b_2$. Since the molecule is not spherically symmetric, the orbital angular momentum ℓ is not a strictly "good" quantum number and the atomic $\Delta\ell = \pm 1$ selection rule is relaxed into more of a "propensity rule". Using this rule, we expect to see transitions of the $p \rightarrow s$ and $p \rightarrow d$ sorts from the $1b_1$ and $3a_1$ orbitals. s states automatically have a_1 symmetry, and there are d states of all four symmetries (a_1, a_2, b_1, b_2). For future reference, sketches of the d states optically accessible from the $1b_1$ (~ $2p_x$) orbital are shown in Fig. 4(b). When an electron is excited to a Rydberg state, the potential it moves in is nearly central, and the orbital angular momentum quantum number ℓ is sensibly employed. For example, the notation $(6da_1, v_1^+ = 1) \leftarrow 1b_1$ describes a transition to the d electron's $n = 6$ state with orbital symmetry a_1, and 1 quantum in the ion core's symmetric stretching (ν_1) vibration. Similarly, the notation $(3a_1)^{-1}$ 3d describes a state in which a $3a_1$ electron has been excited to a 3d state of unspecified symmetry.

Rotational selection rules are also important in determining the occurrence and location of lines in a spectrum. When considering rotational transitions, a reference frame is provided by the molecule's principal axes $\hat{a}$, $\hat{b}$, and $\hat{c}$ (Fig. 5), where $I_a < I_b < I_c$. In describing a rotational level, a state is designated as $J_{K_a K_c}$; in this notation, the total angular momentum J and its projections K_a and K_c on the $\hat{a}$ and

$\hat{c}$ axes are given. Since water does not have axial symmetry, K_a and K_c are not rigorously "good" quantum numbers, but for the purposes of this work we can ignore that fact: The strong optical transitions can be predicted with selection rules which treat K_a and K_c as true angular momentum projections. Different orientations of the transition dipole moment with respect to the molecule's $\hat{a}$, $\hat{b}$, and $\hat{c}$ axes lead to different selection rules for changes in K_a and K_c. In the usual notation, an $\hat{a}$-axis-oriented dipole moment gives "Type A" selection rules and rotational band structure, etc. The selection rules are derived by considering the parities of the wavefunctions of the various rotational states. Figure 5 gives an example of a "Type C" transition (the 1240 A $3pa_1 \leftarrow 1b_1$ band). It has the selection rule $\Delta K_a = \pm 1$. This type of transition causes a change in the rotation about the $\hat{a}$ axis, which is the axis of least moment of inertia (highest rotational constant). "Type A" ($\hat{a}$ axis dipole moment) transitions have $\Delta K_c = \pm 1$, and "Type B" ($\hat{b}$ axis dipole moment) have $\Delta K_a = \pm 1$, $\Delta K_c = \pm 1$. Figure 6 is an energy level diagram which shows the three types of transitions occurring from the 0_{oo} ground state. All three should be present in the $nd \leftarrow 1b_1$ manifold, and populate final states with different symmetries. The rotational band structures of the series should differ as well. Without analyzing the rotational band structure of a member of a series, it is not generally possible to determine its electronic origin frequency.

In order to explain the details of a rotationally-resolved spectrum of a molecule which contains identical nuclei, it is necessary to consider the effects of spin statistics. Since H_2O has two hydrogen atoms, it and H_2 have the same nuclear spin degeneracies. In H_2, even

rotational levels (even J) belong to one spin modification (para), and odd levels (odd J) to the other (ortho). This rule is determined by the requirement that the exhange of identical Fermions cause a sign change in the overall wave function. Nuclear exchange is simulated by an exchange of the spins and a rotation of the molecule by π. The para and ortho spin functions have odd and even exchange symmetry, respectively, and the rotational wave functions have $(-1)^J$ rotational symmetry. For the water molecule, the relevant axis about which the rotation (nuclear exchange) is defined is $\hat{b}$, the C_2 axis. If K_b were used in the notation for the rotational levels, it would be analogous to J in hydrogen. But it is necessary to express the nuclear exchange behavior in terms of K_a and K_c, the quantum numbers actually used. Because a rotation of π about $\hat{b}$ is the same as successive rotations of π about $\hat{a}$ and $\hat{c}$, $(-1)^{K_b} = (-1)^{K_a+K_c}$, and we simply keep track of the oddness or evenness of $(K_a + K_c)$.

When the rule is applied to water in its ground electronic state, para-H_2O has even $(K_a'' + K_c'')$ and a statistical weight of 1, and ortho-H_2O, with odd $(K_a'' + K_c'')$, has a weight of 3. D_2O, on the other hand, contains deuterons, which obey Bose statistics. It has weights of 2 in the even $(K_a'' + K_c'')$ states, and 1 in the odd $(K_a'' + K_c'')$ states.

We have just considered the ground state, which has A electronic symmetry. In other words, a C_2 $(\hat{b})$ rotation does not change the sign of the electronic wave function. When states with B electronic symmetry are involved, the $(K_a + K_c)$ even/odd rule is switched: para (weight 1) states have $(K_a + K_c)$ odd. In fact, the $(1b_1)^{-1}$ H_2O^+ ground state has B electronic symmetry. The excited states of neutral water can have either A or B electronic symmetry, depending the wave function

symmetry of the excited electron.

IV. RESULTS AND ANALYSIS

Photoionization spectra of H_2O and D_2O in the ~ 100K - 110K cm^{-1} (~ 990-900 A) region are shown in Fig. 7 and Fig. 8, respectively. In both spectra, the baseline represents zero ion signal, so that the cross sections of the sharp features can be reckoned with respect to those of the neighboring continua. As was mentioned in the Experimental section, our normalization technique did not allow us to measure the continuum intensities accurately. However, an experiment done by Eland and Berkowitz[31] did not have this problem. Their photoionization spectrum of room-temperature H_2O, obtained with a resolution of 0.14 A (~ 15 cm^{-1}), is shown in Fig. 9. This spectrum can in turn be compared with the quantitative spectrum of Katayama et al.,[2] whose resolution was ~ 0.5 A (~ 50 cm^{-1}). They obtained, for both H_2O and D_2O, a photoionization cross section of ~ 6×10^{-18} cm^2 in the plateau just above the IP, with a gradual rise to ~ 8×10^{-18} cm^2 at 900 A. (The baseline has been suppressed in the spectrum of Berkowitz.)

The gross features of Fig. 9 occur in Fig. 7 and correspondingly for D_2O in Fig. 8. They are a threshold at the beginning of a continuum and a number of rather intense features with ~ 1 A widths in the 970-910 A region. Our spread-out wavelength scale makes it rather difficult to see the modulations in the continuum intensity. The most important improvement visible in our spectra is the presence of very sharp peaks with ~ 5 cm^{-1} widths between the ionization threshold and ~ 104K cm^{-1}. As was mentioned earlier (Figs. 2 and 3), these

newly-observed sharp peaks are difficult to find in a spectrum of room-temperature gas.

The dips in the D_2O spectrum, marked with an asterisk (*) and appearing at ~ 106350 and ~ 109850 cm^{-1}, are artifacts. They were caused when the liquid nitrogen traps on the vacuum chamber's diffusion pumps were refilled. After many hours of running the experiment, the traps accumulated a layer of water and acetylene. Thermal stresses during the fill cycle caused bits of frozen matter to fall off the traps and into the hot oil in the diffusion pumps, causing a burst of gas to enter the chamber. An increased concentration of C_2H_2 with respect to D_2O would cause the $D_2O^+/C_2H_2^+$ ratio to decrease, as observed.

A. Rydberg Series Converging to $\tilde{X}$, $v_1^+ = 1$ of the Ion

(i) Expected Intensities and Missing nd Series

From photoelectron spectroscopy[11] and the thorough visible emission study of the ion[17] it is known that removal of a $1b_1$ (~ $2p_x$ non-bonding) electron has the effect of causing the ion to "open" and "stretch" slightly with respect to the neutral. The two geometries differ by displacements in the ν_1 and ν_2 normal coordinates. Consequently, if the photon energy is far enough above the IP, the ion can be left in the $v_1^+ = 1$ (symmetric stretching) state, or $v_2^+ = 1$ (bending) state. The photoelectron spectra determine the intensities of these channels to be 0.2 ± 0.04 and 0.1 ± .02, respectively, compared with the defined intensity of 1.0 of the $v_1^+ = v_2^+ = 0$ channel. The different channels are expected to have qualitatively similar absorption spectra. Just as the vibrationless channel gives a rather sharp ionization threshold followed by a continuum of nearly constant intensity for the direct ionization process, the channels with the ion

left vibrating should do likewise. Furthermore, the Rydberg series which converge to the higher thresholds include discrete states above the IP; molecules in these states can autoionize and be detected in our spectrum. Otherwise, if they predissociate into neutral products, they will not be detected. With some simplifying assumptions it is possible to sketch how the spectrum should look above the IP if the autoionization yield is 100%. These assumptions are: 1. All observed ionization is due to excitation of the $1b_1$ electron. 2. Within the small energy range we consider, the oscillator strength distribution $df/d\nu$ is constant for each vibrational channel. 3. Only one vibrational channel, the $v_1^+ = 1$ channel, is shown, and only one of the electric-dipole-allowed Rydberg series is shown. Figure 10 is the resulting picture. The heights and frequency spacings of the autoionizing peaks are assumed to have a $1/n^3$ dependence, which is typical of the members of a Rydberg series. According to the Thomas-Reiche-Kuhn sum rule, when several Rydberg series of different symmetries are present, the sum of their oscillator strengths should be continuous across the $v_1^+ = 1$ threshold.

We have detected a pair of Rydberg series in each of the H_2O and D_2O spectra. Their transition frequencies are listed in Table I; for each n, the lower-frequency transition is listed as "a", the higher-frequency one as "b". In the H_2O^+ spectrum, the n = 6 peaks are at 101861 and 101967 cm^{-1}. In the next pair of peaks, n = 7, at 102696 and 102773 cm^{-1}, the relative intensities of the peaks are different: the high-frequency one is weaker. This trend continues as far as the series can be followed, to n = 10 around 103900 cm^{-1}. (The n = 8 peaks are overlapped by other structure.) These series converge to ~ 105000

cm^{-1}.

In the D_2O^+ spectrum, the first clearly observed members of the series occur at n = 8, at 102525 and 102541 cm^{-1}. These series are well resolved until n = 11, around 103400 cm^{-1}. The n = 12 features are overlapped by a broad structure at 103520 cm^{-1}, and only the low-frequency n = 13 peak is observed, at 103635 cm^{-1}. Extrapolation of these series back to n = 7 predicts that features should appear at ~ 101990 cm^{-1}. Clearly, there is no lack of transitions in that neighborhood, but a striking resemblance to the $n \geq 8$ bands is not to be found. The convergence of these series is in the 104300 cm^{-1} region. In contrast with the series observed in the H_2O molecule, in these series, the low-frequency member has the greater intensity, because of the differing nuclear spin statistics in the two molecules.

Note that the series do not have the intensity predicted by the model of Fig. 10. Their total intensity should be, according to the known Franck-Condon factor, 20% of that of the continuum. The observed intensity is about ten times less, suggesting that predissociation is an important decay mechanism of Rydberg states.

We identify the observed series with d orbital upper states, in agreement with previous workers. Ishiguro et al.[7] have found peaks at 101864 cm^{-1} and 102712 cm^{-1} in the H_2O spectrum, and assigned them as being part of the $(nd; v_1^+ = 1) \leftarrow 1b_1$ Rydberg series, with n = 6 and 7, respectively. Mayhew[10] has found a peak at 101958 cm^{-1} and similarly assigned it as a $(6d; v_1^+ = 1) \leftarrow 1b_1$ feature. We consider these transition frequencies to be in reasonable agreement with ours. Theoretically, there are many Rydberg transitions from a $1b_1$ orbital; they include s, p, and d final states. But considering that the $1b_1$

orbital is similar to a $2p_x$ lone pair, it is very "atomic" in character. The $\Delta\ell \neq 0$ selection rule would eliminate the np series. Also, comparison of radial matrix elements for hydrogenic wave functions[32] shows that the 2p → nd series should be much stronger than the 2p → ns series. In the electric dipole approximation, four nd Rydberg series of three different symmetries are predicted: nd_{z^2} (a_1), $nd_{x^2-y^2}$ (a_1), nd_{xy} (a_2), and nd_{xz} (b_1). Sketches of the angular dependences of the orbital wave functions are given in Fig. 4(b). The relative intensities of the four series (in the vibrationless channel) have been calculated by Diercksen et al.[25] Their prediction is that all four series have nearly equal oscillator strengths; typical strengths for n = 6 are ~ 0.02. Since the Rydberg electron does not significantly influence the motion of the core, there is no reason that the relative absorption intensities of the four series should be significantly different in the $v^+ = 1$ state.

Now why are there only two series instead of four present in the ionization spectrum? Are some of the series rapidly predissociated? An answer to these questions must consider the dynamics of the vibrationally-excited Rydberg states. In order to see a Rydberg state in the photoionization spectrum, it is necessary that its autoionization rate be an appreciable fraction of its total decay rate. Rapid predissociation would diminish the autoionization probability. Applying the uncertainty principle to the ~ 5 cm^{-1} linewidths of the observed peaks, the autoionization rate cannot exceed ~ 10^{12}/sec. A ten times larger predissociation rate of 10^{13}/sec would make a Rydberg series difficult to observe. (This is ~ 10 vibrational periods.) On the other hand, the different series need not have the

same autoionization rates; if they had the same predissociation rates, the ones slowest to autoionize would be most weakly observed in our spectrum.

The calculation of autoionization and predissociation rates should probably be done with multichannel quantum defect theory (MQDT).[33] Since this is already challenging for a diatomic molecule, its application to triatomics has apparently not been performed. But we can hypothesize about the missing series in terms of the connection between symmetry and predissociation rate, which is qualitatively understood for the valence excitations.

Even though the words "valence" and "Rydberg" are used to describe excited states, in fact the two are always mixed to some extent. This is explicitly expressed, for example, with the notation $3sa_1/4a_1$, which indicates that the $3sa_1$ Rydberg orbital has a slight $4a_1$ valence component. The decay characteristics of the nd ← $1b_1$ Rydberg excitations (a_1, b_1, and a_2) are partly determined by the valence orbitals they are mixed with. Of the three symmetries, only a_1 has electron density in the molecular plane, and it should have the greatest propensity for dissociative behavior: $4a_1$ is the lowest unoccupied valence orbital, and is thought to be strongly antibonding.[3,19] This conclusion was reached on the basis of observed extremely broad absorption features and large dissociation yields. Even higher-lying orbitals with a_1 symmetry would also be slightly anti-bonding. We speculate that rapid predissociation has made the nda_1 series invisible to us. If the a_1 series were not observed, the b_1 and a_2 series would be left for a total of two series. Coincidentally, we have observed two series, but without detailed

rotational assignments, we cannot determine their symmetries. It is even possible that the two series are really one series with rotational structure.

(ii) Rotational Analysis of H_2O "6a" Feature

The peak we assigned as "6a" in the H_2O^+ spectrum has significant structure, which we observed with high signal-to-noise ratio. Figure 12 shows this region on an expanded scale. Before describing the rotational analysis, we note the presence of the peak which is marked with an arrow (↓) - 40 cm^{-1} to the red of the "6b" feature. The reason we do not assign it as "6a" is that its spacing from "6b" is too small to fit the pattern of the other members of the series.

In performing the rotational analysis, we calculated stick spectra by the following procedure. First, partition functions were calculated for H_2O at ~ 30°K and ~ 50°K. In doing this we remained cognizant of the fact that the two spin species (para and ortho) do not interconvert. Second, we calculated the fraction of the population in each $J''_{K''_a K''_c}$ state. Third, we calculated the rotational contributions to the rovibronic transition frequencies. Energy levels came from the electronic-ground-state tables of Flaud et al.[34] and the ionic-ground-state table of Lew.[17] A diagram of these levels for $J \leq 2$ is shown in Fig. 11. We used the asymmetric rotor rotational line strength tables of Cross, Hainer, and King, as reported by Townes.[35] Stick spectra were constructed for rotational bands of types A, B, and C, at temperatures of ~ 30°K and 50°K.

Some remarks about the thermal rotational state distribution are in order at this point. The most intense features in the stick spectra originate from the 0_{00} and 1_{01} states, which are the two lowest in

energy, and the only ones populated at extremely low temperatures. (It is assumed that nuclear spin relaxation is forbidden.) The $J'' = 1$ states are at 24, 37, and 42 cm^{-1}, on the order of kT. $J'' = 2$ states begin at ~ 70 cm^{-1} and extend to ~ 135 cm^{-1}. At 50°K, kT ~ 30 cm^{-1}, and only the lowest of the $J'' = 2$ states contribute to the spectrum. Crude calculations of expected spectra can in fact be done by including only the four $J'' = 0,1$ states 0_{00}, 1_{01}, 1_{11}, and 1_{10}. In the D_2O spectrum, and for the same "rotational temperature", more states would need to be included because the spacing between rotational levels is smaller.

Only the "6a" band showed a convincing resemblance to any of the spectra we calculated. The calculated type A ($\Delta K_c = \pm 1$) spectrum of a 50°K sample proved to have intense lines at almost all the right frequencies. Even so, the relative intensities of the lines in the stick spectrum did not agree with those in the experimental spectrum. The source of this problem is easily explained: the branching ratio between predissociation and autoionization depends on the final rotational state. In fact, studies with multiphoton ionization[22-24] have shown that the predissociation rate depends strongly on K_a', the rotation about the â axis. There is not yet a theoretical calculation of this effect. We have, rather arbitrarily, halved the intensities of the $K_a' = 1$ lines in the stick spectrum in order to improve its fit with the experimental spectrum. Original heights are shown with asterisks (*).

The â-oriented "Type A" transition causes a $1b_1$ ($2p_x$) electron to be excited into an a_2 state (see Fig. 4). This excited state cannot be occupied by an s electron, whose wave function must have a_1 symmetry,

or a p electron, whose states are of a_1, b_1, and b_2 symmetry. It must contain a d electron. Consequently, we call this the $nda_2 \leftarrow 2pb_1$ molecular analog of the atomic $d_{xy} \leftarrow p_x$ transition induced by a y-oriented ($\hat{a}$-axis) electric field. The excitation of the totally-symmetric (a_1) ν_1 vibration during the transition does not change the upper-state symmetry or our symmetry assignment.

Unfortunately, we have not been able to assign, nor did we see, clear rotational structure in any of the other Rydberg features. This is not surprising because the rotational bandshapes look very different in Rydberg states with large n. As the orbiting Rydberg electron is more highly excited, final states of different n become closer together in energy than the rotational level spacing. In this regime a change of basis is appropriate, in which the electronic energy assumes the rôle of a perturbation to the H_2O^+ core rotational energy. Electronic states with different n, ℓ, and orbital symmetry share the same core rotational state $N^+_{K_a^+K_c^+}$. The ordering in energy of the highly-excited Rydberg states is completely different than in the lower states. Line intensities and rotational bandshapes become drastically altered, so that it becomes impossible to identify a band as type A, B, or C.

This phenomenon has been observed in diatomics such as H_2 [36] and Na_2,[37] in which it has been known as "ℓ uncoupling", since the orbital angular momentum ℓ of the excited electron is no longer locked in space with respect to the ion core. The theory, experimentally confirmed for diatomics, apparently is not well developed for asymmetric rotors like H_2O, which have a nasty rotational energy level structure to begin with. Herzberg has shown that ℓ-uncoupling is nearly complete in H_2 by the time n = 10 for a p electron. In H_2O^+, the rotational constant A -

28 cm^{-1} is not very different from the H_2^+ B value of ~ 30 cm^{-1}. This similarity implies that our spectrum, even with its paucity of rotational features, probably includes the effects of ℓ-uncoupling because it includes states with n ~ 10. It would be useful to get data with even better signal-to-noise ratio to analyze with this in mind.

(iii) Convergence Limits and the Ionization Potential

Whenever a Rydberg series is observed, it is possible to find its convergence limit, which is the energy required to form an ion in a given rovibronic state. In both H_2O and D_2O, we have two series rotationally resolved; this situation has not presented itself in previous work on water, nor, to our knowledge, published work on any other polyatomic molecule. Congestion from the large number of thermally populated rotational levels in room-temperature samples has made it impossible to distinguish the a_1, a_2, and b_1 series and find their rotational band origins. We have a better chance to find accurate ionization potentials. In this work, the ion has $v_1^+ = 1$, or one quantum of symmetric-stretching motion. The vibrational frequency ν_1^+ is related to the IP's (all energies in cm^{-1}):

$$IP(v_1^+ = 1) = IP(v_1^+ = 0) + \nu_1^+. \qquad (1)$$

This equation is exact if the rotational state of the ion (i.e. the rotational energy) is the same in both the $v_1^+ = 0,1$ vibrational states.

Our ionization potentials should be checked for consistency with IP values obtained from other experiments. The ionization potentials have been gotten in three ways: the first, and least accurate, was by

observing the steps in the H_2O^+ photoionization yield spectrum (Fig. 10). Since the steps have ill-defined onsets, their positions are hard to determine exactly. The second method, photoelectron spectroscopy, gives bands (with rotational structure) at distinct energies corresponding to different ion vibrational states: IP($v_i^+ = 0$), IP($v_i^+ = 1$), ... The resolution obtainable with photoelectron spectroscopy is on the order of a few tenths of a meV, or tens of cm^{-1}. Band centers are determined to within a small fraction (a few cm^{-1}) of their widths if the bands are known to have symmetric intensity distributions (rotational structures). The low resolution, and calibration difficulties normally limit the accuracy of an IP determination to a few tens of cm^{-1}. In spite of that, a vibrational frequency, or the separation between IP's (photoelectron bands) can be determined much more accurately because it is not affected by a constant voltage offset (calibration error). Finally, the most accurate IP determination is done with optical spectroscopy by following a Rydberg series to high n values and calculating its convergence limit. If the rotational structure of each band is known and resolved, band origins can be determined extremely accurately, with available optical resolutions of better than 1 cm^{-1}. Calibration is normally not a problem.

In estimating the convergence limits of the "a" and "b" series (Table I), we have made the assumption that all the members within each series ought to be described by the same value of the quantum defect δ in the expression $E(n) = IP - Ry/(n - \delta)^2$. The values of δ and the $n = \infty$ convergence limits are listed in the Table. Our uncertainties in the IP's are due to ambiguities in the choice of the "best fits" and to the calibration uncertainty of $\pm$ 3 cm^{-1}. It is seen

that the ∞a and ∞b convergence limits are not coincident. This is not due to error or sloppiness, but to the fact that we have not yet accounted for the rotational energies of the initial state and ion core. In other words, it is time to consider the caveat which accompanied Eq. (1).

To do a proper job of finding the $v^+ = 1$ IP from the Rydberg series would require that we identify the initial rotational states $J''_{K_a''K_c''}$ and final core states $N^+_{K_a^+K_c^+}$ exactly. We are unable to do that because a rotational analysis has not been performed, but we <u>can</u> make tentative choices for each of the "a" and "b" series. First, we consider the observed intensities: the "a" series is the weaker one in H_2O^+, and the stronger one in D_2O^+. The different nuclear spin statistics in the two molecules are clearly implicated. Thus, H_2O^+ "a" and "b" series are associated with $J''_{K_a''K_c''}$ states of statistical weights 1 and 3, respectively. Conversely, the D_2O^+ "a" and "b" series get the weights 2 and 1. Second, since a single line is to be fit in each of the series members, only the initial and final states which cause the strongest autoionization signals should be included. This means that upper states with $K_a' \geq 1$ are rejected on the premise that they are predissociative. Also, lower states with small populations are ignored.

This leaves (in H_2O) the 0_{00} and 1_{01} initial states, which have the largest populations. After determining the strongest ionizing lines from both of them and ensuring that the selection rules for autoionization

are obeyed, a limited number of $N^+_{K_a^+K_c^+}$ choices will remain. Since the vibrational autoionization involves the totally- symmetric ν_1 mode, neutral and ionic states of the same electronic symmetry are coupled.

Also, with the ℓ-uncoupled Rydberg electron exerting no torque on the core, no core rotational transitions occur

In this case the autoionization selection rule is simple: no nuclear spin flips (para ↔ ortho conversions) or changes in core rotational quantum numbers occur.

Below the onset of ℓ uncoupling, the transition intensities can be estimated in the well-understood "coupled" basis. The 0_{00} level then has equally intense electric dipole transitions to the upper states 1_{01}, 1_{11}, and 1_{10}. Remembering the nuclear spin statistics, the initial state 0_{00} has para symmetry, as must $N^+_{K_a^+K_c^+}$. Thus, the choices on nuclear spin grounds include the ion states 1_{01} and 1_{10}. Only the first of these has $K_a' = 0$, one of our criteria.

We do not mean to imply that we were actually imposing angular momentum selection rules for the two separate excitation and autoionization processes

$$H_2O + h\omega \rightarrow \ell\text{-uncoupled Rydberg state } H_2O^*$$

$$\ell\text{-uncoupled Rydberg state } H_2O^* \rightarrow H_2O^+ + e^-.$$

More accurately, we made sure, by the use of the well-understood angular momentum basis (i.e. ignoring ℓ-uncoupling), that the overall process

$$H_2O\ (J''_{K''_aK''_c}) + h\omega \rightarrow H_2O^+\ (N^+_{K_a^+K_c^+}) + e^-$$

can give a plausible answer for $N^+_{K_a^+K_c^+}$, which determines the series convergence limit. The final states derived by this procedure have the

correct symmetries. Use of the incorrect (ℓ-coupled) basis could only cause an error in the relative intensities of the symmetry-allowed channels.

Based on the criteria above, it is expected that the 0_{00} ground state can contribute to the 1_{01} ionic state, 21 cm^{-1} above the ion's 0_{00} level. For the 1_{01} ground state, the procedure is the same. In the absence of ℓ-uncoupling, the transition to the 2_{02} level is the strongest. The 2_{02} state also meets the $K_a' = 0$ and nuclear-spin-allowed criteria. This means that the ionic rotational states associated with the "a" and "b" series are 1_{01} and 2_{02}, respectively.

Since the 1_{01} initial state for the "b" series is 24 cm^{-1} above the 0_{00} ground state, the extrapolated ∞b convergence limit has to be increased by 24 cm^{-1} to give the absolute final energy. Figure 13 is a diagram representing the energy levels involved. With all the rotational levels known, it is possible to predict the difference in observed extrapolated convergence limits (∞b-∞a). In the hypothetical scheme just used, this convergence-limit difference should be 17 cm^{-1} for H_2O. Our experimental value of 20 ± 7 cm^{-1} is in good agreement.

This same procedure may be followed for D_2O. All of the rotational constants and energies are roughly half their H_2O values because the deuterium atoms, the major source of the moments of inertia, are twice as massive as hydrogen atoms. The splitting between the ∞a and ∞b convergence limits is thus predicted to be ~ 9 cm^{-1}, in good agreement with our 10 ± 11 cm^{-1} result.

To find the $N^+ = 0$, $v_1^+ = 1$ IP's we subtract 21 cm^{-1}, the rotational energy in the H_2O^+ 1_{01} state, from the H_2O ∞a limit, and 11 cm^{-1} from

the D_2O ∞a limit. The results are 104982 ± 5 cm^{-1} for H_2O^+ ($v_1^+ = 1$) and 104289 ± 5 cm^{-1} for D_2O^+ ($v_1^+ = 1$). These values will be used in Eq. (1) to determine the IP of the $v_1^+ = 0$ channel.

Ionization potentials previously determined have not had the rotational correction taken into account, because the rotational lines have never been resolved in the Rydberg or photoelectron spectra. Asbrink and Rabalais[38] did, however, see an asymmetric bandshape in the $v_1^+ = 0$ photoelectron band, obtained with a room temperature sample. In spite of the fact that this band was ~ 400 cm^{-1} wide, they claimed to locate the rotationless origin (the IP) to within ± 8 cm^{-1}. Their assumption was that the rotational transition between neutral and ion must be "type C", because the initial neutral (A_1) and final ion (B_1) states are connected by a ĉ-oriented (b_1) dipole moment. They superimposed the stick spectrum calculated by Johns[4] for the genuine 1240-Å type C transition on their spectrum and attempted to align the origins. They did not explain why the different angular momentum and symmetry states of the liberated d electron could be ignored; the overall symmetry of the (ion + electron) final state is really a mixture of B_1 multiplied by b_1, a_1, and a_2. This gives not just type C, but type A, B, and C transitions as in Fig. 6. There does not appear to be any <u>a priori</u> reason that the "type C" channel has the bulk of the intensity.

Our own estimate of the ($v_1^+ = 0$, $N^+ = 0$) IP comes from subtracting ν_1^+ from the ($v_1^+ = 1$, $N^+ = 0$) IP, as in Eq. (1). Although our experiment did not find ν_1^+, the value obtained by taking the difference of the IP's from photoelectron spectroscopy should be reliable. Reutt et al.[13] have recently recorded photoelectron spectra of molecular beam

samples of H_2O and D_2O, with high signal-to-noise ratio and good calibration. Uncertainties in the ν_1^+ frequencies are quite small: ν_1^+ = 3205 ± 4 cm^{-1} for H_2O^+ and 2342 ± 4 cm^{-1} for D_2O^+. Upon subtraction of these frequencies from the (ν_1^+ = 1, N^+ = 0) convergence limits, the rotationless IP's are discovered: 101777 ± 7 cm^{-1} for H_2O and 101947 ± 7 cm^{-1} for D_2O. These values should be better than results of previous experiments, in which the rotational structure was not analyzed in detail. Previous findings, and our new results, are summarized in Table II.

B. Bands Associated with Excitation of a $3a_1$ Electron

(i) Change of Geometry, and Rovibronic Structure

Until now the concern has been the spectral structure due to excitation of an electron in the nonbonding $1b_1$ orbital, the highest-energy filled orbital. But there are also allowed transitions in the 900-1000 A range from the next highest filled orbital ($3a_1$), which involves an oxygen $2p_z$ electron. This orbital has appreciable electron density in the plane of the molecule, between the H atoms, and is important in H-O-H bonding. Removal of a $3a_1$ electron weakens the H-O-H bond and causes the ion to have a quasi-linear equilibrium structure. Similarly, the equilibrium geometry should be nearly linear in the Rydberg states of the $(3a_1)^{-1}$ manifold. Photoexcitation causes a sudden transition between the bent (neutral) and linear (ion) geometries, with the consequence that the ν_2 (bending) mode is highly excited. This is strikingly displayed in the $(3a_1)^{-1}$ band of a photoelectron spectrum; many different v_2^+ states are populated, and the most likely value of v_2^+ is about 8 for H_2O^+ and about 12 for D_2O^+. There is almost zero probability for the v_2^+ = 0 state to be created,

accounting for the lack of a sharp increase in the ionization yield as the wavelength is decreased to ~ 900 A, the location of the $(3a_1)^{-1}$, $v_2^+ = 0$ IP.

In an absorption spectrum, one expects transitions to $(3a_1)^{-1}$ Rydberg states, with states having large values of v_2^+ preferentially excited. In photoelectron spectra, the vertical transition to the v_2^+ ($n = \infty$) state with the highest Franck-Condon factor occurs around 118000 cm^{-1}. The $n = 3$ excitations should be seen $1Ry/(3)^2$ ~ 12000 cm^{-1} lower, at ~ 106000 cm^{-1} in absorption spectra. If autoionization efficiently competes with predissociation, these excitations above the $(1b_1)^{-1}$ IP should also be seen in photoionization spectra. Indeed they are; Katayama et al.[2] identified features in the absorption and ionization spectra due to bending vibrations. The most striking examples occur in our spectra at ~ 104.2K and 106.1K cm^{-1} in the H_2O^+ spectrum (Fig. 7), and ~ 106.6K, 107.3K, and 108.0K cm^{-1} in the D_2O^+ spectrum (Fig. 8). The H_2O^+ peaks occur at ~ 961 and 942 A in the spectrum of Eland and Berkowitz[31] (Fig. 9). There are other peaks seen in their spectrum but not prominently in ours, notably at ~ 952 A (~ 105.0K cm^{-1}), and they all tend to have amplitudes of 10-20% with respect to the continuum (≡ 100%). Also, they occupy 1-2 A (~ 100-200 cm^{-1}) in the room-temperature spectrum. In our spectra, the sharpest bands are only ~ 50 cm^{-1} wide overall and have about one or two times the intensity of the continuum at their peaks. We attribute this sharpening to a condensation of the rotational structure which occurs when a sample is cooled. Weak features at 104078 and 105994 cm^{-1} in the H_2O^+ spectrum (Fig. 7), which are marked with arrows, appear much stronger when the sample gas is warmer because of poor pulsed valve

performance. They must originate from rotational levels which are depopulated by cooling. When the bandwidth of a feature is dominated by lifetime broadening, this sharpening of the structure does not occur. Higher members of the H_2O ν_2 progression (coincidentally, vertically aligned in the figure), at ~ 108.1K and 110.0K cm^{-1} are quite broad and appear to be rather weak.

None of these bands has previously had a thorough rovibronic analysis. Katayama et al. obtained their absorption spectra with a resolution sufficient to find that the individual rotational lines were diffuse, being a few cm^{-1} in breadth. This caused the spectrum to appear congested, and rotational assignments were not performed. They listed of the frequencies of the strongest absorption lines, and their list includes most of the sharp transitions seen in our spectra. The transition frequencies we report agree with theirs to within 3 cm^{-1}, our calibration accuracy.

Some features in our H_2O^+ spectrum, for example, at ~ 104.2K cm^{-1} appear to be well-resolved and thus analyzable. Accepting the hypothesis that the three peaks in this band come from a linear ← bent transition, previous rotational analyses of other similar transitions in H_2O^+ [17] and NH_2 [14] can serve as examples for our own assignments. We succeeded in assigning rotational structure in some of the $(3a_1)^{-1}$ bending features.

The fact that the linear excited-state configuration has a doubly degenerate bending vibration changes the rotational selection rules because vibrational angular momentum is involved. The origin of the degeneracy is in the $1b_1$ and $3a_1$ ($2p_x$ and $2p_z$) orbitals, which become identical in the linear configuration. Then they are called $p\pi_u$

orbitals, and the ground state has Σ electronic symmetry, which correlates with the A_1 symmetry of the bent ground state. (The Greek letters identify the axial component of the electronic angular momentum.)

As shown in Fig. 11, in a linear state (like H_2O^+ $\tilde{A}$), the rotational energy levels within a vibronic (K) manifold are given by $BJ(J + 1)$, without regard for K_a and K_c. But for the purpose of listing transitions, it is convenient to retain these projection quantum numbers. Each J state ($J \geq K$) contains both para and ortho nuclear spin modifications, except for $J = 0$, which can have only the 0_{00} level, para in H_2O^+.

Transitions from the Σ (A_1) lower state to the Π upper state have the transition dipole moment perpendicular to the internuclear axis. The selection rule $\Delta\Lambda = 1$ is obeyed in this case.[39] The corresponding selection rule in the bent-molecule basis is $\Delta K_a = \pm 1$, $\Delta K_c = 0$; this would give rise to a "type C" band.

But when the vibrational angular momentum $\ell = v_2, v_2 - 2, v_2 - 4 \ldots -v_2$ is included, Λ and ℓ are not good quantum numbers because the electronic and vibrational angular momenta interact. The "vibronic" quantum number to use, $K = |\ell \pm \Lambda|$, is analogous to K_a in a bent molecule. The resulting electric dipole selection rule is $K = K_a'' \pm 1$. K is denoted with the capital Greek letters Σ, Π, Δ, Φ, etc. When $\Lambda = 1$, it is seen that even values of v_2 lead to even values of ℓ, odd values of K, and thus Π, Φ, ... states, while odd values of v_2 give Σ, Δ, ... states. Thus the type of vibronic structure observed in the spectrum alternates when v_2 goes from odd to even, etc.

The information just given is sufficient for rotationally analyzing

a band due to a single upper (K) state, as will be done here. But for historical completeness it is important to mention that the different vibronic (K) levels within a ν_2 band have a strong Renner-Teller splitting: The degenerate $p\pi_u$ orbitals, mixed by the interaction between vibrational and electronic angular momenta, are strongly nondegenerate in-plane $3a_1$ and out-of-plane $1b_1$ components when the molecule is bent. Then they are ~ 10,000 cm^{-1} different in energy, as manifested in the separation between the IP's $(1b_1)^{-1}$ and $(3a_1)^{-1}$. The different K states are differently perturbed by the vibronic interaction, whose strength is phenomenologically expressed as GK^2, with G ~ - 25 cm^{-1}. According to this relationship, the $\Sigma - \Delta$ (K = 0)/(K = 2) splitting of odd ν_2 levels is ~ 100 cm^{-1}, but the $\Pi - \Phi$ splitting of even ν_2 states is much larger, at ~ 200 cm^{-1}. When the K structure in a spectrum is not resolved, only the width of a ν_2 band can be discerned: the even ($\Pi - \Phi$) bands are "broad", and the odd ($\Sigma - \Delta$) bands are "sharp".

(ii) Rotational Analysis of the Π Bands

Our spectrum is comparatively easy to analyze because only a few transitions are observed, and those are well resolved. In fact, the "broad-sharp" alternation with ν_2 has become more of a "band-no band" alternation: bands coming from states with $K_a'' \neq 0$ (i.e. everything but the K = 1 Π bands) are severely weakened by the rotational cooling of the sample.

Our analysis applies to the bands at 104.2K and 106.1K cm^{-1} in the H_2O^+ spectrum (Fig. 7). Figure 14 illustrates the transitions that contribute to these bands and gives the resulting stick spectrum. The final state has Π ($K_a' = 1$) symmetry and the $\Delta K_a = \pm 1$ rule applies, as

described above. Initial states can have $K_a'' = 0,2$; the latter are negligibly populated. Thus only two states, 0_{00} and 1_{01}, contribute to the spectrum. The 0_{00} level is the source of an R branch transition to $J' = 1$, while the 1_{01} level has Q and R branch transitions to $J' = 1$ and 2, respectively. Three peaks are predicted and observed.

The molecule's geometry in the upper state influences the combination difference (peak splitting) R(1) - Q(1), which depends only on the excited-state moments of inertia. This difference is 4B, regardless of whether the upper state is linear, because the 2_{11} level's rotational energy is A + 4B + C, and the 1_{11} level's energy is A + C. B varies with the HOH apex angle, being smallest at 180°, when the moment of inertia is largest. Our simulation employed the $(3a_1)^{-1}$ ionic value B = 9 cm^{-1},[17] giving a predicted Q-R branch splitting of 36 cm^{-1}. Considering that the observed peaks are broad and that B varies with v_2, the observed splitting of 37 ± 1 cm^{-1} in both the 104.2K and 106.1K cm^{-1} bands is in good agreement. We can reasonably conclude that the upper states are Rydberg analogs of the quasi-linear $(3a_1)^{-1}$ ionic $\tilde{A}$ state. As discussed in subsection (i), the principal quantum number of the excited electron must be 3.

(iii) v_2 Numbering and 3d Energy Level

If the geometry and vibrational level spacings are the same in the n = 3 Rydberg state we have observed and in the ion's (n = ∞) $\tilde{A}$ state, our spectra should look like $(3a_1)^{-1}$ photoelectron spectra. The v_2 assignments in the latter could then be applied to our spectra. We did this by plotting the peaks observed in the optical (this work) and photoelectron spectra on separate pieces of paper and adjusting the $Ry/(3 - \delta)^2$ relative energy difference for a coincidence. The high

resolution photoelectron spectra of Reutt et al.[13] are excellent for this purpose. The various K (Σ, Π, Δ ...) components were not sharply resolved, but were reliably assigned after deconvolution of the spectra.

Such a method is not very reliable if only one isotopic species is employed, because the v_2 levels have rather uniform spacings and there are many energy offsets which give peak coincidences. But the electronic energy difference, which is $1Ry/(3 - \delta)^2$, should be the same for H_2O and D_2O. When data on both molecules, whose v_2 spacings are incommensurate, are forced to coincide simultaneously, there is a unique solution. Figure 15 illustrates the resulting situation. The splitting between the $n = 3$ and $n = \infty$ states should not depend much on differences in vibrational zero-point energies in the molecules, and this test is exceedingly reliable. We have assigned the Σ and Π bands according to their v_2 numbering, both in Tables IIIa and IIIb, and in Figs. 7 and 8. Also, we have computed the difference between each optical transition frequency and the corresponding ion energy level as determined from photoelectron spectroscopy. The result is that $\Delta E \approx 11900$ cm^{-1}, and the quantum defect $\delta \approx -.037$. This value of δ is consistent with that expected for a d electron which has slight overlap with the core. If the similarity in vibrational behavior is maintained even at the lowest v_2 levels ($v_2 = 1$), then the predicted energies of the 3d states there are ~ 99740 cm^{-1} for H_2O and ~ 99200 cm^{-1} for D_2O.

Previous authors have differed significantly on the v_2 numbering of the bands, and thus the energy of the $(3a_1)^{-1}$ $n = 3$ origin. Ishiguro et al.[7] proposed a numbering in which all v_2 values were increased by one unit with respect to ours. This caused their $n = 3 - n = \infty$ splittings to differ by ~ 200 cm^{-1} between H_2O and D_2O, whereas ours is

the same to within ~ 20 cm^{-1} for most bands. Evidently their decision concerning the oddness or evenness of the v_2 bands in the optical spectrum was incorrect; the numbering given for the photoelectron spectrum they employed[12] agrees with ours.[13] Wang et al.[3] proposed a v_2 numbering which differed by 4 units for H_2O and 7 units for D_2O. The photoelectron data they used[11] erred by one unit in v_2 for D_2O^+. Considering that the levels below $v_2 \sim 4$ have never been observed optically due to the poor Franck-Condon factors and congested spectral regions they occur in, such confusion is understandable.

By knowing the principal quantum number ($n = 3$) of this v_2 progression and the quantum defect ($\delta = -.037$), it is possible to predict where transitions to higher Rydberg states should be observed. For example, $n = 4$ v_2 levels should be 5165 cm^{-1} above their $n = 3$ counterparts. This predicts the $n = 4$, $v_2 = 6$ $^1\Pi$ band to appear near 109360 cm^{-1} in the H_2O spectrum. There is indeed some structure at that frequency, confirming the prediction. It is a good deal weaker than the $n = 3 \leftarrow n = 2$ transition, as would be expected if it were really due to the $n = 4$ state.

(iv) $(3a_1)^{-1}$ 3d Oscillator Strength

It is possible to estimate the oscillator strength of the $n = 3$ band which contains the v_2 progression just discussed. Since the continuum cross section is known,[2] it is possible to find the cross section under the peaks and use the relation[31]

$$f = 1.13 \times 10^{12} \int \sigma(\nu) d\nu,$$

where σ is in cm^2 and ν is in cm^{-1}. The cross section of the

photoionization continuum is ~ 10^{-17} cm^2; the H_2O peaks are twice as intense as the continuum, rather triangular, and ~ 40 cm^{-1} across. The total oscillator strength of all the peaks in the v_2 progression is a few times 10^{-3}. It is assumed that the autoionization yield is 100%; if not, the oscillator strength has been underestimated by the inverse of the actual ionization efficiency.

Diercksen et al.[25] calculated oscillator strengths for transitions from $3a_1$ to Rydberg states of all symmetries possible for s, p, and d electrons. They expressed the symmetries in the bent-molecule basis, as is appropriate when a "vertical" transition with no nulcear geometry change occurs. $3d \leftarrow 3a_1$ f values range from 0.004 for the b_1 series to 0.032 for the b_2 series. Our value of a few times 10^{-3} fits the former better. If the b_2 and a_1 symmetries contain states that are highly predissociative, only the b_1 series would occur in the spectrum.

In fact, another series of comparable strength is visible in the H_2O^+ spectrum: its peaks are labeled A, B, C, D, and E (Fig. 7). The "E" peak has a shape similar to a smoothed version of the 3d Π bands of $v_2 = 6,8$. The spacing between v_2 levels is smaller than for the progression just assigned. This might occur if the excited orbital were slightly antibonding, causing a smaller bending force constant, increased O-H bond length, and larger effective mass for the bending motion. The D_2O^+ spectrum has additional peaks as well, near the $n = 3$, $v_2 = 13$ Σ, $v_2 = 16$ Π, $v_2 = 15$ Σ, and $v_2 = 17$ Σ bands, as well as at ~ 105350, ~ 107500, and 108310 cm^{-1}. There does not seem to be a pattern in their locations or shapes which is easy to recognize.

(v) Dynamics

So far the issue of intramolecular dynamics has not been

considered. In our spectra, the information is in the form of peak heights, widths, and shapes. Peak heights can lead to determinations of branching ratios if total absorption cross sections are known. Also, widths help to determine homogeneous lifetimes. The H_2O highly-resolved $v_2 = 6,8$ Π bands show evidence of states with 0.5 psec lifetimes, as judged from 10 cm^{-1} homogeneous linewidths. Other peaks, "C" for example, are even broader; it is hard to tell exactly how broad individual lines are because the rotational structure is not resolved. 50 cm^{-1} is a plausible guess, making the lifetime ~ 0.1 psec.

Peak asymmetries are the result of interferences between interacting, optically-accessible channels such as autoionizing (discrete) and ionic (continuum) states. As described by Fano,[40] the fitting of lineshapes gives parameters which are simply interpreted in terms of interaction matrix elements. In a Fano profile, a peak in the ionization cross section is always adjacent to a dip, and the ratio of the peak height and dip depth is used to calculate the magnitude of the discrete state-continuum interaction. Dips are weak and hard to see when the interaction is slight.

A modest improvement in the signal-to-noise ratio of our H_2O^+ spectrum between 106000 and 106200 cm^{-1} would enable such a lineshape analysis of an isolated, autoionizing resonance. It would help to get the water sample colder so that only two initial states (0_{00} and 1_{01}) are significantly populated. This is certainly feasible. Then dips would be easier to detect because a dip, whose contribution comes from a single quantum-state population, would be less diluted by the continuum, which is due to all populations. A careful measurement of the photoionization and photodissociation spectra would give the

ionization-dissociation branching ratio, the lineshapes, and the chance to understand a great deal more about the excited states of water.

V. CONCLUSION

We have obtained and partially analyzed photoionization spectra of cold H_2O and D_2O molecules. Our resolution (~ 1 1/2 cm^{-1}) and signal-to-noise ratio were both about ten times better than those in previously reported spectra. This has allowed us to obtain new information about the all-important water molecule. Autoionizing Rydberg series converging to $v^+ = 1$ have been newly observed, and their convergence limits found. By using accurately known values for v^+, we have made improved estimates of the ionization potential. Also, a Rydberg state lifetime (for n ~ 7 - 10) of ~ 1 psec was deduced on the basis of observed linewidths. Several Rydberg series which were expected, did not appear, leading to the conclusion that they are predissociated.

Several rovibronic bands which are part of the $(3a_1)^{-1}$ manifold gave strong autoionization signals and were exposed much more cleanly than ever before, and some were rotationally analyzed. We have compared the energies of the autoionizing states with ionic energy levels determined by photoelectron spectroscopy. From this comparison, we have determined the assignments of v_2 and deduced the adiabatic ($v_2 = 1$) $(3a_1)^{-1}$ 3d energy level. Lifetimes in some of the v_2 levels appear to be ~ 0.5 psec. This information is useful in formulating theories about the electronic states responsible for the decays.

A really thorough understanding of the highly excited water molecule must be based on accurate data concerning all possible final

states. The ionic state is one which is obviously suitable for high-resolution work. Although work has already been done in analyzing the photodissociation spectra,[19] it would be useful to repeat the measurements with a molecular beam sample and higher resolution. This is a much more challenging endeavor than obtaining a photoionization spectrum because fluorescence detection is inherently inefficient with respect to ion detection. But with improvements in the molecular beam source, and large averaging times, it is certainly feasible. Then the missing Rydberg series, supposedly rapidly predissociated, should become visible, even above the IP. With them would come the chance to examine the intramolecular dynamics and their dependences on electronic, vibrational, and rotational state. If this were done it would probably not be long before multichannel quantum defect theory, currently used on diatomics, was stretched to fit triatomic molecules as well.

References

1. W. C. Price, J. Chem. Phys. 4, 147 (1936).

2. D. H. Katayama, R. E. Huffman, and C. L. O'Bryan, J. Chem. Phys. 59, 4309 (1973).

3. H.-t. Wang, W. S. Felps, and S. P. McGlynn, J. Chem. Phys. 67, 2614 (1977).

4. J. W. C. Johns, Can. J. Phys. 41, 209 (1963).

5. P. L. Smith, K. Yoshino, H. E. Griesinger, and J. H. Black, Astrophys. J. 250, 166 (1981).

6. S. Bell, J. Mol. Spectrosc. 16, 205 (1965).

7. E. Ishiguro, M. Sasanuma, H. Masuko, Y. Morioka, and M. Nakamura, J. Phys. B 11, 993 (1978).

8. P. Gürtler, V. Saile, and E. E. Koch, Chem. Phys. Lett. 51, 386 (1977).

9. J. P. Connerade, M. A. Baig, S. P. McGlynn, and W. R. S. Garton, J. Phys. B 13, L705 (1980).

10. C. A. Mayhew, Ph.D. Thesis, University of London, 1985.

11. K. Karlsson, L. Mattson, R. Jadrny, R. G. Albridge, S. Pinchas, T. Bergmark, and K. Siegbahn, J. Chem. Phys. 62, 4745 (1975).

12. R. N. Dixon, G. Duxbury, J. W. Rabalias, and L. Asbrink, Mol. Phys. 31, 423 (1976).

13. J. E. Reutt, L. S. Wang, Y. T. Lee, and D. A. Shirely, J. Chem. Phys. 85, 6928 (1986).

14. K. Dressler and D. A. Ramsay, Phil. Trans. Roy. Soc. London, Ser. A 251, 69 (1959).

15. J. A. Pople and H. C. Longuet-Higgins, Mol. Phys. 1, 372 (1958).

16. Ch. Jungen and A. J. Merer, in Molecular Spectroscopy: Modern

Research, K. N. Rao, ed., (Academic Press, New York, 1976), Ch. 3, Vol. 2.

17. H. Lew, Can. J. Phys. 54, 2028 (1976).

18. L. C. Lee and M. Suto, Chem. Phys. 110, 161 (1986).

19. O. Dutuit, A. Tabche-Fouhaile, I. Nenner, H. Frohlich, and P. M. Guyon, J. Chem. Phys. 83, 584 (1985).

20. G. N. Haddad and J. A. R. Samson, J. Chem. Phys. 84, 6623 (1986).

21. M. N. R. Ashfold, J. M. Bayley, and R. N. Dixon, J. Chem. Phys. 79, 4080 (1983).

22. M. N. R. Ashold, J. M. Bayley, and R. N. Dixon, Chem. Phys. 84, 35 (1984).

23. M. N. R. Ashold, J. M. Bayley, and R. N. Dixon, Can. J. Phys. 62, 1806 (1984).

24. G. Meijer, J. J. ter Meulen, P. Andresen, and A. Bath, J. Chem. Phys. 85, 6914 (1986).

25. G. H. F. Diercksen, W. P. Kraemer, T. N. Rescigno, C. F. Bender, B. V. McKoy, S. R. Langhoff, and P. W. Langhoff, J. Chem. Phys. 76, 1043 (1982).

26. C. T. Rettner, E. E. Marinero, R. N. Zare, and A. H. Kung, J. Phys. Chem. 88, 4459 (1984).

27. R. H. Page, R. J. Larkin, A. H. Kung, Y. R. Shen, and Y. T. Lee, to be published

28. K. Radler and J. Berkowitz, J. Opt. Soc. Am. 68, 1181 (1978).

29. J. R. Nestor, Appl. Opt. 21, 4154 (1982).

30. T. Hayaishi, S. Iwata, M. Sasanuma, E. Ishiguro, Y. Morioka, Y. Iida, and M. Nakamura, J. Phys. B 15, 79 (1982).

31. J. Berkowitz, Photoabsorption, Photoionization, and Photoelectron

Spectroscopy (Academic Press, New York, 1979).

32. E. U. Condon and G. H. Shortley, The Theory of Atomic Spectra (Cambridge Univ. Press, New York, 1959).

33. M. J. Seaton, Rep. Prog. Phys. 46, 167 (1983).

34. J. M. Flaud, C. Cany-Peyret, and J. P. Flaud, Mol. Phys. 32, 499 (1976).

35. C. H. Townes and A. L. Schawlow, Microwave Spectroscopy (McGraw-Hill, New York, 1955).

36. G. Herzberg and Ch. Jungen, J. Mol. Spectrosc. 41, 425 (1972).

37. S. Martin, J. Chevaleyre, M. Chr. Bordas, S. Valignat, M. Broyer, B. Cabaud, and A. Hoareau, J. Chem. Phys. 79, 4132 (1983).

38. L. Asbrink and J. W. Rabalais, Chem. Phys. Lett. 12, 182 (1971).

39. G. Herzberg, Molecular Spectra and Molecular Structure. III. Electronic Spectra of Polyatomic Molecules (Van Nostrand Reinhold, New York, 1966).

40. U. Fano, Phys. Rev. 124, 1866 (1961).

Table I. Rydberg series converging to H_2O^+, D_2O^+ ($\tilde{X}$, $v_1^+ = 1$).

H_2O			D_2O		
n	$\nu(cm^{-1})$	δ	n	$\nu(cm^{-1})$	δ
6a	101861	0.09	8a	102525	0.14
6b	101967	0.01	8b	102541	0.12
7a	102696	0.10	9a	102903	0.14
7b	102773	0.02	9b	102927	0.09
8a			10a	103171	0.14
8b	103306	0.01	10b	103185	0.12
9a	103616	0.11	11a	103375	0.11
9b	103660	0.03	11b	103405	-.01
10a	103886	0.09	12a		
10b	103926	0.00	12b		
			13a	103635	0.15
			13b		
∞a	105003	± 5	∞a	104300	± 5
∞b	105023	± 5	∞b	104310	± 10

Table II. Ionization potentials from various experiments.

(all values in cm^{-1})

Reference	H_2O		D_2O		Method
	$v_1^+ = 0$	$v_1^+ = 1$	$v_1^+ = 0$	$v_1^+ = 1$	
This work	101777 ± 7	104982 ± 5	101947 ± 7	104289 ± 5	series limit[a]
Karlsson et al.[11]	101746 ± 8	104989 ± 16	101891 ± 8	104255 ± 8	PES[b]
Reutt et al.[13]	101805 ± 30	105010 ± 30	101944 ± 30	104286 ± 30	MBPES[c]
Gurtler et al.[8]	101720		101930		absorption; series limit
Ishiguro et al.[7]	101770		101930		absorption; series limit
Mayhew[10]	101740 ± 10		101910 ± 10		absorption; series limit

[a]extrapolated to ($v_1^+ = 1$, $N^+ = 0$)
[b]photoelectron spectroscopy
[c]molecular beam photoelectron spectroscopy

Table IIIa. Features due to H_2O $3d \leftarrow 3a_1$ transitions, and corresponding ion vibrational levels.

v_2	$\nu(cm^{-1})$	assignment	$\nu^+(cm^{-1})$	$\nu^+ - \nu(cm^{-1})$
4	102330	Π Q(1)		
	102360[a]	Π R(0),R(1)	114237 ± 30	11877
5	103250[a]	Σ	115130	11880
6	104078[b]			
	104172	Π Q(1)		
	104198	Π R(0)	116069	11871
	104209	Π R(1)		
7	105030[a]	Σ	117066	12036
8	105994[b]			
	106081	Π Q(1)		
	106106	Π R(0)	118077	11971
	106118	Π R(1)		
9	107082	Σ	118998	11916
10	108070[c]	Π	119974	11904
11	109080[c]	Σ	120990	11910
12	110020[c]	Π	122033	12013

a: uncertain; overlapping structure
b: "warm" feature
c: broad

Table IIIb. Features due to D_2O $3d \leftarrow 3a_1$ transitions, and corresponding ion vibrational levels.

v_2	$\nu(cm^{-1})$	assignment	$\nu^+(cm^{-1})$	$\nu^+ - \nu(cm^{-1})$
9	104440	Σ	116330	11890
10	105157	Π	117054	11897
11	105862	Σ	117756	11894
12	106582	Π	118487	11905
13	107298	Σ	119196	11898
14	108030	Π	119956	11926
15	108769	Σ	120653	11884
16	109562	Π	121440	11878
17	110267	Σ	122147	11880

Figure Captions

Fig. 1 XUV generation-photoionization apparatus. A supersonic beam of water seeded in neon is delivered via a pulsed valve and skimmer. The beam passes through a set of ion extraction optics. XUV light is generated by frequency tripling in a pulsed jet of xenon or argon. This light ionizes the water molecules in the supersonic beam. Ions are extracted through a mass filter, and counted. Walls which separate differentially-pumped regions are not shown, except for the sleeve and cone which direct the tripling gas into a cryopump.

Fig. 2 Photoionization spectra obtained with different sample temperatures. (a) "Warm" sample obtained by using too high a nozzle stagnation pressure. (b) "Cold" sample (normal operating conditions). Rotational temperature is ~ 50°k.

Fig. 3 Photoionization spectra of H_2O^+ near threshold obtained with (a) room temperature gas and (b) the supersonic beam.

Fig. 4 (a) H_2O molecular orbitals derived from oxygen 2p electrons. (b) d orbitals which can be populated in optical transitions from the $1b_1$ (~ $2p_x$) orbital.

Fig. 5 (a) Principal axes ($\hat{a}$, $\hat{b}$, and $\hat{c}$) in H_2O. The "type" of rotational transition is determined by the axis along which the transition dipole points. (b) A type "C" transition, in this case involving orbitals of symmetry a_1 and b_1 (shown). The $1b_1$ orbital is aligned with the $\hat{c}$ axis. In this transition, the rotational selection rule is $\Delta K_a = \pm 1$.

Fig. 6 Final-state symmetries and energy levels populated by different types of rotational transitions with the 0_{00} level

as the lower (initial) state. The rotational transitions accompany the nd ← $2pb_1$ electronic transition.

Fig. 7 Photoionization spectrum of H_2O^+. Members of "a" and "b" Rydberg series converging to $v^+ = 1$ are denoted with their principal quantum numbers. Autoionization features from $(3a_1)^{-1}$ 3d states with ν_2 excited are labeled with their ν_2 quantum numbers and the vibronic symmetries of the upper states. Letters A, B, ... identify an unassigned ν_2 progression.

Fig. 8 As in Fig. 6, but for D_2O. Asterisks (*) indicate artifacts in the spectrum. See text for details.

Fig. 9 Photoionization spectrum of H_2O^+ at room temperature, obtained by Eland and Berkowitz with 0.14 A (~ 15 cm^{-1}) resolution. The intensity scale is the same in both parts of the spectrum, but the baseline has been suppressed in the second portion. The cross section of the ionization continuum varies from ~ 6 × 10^{-18} cm^2 near threshold to ~ 8 × 10^{-18} cm^2 at 900 A.

Fig. 10 Sketch of the appearance of a single autoionizing Rydberg series, with unit ionization yield. In this case the ratio of the intensity of the autoionizing series converging to $v^+ = 1$ to the continuum, is just the ratio of the $v^+ = 1$ and $v^+ = 0$ Franck-Condon factors, assumed to be 0.2 here.

Fig. 11 Rotational energy levels in ground-state H_2O, and the ground and first excited states of H_2O^+. Electronic spin splittings are ignored in the H_2O^+ levels. H_2O levels were taken from Flaud et al.;[34] H_2O^+ $\tilde{X}$ levels are from Lew;[17] and H_2O^+ $\tilde{A}$ energies were calculated with the rotational constant B = 9

cm^{-1}. Nuclear spin labels appropriate for H_2O are shown; the para modification has degeneracy 1, and the ortho modification has degeneracy 3. At 50°K, kT ~ 30 cm^{-1}, and the H_2O $\tilde{X}$ state has most of its population in J = 0,1 levels.

Fig. 12 Detail of n = 6, v_1 = 1 H_2O Rydberg state spectrum, and stick spectrum calculated with type A selection rules. Intensities of $K_a' = 1$ sticks have been halved; their original heights are shown with asterisks (*). The downward arrow (↓) marks an unassigned transition.

Fig. 13 Energy level diagram showing how ∞a and ∞b extrapolated $v^+ = 1$ convergence limits are corrected for ground- and excited-state rotational energy offsets. The $v^+ = 1$, $N^+ = 0$ IP is thus determined. It can be used to find the $v^+ = 0$ IP if ν^+ is known.

Fig. 14 (a) Energy level diagram of states contributing to Π upper state in a linear ↔ bent transition. Realistic ground- and excited-state rotational constants have been used. (b) Resulting stick spectrum. Splittings are in excellent agreement with observations.

Fig. 15 v_2 levels in $(3a_1)^{-1}$ ionic and $(3a_1)^{-1}$ 3d neutral states of H_2O and D_2O. The separation between homologous v_2 levels in the neutral molecule and its ion is independent of isotopic substitution and v_2 level. There is a unique value of $\Delta E = Ry/(3-\delta)^2$ which provides a simultaneous fit to the levels of both isotopomers. ΔE and δ are thus determined. With the v_2 numbering known in the ion's levels, it is determined in the neutral's as well.

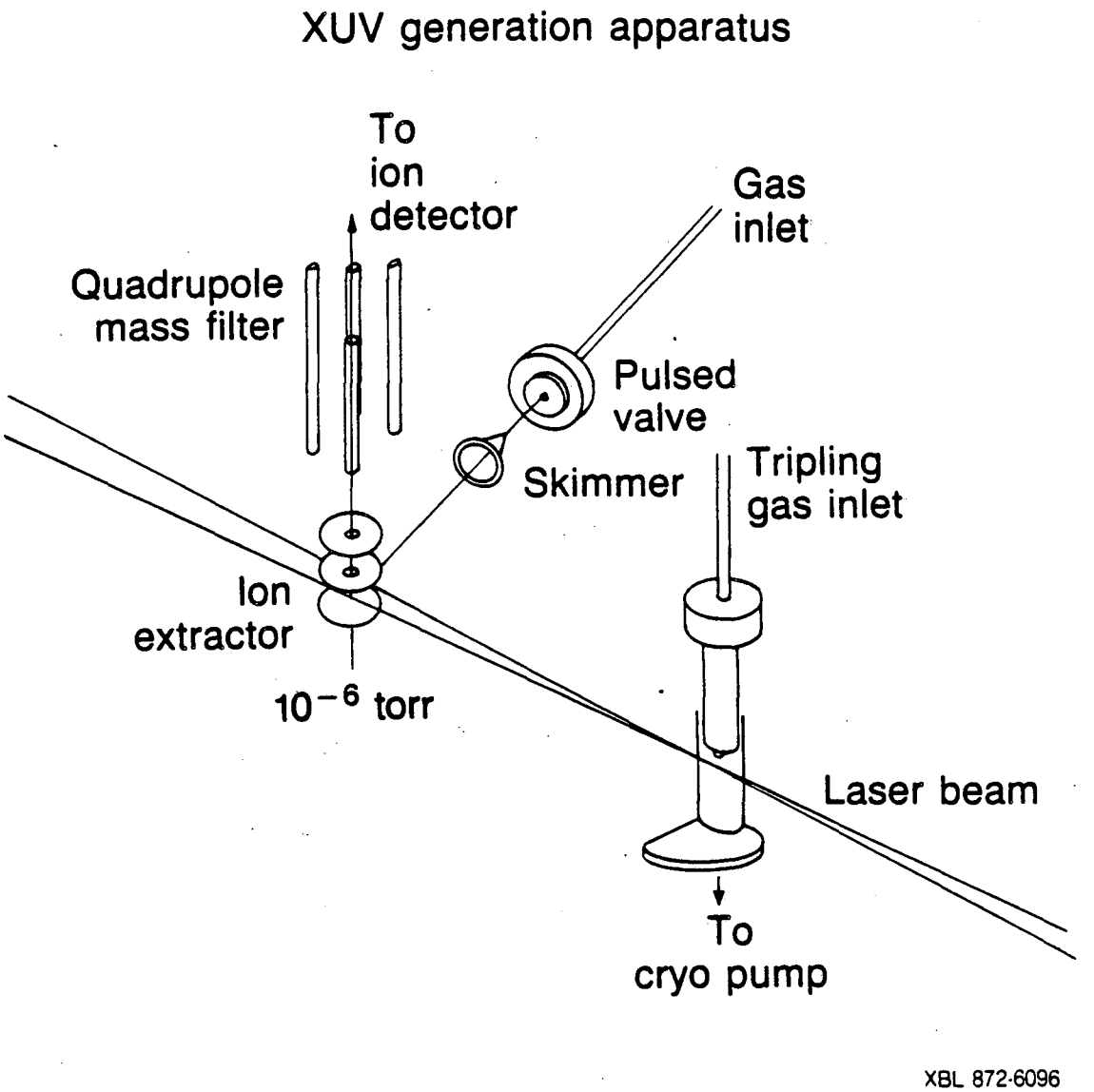
XUV generation apparatus
To
ion
detector
Gas
inlet
Quadrupole
mass filter
Pulsed
valve
Skimmer
Tripling
gas inlet
Ion
extractor
10^{-6} torr
Laser beam
To
cryo pump
XBL 872-6096

Figure 1.

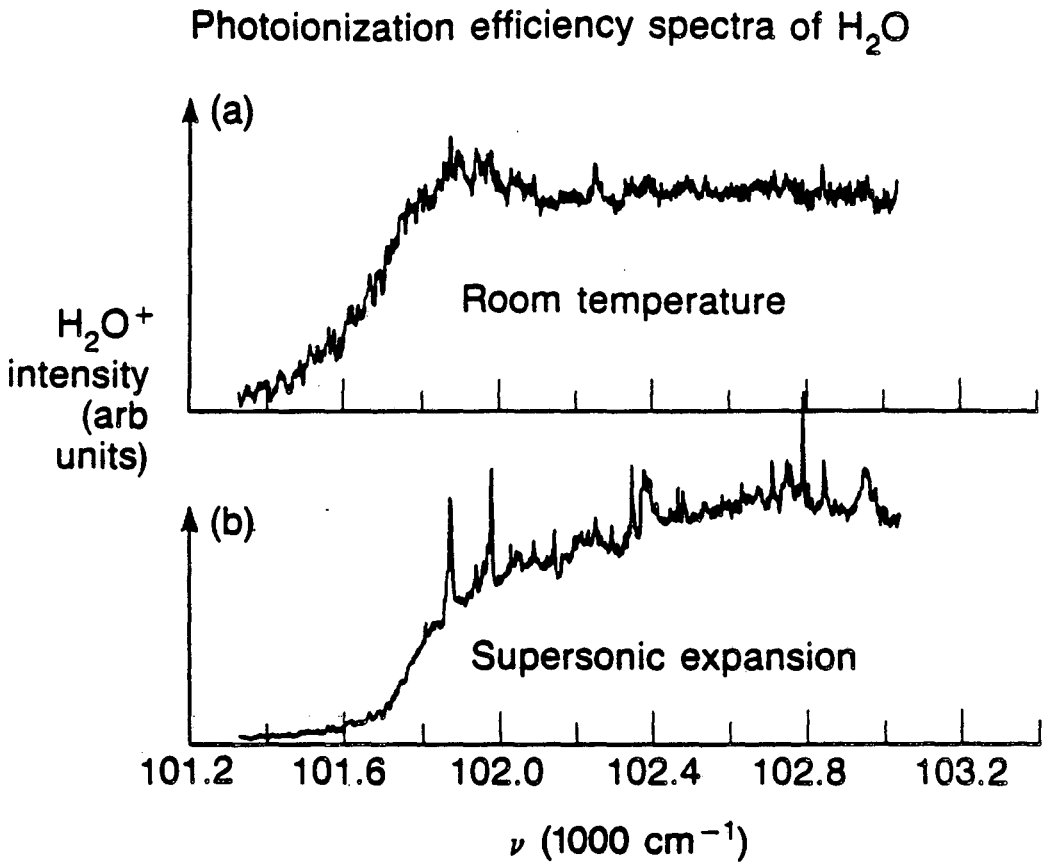
Photoionization efficiency spectra of H_2O
(a)
Room temperature
H_2O^+ intensity (arb units)
(b)
Supersonic expansion
101.2
101.6
102.0
102.4
102.8
103.2
ν (1000 cm^{-1})
XBL 872-6151

Figure 2.

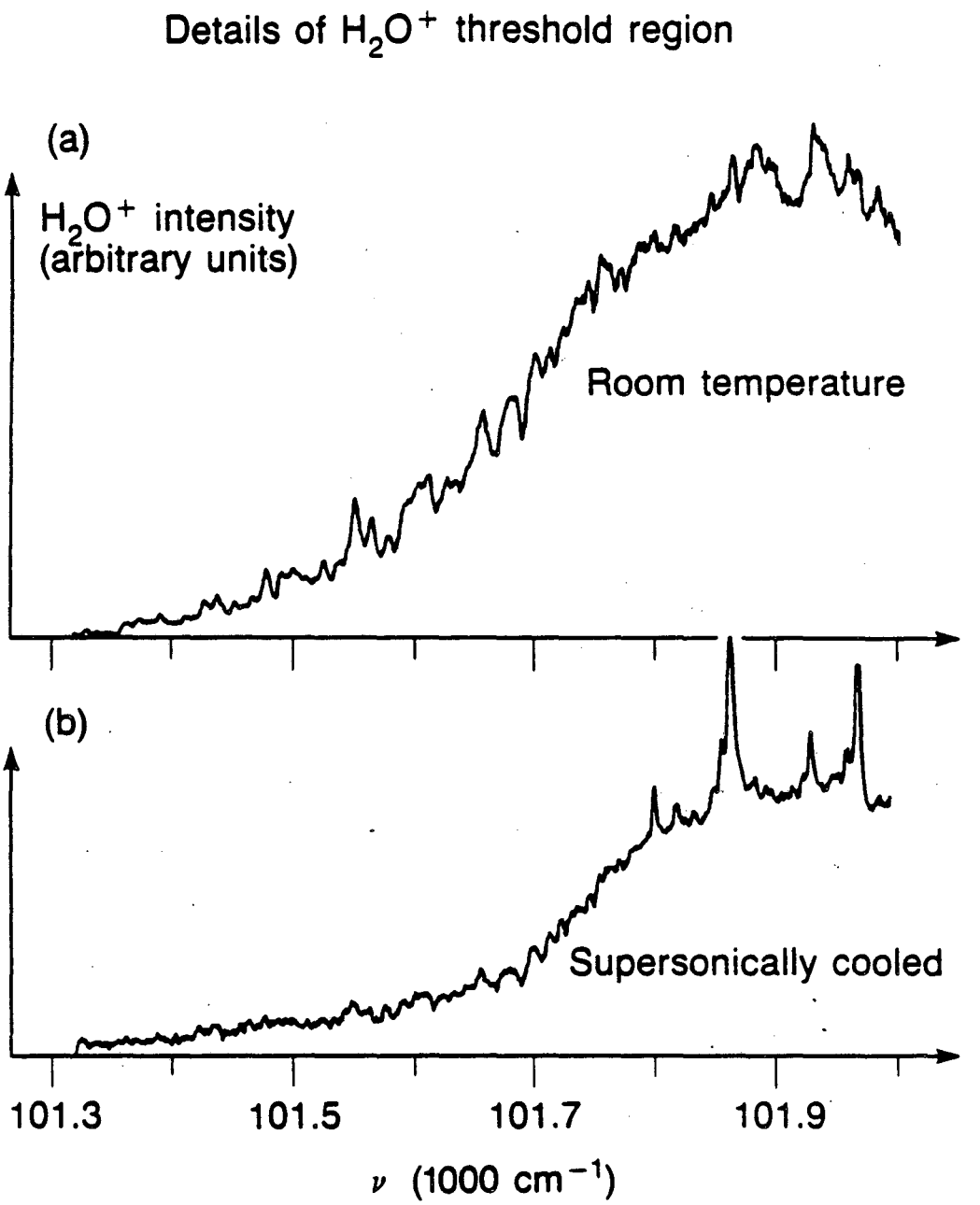

XBL 872-6127

Figure 3.

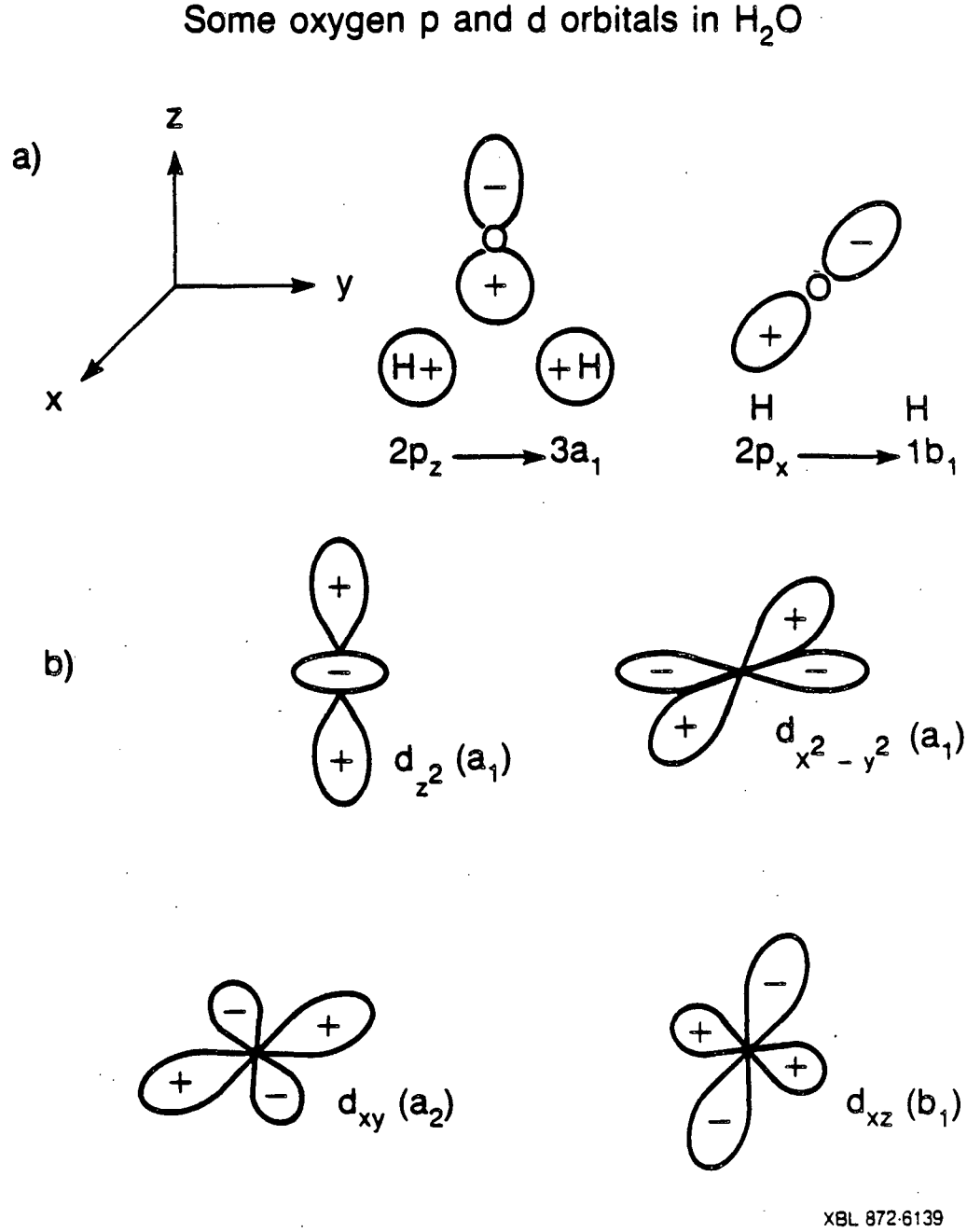
Some oxygen p and d orbitals in H_2O
a)
z
y
x
H+
+H
$2p_z \longrightarrow 3a_1$
H
H
$2p_x \longrightarrow 1b_1$
b)
d_{z^2} (a_1)
$d_{x^2-y^2}$ (a_1)
d_{xy} (a_2)
d_{xz} (b_1)
XBL 872-6139

Figure 4.

Example of a "Type C" transition

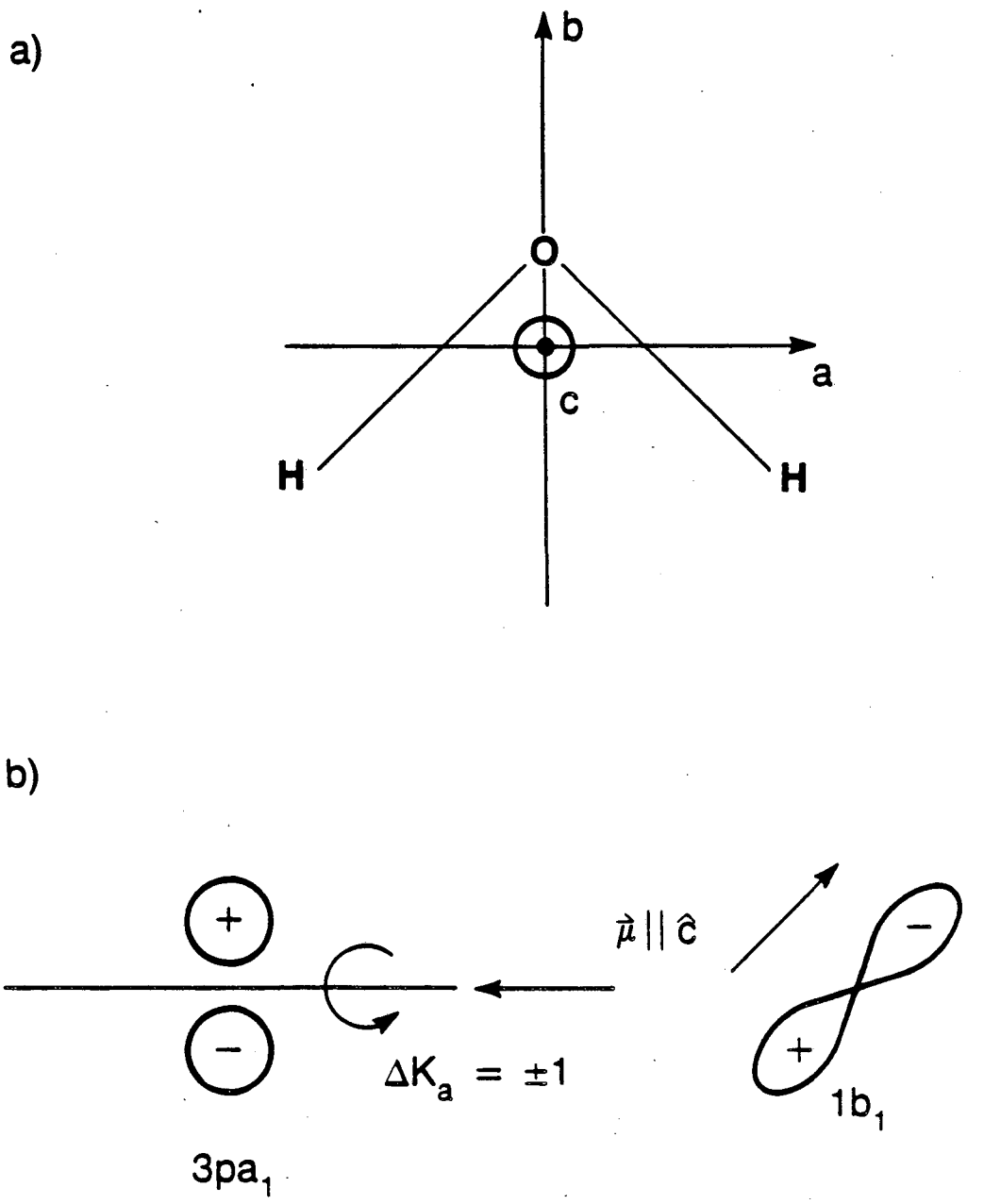

XBL 872-6138

Figure 5.

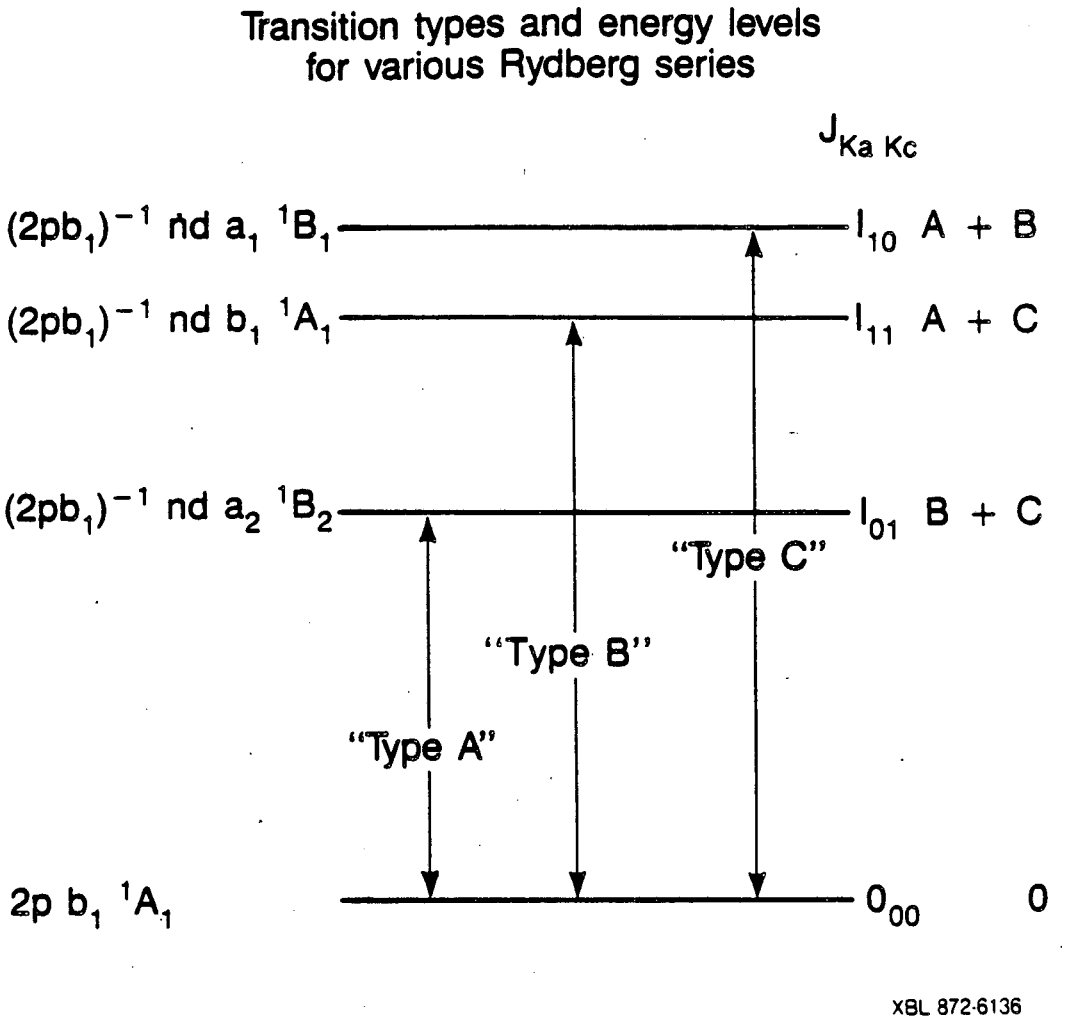
Transition types and energy levels
for various Rydberg series
$J_{Ka\ Kc}$
$(2pb_1)^{-1}$ nd a_1 $^1B_1$
I_{10} A + B
$(2pb_1)^{-1}$ nd b_1 $^1A_1$
I_{11} A + C
$(2pb_1)^{-1}$ nd a_2 $^1B_2$
I_{01} B + C
"Type C"
"Type B"
"Type A"
2p b_1 $^1A_1$
0_{00}
0
XBL 872-6136

Figure 6.

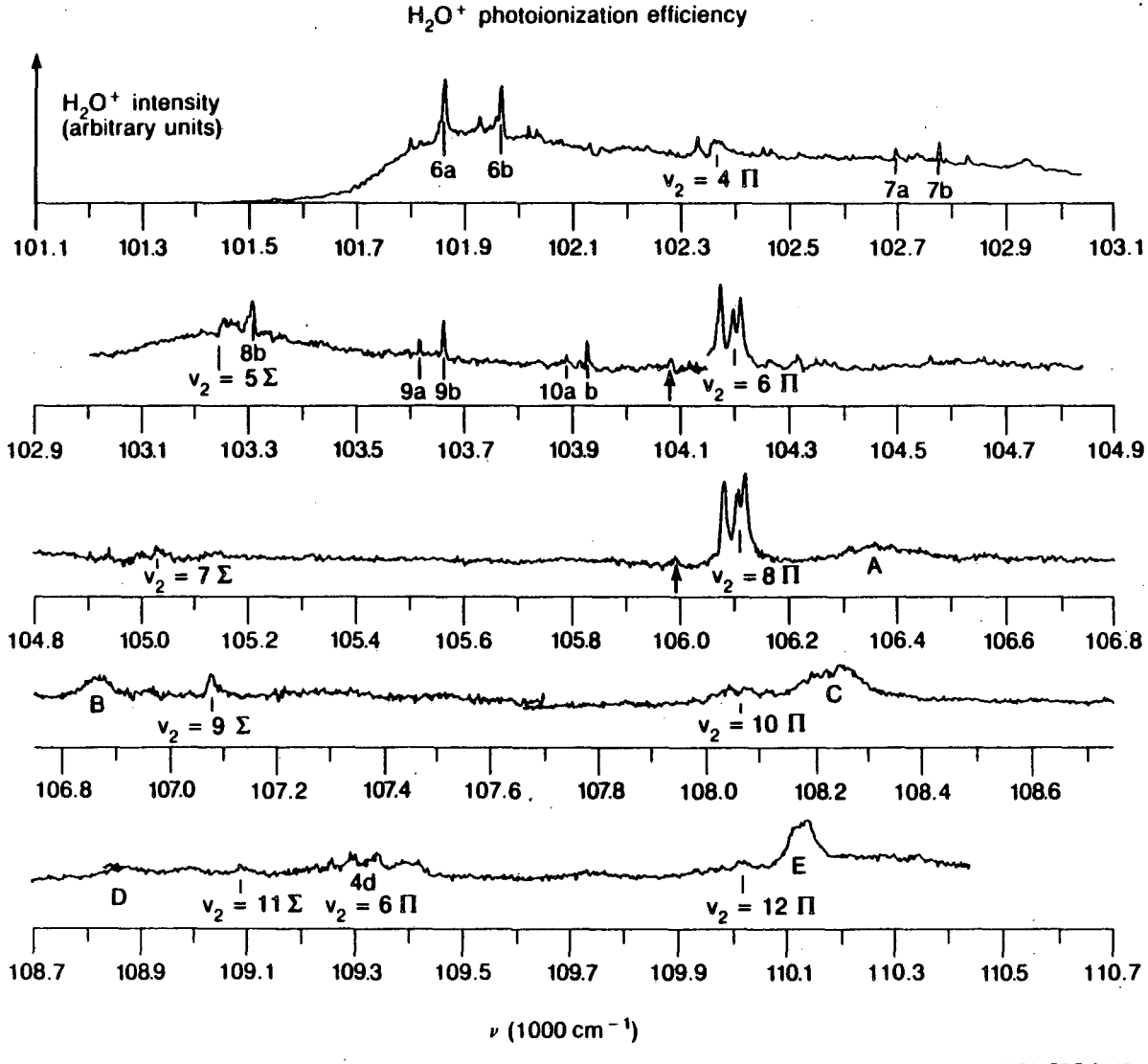
H_2O^+ photoionization efficiency
H_2O^+ intensity (arbitrary units)
6a
6b
$v_2 = 4\ \Pi$
7a
7b
101.1
101.3
101.5
101.7
101.9
102.1
102.3
102.5
102.7
102.9
103.1
8b
$v_2 = 5\ \Sigma$
9a 9b
10a b
$v_2 = 6\ \Pi$
102.9
103.1
103.3
103.5
103.7
103.9
104.1
104.3
104.5
104.7
104.9
$v_2 = 7\ \Sigma$
$v_2 = 8\ \Pi$
A
104.8
105.0
105.2
105.4
105.6
105.8
106.0
106.2
106.4
106.6
106.8
B
$v_2 = 9\ \Sigma$
C
$v_2 = 10\ \Pi$
106.8
107.0
107.2
107.4
107.6
107.8
108.0
108.2
108.4
108.6
D
4d
$v_2 = 11\ \Sigma$
$v_2 = 6\ \Pi$
E
$v_2 = 12\ \Pi$
108.7
108.9
109.1
109.3
109.5
109.7
109.9
110.1
110.3
110.5
110.7
ν (1000 cm^{-1})
XBL 872-6148

Figure 7.

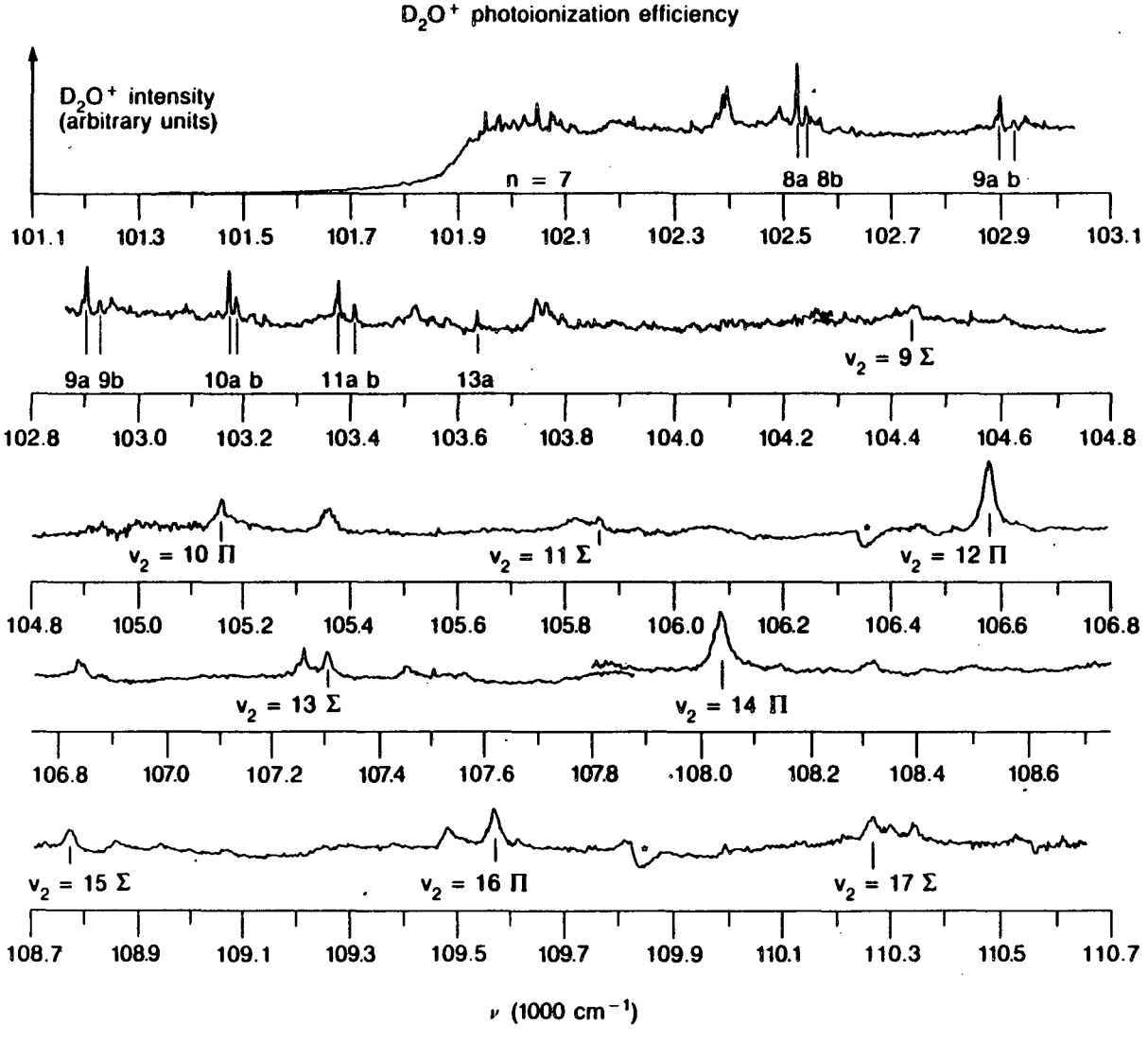

XBL-872-6140

Figure 8.

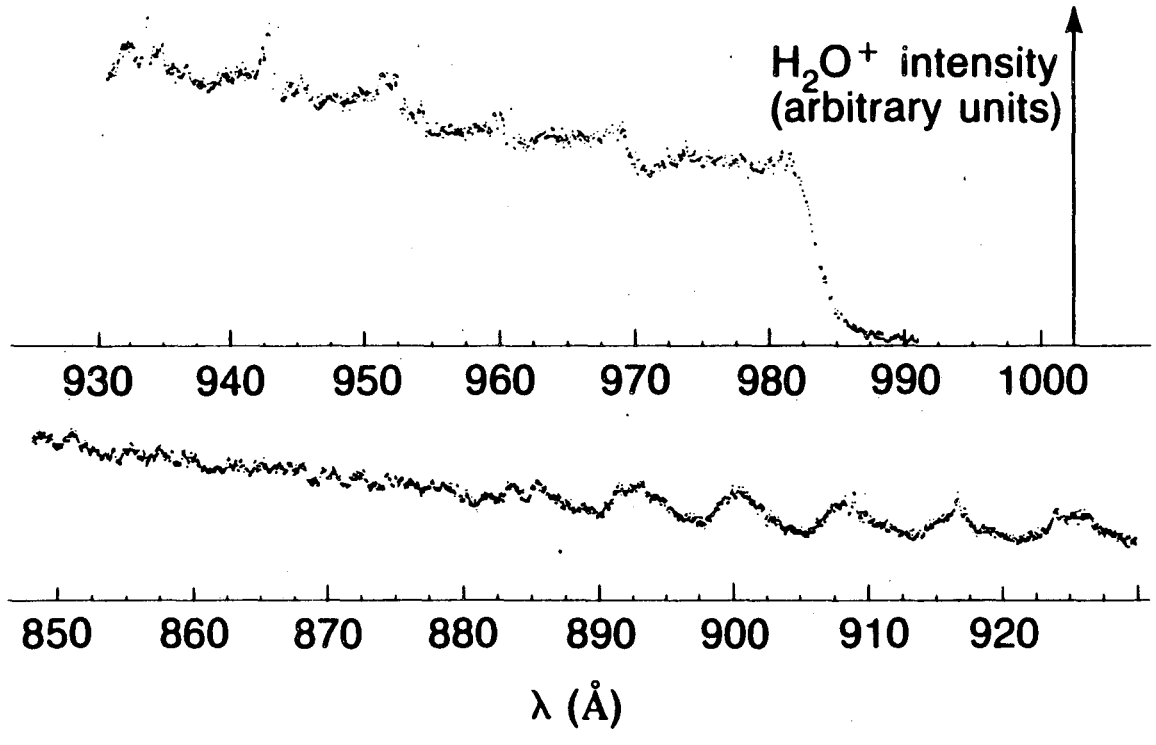

XBL 872-6125

Figure 9.

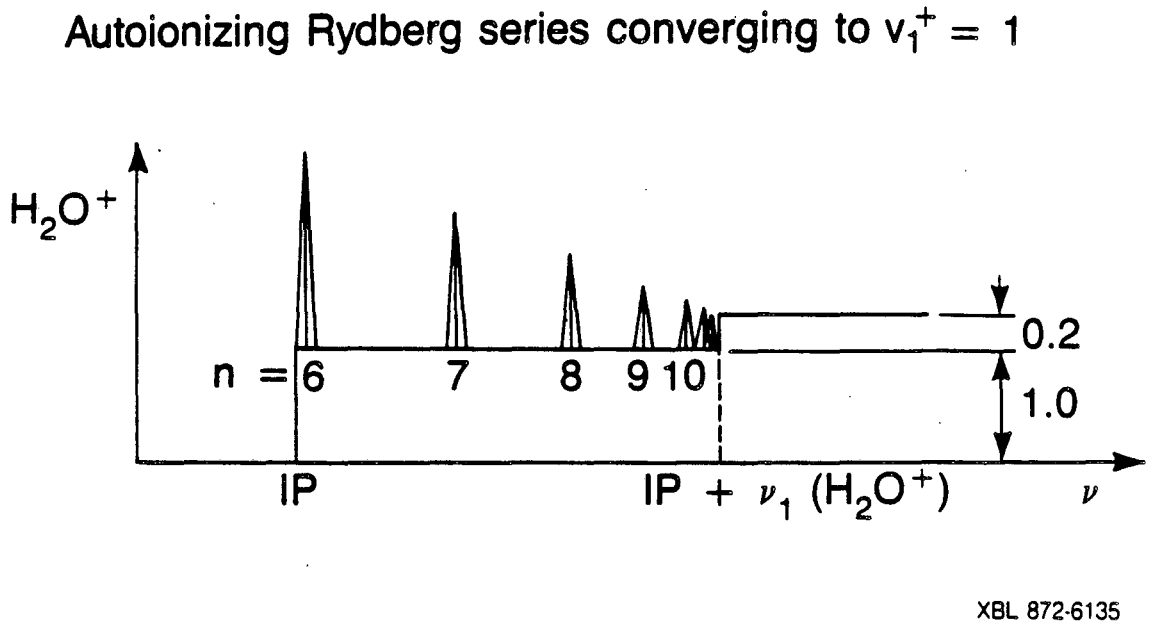
Autoionizing Rydberg series converging to $v_1^+ = 1$
H_2O^+
n = 6
7
8
9 10
0.2
1.0
IP
IP + ν_1 (H_2O^+)
ν
XBL 872-6135

Figure 10.

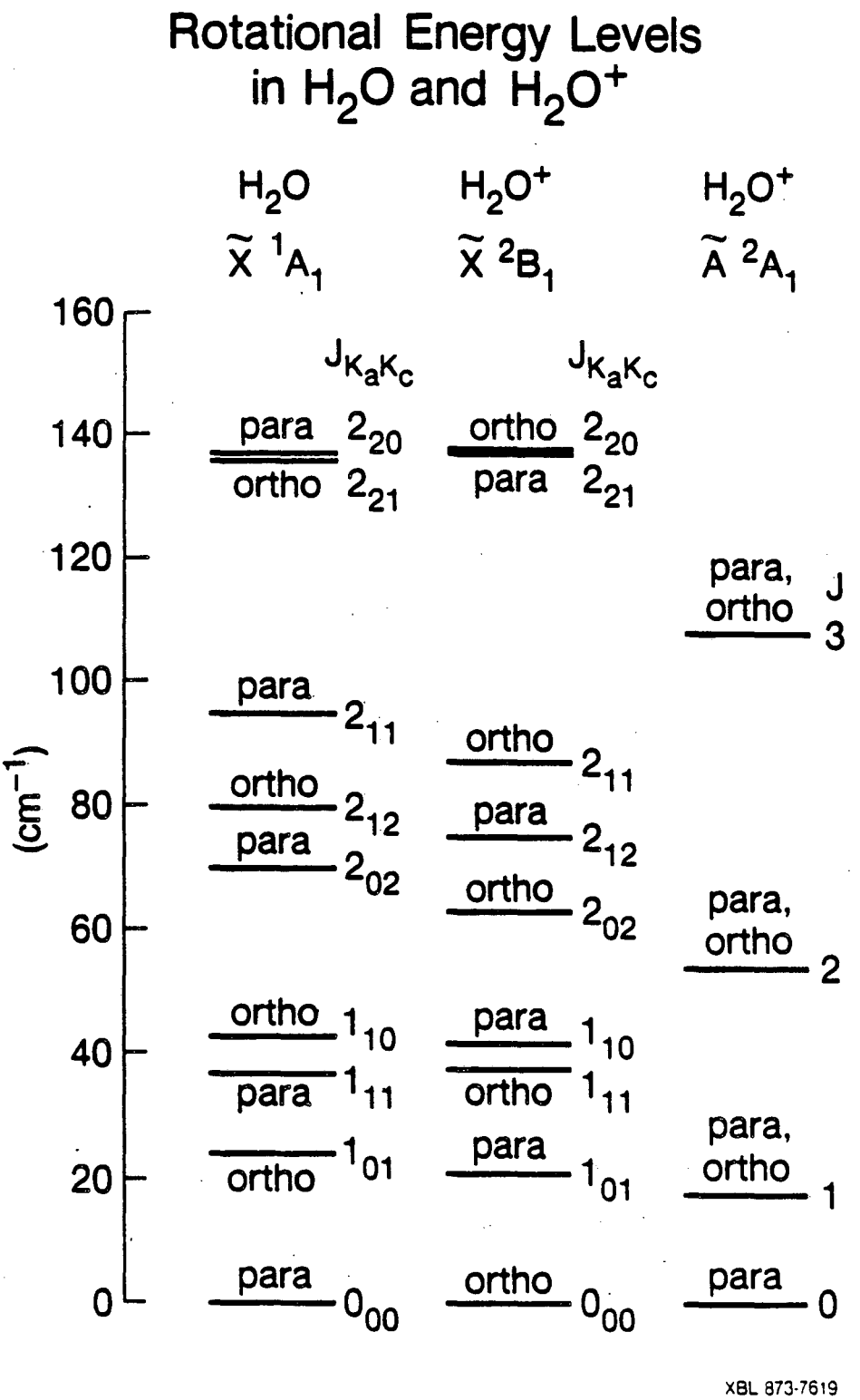
Rotational Energy Levels
in H_2O and H_2O^+
H_2O
$\tilde{X}\ ^1A_1$
H_2O^+
$\tilde{X}\ ^2B_1$
H_2O^+
$\tilde{A}\ ^2A_1$
$J_{K_aK_c}$
$J_{K_aK_c}$
160
140
120
100
80
60
40
20
0
(cm^{-1})
para 2_{20}
ortho 2_{21}
ortho 2_{20}
para 2_{21}
para, ortho J
3
para 2_{11}
ortho 2_{12}
para 2_{02}
ortho 2_{11}
para 2_{12}
ortho 2_{02}
para, ortho
2
ortho 1_{10}
para 1_{11}
para 1_{10}
ortho 1_{11}
para 1_{01}
ortho 1_{01}
para, ortho
1
para 0_{00}
ortho 0_{00}
para
0
XBL 873-7619

Figure 11.

Comparison of Experimental Spectrum With Stick Spectrum of a Type A Band

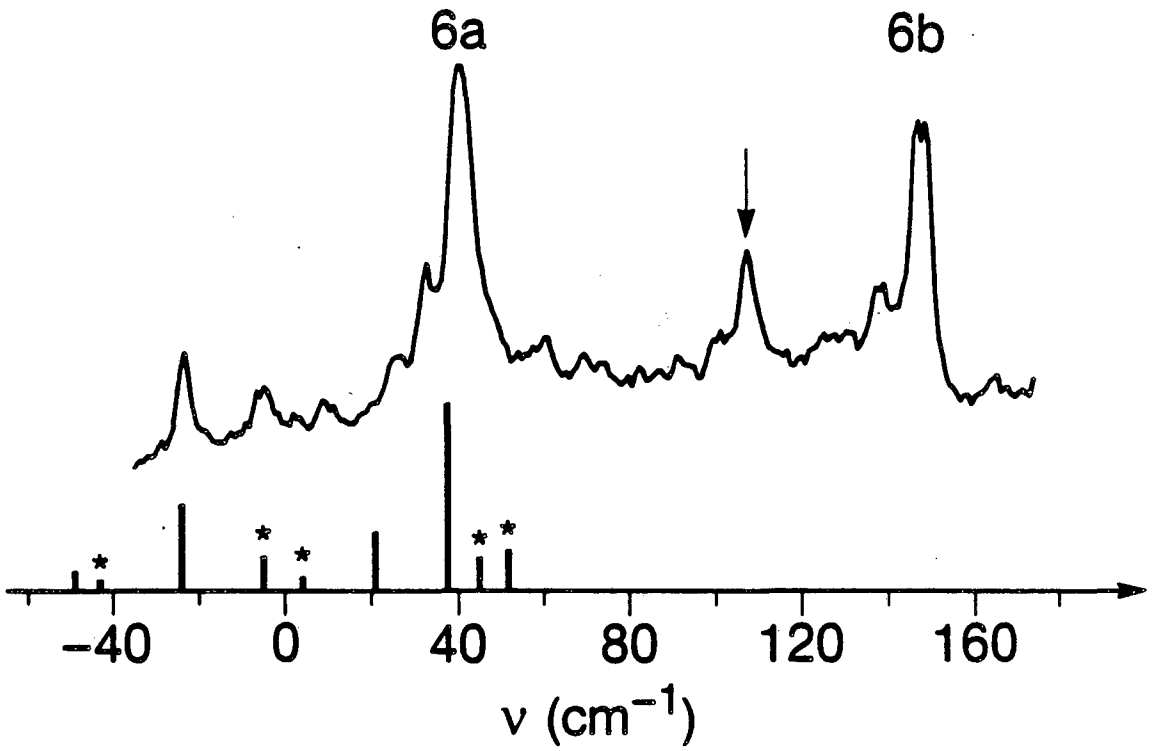

XBL 873-7623

Figure 12.

Determination of Rotationless ($N^+ = 0$) Convergence Limits of $v_1^+ = 1$ "a" and "b" Series

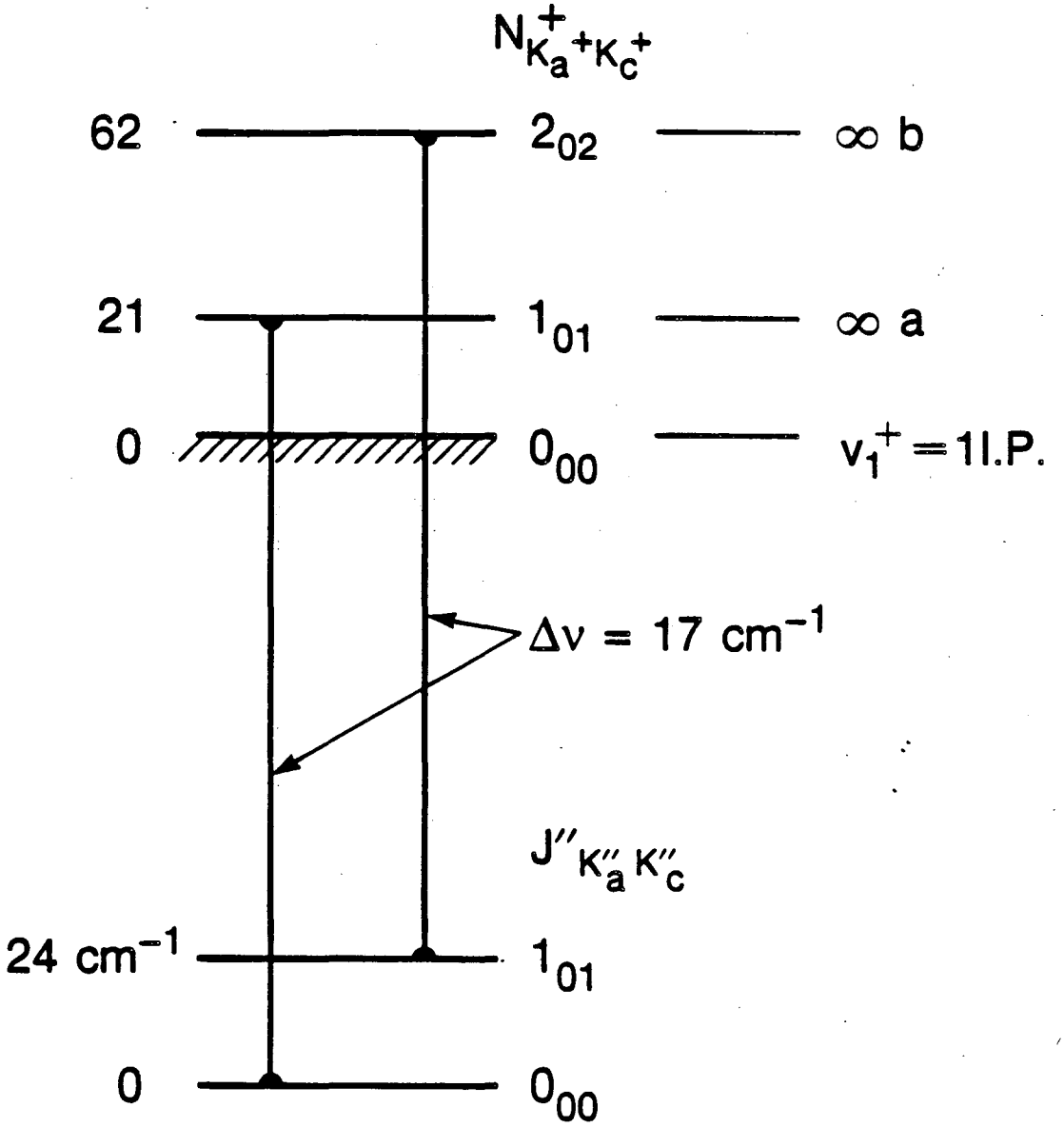

Figure 13.

XBL 873-7621

Rotational Structure of Π Bands in a Linear ← Bent Transition

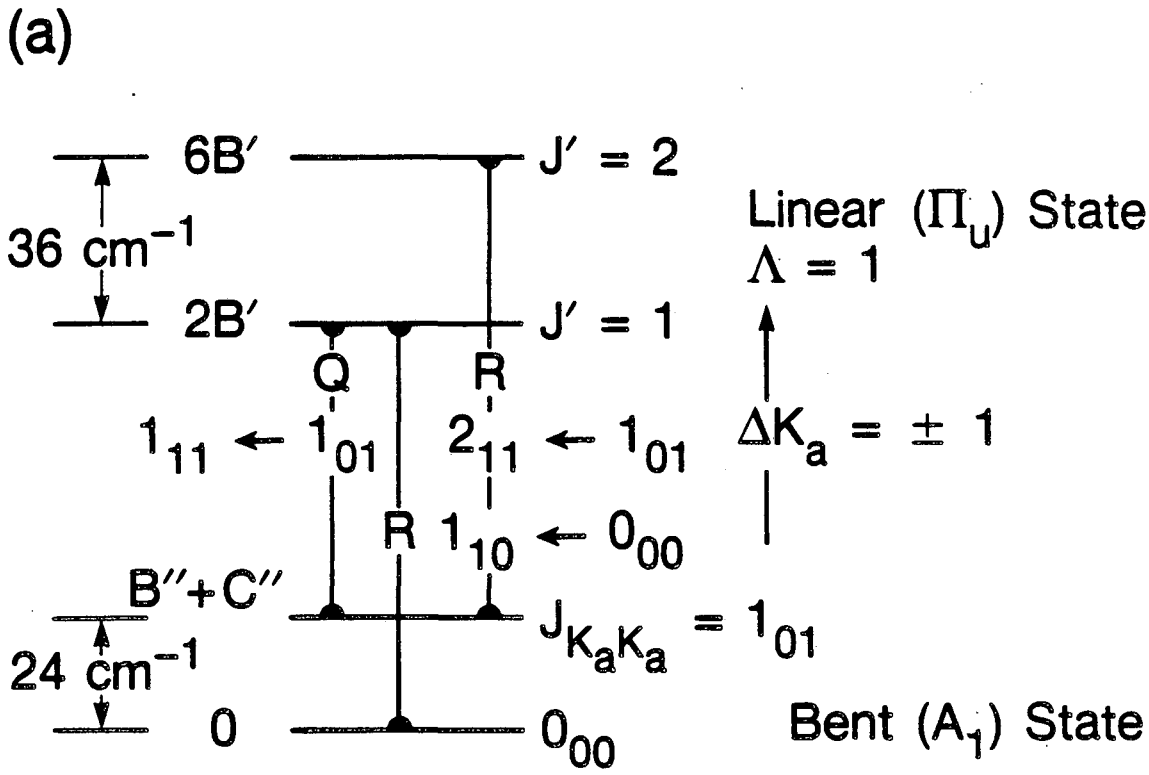

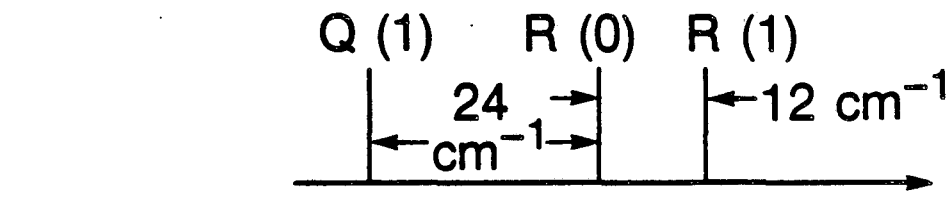

XBL 873-7618

Figure 14.

Assignment of V_2 Levels and $(3a_1)^{-1}$ 3d Energy

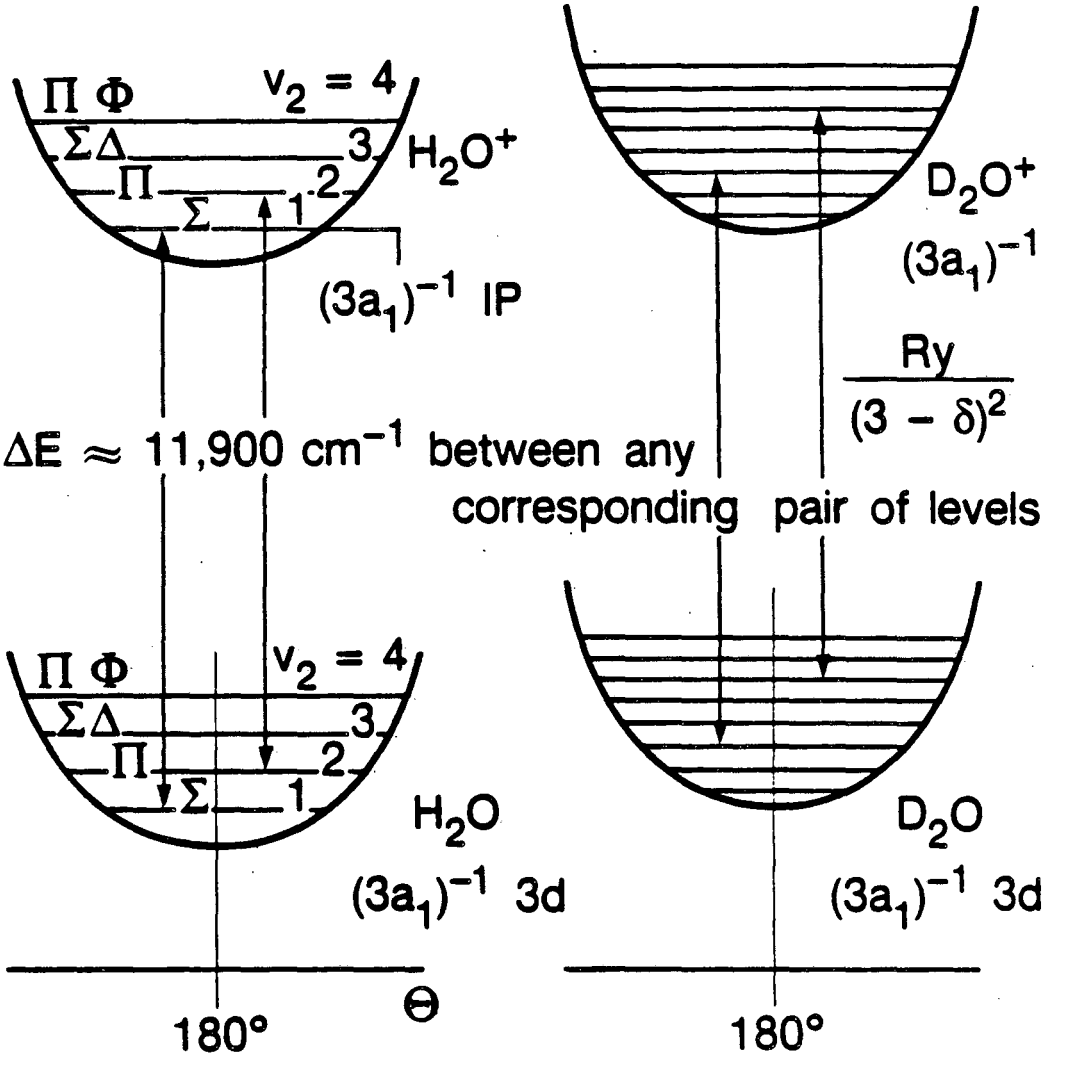

XBL 873-7622

Figure 15.

VOLUME 56, NUMBER 4 PHYSICAL REVIEW LETTERS 27 JANUARY 1986

VII. A. Rydberg Spectroscopy of H_2 via Stepwise Resonant Two-Photon Ion-Pair ($H^+ + H^-$) Production

A. H. Kung

San Francisco Laser Center, Department of Chemistry, University of California, Berkeley, California 94720

and

Ralph H. Page,[a] R. J. Larkin,[b] Y. R. Shen,[a] and Yuan T. Lee[c]

Materials and Molecular Research Division, Lawrence Berkeley Laboratory, University of California, Berkeley, California 94720

(Received 22 October 1985)

High-resolution spectra of new Rydberg states of H_2 in the extreme-uv region were obtained by two-step doubly resonant excitation followed by H^--ion detection. Resolved Fano-line profiles showing a sign reversal of the profile index along the Rydberg series were observed for the first time in H_2. Dynamical information such as lifetimes and relative transition strengths was also derived.

PACS numbers: 33.20.Ni, 33.70.−w, 33.80.Eh, 33.80.Rv

Recently, extensive spectroscopic work on H_2, especially in the range of photon energy below 17 eV, has led to a good understanding of the autoionization process through Rydberg transitions that converge to $H_2^+(X\,^2\Sigma_g^+)$ and up to $v^+ = 7$.[1-5] Extension of the same level of understanding to series that converge to higher vibrational states ($v^+ > 7$) and to other important processes such as ion-pair formation and dissociative ionization is, however, inhibited by the limited amount of data available above 17 eV. Spectroscopic study of these highly excited states is made difficult by weak transition probability and the lack of intense light sources at these frequencies. With the recent advances in the development of tunable coherent extreme-uv sources,[6,7] it is now possible to apply nonlinear optical spectroscopy to the investigation of these highly excited states. By use of resonant two-photon excitation,[8] the weak transition probabilities due to small Franck-Condon factors for single-photon excitation can be greatly improved. New excited states whose transitions cannot be reached from the ground state can be studied. The spectrum can also be simplified by selective labeling of the rotational states. In this paper, we report the first application of two-step doubly resonant excitation followed by negative (H^-) ion detection to study the Rydberg states of H_2 above 17 eV. High-resolution spectra of new Rydberg states with high convergence limits (to $H_2^+ X\,^2\Sigma_g$, $v^+ = 9$, $N^+ = 1, 3$) were obtained and analyzed. The Fano-line profiles were resolved and reversal of the profile index along the series was observed, the latter for the first time in H_2. Dynamical information such as lifetimes and relative transition strengths from low electronic states to Rydberg states and the ion-pair dissociation continuum was deduced. Use of H^- detection was essential in this study because the alternative method of probing these Rydberg states via autoionization and detecting H_2^+ results in a two orders of magnitude larger ion signal but yields a very poor spectrum dominated by an intense ionization continuum. The H^- continuum arising from direct ion-pair formation, on the other hand, is relatively weak, rendering the observation of the Rydberg structure comparatively easy. Ion-pair formation via single-photon excitation was previously used by Chupka, Dehmer, and Jivery to study Rydberg states of H_2.[9] In this study we extended this detection technique to Rydberg states that have *gerade* symmetry. The combination of this detection with the use of coherent laser sources provided both good signal strength and improved frequency resolution, making possible the extraction of dynamical information on these new states. It should be pointed out that the use of H^- detection confines the study to a subset of molecular states that are coupled to the ion-pair continuum. Nevertheless, knowledge of this subset is essential to the understanding of the H_2 ionization and predissociation processes.

Described below are the two-photon excitation scheme and the subsequent ionization or dissociation of H_2 applicable to this experiment (see Fig. 1). Excitation:

$$H_2 + h\nu_1 \rightarrow H_2^*(B\,^1\Sigma_u^+ \text{ or } C\,^1\Pi_u), \quad (1a)$$

$$H_2^* + h\nu_2 \rightarrow H_2^{**}. \quad (1b)$$

Autoionization:

$$H_2^{**} \rightarrow H_2^+ + e. \quad (2)$$

Ion-pair formation:

$$H_2^{**} \rightarrow H^+ + H^-. \quad (3)$$

The dominant channel in the region of interest is the formation of H_2^+ by direct ionization. The thresh-

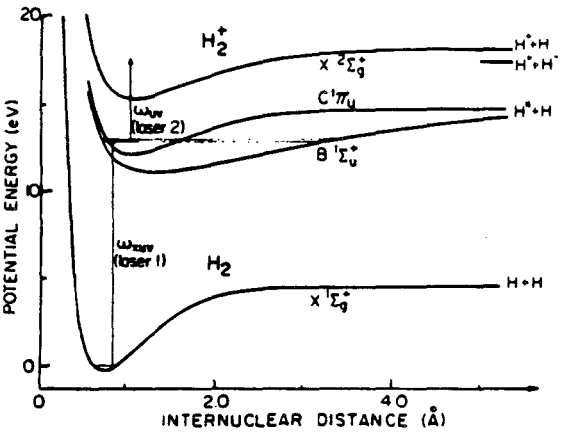

FIG. 1. Potential energy diagram for H_2 showing the levels of interest, from Sharp (Ref. 10).

old for this process is 15.43 eV. In the range of a few electronvolts above this threshold, the spectrum obtained by detecting H_2^+ consists of autoionizing lines superimposed on a continuum; the latter generally dominates as the excitation energy increases.[2] Ion-pair formation has a threshold at 17.34 eV. The intensity of the ion-pair channel immediately above its threshold is low. The interference of Rydberg states with this ion-pair continuum allows us to probe the Rydberg line spectrum in this region with high accuracy by measuring the excitation-frequency dependence of the H^--ion signal.[9]

In the experiment, the frequency-tripled output of a frequency-doubled Nd-doped yttrium aluminum garnet laser–pumped dye laser (laser 1) was tuned to selectively excite either the $v'=2$, $J'=1$ level of the $C\ ^1\Pi_u$ state of a pulsed beam of H_2 at 103 509.24 cm^{-1} or the $v'=12$, $J'=0$ level of the $B\ ^1\Sigma_u^+$ state at 103 700.91 cm^{-1}.[11] From these levels, the molecules were further excited by a second laser (laser 2). This second laser was a frequency-doubled Nd-doped yttrium aluminum garnet laser–pumped dye laser, which was tuned to have the sum of the frequencies of lasers 1 and 2 span the region from below the ion-pair formation threshold to well above that threshold. The H^- ions produced were detected by a time-of-flight mass spectrometer. The ion signals were averaged by a boxcar integrator and digitized for analysis. The signal level was as big as 100 ion counts per laser pulse. Wavelength calibration of laser 2 was performed by use of the optogalvanic effect with an argon-discharge lamp.

Figure 2(a) presents a portion of the spectrum obtained by tuning laser 2 with $C\ ^1\Pi_u(v'=2, J'=1)$ as the intermediate state. Its exhibits many sharp dips superimposed on a structured continuum. Analysis shows that the dips can be assigned to transitions to

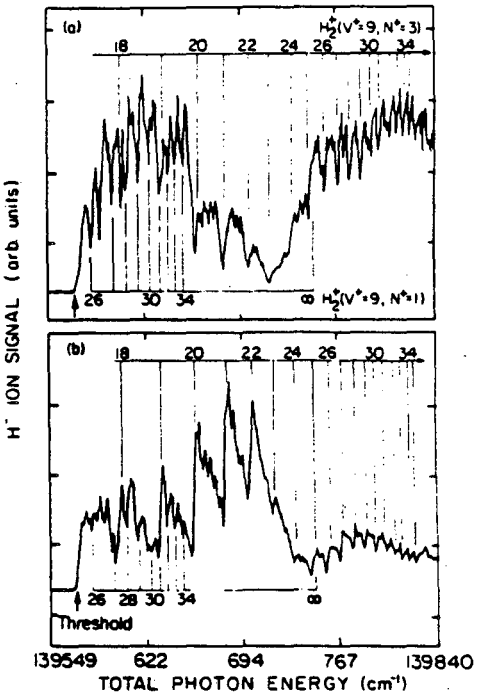

FIG. 2. Resonant two-photon ion-pair spectra of H_2 from the onset of H^- production threshold, indicating transitions assigned to series that converge to $H_2^+(X\ ^2\Sigma_g^+, v^+=9, N^+=1, 3)$. (a) Intermediate state: $C\ ^1\Pi_u(v'=2, J'=1)$. (b) Intermediate state: $B\ ^1\Sigma_u^+(v'=12, J'=0)$. Spectrum (a) is obtained with 20 times higher gain than (b).

the high-n states of two distinct Rydberg series converging to the ion-core levels specified by the rotational quantum numbers $N^+=1$ and $N^+=3$ and the vibrational quantum number $v^+=9$. The effective principal quantum numbers n^* of the observed states can be determined; a portion of them is listed in Table I. Here, n^* is defined by the Rydberg series formula $\nu = S - R/n^{*2}$, where ν is the measured frequency in inverse centimeters, S is the theoretical series limit given by Wind,[12] and $R = 109\,707.42\ cm^{-1}$ is the Rydberg constant for H_2. Our present signal-to-noise ratio limits the determination of n^* to ~ 36. Figure 2(b) gives the spectrum in the same region with $B\ ^1\Sigma_u^+(v'=12, J'=0)$ as the intermediate state. The lines in this spectrum can be identified as arising from transition to the same Rydberg series displayed in Fig. 2(a). Their positions relative to the ionization level of the series $(v^+=9, N^+=1, 3)$ agree with those deduced from Fig. 2(a) to within 1 cm^{-1}, which is well within our experimental resolution of 1.5 cm^{-1}.

From the values of n^*, the quantum defect for the $N^+=1$ series is thus determined to be 0.1 ± 0.1,

TABLE I. Fano-profile parameters for Rydberg series converging to $H_2^+(v^+=9, N^+=3)$.

Principal quantum number	Line center (± 0.5) (cm^{-1})	n^*	Linewidth (cm^{-1})	Lifetime (psec)	$q(\pm 0.05)$ $C\,^1\Pi_u$[a]	$q(\pm 0.05)$ $(B\,^1\Sigma_u^+)$[a]
25	139746.5	25.84	3.0 ± 0.5	1.7	[b]	0.40
26	139757.6	26.76	1.5 ± 0.3	3.5	0.00	0.2
27	139768.2	27.74	1.2 ± 0.2	4.3	0.00	0.60
28	139777.5	28.69	0.8 ± 0.1	6.5	−0.10	0.55
29	139786.0	29.65	0.6 ± 0.1	8.7	0.10	0.10
30	139794.0	30.65	2.0 ± 0.3	2.6	0.00	0.00
31	139801.8	31.73	1.4 ± 0.2	3.7	0.10	−0.30
32	139808.6	32.77	3.0 ± 0.5	1.7	−0.10	−0.30
33	139814.1	33.69	0.4 ± 0.1	13.1	0.00	−0.80
34	139819.0	34.58	0.3 ± 0.1	17.5	[b]	−0.80
35	139824.2	35.60	1.1 ± 0.2	4.7	[b]	−0.15

[a]Intermediate state. [b]Not measured.

whereas that for the $N^+=3$ series is 0.7 ± 0.15. The perturbations among adjacent Rydberg states in H_2, the limited signal-to-noise ratio for the higher-n states, and the limited frequency resolution have prevented us from determining the orbital quantum number (s or d) of these series and from obtaining finer limits for the quantum defects. However, these measurements are an important first step in providing data for spectroscopists to use to improve our understanding of these high-lying states of H_2. Some additional lines which do not belong to these series also appear in the spectra. These, along with the broad structures in the spectra, are not yet assigned. The broad structures are likely to arise from transitions to low-n states of Rydberg series with v^+ higher than 9.

While the Rydberg line positions in the two cases with different intermediate states agree, the line shapes observed are very different. Those in Fig. 2(a) are sharp dips but those in Fig. 2(b) have asymmetric Fano profiles with changing profile indices. We have used Fano's line-shape formula,[13,14] which takes into account the interaction of discrete autoionizing states with a continuum, to fit individually the observed lines with $n \geq 25$ in Fig. 2 (those lying above the $v^+=9$, $N^+=1$ series limit of 139746.58 cm^{-1}). The results for Fig. 2(b) are shown in Fig. 3. Values of the profile index q and linewidths deduced are given in Table I. Here $q = A^*|\langle i|z|n\rangle|/|\langle i|z|a\rangle|$, where $\langle i|z|n\rangle$ is the dipole matrix element from the intermediate state $\langle i\rangle$ to the discrete autoionizing state $\langle n\rangle$, $\langle i|z|a\rangle$ the matrix element from $\langle i\rangle$ to the continuum state $\langle a\rangle$, and A is independent of state $\langle i\rangle$ and is inversely proportional to the strength of the interaction between states $\langle n\rangle$ and $\langle a\rangle$. The laser linewidth has been deconvolved to obtain the transition widths. We did not try to fit the lines with $n < 25$ because their profiles are distorted by strong perturbation between the $N^+=1$ and $N^+=3$ series. The lifetimes obtained from the inverse linewidths are also listed in Table I.

An interesting result from the line-shape analysis is the revelation of a change of the sign of the profile index q (q reversal) at $n \geq 31$ (see Fig. 3). This sign reversal arises from a relative phase shift in the two transition-matrix elements that determine q. The phenomenon has been analyzed theoretically by several authors.[15–17] In this experiment, the reversal is the result of the interaction of the $N^+=3$ series with a broad state of finite bandwidth which appears to be centered around the $n=30$ transition. Unfortunately,

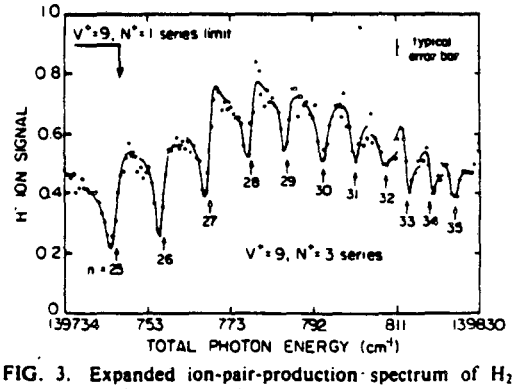

FIG. 3. Expanded ion-pair-production spectrum of H_2 between the $N^+=1$ and $N^+=3$ series limits showing the fitted Fano line profiles: Solid curves, calculated profile; circles, experimental points; and arrows, fitted line center positions.

the origin of this broad state is not yet clear. Connerade has previously reported evidence of similar q reversal in the Rydberg spectra of Tl[15] and of CH_3Br.[18] This is, however, the first time that q reversal has been observed in a diatomic molecule.

A more advanced and complete analysis of these spectra involves the use of multichannel quantum-defect theory initially applied by Fano[19] and more recently refined and extended by Jungen and his colleagues[3,4] to calculate successfully the H_2 ionization spectra. Because of the scope of this work, multichannel quantum-defect theory treatment has not been attempted.

Our results also reveal important information about the relative transition probabilities between high-lying electronic states of H_2. It is known that $C\,^1\Pi_u$ is a "Rydberg-type" state ($n=2$) whereas $B\,^1\Sigma_u^+$ is an "ion-pair-like" state.[20] This suggests that transitions from $B\,^1\Sigma_u^+$ to the ion-pair continuum should be stronger than those from $C\,^1\Pi_u$ to the ion-pair continuum. This was indeed observed in our experiment: The H^- continuum signal was ten times stronger when we excited via the B level than via the C level. On the other hand, one would also expect electronic transitions from $C\,^1\Pi_u$ to the high-lying Rydberg states to be stronger than those from $B\,^1\Sigma_u^+$ to the Rydberg states. Experimentally, however, we found that the reverse was true. A comparison of the magnitudes of q in columns 6 and 7 in Table I shows that the transitions from $C\,^1\Pi_u$ to the Rydberg states are even weaker by about an order of magnitude than the transitions from $B\,^1\Sigma_u^+$ to the ion-pair continuum. This can be easily understood by realizing that in our case, transitions from $C\,^1\Pi_u$ to the Rydberg states should have small Franck-Condon factors because of the larger change in the vibrational quantum number ($v=2 \rightarrow v=9$). If it were not for the interaction between the Rydberg states and the ion-pair continuum that leads to preionization and intensity borrowing, these transitions would not have been observed. For the transitions from B to the Rydberg states, Δv is only 3 in our case. This is consistent with the observation of Pratt, Dehmer, and Dehmer who, using multiphoton photoelectron spectroscopy, have shown a near-unity Franck-Condon factor for transitions from $C\,^1\Pi_u$ to high-lying Rydberg states with $\Delta v = 0$.[21]

This work was supported by the Director, Office of Energy Research, Office of Basic Energy Sciences of the U. S. Department of Energy under Contract No. DE-AC03-76SF-00098. The work of one of us (A.H.K.) was also supported by the National Science Foundation under Grant No. CHE 83-03208.

---

[a]Also affiliated with the Department of Physics, University of California, Berkeley, Cal. 94720.

[b]Present address: United Technologies Research Center, Optics and Applied Technology Laboratory, West Palm Beach, Fla. 33402.

[c]Also affiliated with the Department of Chemistry, University of California, Berkeley, Cal. 94720.

[1]G. Herzberg and Ch. Jungen, J. Mol. Spectrosc. **41**, 425 (1972).

[2]P. M. Dehmer and W. A. Chupka, J. Chem. Phys. **65**, 2243 (1976).

[3]Ch. Jungen and D. Dill, J. Chem. Phys. **73**, 3338 (1980).

[4]M. Raoult and Ch. Jungen, J. Chem. Phys. **74**, 3388 (1981).

[5]H. Rottke and K. H. Welge, J. Phys. (Paris), Colloq. **46**, C1-127 (1985).

[6]E. E. Marinero, C. T. Rettner, R. N. Zare, and A. H. Kung, Chem. Phys. Lett. **95**, 486 (1983); C. T. Rettner, E. E. Marinero, R. N. Zare, and A. H. Kung, J. Phys. Chem. **88**, 4459 (1984).

[7]R. Hilbig, A. Lago, and R. Wallenstein, Opt. Commun. **49**, 297 (1984).

[8]D. J. Kligler and C. K. Rhodes, Phys. Rev. Lett. **40**, 309 (1978).

[9]W. A. Chupka, P. M. Dehmer, and W. T. Jivery, J. Chem. Phys. **63**, 3929 (1975).

[10]T. E. Sharp, At. Data **2**, 119 (1971).

[11]I. Dabrowski and G. Herzberg, Can. J. Phys. **52**, 1110 (1974).

[12]H. Wind, J. Chem. Phys. **43**, 2956 (1956).

[13]U. Fano and J. W. Cooper, Rev. Mod. Phys. **40**, 441 (1968).

[14]M. B. Robin, *Higher Excited States of Polyatomic Molecules* (Academic, New York 1974), p. 32.

[15]J. P. Connerade, Proc. Roy. Soc. London, Ser. A **362**, 361 (1978).

[16]A. M. Lane, J. Phys. B **17**, 2213 (1984).

[17]A. Giusti-Suzor and H. Lefebvre-Brion, Phys. Rev. A **30**, 3057 (1984).

[18]J. P. Connerade, M. A. Baig, and S. P. McGlynn, J. Phys. B **14**, L67 (1981).

[19]U. Fano, Phys. Rev. A **2**, 353 (1970), and J. Opt. Soc. Am. **65**, 979 (1975).

[20]G. Herzberg, *Spectra of Diatomic Molecules* (Van Nostrand, New York, 1950), 2nd ed.

[21]S. T. Pratt, P. M. Dehmer, and J. L. Dehmer, Chem. Phys. Lett. **105**, 28 (1984).

VII. B. Appendix to "Rydberg Spectroscopy of H_2 via Stepwise Resonant Two-Photon Ion-Pair ($H^+ + H^-$) Production" [Phys. Rev. Lett. 56, 328 (1986)]

The purpose of this Appendix is to provide a final resting place for the large amount of data I have organized in connection with the ion-pair experiment. Also, the work can be put in slightly better perspective if it is discussed a bit more.

Figure 1 shows ion intensities vs. total energy, with ω_1 tuned to the $B \leftarrow X$ (13,0) P(1) transition, and ω_2 scanning. The H^+ and H_2^+ signals were detected simultaneously during a scan which was different from the one which gave the H^- signal. (We could not detect both polarities of ions simultaneously.) The point of interest is that the H^+ and H^- spectra between the H^- threshold and 140.3 K cm^{-1} appear to have features in common. Though this data was not reproduced by us, it shows that the ion-pair ($H^+ + H^-$) channel can be as intense as that which produces the continuum H^+ signal.

The glut of H^- data we obtained is shown in Figs. 2-7, plotted as a function of total energy. There are clearly many spectral features, a small fraction of which have been assigned. It will take an enthusiastic hard-core spectroscopist to sort the rest of them out. More experiments with different intermediate states will probably prove to be useful for assigning many of the bumps and dips. Most of our H^- spectra have a pretty substantial peak near 140370 cm^{-1}. There must be something important about that energy!

Figure Captions

Fig. 1 Ion signals obtained with the B $^1\Sigma_u^+$ (v = 13, J = 0) state as intermediate. Positive and negative ion signals were recorded separately. The H^+ and H^- spectra have features in common in the 139700-140300 cm^{-1} range; these are due to the ion-pair ($H^+ + H^-$) channel.

Fig. 2 H^- spectrum obtained with B $^1\Sigma_u^+$ (v = 12, J = 0) as intermediate state.

Fig. 3 H^- spectrum obtained with B $^1\Sigma_u^+$ (v = 12, J = 1) as intermediate state.

Fig. 4 H^- spectrum obtained with B $^1\Sigma_u^+$ (v = 12, J = 2) as intermediate state.

Fig. 5 (a) and (b) H^- spectrum obtained with B $^1\Sigma_u^+$ (v = 13, J = 0) as intermediate state.

Fig. 6 H^- spectrum obtained with C $^1\Pi_u^-$ (v = 2, J = 1) as intermediate state.

Fig. 7 H^- spectrum obtained with C $^1\Pi_u^+$ (v = 2, J = 2) as intermediate state.

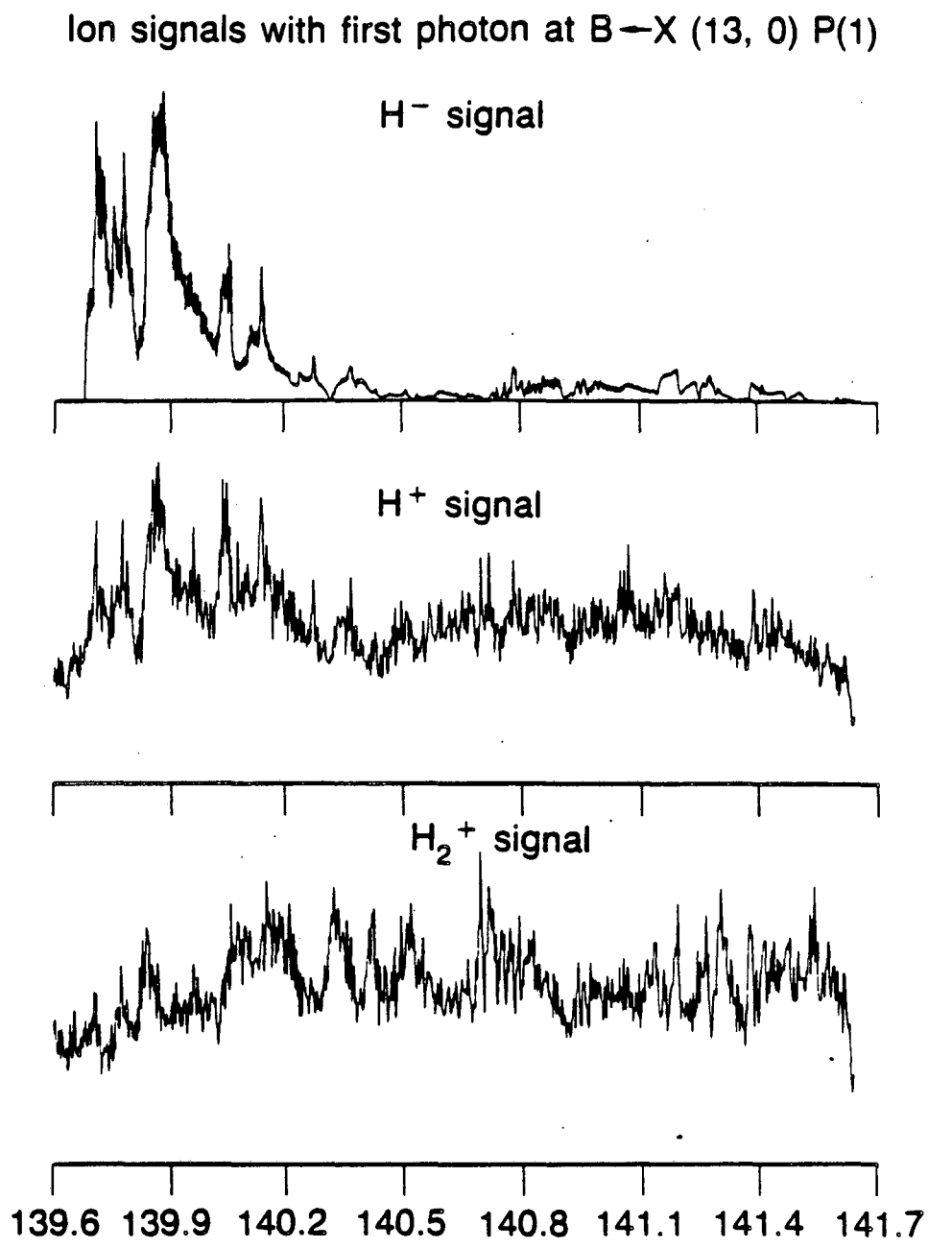

XBL 872-6094

Figure 1.

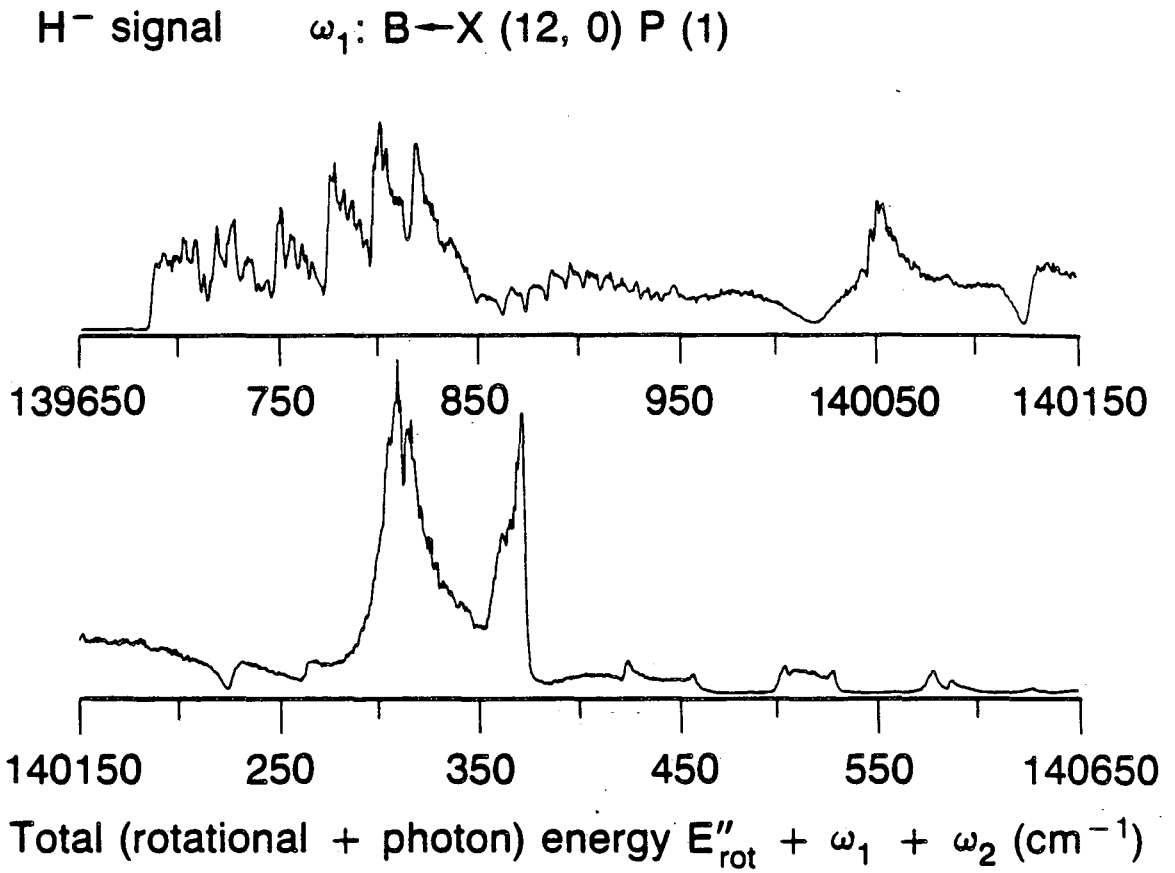

XBL 872-6154

Figure 2.

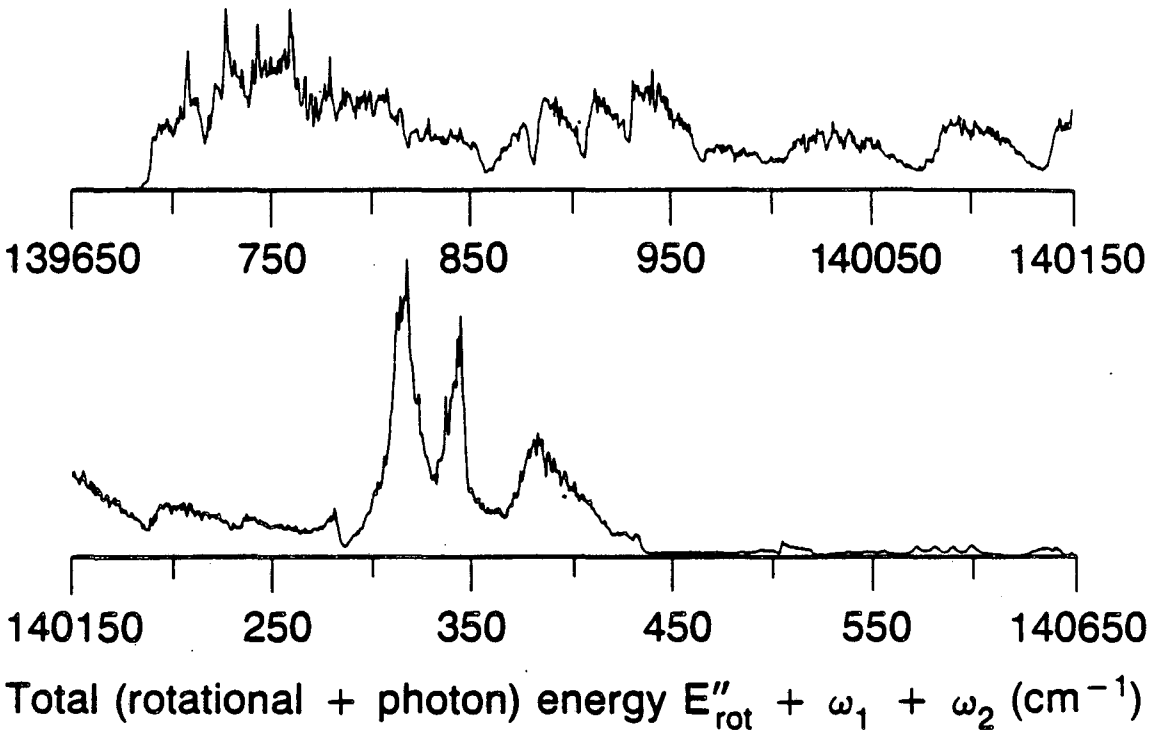

XBL 872-6088

Figure 3.

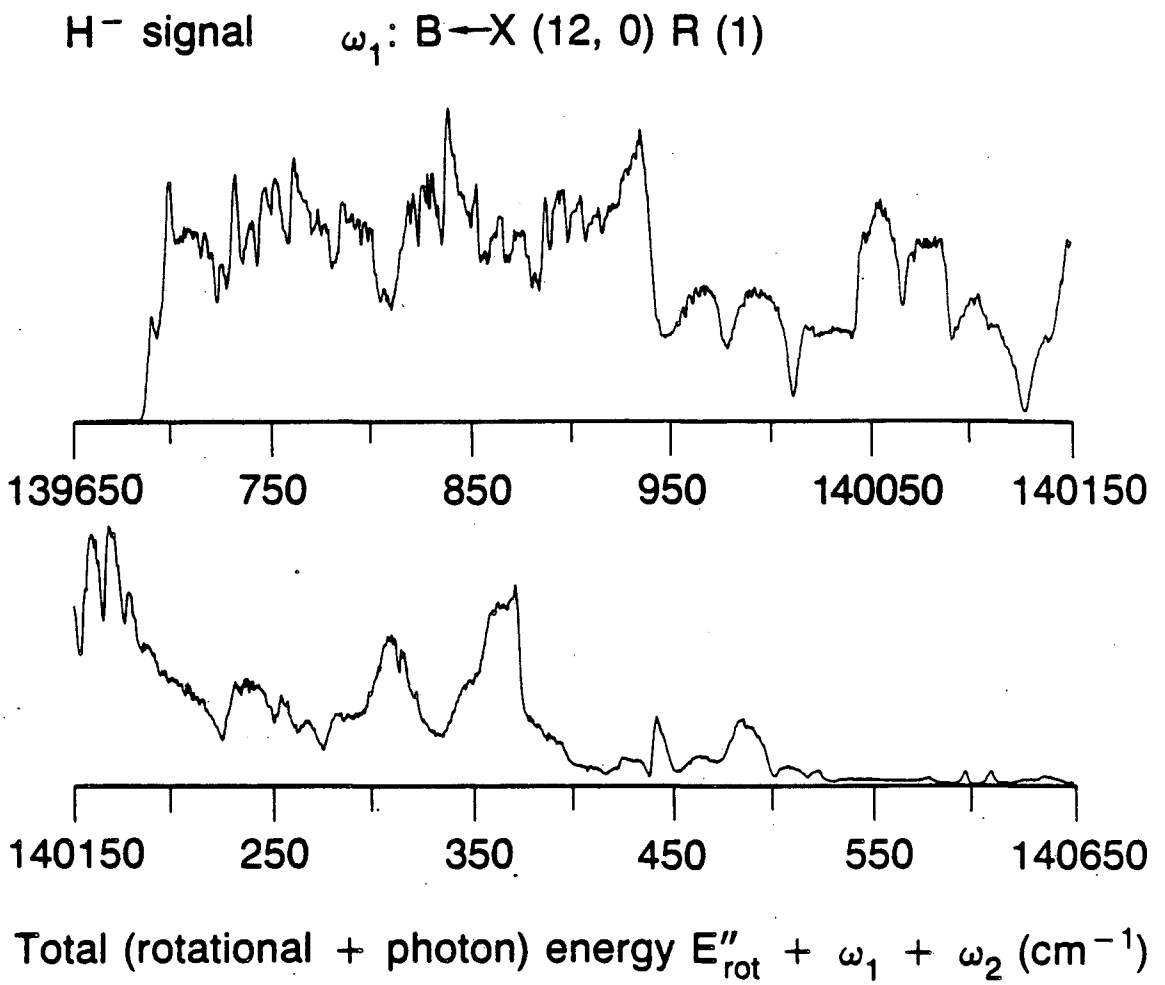

XBL 872-6089

Figure 4.

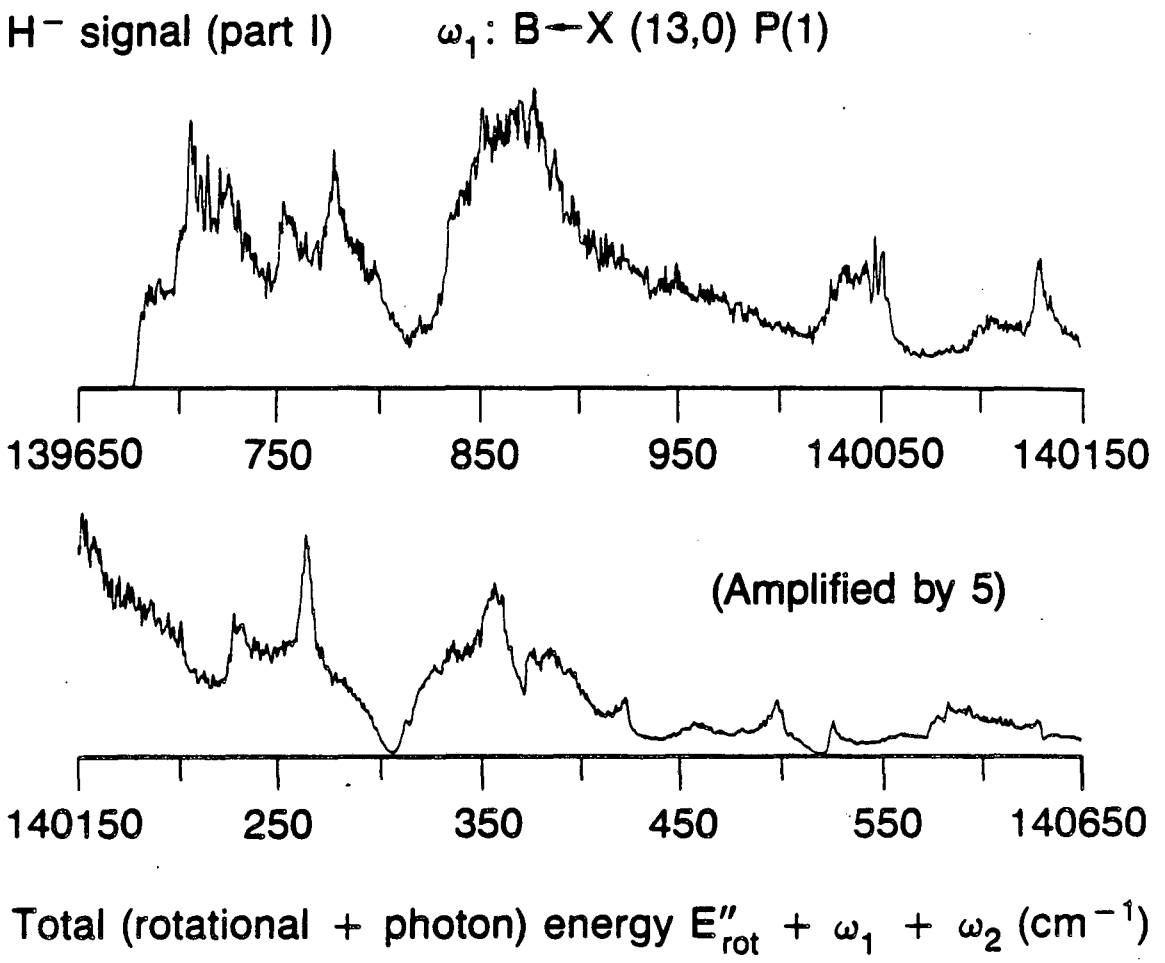

XBL 872-6086

Figure 5(a).

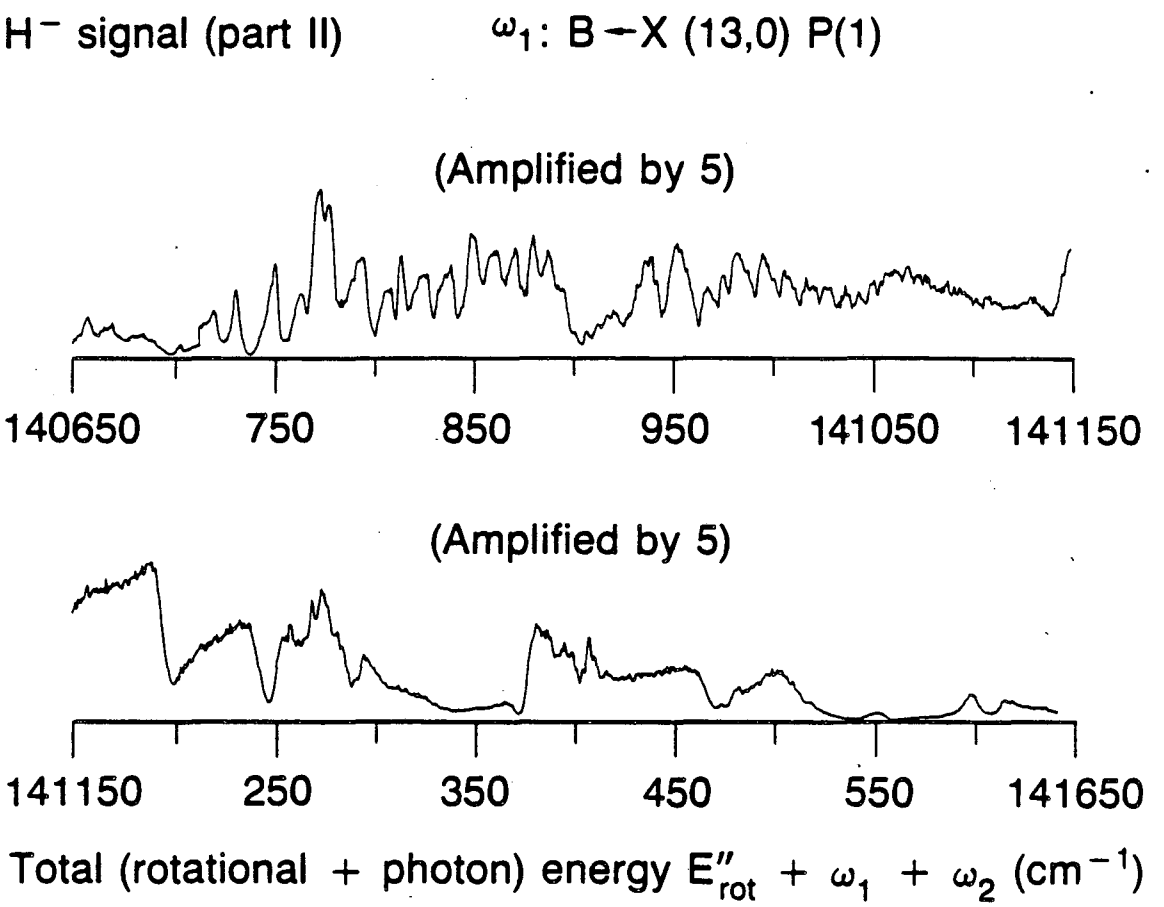

XBL 872-6085

Figure 5(b).

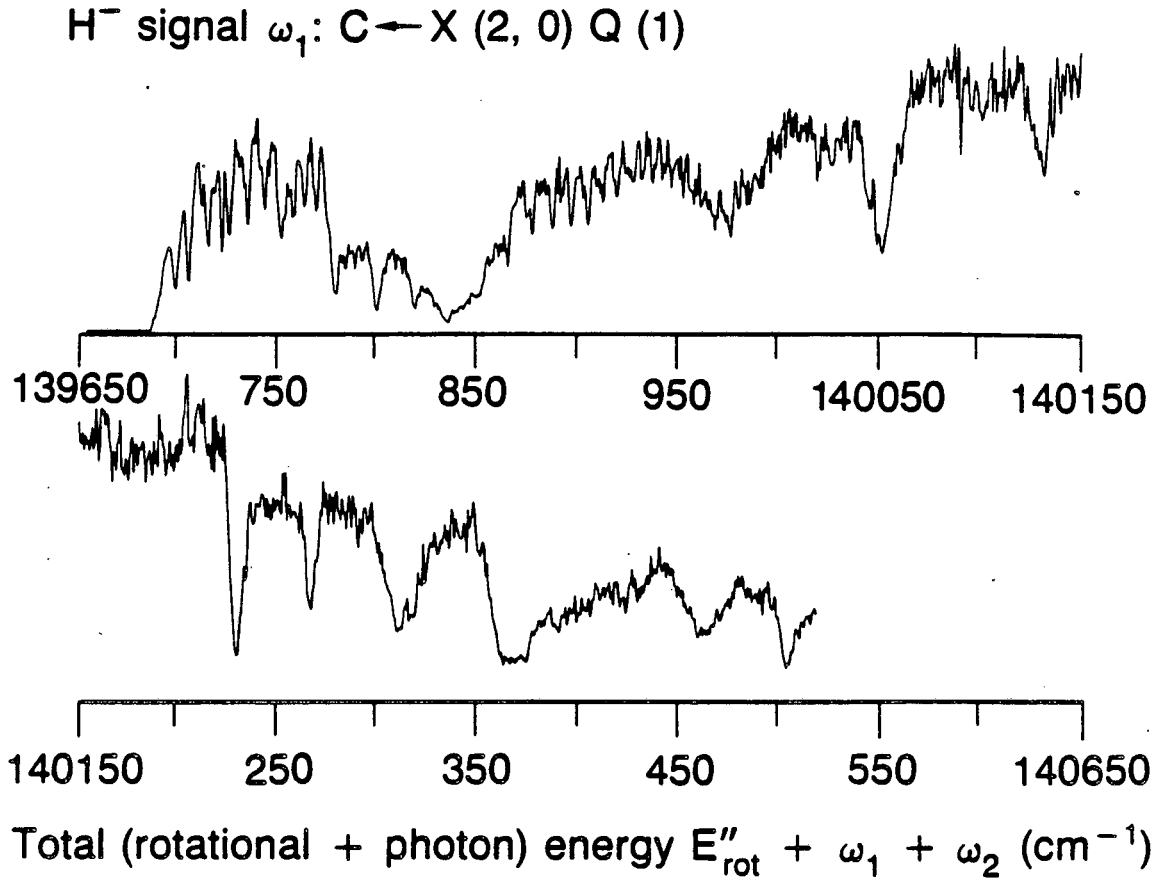

XBL 872-6090

Figure 6.

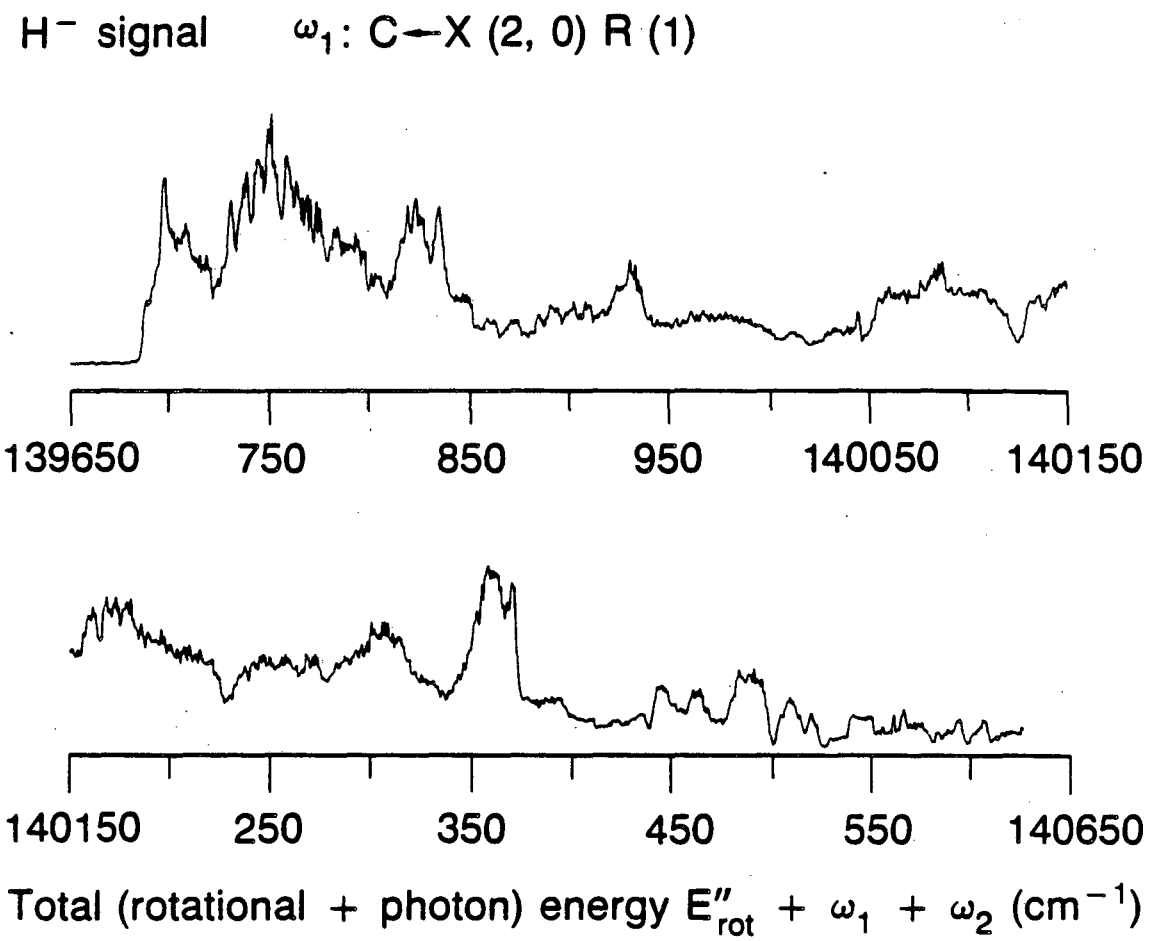

XBL 872-6092

Figure 7.

VII. C. XUV-VISIBLE DOUBLE RESONANCE IN THE NO MAN'S LAND OF H_2: SINGLET GERADE LEVELS OF MEDIUM PRINCIPAL QUANTUM NUMBER (n ~ 5)

I. Introduction

As the most theoretically tractable neutral molecule that can be imagined, H_2 has always had a special place in the minds and hearts of chemists and physicists, and especially spectroscopists. Optical spectroscopy is the best way to find the energy levels and measure the excited-state dynamics of the isolated molecule. And theory is never far behind in using fundamental physical principles to provide a quantitative explanation of the experimental results. There have been, appropriately, encyclopedic publications which have compiled the extant information on the H_2 optical spectrum and potential energy curves.[1-3] It is in no way claimed that the work is complete; many energy levels are left undetermined, and many transitions that have been observed remain unassigned.

In recent years much progress has been made in learning about the excited states of H_2. Since the H_2 ground state has gerade (g) symmetry, absorption spectroscopy has been well suited to finding the transitions to electronic states of ungerade (u) symmetry. Detail has not been spared in the examination of the lowest excited states[4] and the highly-excited Rydberg states.[5] Analysis of lineshapes observed in absorption and ionization spectra[6-8] has given information about the molecular decay processes of autoionization and predissociation. In fact, multichannel quantum defect theory[9] now includes these processes concurrently.

The gerade levels, on the other hand, present a more challenging

problem because the are not reached with single photon absorption from the ground state. But these levels can be populated by electron impact[10] or in a discharge.[11,12] Radiation in the IR-near UV range is emitted as populations in these levels decay radiatively into ungerade levels. Rapidly predissociated gerade levels cannot realistically be studied with the emission technique because the light which is emitted is weak and spectrally diffuse. Also, the extremely dense spectrum observed in a discharge is extremely difficult to sort out and assign; many excited states are populated and they each have many alternative final states into which to decay. So far, the highest well-studied levels have a principal quantum number n = 3.

Eyler and Pipkin[13,14] have observed transitions to the n = 4 gerade levels of the triplet manifold by starting with a metastable population in the n = 2 ungerade level. Such a technique (which does not work for the short-lived singlets) allowed them to use fluorescence excitation spectroscopy, the results of which indicated that the upper state levels which had vibrational excitation were usually predissociative, with lifetimes as low as 100 psec. They made a simple model of the ion core-electron interaction and did numerical calculations which reproduced the observed energy levels to within a few cm^{-1}. Ab initio theoretical calculations, which normally are even more accurate, have apparently not been performed for the n = 4 states.

One might expect that laser light sources would make the two-photon spectroscopic study of the gerade states an easy matter. After all, two-photon studies have been performed on many molecules. Actually, this is not the case; even if two-photon excitation is used, vacuum ultraviolet light (below 2000 A) must be generated to reach any of the

singlet gerade states, which are all at least ~ 100000 cm^{-1} above the ground state. When there is no intermediate resonance near the one-photon energy, high power must be used. Fortuitously, the 193-nm ArF laser is well suited to the study of the n = 2 state at ~ 104000 cm^{-1}.[15]

Thus there is an important gap in our knowledge of the gerade states of hydrogen above n = 2. The n = 3 level is only partially characterized experimentally[10-12] and theoretically.[16-19] Much unknown territory exists beginning in the vibrationally excited levels of n = 3 and extending all the way to n = ∞. We have termed the region in which n is between 3 and ~ 10 the "no man's land" because so little is known about it and because many complex and interesting effects should be visible there. Figure 1 is a set of potential energy curves, largely taken from Sharp,[3] which will help to explain why this region is interesting.

One important attribute of the region above ~ 119000 cm^{-1} is that predissociation into electronically excited products [H (n = 1) + H^* (n = 2)] becomes possible. This decay channel is a source of difficulty with emission spectroscopy. Another exotic feature of this area is that the gerade states include the double-well states (E,F; G,K; H,$\bar{H}$; etc.). These double-minimum potentials result from avoided crossings between singly-excited and doubly-excited electron configurations. [For example, E $^1\Sigma_g^+$ ($1s\sigma_g$ $2s\sigma_g$) interacts with F $^1\Sigma_g^+$ ($2p\sigma_u$ $2p\sigma_u$). The $1s\sigma_g$ designation is understood to be a part of all one-orbital labels in Fig. 1.] Theoretical calculations have predicted the energy levels[18] of some of these interesting states, but an experimental map of them has not been produced. Still another interesting phenomenon occurs at this energy: "ℓ uncoupling",[20] in which the excited electron gets so

far from the H_2^+ core that its motion is only weakly influenced by the core's anisotropy. The orbital angular momentum ℓ (s, p, d, etc.) ceases to have a well-defined projection λ (σ, π, δ, etc.) on the internuclear axis, and the electronic symmetry designation Λ (Σ, Π, Δ, etc.) loses its relevance. As this happens, the states of different electronic symmetry Λ can perturb each other. It is known in the case of the ungerade np states that ℓ-uncoupling is basically absent at n = 2 and complete by n ~ 10.[5] It would be interesting to see what differences exist for gerade states.

All in all, the singlet gerade n = 3-10 manifold is likely to be rife with perturbations and interesting effects. A very incisive spectroscopic technique will be required to get unambiguous information in this challenging area. In this article we describe such a spectroscopic technique and present some preliminary results on what we believe are the n = 4,5 levels. We have used XUV-visible double resonance to study transitions from selected rovibronic levels in the H_2 2p state. There is a signature of rapid predissociation of final states belonging to a certain electronic symmetry class. Further data acquisition with a setup similar to ours will quickly provide a treasure trove of useful line assignments, predissociation rates, oscillator strengths, and lineshape parameters. Such information would be sufficient for a traditional thorough spectroscopic analysis including ℓ uncoupling, interstate perturbations, and decay processes.

II. Technique

Figure 1 shows the energy levels and transitions involved in our experiment. Stepwise two-photon excitation is used to reach the levels

under study. The first photon, at ω_1 in the XUV, is fixed to pump the H_2 1s → 2p transition, so that molecules are temporarily in the B ($^1\Sigma_u^+$) or C ($^1\Pi_u$) state, with exactly known vibrational and rotational quantum numbers v, J'. At slightly less than 1 nsec, the radiative decay lifetimes of these states are a few times shorter than the laser pulsewidths used. A tunable visible (green) pulse of light at $\omega_2/2$, synchronized with the XUV (ω_1) pulse, induces the 2p → ns,nd transition. Figure 1 also contains a curve which schematically represents the presence of resonant levels with n = 4,5. The total density of (n, v, J) states in this region is rather large. But only three values of final-state angular momentum are allowed by the $\Delta J = 0, \pm 1$ selection rule, making the spectrum much sparser. Also, poor wave-function overlap (small Franck-Condon factors) may weaken many transitions to the point of invisibility.

An important ingredient in our scheme is the presence of a large flux of near UV photons which ionize atoms or molecules in states with $n \geq 2$. In this particular setup, which was also used to study ion-pair ($H^+ + H^-$) production,[21] two colors of near UV light were present: a beam at $\omega_1/3$, used to generate ω_1 by frequency tripling, and the scanned beam at $\omega_2 > \omega_1/3$, sufficiently energetic to reach from the B/C state to the ion-pair continuum at ~ 139000 cm^{-1}. Either of these near-UV beams, which caused nonresonant ionizing transitions, would have been sufficient for the experiment we describe here. When $\omega_2/2$ is not tuned to a resonance, the most intense ion signal observed is the H_2^+ continuum. H^+ and H^- signals occur via the ion-pair continuum, which is reached by ω_2 but not by $\omega_1/3$. Also, H^+ can be generated by photodissociation of H_2^+; this could be the major source of the H^+

continuum. All of these ion signals change in magnitude when $\omega_2/2$ is tuned to a n = 4,5 resonance at ~ 122000 cm^{-1}. A large H^+ signal is created by the near UV ionization of H_2^* (n = 4) or its predissociation product H^* (n = 2). [Although not shown in Fig. 1, the $H + H^+ + e^-$ threshold at ~ 146000 cm^{-1} is reached by the near UV excitation of H (n = 1) + H^* (n = 2), or the dissociative ionization of H_2^* (n = 4).] The population in the H_2 (n = 2) state, the precursor of the H_2^+ and H^- signals, is also diminished by the $\omega_2/2$ resonance. Dips in the H_2^+ and H^- ion signals are correlated with peaks in the H^+ signal. The important advantage of this experiment is that all $\omega_2/2$ resonances, predissociative or not, lead to H^+ signals, which are superimposed on a much weaker background. There are no levels which are invisible, as in the case of emission spectroscopy. This scheme has previously been used by Rottke and Welge,[22] but they did not have the ability to create populations in the C state. Also, they did not attempt to explore the "no man's land" well below the IP, but concentrated on the Rydberg states with higher n.

III. Experimental

Our setup has already been briefly described.[21] A forthcoming publication[23] will provide details of the continuously-tunable XUV source. Figure 2 is a sketch of the vacuum chamber's internal components. Basically, the apparatus was an ion extractor in a vacuum chamber with entry ports for laser and molecular beams. The H_2 was supplied by a Lasertechnics pulsed valve enclosed in a differentially pumped region with a skimmer. Upon being skimmed, the beam passed into the 10^{-6} torr experimental chamber and between the ion-extractor

plates. The pulsed nature of the experiment allowed time-of-flight mass spectrometry, with ion flight times varying as $\sqrt{M}$. The quadrupole mass filter was adjusted to act as an ion guide. Ions of either polarity could be chosen for extraction and detection by the Johnston electron multiplier, which was enclosed in the differentially-pumped flight tube at $< 10^{-8}$ torr.

On its way to the ion-extraction/molecular beam intersection, the $\omega_1/3$ (near UV ~ 290 nm) beam came to a focus in a pulsed free jet[24] of CO, an efficient gas for tripling at that wavelength.[23] A conversion efficiency from near UV to XUV of ~ 10^{-6} was probably achieved; this would have made the photon flux ~ 10^{10}/shot. The CO jet, which issued from an NRC pulsed vale, was in its own differentially-pumped portion of the main experimental chamber. The ω_2, $\omega_2/2$ beam entered at right angles to the ω_1, $\omega_1/3$ beam, and antiparallel to the H_2 beam. All laser beams had parallel polarizations except for $\omega_2/2$, whose electric vector was perpendicular to the other three. We did not vary the polarizations in this experiment.

We used standard Nd:YAG lasers to pump Rhodamine 610 and Fluorescein 548 dye lasers ($\omega_1/6$ and $\omega_2/2$, respectively). After frequency doubling, pulse energies were about 10 mj in each of the near UV ($\omega_1/3$ and ω_2) wavelengths. Severe losses in the UV-coated dielectric mirrors reduced the $\omega_2/2$ energy to a few tenths of a millijoule; this was no handicap, because the observed transitions were strong. Spot sizes at the ion extractor were ~ 10 mm^2. Synchronization of the ~ 5 nsec pulses was maintained with cable-adjusted trigger pulse delays and photodiodes monitoring the visible dye laser light. Resolutions in the XUV and visible beams were about

1.5 and 0.3 cm^{-1}, respectively. XUV wavelength calibration was done with the B ← X and C ← X transition frequency tables of Dabrowski and Herzberg.[4] We used an argon-filled voltage-regulator tube for optogalvanic calibration of the visible (scanning) laser frequency. Our overall accuracy is to within 1 cm^{-1} in the computation of the total (XUV + visible) energy.

Points to note are these: 1. The widely tunable, windowless XUV system gives access to many intermediate states in the double resonance. 2. Mass-resolved H^+ ion detection allows selective probing of resonant states near 122000 cm^{-1}.

IV. Results

Figure 3 shows the behavior of each of the three ion signals, H^-, H_2^+, and H^+, as a function of $\omega_2/2 \sim 18000$ cm^{-1}. In this series of spectra the intermediate state $2p\pi\ ^1\Pi_u$ C (v = 2, J' = 1) was prepared via the C ← X (2,0) Q(1) transition from the X (V = 0, J" = 1) ground state. (In the standard notation for the transition, the electronic states are given, then the final and initial vibrational quantum numbers, and finally the rotational branch of the initial angular momentum state.) Both positive ion signals, H_2^+ and H^+, were recorded simultaneously. In all three spectra, the baseline represents zero signal. The intense H^+ signals are clearly correlated with dips in the H_2^+ and H^- continua, the result of depopulating the C (intermediate) state. The small H^- peak below the H^- threshold is due to three-photon (XUV + visible + near UV) ion-pair production as opposed to the normal (XUV + near UV) process. Filtering out the visible light eliminated this small peak and all sharp features in the H^+, H_2^+ spectra. Our

previous publication[21] presented a similar H^- spectrum, obtained with $\omega_2/2$ filtered out. (Much more unpublished H^- data may be had upon request.[25])

We studied the (ω_2, $\omega_2/2$) power dependence of the H^+ features at 18142 and 18159 cm^{-1}. Our observation was that the sharper peak exhibited saturation broadening of the linewidth, and grew much more slowly in amplitude with increasing power than did the broad peak. All spectra shown here were recorded with full power. The sharp dip in the H_2^+ signal at 18159 cm^{-1} has an amplitude of 48 ± 2% with respect to the continuum, while the broad dip is only ~ 14%. Evidently the behavior at the sharp transition mimics that of a saturated two-level system with a homogeneous linewidth less than the laser linewidth. If the upper and lower levels were only weakly depleted by ionization and predissociation, complete saturation would equalize the populations in the two levels, causing a 50% dip in the lower (C state) level's population. This is almost exactly what is observed. The presence of a larger dip would imply that the upper state experienced irreversible decay during the time of the laser pulse. In this case, such decays include not only predissociation and ionization, but in addition fluorescence to levels with u symmetry. Evidently the upper-state lifetime is at least a few times the laser pulsewidth, or a few tens of nsec. This is in excellent agreement with the measured spontaneous emission lifetimes of some 3d states of H_2,[10-12] which are in the 20-100 nsec range. The broad peak, with a linewidth of 5 cm^{-1}, did not show signs of saturation. The corresponding homogeneous lifetime is thus ~ 1 psec, which is too short for detection with emission spectroscopy or measurement by techniques like the Hanle effect. This

short lifetime is presumably due to predissociation into H (n = 1) + H^* (n = 2).

Our two-level model of the sharp transition, which ignores decay, is justified a posteriori by noting that the photoionization cross section from the C levels is probably not too different from the B (v = 0,3) state value of ~ 10^{-18} cm^2.[26] The UV photon flux, on the order of $10^{17}/cm^2$, thus did not affect the population distribution between the upper and lower levels significantly, because the product of photon flux and absorption cross section was only ~ 0.1. More extensive measurements would warrant a more ambitious theoretical treatment including predissociation, upper- and lower-state fluorescence, ionization from both states, and the upper-state H^+/H_2^+ branching ratio. The fact that the photoionization cross sections are not known prohibits a quantitative analysis of the ion yields observed in the H^+, H_2^+ spectra.

In Figure 4 the major results of our experiment are presented. Several intermediate states in the H_2 2p manifold were used in obtaining the H^+ spectra, which are plotted as a function of total energy ($E''_{rot} + \omega_1 + \omega_2/2$) above the X (v = 0, J" = 0) ground state. E''_{rot} is the initial rotational energy BJ"(J" + 1). With the spectra thus arranged, transitions to a common upper state appear vertically aligned. For example, to within our frequency calibration accuracy, coincidences in energy occur between peaks c and ℓ; e and n; and j and p. the vertical scale represents the observed signal levels, with no change in sensitivity between the different bands. We did not normalize these signals to the intermediate-state H_2^* (B/C) population or to the $\omega_2/2$ power, which varied only a factor of two or so across

the spectra.

All of the spectra show a weak H^+ continuum; with B (v = 12) as the intermediate state, no peaks are cleanly observed. With C (v = 2) as the intermediate state, many intense peaks are seen which can be sorted into two categories: "sharp" and "broad". The sharp peaks (b, d, e, g, n, o) have widths of 2-3 cm^{-1}, which is slightly larger than the laser bandwidth; their widths are partly due to saturation. On the other hand, the broad peaks are definitely homogeneously broadened, with widths ~ 10 cm^{-1}. Several of the peaks (i, most noticeably) are slightly asymmetric, indicating a weak interference between the transitions to discrete and continuum states.[27] An H^+ signal is present even with laser 2 turned off; the observed continuum is only partially due to $\omega_2/2$. When two peaks appear close together, it sometimes happens (a and b; h and i) that the steep sides face each other. This interesting effect deserves further experimental study, and theoretical analysis with multichannel quantum defect theory.

The variation in predissociation lifetime between the "sharp" and "broad" states is extreme. As discussed earlier in this section, the lifetime of the level responsible for peak d is at least in the tens of nsec. On the other hand, peak m has a breadth of 22 cm^{-1}, with an associated lifetime of ~ 250 fsec. The ratio of the lifetimes of the sharp and broad states is about 10^5!

V. Discussion

A. Cross Sections

In assigning the transitions we should be able to explain in a simple way the intensity level which is characteristic of the peaks in

the H^+ spectra. There is no completely straightforward way to reckon the intensities. However, it is possible to compare the intensities of the competing ion-producing transitions from the C state, which are (1) near UV ionization to produce H_2^+ and (2) visible excitation to a state which ultimately produces H^+. If the cross section of one of these processes is known, the other can be determined. The most reliable method is probably to use Fig. 3 to compare the amplitude of the H_2^+ continuum with the depths of the dips. For this purpose, the broad dip (also seen as "c" in Fig. 4) is the best because its shape is not affected by saturation. First, the UV photoionization cross section from the C state can be delimited by noting that the $H_2^+ \leftarrow C$ transition has better wave-function overlap (larger Franck-Condon factors) than the $H_2^+ \leftarrow B$ transition, whose cross section is $\sim 10^{-18}$ cm^2 [26] at 266 nm. A reasonable upper bound for the $H_2^+ \leftarrow C$ transition cross section is the typical photoionization value of $\sim 10^{-17}$ cm^2.[28] Thus the H_2^+ continuum cross section is 10^{-18}–10^{-17} cm^2. The ratio of the UV to visible power was on the order of 50, and the dip's amplitude was 14%. The estimate of the visible cross section is then (50)(.14) times larger, or $\sim 10^{-17}$–10^{-16} cm^2. An estimate of the oscillator strength f of the transition causing the dip comes from the relation[28] $f = 1.13 \times 10^{12} \int \sigma(\nu)d\nu$, in which σ has the units of cm^2 and ν is in cm^{-1}. This puts the value of f within about half an order of magnitude of 10^{-3}. Compared with integrated oscillator strengths of ~ 0.1 for the $3d \rightarrow 2p$ spontaneous emission lifetimes of $\sim$ 30 nsec, this is relatively weak. But this is a reasonable value when the possibility of a small Franck-Condon factor between C ($v = 2$) and the as-yet unidentified upper state is taken into account. In fact, the lack of

distinguishable peaks in the B (v = 12) intermediate state H^+ spectra must be due to greatly diminished Franck-Condon factors for a transition from a v = 12 state to a Rydberg-like state with a much smaller value of v.

B. Selection Rules

Before proceeding with detailed assignments of the transitions, we describe the selection rules for the optical excitation and predissociation of the upper states. These rules are of profound importance in determining the structure of the spectra, and are discussed in standard texts.[20,29] The upper states reached with the $\omega_2/2$ (visible) light are described with the complete label $n\ell\lambda^s\Lambda_g^s(v,J)$. n, v, and J are the principal, vibrational, and rotational quantum numbers. ℓ is the electronic orbital angular momentum quantum number, and $\lambda \leq \ell$ is its projection on the internuclear axis. In this case, we are only considering one-electron excitations, and the unexcited electron remains in the $1s\sigma$ state. Then the symmetry species Λ (Σ, Π, Δ, ...) is the same as λ (σ, π, δ, ...). The superscript s (+ or -) describes the oddness or evenness of the electronic wavefunction when the electrons are reflected through a plane containing the nuclei. In H_2, Σ^- functions do not exist because the σ orbital inherently possesses (+) symmetry. If we were considering an atom, the electronic function $|\lambda\rangle$ would have an axial dependence $\exp(i\lambda\phi)$. For a diatomic molecule, the label $\lambda^{\pm}$ describes the function with definite reflection symmetry $1/\sqrt{2}(|\lambda\rangle \pm |-\lambda\rangle)$, which varies as $\cos\lambda\phi$ or $\sin\lambda\phi$. The plane about which ϕ is measured can be defined because $\bar{J}$ and the internuclear axis provide reference axes. As usual, the total angular momentum J is larger than the projection Λ.

To understand the parity of the overall molecular wavefunction, the nuclear (vibrational and rotational) and electronic wavefunctions can be considered separately; their product is the total wavefunction. The nuclear spin function's parity can be ignored because no spin flips occur in this experiment. But anticipating the need to consider allowed final states in different angular momentum coupling cases, it is useful to keep in mind that the para (total nuclear spin of zero) modification is always associated with even values of the core angular momentum, and the ortho (total spin one) states belong with odd core angular momenta.

The parity of the overall wavefunction does not depend on the vibrational quantum number v; the vibrational function only depends on the internuclear separation and has even parity. The parity of the rotational wavefunction is $(-1)^J$. The parity of the electron function Λ^S is s. (Formally, our use of the word "parity" in describing the electronic functions is wrong, because their properties are not defined with respect to inversion through the origin. But a rotation of all particles by π about an axis perpendicular to the internuclear axis, does not change the electronic functions because they are defined with respect to the relative positions of electrons and nuclei. s describes the reflection symmetry about a plane containing the internuclear axis. Carrying out the rotation and reflection symmetry operations in succession is equivalent to a true inversion.) For the purpose of considering electronic transitions, the relevant parity is determined by the electronic and rotational functions: it is $s(-1)^J$ for a $\Lambda^S(v,J)$ state. During an electric dipole transition, the usual rules apply: $\Delta J = 0, \pm 1$ but $J = 0 \not\leftrightarrow J = 0$, and $\Delta\Lambda = 0, \pm 1$. The parity change requires

that either s or J changes: thus in P ($\Delta J = -1$) and R ($\Delta J = 1$) transitions, s does not change ($+ \leftrightarrow +$ and $- \leftrightarrow -$), but in Q ($\Delta J = 0$) transitions, $+ \leftrightarrow -$. With the "atomic orbital" representation we are using, the rule $\Delta \ell = \pm 1$ also applies; the 2p nature of the B and C (intermediate) states means that only s and d final states are accessible.

The predissociation selection rules are considerably simpler than their electric dipole counterparts. In the absence of external fields, the total energy, angular momentum J, parity (g/u), and electronic parity s are conserved. Depending on the mechanism of predissociation, ℓ and Λ may not be conserved.[29]

C. ℓ Uncoupling

For low values of n (below 3), the excited electron is still close to, and following, the nuclei in the H_2^+ core. The projection quantum number Λ ($= \lambda$) is well defined, but for a given J, the $\Lambda^{\pm}$ components are slightly split by the interaction of the nuclear and electronic angular momenta, a phenomenon known as "lambda doubling". "ℓ uncoupling" occurs between $n \sim 3$ and $n \sim 10$, above which the Λ components of a state with defined J and ℓ are heavily mixed. The electron appears to be basically ignorant of the core's asymmetry. The preferred basis then employs N^+, the H_2^+ core rotational quantum number, instead of Λ, to describe the angular momenta. In spite of the fact that the different Λ levels lose their identity, the reflection symmetry s (+ or −) is still a "good" quantum number. In the representation $|J,N^+\rangle$, the $\Lambda^{\pm}$ components belong to different values of N^+ and are widely separated in energy. A correlation diagram describing this transition from "Hund's case (b)" to "Hund's case (d)"

is given by Eyler and Pipkin.[14] We have reproduced it here as Fig. 5, with a notation consistent with the rest of the text. The construction of this diagram is straightforward: the connection between $|J,\Lambda^s\rangle$ and $|J,N^+\rangle$ is made by following simple rules. First, the nuclear spin state (para or ortho) is the same in both cases (b) and (d). Second, the total angular momentum J is conserved. Third, the noncrossing rule is obeyed: lines leading from $|J,\Lambda^s\rangle$ states with the same J and s cannot cross. Starting at the bottom of the case (d) side of the diagram, lines are drawn from the $|J,N^+\rangle$ states to the lowest $|J,\Lambda\rangle$ states fulfilling the symmetry requirements. In case (b), the rotational energy $BJ(J + 1)$ is measured with respect to the origin of each Λ state. In case (d), the rotational energy is, analogously, $BN^+(N^+ + 1)$.

Unfortunately, this diagram is more for illustration than practical employment, because in the medium-n "no man's land", the behavior is between cases (b) and (d). The rotational levels have separations roughly comparable with those between states of different Λ. Neither the rotational nor the electronic energy may be considered as a perturbation to the other. Energy levels are found by diagonalization of the complete Hamiltonian. Yet another problem is that even in case (b), the relative position of the Σ, Π, and Δ levels is a function of the vibrational quantum number. With different electron densities at the core, the different Λ^s states have different bond stretching force constants and different vibrational frequencies. Also, the anisotropy of the core increases with v, because the average internuclear separation increases with vibration due to anharmonicity. The increase in anisotropy creates a larger orienting force on the orbiting Rydberg

electron, and the tendency toward ℓ uncoupling is decreased. The degree of ℓ uncoupling is a function of all the variables n, Λ, v, and J. Our diagram is mostly useful for illustration of the limiting behavior at high and low n. To find accurate level positions, perturbations from different (n,v) states must be included, as well as the effects s-d wavefunction mixing. These perturbations from different electronic states vanish in a truly central (hydrogenic) potential.

D. Predissociation

All the aforementioned rules result in the following experimental scenario: The visible light excites a transition from $C(2p\pi\Pi_u^+)$ to $ns\sigma\Sigma_g^+$ or $nd\lambda\Lambda_g$ ($\lambda = \sigma, \pi, \delta$; $\Lambda = \Sigma^+, \Pi^\pm, \Delta^\pm$). The p → d transition has larger matrix elements[30] and is much more probable. Λ^+ components mix among themselves, as do Λ^- components. Energy levels do not follow a simple pattern. Predissociation occurs rapidly for levels of one s (+/-) electronic symmetry, and undetectably for the other. As a result, "broad" and "sharp" lines occur in the spectrum. In this case, the electronic states that cause predissociation would most likely be G, K, which have + symmetry. The I $\Pi^\pm$ state could predissociate states of both symmetries, but that is not what our spectra appear to suggest, since very sharp lines are observed. Eyler and Pipkin have noted in their study of n = 4 triplets[14] that only the Λ^+ states above the H (n = 1) + H (n = 2) threshold are predissociated, but the Λ^- states are not. Their assignments of the levels and symmetries are confirmed by theory. Although several mistakes were made in assignment, Dieke's ambitious list[2] includes few Λ^+ levels above 120000 cm^{-1}. In our assignments, we have embraced the heretofore uncontradicted notion that

"sharp" lines belong with Λ^- levels, and "broad" lines with Λ^+ levels.

E. Assignments

Table I is a list of the observed lines including each intermediate state's symmetry designation, the visible transition frequency, the total energy of the final state, the FWHM linewidth, and our assignment. Assignments are subject to change when more data are available.

Working from the top down in Fig. 4, we begin with the H^+ spectrum obtained with the C $2p\pi^-$ $\Pi_u^-(v = 2, J' = 1)$ intermediate state. Five features of roughly equal strength are apparent, and three are sharp. The sharp lines can only come from a Λ^- state, as has just been discussed. Since there are no s orbital Σ^- states, this rules out the ns ← 2p transition. Therefore these lines belong to an nd ← 2p manifold. The allowed final states are $d\sigma^+$ $\Sigma^+(J = 1)$, $d\pi^+$ $\Pi^+(J = 1)$, $d\pi^-$ $\Pi^-(J = 2)$, and $d\delta^-$ $\Delta^-(J = 2)$, where the rule "J must change or s must change" has been applied. There is a remarkable spectroscopic regularity: the pairs of peaks (a,b) and (c,d) both have separations of 17 cm^{-1}. Also, more sharp peaks are present (three) than are predicted [only two: $\Pi^-(J = 2)$ and $\Delta^-(J = 2)$]. These pairs of sharp and broad peaks must belong to different (n,v) combinations. Thus it is necessary to determine what d-electron states have (n,v) levels in the 121600-122100 cm^{-1} range. This is not a trivial matter because the vibrational characteristics of the states in this region are not easy to predict, especially near the dissociation limit. For example, the n = 3 I state does not have an accurately-determined potential energy curve. Also, around n ~ 4-5, increasing n by one unit gives about the same energy change (~ 2000 cm^{-1}) as does increasing v by one unit. But

it is still possible to narrow the (n,v) field considerably. We note that $n \geq 3$ for a d electron, and by using the Rydberg formula $E(n) = IP - Ry/n^2$, eliminate $n \geq 7$ because the energy is too high. (IP ~ 124500 cm^{-1}, and the quantum defect need not be considered in this case -- it is near zero for a d electron.) It is also possible to estimate the positions of the vibrational levels. Quadrelli and Dressler[16] have provided approximate frequency (ω_e) and anharmonicity ($\omega_e x_e$) values for the $n = 3$ I Π_g^- and J Δ_g^- states of d electrons. For the Π states these are 2242 and 65 cm^{-1}, respectively, while for the Δ states they are 2347 and 67 cm^{-1}. The values for the H_2^+ ion ($n \to \infty$) are in between: $\omega_e = 2321$ cm^{-1} and $\omega_e x_e = 66$ cm^{-1}. Plausible (n,v) combinations are ($n = 3$, $v = 6$), ($n = 4$, $v = 2$), ($n = 5$, $v = 1$) and ($n = 6$, $v = 0$). We consider the middle two possibilities to be the most likely for two reasons.

First, a <u>rough</u> rationalization of the nearly-equal intensities of the (a,b) and (c,d) pairs induces us to choose final states with roughly similar Franck-Condon factors. It has been shown in a study of the H_2^+ X ← H_2 C transition that $\Delta v = 0, \pm 1$ transitions are strongly favored when the initial state has $v \leq 2$.[31] The similarity between the H_2^+ and $n \sim 5$ Rydberg potential curves leads us to expect similar behavior. Considering the isoenergetic (n,v) choices, with the favorable Franck-Condon factors for low v values comes an increase in n, and a decrease in the 2p → nd electric dipole matrix element. Relative intensity calculations for the four (n,v) combinations above can be done by multiplying the Franck-Condon factors of Pratt[31] by the squared dipole moments of Condon and Shortley.[30] The results, again in order of increasing n, are 1.5×10^{-3}, 1, 0.06, and 7×10^{-6}. The ($n =$

4, v = 2) and (n = 5, v = 1) intensities differ by a factor of 16, but are the closest of any pair.

A second, even more convincing reason to vote for (n = 4, v = 2) is that this level has been observed in the triplet manifold.[14] It has been shown for the 3d state that the $J\delta^- \ ^1\Delta_g^-$ and $j\delta^- \ ^3\Delta_g^-$ levels are only 12 cm^{-1} apart.[19] In the δ state, the d electron has very little contact with the core electron, so the energy does not depend much on the relative orientation of the spins. (This is true for the Δ, but not the Π and Σ states, which have greater core overlaps.) The coincidence of the potential curves should be even closer when n is increased and the electrons are even further apart. Eyler and Pipkin[14] found the (n = 4, v = 2) $^3\Delta^-$(J = 2) state at a total energy of 122042.6 cm^{-1}. (We have computed this energy by using the $2p^3\Pi$ energy of Dieke,[2] as recalibrated by Miller and Freund.[32] Eyler and Pipkin observed a visible transition from this triplet lower level in an experiment conceptually similar to ours, which used the singlet analog.) To within our accuracy, this is exactly the same location as the sharp peaks e and n. We therefore assign peak e (and n) to the upper state $4d\delta^-\Delta^-$(v = 2, J = 2). This "vertical" (Δv = 0) transition is nearly as strong as any others in our H^+ spectra, and was earlier estimated to be the strongest of the four (n,v) alternatives.

With the (n = 4, v = 2) Δ^-(J = 2) state as a benchmark, assignment of the rest of the features in the $C\Pi^-$(v = 2, J' = 1) H^+ spectrum is less difficult. First, we note that the Π levels (for a given J) are a few hundred cm^{-1} below the Δ levels, and that the Σ^+ levels are similarly a few hundred cm^{-1} below the Π levels.[2] The Λ splitting is due to the fact that the electrons with lower orbital angular momentum

projection quantum numbers λ (= Λ) have greater electron densities near the core, and lower energies. Second, we recall that $\Pi^{\pm}$ states should appear in the spectrum. So we assign the broad/sharp pairs as $\Pi^{+}(J = 1)/\Pi^{-}(J = 2)$ states of different (n,v) bands. The $\Sigma^{+}(J = 1)$ states are evidently too low in energy to be seen on our scale. [We have truncated the spectra; no peaks are detected down to 121400 cm^{-1} in the $C\Pi^{-}(v = 2, J' = 1)$ spectrum or down to 121500 cm^{-1} in the $C\Pi^{+}(v = 2, J' = 1)/B\Sigma^{+}(v = 12, J' = 3)$ spectrum.] Use of the Rydberg formula, and H_2^+ vibrational constants, allows us to estimate the relative positions of the (n,v) levels. With respect to (n = 4, v = 2), (n = 6, v = 0) is 503 cm^{-1} to the red, and (n = 5, v = 1) is 346 cm^{-1} to the blue. The observed separation of ~ 150 cm^{-1} between the (a,b) and (c,d) pairs fits the latter possibility better. Also, the transition to (n = 6, v = 0) is supposed to be several orders of magnitude weaker. Given the approximate nature of our line position estimate and the likelihood of perturbations (as evidenced by erratic spacings in energy levels observed to date), this is satisfactory agreement. However, the striking similarity in intensity, lineshape and $\Pi^{+}(J = 1)/\Pi^{-}(J = 2)$ splitting (17 cm^{-1}) between the (a,b) and (c,d) pairs is still puzzling. This 17 cm^{-1} splitting is between the values that are expected when the orbital angular momentum is completely coupled to, or decoupled from, the core. In the first case the J = 2 level is at BJ(J + 1) = 180 cm^{-1} rotational energy, since B = 30 cm^{-1}. The J = 1 level is = 120 cm^{-1} below, at = 60 cm^{-1}. When ℓ uncoupling has occurred, the N^{+} = 1,3 states are involved. B is roughly the same, at = 30 cm^{-1}, and the splitting is = 300 cm^{-1}, but now the $\Pi^{+}(J = 1)$ level is <u>higher</u> in energy than the $\Pi^{-}(J = 2)$ level.

The lack of an obvious pattern in the spectra makes assignment of the rest of the transitions less straightforward, and some features will not be assigned. The features in the next spectrum down in Fig. 4 are due to transitions from the C $2p\pi^+$ $\Pi^+(v = 2, J' = 1)$ state. The contribution from the overlapped B(v = 12) state is ignorable, as the bottom two B(v = 12) spectra attest. Possible final states are $\Sigma^+(J = 0)$, $\Sigma^+(J = 2)$, $\Pi^-(J = 1)$, $\Pi^+(J = 2)$, and $\Delta^+(J = 2)$. Of these, $\Delta^+(J = 2)$ should be much higher in energy than $\Delta^-(J = 2)$, and off the energy scale. Also, the Σ states belong to the red of the region we scanned. [But this does not rule out the appearance of (n,v) combinations other than (4,2) and (5,1).] This leaves $\Pi^-(J = 1)$ and $\Pi^+(J = 2)$ states. The only "sharp" (Λ^-) line in this spectrum is g, which we assign as $5d\pi^-\Pi^-(v = 1, J = 1)$, because it is below the analogous $\Pi^+(J = 1)$ component. Further, we assign peak h as $5d\pi^+\Pi^+(v = 1, J = 2)$ and f as $4d\pi^+\Pi^+(v = 2, J = 2)$. This assignment is in accordance with the correlation diagram's prediction. Peaks i and j are left unassigned, but note that j and p coincide in energy.

Next, the $2p\pi^+C\Pi^+(v = 2, J' = 2)$ spectrum gives two coincidences with the $\Pi^-(J' = 1)$ spectrum: (ℓ,c) and (n,e). Allowed final states have $\Lambda^+(J = 1,3)$ and $\Lambda^-(J = 2)$. The sharp peak n is of the latter variety and is the $\Delta^-(J = 2)$ member of the (n = 4, v = 2) band, the first transition assigned. Peak ℓ is broad and corroborates our $\Pi^+(J = 1)$ assignment of peak c. We suggest that feature m is the $\Pi^+(J = 3)$ member of the (n = 4, v = 2) manifold; it is well to the blue of the J = 1,2 features, as it should be. Peak k is unassigned.

The C ← X (2,0) R(2) transition prepares the $\Pi^+(J' = 3)$ intermediate state. Starting with three units of angular momentum, P,

Q, and R transitions can occur to each of the three Λ species (except, with no Σ^- states, there is no $\Sigma^- \leftarrow \Pi^+$ Q branch.) Many lines [e.g. $\Pi^+(J = 1,2)$] should occur, and their lack is puzzling; some are probably outside our energy region. However, the $\Pi^-(J = 3)$ line should be visible; this is the assignment of peak o, in the $(n = 4, v = 2)$ group. Peak p lines up with peak j. $J = 2$ is the only final state angular momentum both peaks could belong to, because they were reached by $\Delta J = \pm 1$ transitions from states with $J' = 1$ and $J' = 3$. According to the selection rules, we label these peaks as $\Lambda^+(J = 2)$, and leave (n,v) undetermined.

F. Future Studies

We have demonstrated a technique for penetrating the manifold of H_2 states above 122 000 cm^{-1}. There are many avenues for increasing the amount of useful data. A first step would be to employ more intermediate states and scan $\omega_2/2$ over a much wider frequency range. This would make the list of assigned levels much more comprehensive. Accurate cross section measurements can give improved values for oscillator strengths of the observed transitions. Also, collecting data with different relative polarizations in the ω_1 and $\omega_2/2$ beams[22] would give additional insight concerning the propensities to form final states with different angular momenta.

It should be possible with our technique to find the different levels of the double-minimum $H,\overline{H}$ state. ($\overline{H}$ is slightly to the right of the region covered by Fig. 1.) For this purpose it would be advantageous to use high vibrational levels in the B state, in order to maximize the Franck-Condon overlap. Our XUV source, which is tunable to above 110000 cm^{-1},[23] is capable of reaching $B(v = 19)$. The outer

classical turning points of B states in this region are at ~ 4 Å, which is also where some H vibrational states have their inner classical turning points. Even if the transitions had very small oscillator strengths, the use of a powerful visible dye laser would give good pumping efficiency.

Even further selectivity in the detection of the H(1s) + $H^*(2\ell)$ predissociation products could be had by probing $H^*(2\ell)$ via the $H^+ + e^-$ ← $H(n = 3)$ ← $H^*(2\ell)$ scheme. The different Λ components of the final states have different probabilities to produce 2s or 2p atoms upon predissociation.

Finally, the study of the isotopic variants of H_2 would be most illuminating. In particular, the HD molecule has different symmetry properties and ought to display somewhat different dynamics as a result. "g" and "u" states are slightly mixed, and more predissociation channels become available.

VI. Conclusion

We have reported preliminary results concerning the energy levels of the simplest molecule. These levels are labeled with particular values of J, ℓ, and Λ, and some have not been observed before. The effect of the electronic wavefunction's symmetry on the predissociation rate is decisive and strikingly apparent. Our spectra encompass transitions to states whose lifetimes apparently vary by about five orders of magnitude, from hundreds of fsec to tens of nsec. Detection of the predissociation products guaranteed that the short-lived states did not go undetected.

The technique we have employed is generally applicable to other

molecules requiring XUV excitation to reach the lower states (F_2, for example). A great deal of progress in understanding the level structure and dynamics in the complex and congested middle regions (n ~ 3-10) of a molecule's electronic manifold will result from the diligent application of our method.

References

1. O. W. Richardson, Molecular Hydrogen and Its Spectrum (Yale Univ. Press, New Haven, 1934).
2. H. M. Crosswhite, ed., The Hydrogen Molecule Wavelength Tables of Gerhard Heinrich Dieke (Wiley-Interscience, New York, 1972).
3. T. Sharp, At. Data 2, 119 (1971).
4. I. Dabrowski and G. Herzberg, Can. J. Phys. 52, 1110 (1974).
5. G. Herzberg and Ch. Jungen, J. Mol. Spectrosc. 41, 425 (1972).
6. M. Rothschild, H. Egger, R. T. Hawkins, J. Bokor, H. Pummer, and C. K. Rhodes, Phys. Rev. A 23, 206 (1981).
7. M. Glass-Maujean, J. Breton, and P. M. Guyon, Chem. Phys. Lett. 63, 591 (1979).
8. P. M. Dehmer and W. A. Chupka, J. Chem. Phys. 65, 2243 (1976).
9. Ch. Jungen, Phys. Rev. Lett. 53, 2394 (1984).
10. R. L. Day, R. J. Anderson, and F. A. Sharpton, J. Chem. Phys. 71, 3683 (1979).
11. J. van der Linde and F. W. Dalby, Can. J. Phys. 50, 287 (1972).
12. C. W. T. Chien, F. W. Dalby, and J. van der Linde, Can. J. Phys. 56, 827 (1978).
13. E. E. Eyler and F. M. Pipkin, J. Chem. Phys. 77, 5315 (1982).
14. E. E. Eyler and F. M. Pipkin, Phys. Rev. A 27, 2462 (1983).
15. E. E. Marinero, R. Vasudev, and R. N. Zare, J. Chem. Phys. 78, 692 (1983).
16. P. Quadrelli and K. Dressler, J. Mol. Spectrosc. 86, 316 (1981).
17. L. Wolniewicz and K. Dressler, J. Mol. Spectrosc. 77, 286 (1979).
18. L. Wolniewicz and K. Dressler, J. Chem. Phys. 82, 3292 (1985).
19. J. Rychlewski, J. Mol. Spectrosc. 104, 253 (1984).

20. G. Herzberg, Molecular Spectra and Molecular Structure. I. Spectra of Diatomic Molecules (Van Nostrand Reinhold, New York, 1950).

21. A. H. Kung, R. H. Page, R. J. Larkin, Y. R. Shen, and Y. T. Lee, Phys. Rev. Lett. 56, 328 (1986).

22. H. Rottke and K. Welge, J. Phys. (Paris), Colloq. 46, C1-127 (1985).

23. R. H. Page, R. J. Larkin, A. H. Kung, Y. R. Shen, and Y. T. Lee, to be published.

24. C. T. Rettner, E. E. Marinero, R. N. Zare, and A. H. Kung, J. Phys. Chem. 88, 4459 (1984).

25. R. H. Page, Ph.D. Thesis, Univ. of California, Berkeley, 1987.

26. W. Meier, H. Rottke, H. Zacharias, and K. H. Welge, J. Chem. Phys. 83, 4360 (1985).

27. U. Fano, Phys. Rev. 124, 1866 (1961).

28. J. Berkowitz, Photoabsorption, Photoionization, and Photoelectron Spectroscopy (Academic Press, New York, 1979).

29. H. Lefebvre-Brion and R. W. Field, Perturbations in the Spectra of Diatomic Molecules (Academic Press, Orlando, 1986).

30. E. U. Condon and G. H. Shortley, The Theory of Atomic Spectra (Cambridge Univ. Press., London, 1959).

31. S. T. Pratt, P. M. Dehmer, and J. L. Dehmer, Chem. Phys. Lett. 105, 28 (1984); J. Chem. Phys. 85, 3379 (1986).

32. T. A. Miller and R. S. Freund, J. Chem. Phys. 61, 2160 (1974).

Table I. Observed double resonance lines.

Intermediate State	peak	visible frequency	final energy	FWHM	assignment $A^s(n,v,J)$
$C\Pi^-(v = 2,J=1)$	a	18003 ± 1 cm^{-1}	121631 ± 1 cm^{-1}	8 cm^{-1}	$\Pi^+(4,2,1)$
	b	18020	121648	3	$\Pi^-(4,2,2)$
	c	18142	121770	5	$\Pi^+(5,1,1)$
	d	18159	121787	3	$\Pi^-(5,1,2)$
	e	18414	122042	2	$\Delta^-(4,2,2)$
$C\Pi^+(v = 2,J = 1)$	f	18039	121667	7	$\Pi^+(4,2,2)$
	g	18105	121733	1.3	$\Pi^-(5,1,1)$
	h	18217	121845	11	$\Pi^+(5,1,2)$
	i	18258	121886	4.5	
	j	18408	122036	5.5	$\Lambda^+(n_i,v_i,2)$
$C\Pi^+(v = 2,J = 2)$	k	18011	121749	8.5	
	ℓ	18031	121769	6	$\Pi^+(5,1,1)$
	m	18246	121984	22	$\Pi^+(4,2,3)$
	n	18303	122041	1.6	$\Delta^-(4,2,2)$
$C\Pi^+(v = 2,J = 3)$	o	17987	121883	1.6	$\Pi^-(4,2,3)$
	p	18140	122036	4	$\Lambda^+(n_i,v_i,2)$

Figure Captions

Fig. 1. XUV-visible double resonance spectroscopic scheme. The XUV photon (ω_1) populates the 2p B $^1\Sigma_u^+$ (v = 12) or 2p C $^1\Pi_u^+$ (v = 2) state. Visible light around 18000 cm^{-1} induces transitions to higher (n,v) states which predissociate to form H (n = 1) + H^* (n = 2). The n = 2 atoms are ionized by the UV ($\omega_1/3$ or ω_2) light present.

Fig. 2. Experimental apparatus for XUV generation and spectroscopy with a molecular beam sample. The second laser beam (not shown) propagates opposite the molecular beam.

Fig. 3. H^-, H_2^+, and H^+ ion signals. H^+ peaks are correlated with dips in the H_2^+ and H^- signals; this reflects the fact that the intermediate-state population is depleted. The sharp dip at 18159 cm^{-1} is saturation broadened.

Fig. 4. Double-resonance H^+ spectra plotted as a function of intermediate state and total upper-state energy. Raw signal levels are shown. Wavenumbers and assignments of the labeled peaks are given in Table I.

Fig. 5. Correlation diagram describing the ℓ-uncoupling transition from Hund's case (b) to case (d).

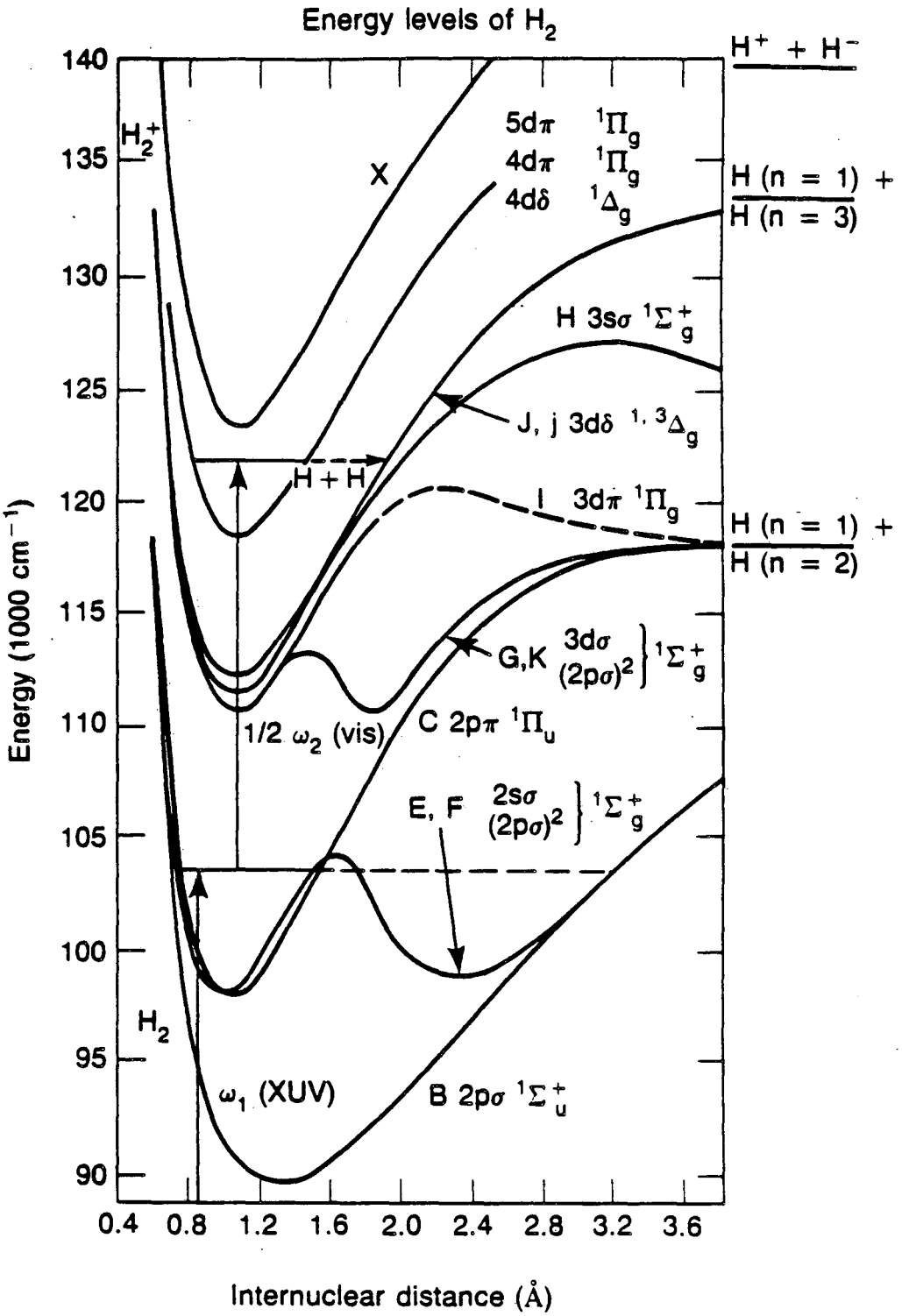

Figure 1.

XBL 872-6194

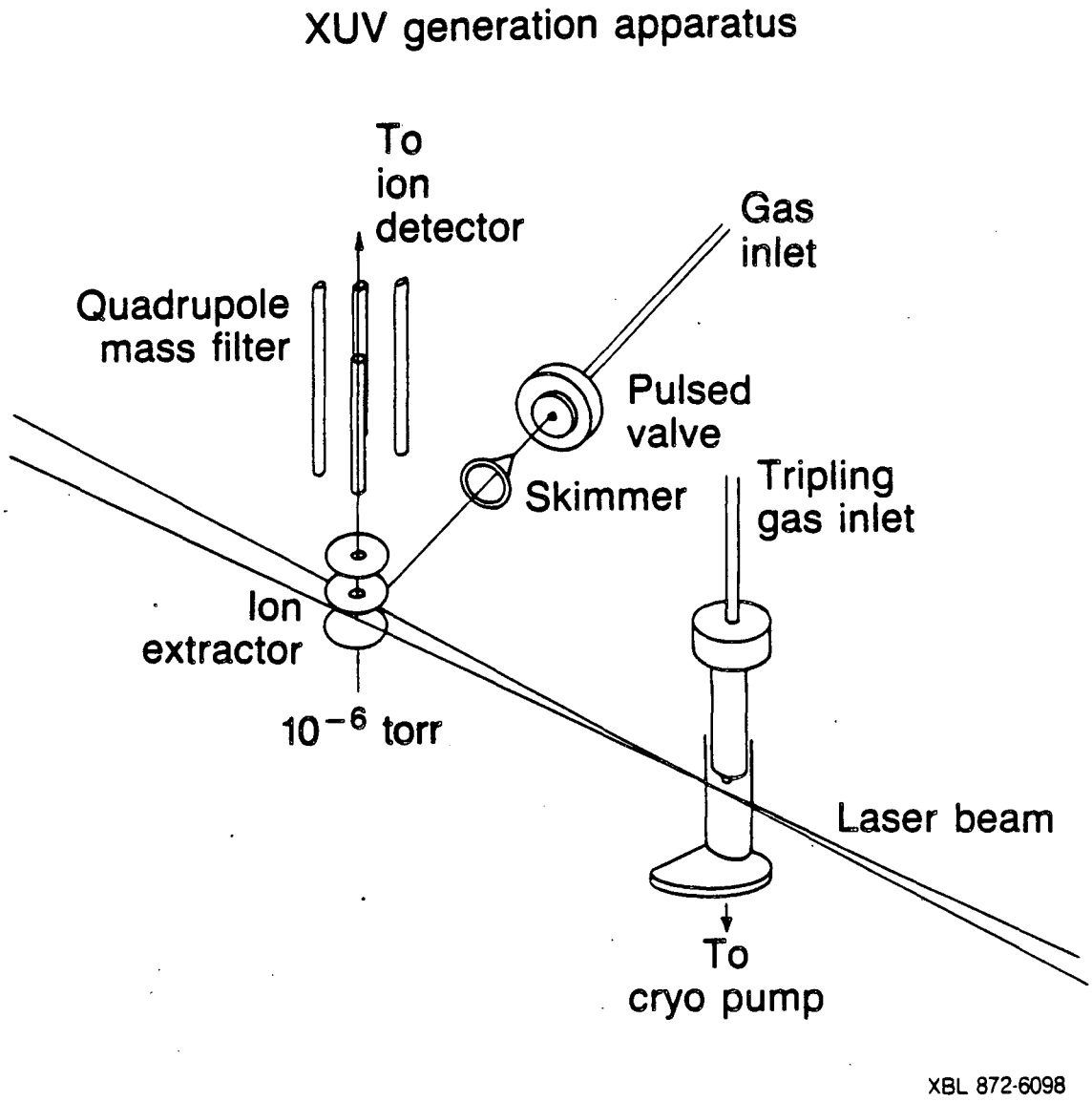
XUV generation apparatus
To
ion
detector
Gas
inlet
Quadrupole
mass filter
Pulsed
valve
Skimmer
Tripling
gas inlet
Ion
extractor
10^{-6} torr
Laser beam
To
cryo pump
XBL 872-6098

Figure 2.

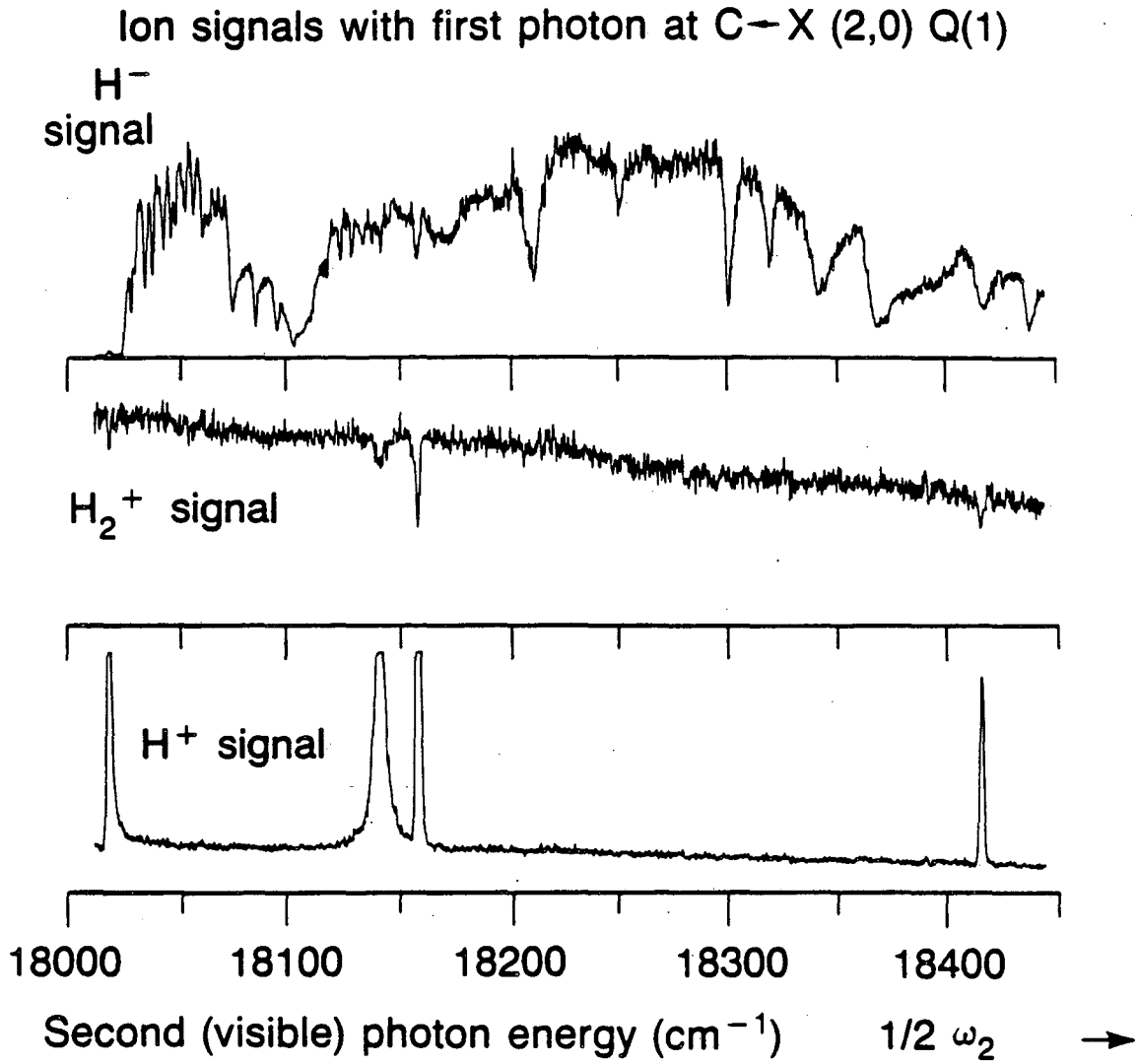

XBL 872-6177

Figure 3.

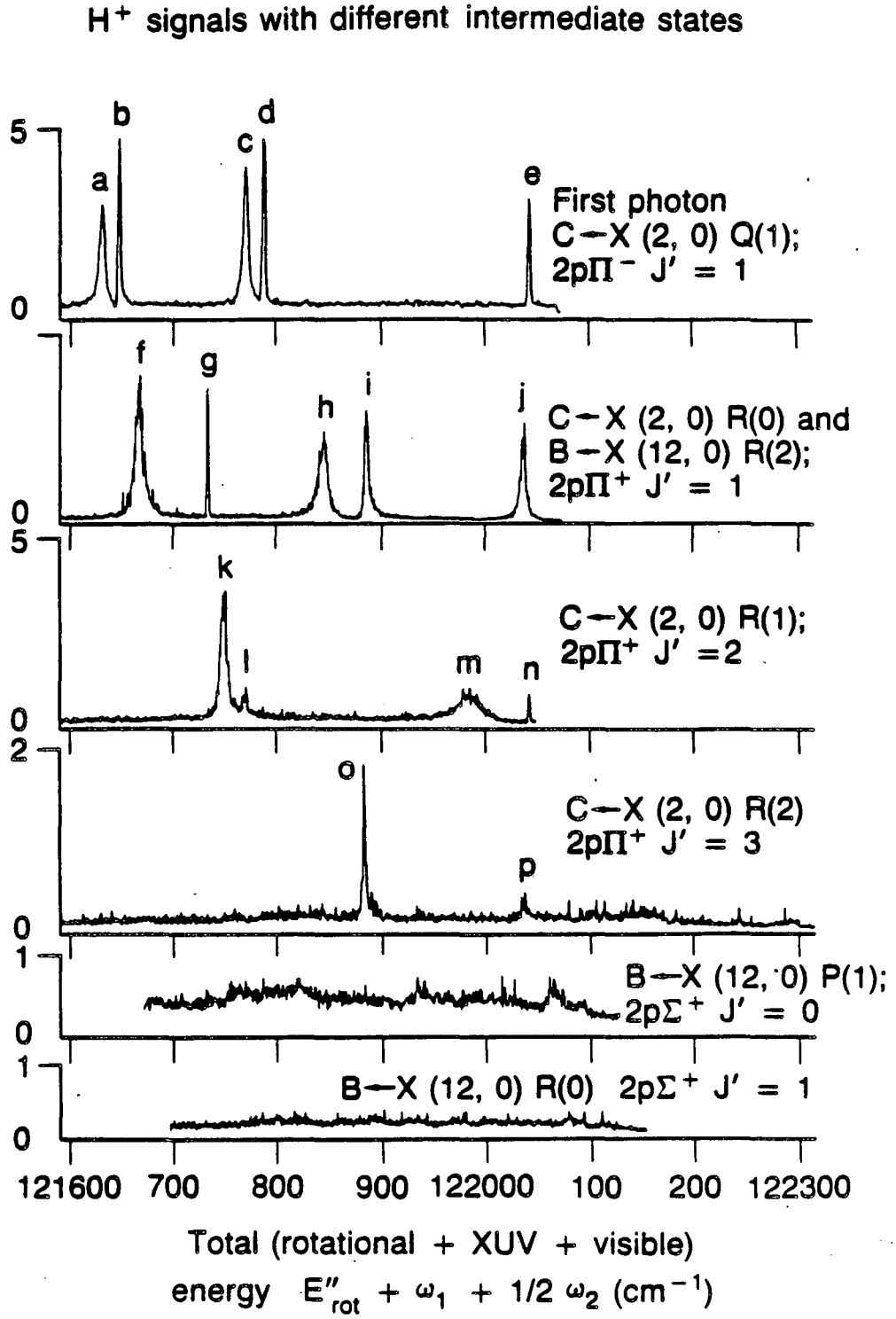

XBL 872-6161

Figure 4.

L Uncoupling for a d Electron

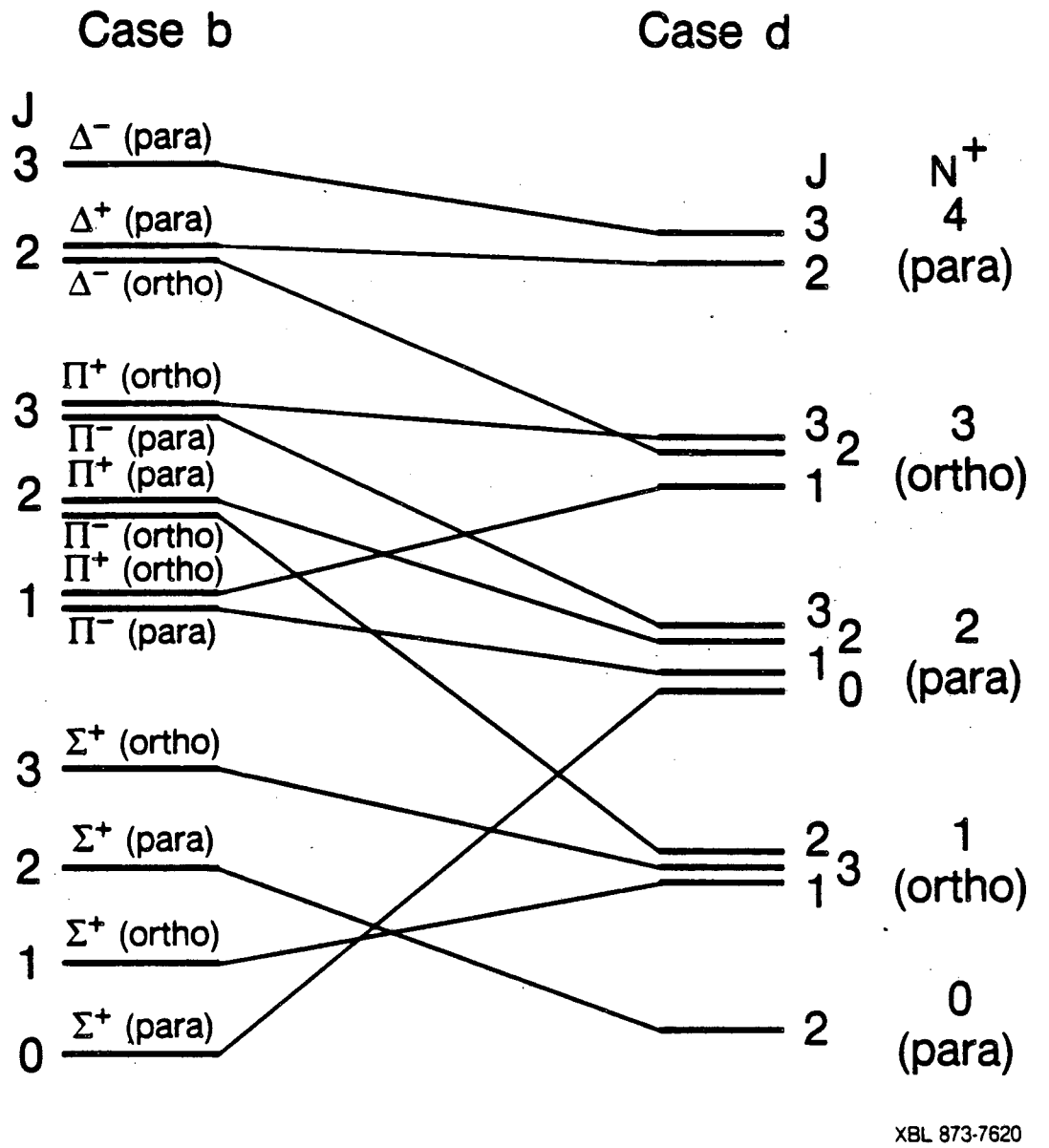

Figure 5.

VIII. CONCLUSION

There is no point in listing the conclusions drawn from the experiments described in this thesis, because they are presented in the chapters themselves and in the abstract. Instead, it is better to remind the reader of the natures of the research topics, and hope he remembers that the problems can be studied with supersonic beams and nonlinear spectroscopy. After all, it is not yet possible to write the final word concerning any of the research described here. The motivation remains!

One problem we worked on was the van der Waals (and hydrogen-bonded) clusters. It is still of interest to find the intermolecular vibrational modes, and the coupling between them and the intramolecular vibrational modes. The mechanism and rate of vibrational predissociation are still difficult puzzles.

A related problem was the C-H stretching local modes of benzene. Again, it is a challenge to understand the intramolecular vibrational couplings (or lack of them) that allow a local mode to exist, and to appear to decay irreversibly.

Still another related problem is to understand a large molecule's vibrational force field, or at least the harmonic part of it. We put some effort into finding some vibrational frequencies in the benzene molecule's first excited state. There are still more to discover and explain.

The problem of pumping molecules to highly excited electronic states was partially solved by our construction of a tunable XUV source. There are improvements to be made in the tunability,

intensity, and resolution.

It is a very large problem to detect, identify, and understand the excited states of molecules of fundamental importance, such as H_2O. Our venture into the photoionization spectroscopy of this molecule gave a non-negligible step forward in describing its autoionization and predissociation properties. Many excited states remain to be observed.

Even to understand the excited-state behavior of H_2, the simplest molecule of all, will take a lot of work. We had a look at its ion-pair ($H^+ + H^-$) channel and Rydberg states associated with a highly-vibrationally-excited H_2^+ core. A very brief foray into the states with medium principal quantum number showed that there is much to be learned about the energy level structure and predissociation properties.

LAWRENCE BERKELEY LABORATORY
TECHNICAL INFORMATION DEPARTMENT
UNIVERSITY OF CALIFORNIA
BERKELEY, CALIFORNIA 94720